

**NEUROPROTECTIVE ACTIVITY OF *PARKIA TIMORIANA* IN
ALUMINUM CHLORIDE MEDIATED ALZHEIMER'S DISEASE
RATS**

**A THESIS SUBMITTED IN PARTIAL FULFILLMENT OF THE
REQUIREMENTS FOR THE DEGREE OF DOCTOR OF
PHILOSOPHY**

NISEKHOTO NISA

MZU REGN NO.: 2010594

Ph.D. REGN NO.: MZU/Ph.D./1539 OF 04.11.2020



**DEPARTMENT OF ZOOLOGY
SCHOOL OF LIFE SCIENCES
JULY, 2024**

**NEUROPROTECTIVE ACTIVITY OF *PARKIA TIMORIANA* IN
ALUMINUM CHLORIDE MEDIATED ALZHEIMER'S DISEASE
RATS**

BY

Nisekphoto Nisa

Department of Zoology

Name of supervisor: Prof. G. Gurusubramanian

Submitted

**In partial fulfillment of the requirement of the Degree of Doctor of
Philosophy in Zoology of Mizoram University, Aizawl.**



Department of Zoology
School of Life Sciences
MIZORAM UNIVERSITY
(A Central University)

Dr. G. Gurusubramanian Ph.D
Dean and Professor

Phone: 9862399411 (M)

CERTIFICATE

I certify that the thesis entitled “**Neuroprotective activity of *Parkia timoriana* in aluminum chloride mediated Alzheimer’s disease rats**” submitted to Mizoram University for the award of the degree of Doctor in Philosophy in Zoology by **Nisekphoto Nisa** is a record of research work carried out during the period of 2020-2024 under my guidance and supervision, and that this work has not formed the basis for the award of any degree, diploma, associateship, fellowship or other titles in this university or any other university or institution of higher learning.

Dated:

Place: Aizawl

(PROF. G. GURUSUBRAMANIAN)

Department of Zoology

Mizoram University

DECLARATION

Mizoram University

July, 2024

I, **Nisekphoto Nisa**, hereby declare that the subject matter of this thesis entitled “**Neuroprotective activity of *Parkia timoriana* in aluminum chloride mediated Alzheimer’s disease rats**” is the record of work done by me, that the contents of this thesis did not form basis of the award of any previous degree to me or to the best of my knowledge to anybody else, and that the thesis has not been submitted by me for any research degree in any other University/Institute.

This is being submitted to the Mizoram University for the degree of **Doctor of Philosophy** in Zoology.

(NISEKHOTO NISA)

Department of Zoology

Mizoram University

(PROF. H. T. LALREMSANGA)

Head

Department of Zoology

Mizoram University

(PROF. G. GURUSUBRAMANIAN)

Supervisor

Department of Zoology

Mizoram University

ACKNOWLEDGEMENT

First and foremost, I would like to express my deepest gratitude to God Almighty for His abundant blessings and unwavering guidance throughout this academic journey. Without His grace, this achievement would not have been possible.

I am profoundly grateful to my supervisor, **Prof. G. Gurusubramanian**, for his invaluable guidance, continuous support, and insightful feedback throughout my research. His mentorship has been instrumental in shaping this work and my development as a researcher.

I would also like to extend my heartfelt thanks to the HOD, **Prof. H.T. Lalremsanga**, and all the teachers, **Dr. Vikas Kumar Roy**, **Dr. Amit Kumar Trivedi**, **Dr. Zothansiana**, **Dr. Esther Lalhmingliani**, **Dr. M. Vabeiryureilai**, and **Dr. Kiran R. Kharat**, who have imparted knowledge and wisdom, inspiring and encouraging me to pursue excellence in my academic endeavors.

My sincere appreciation goes to my parents for their unconditional love, encouragement, and sacrifices. Their constant support and belief in me have been my greatest source of motivation.

I would like to give a special thanks to my dear friends, **Dr. Bidanchi R. Momin**, **Dr. Manikandan B.**, and **Mr. Brilliant N. Marak** for their extraordinary support and assistance in my research. Their valuable insights, encouragement, and constant help have been pivotal in the completion of this thesis.

Special thanks to my labmates, **Mr. Saeed-Ahmed Lasker**, **Dr. Dinata Roy**, **Ms. Bhanushree Baishya**, **Dr. Pori Buragohain**, **Mr. Abhinash Giri**, **Ms. Arati Chetri**, **Mr. Andy Lalremruata**, **Ms. Sonia Chakma**, and **Mr. Gumaa Abdelmuala Abdelgani-Baraka**, for their assistance, and the collaborative spirit that made the lab a nurturing environment for research. The countless discussions, shared challenges, and mutual support have enriched my Ph.D. experience immensely.

I express my sincere gratitude to CSIR for granting me the junior research fellowship and supporting me financially.

Lastly, I would like to acknowledge my friends, relatives and colleagues who have been a source of support and encouragement throughout this journey.

Thank you all for being part of this incredible journey.

Dated:

Place: Aizawl, Mizoram

(NISEKHOTO NISA)

TABLE OF CONTENTS

Content	Page no.
CERTIFICATE	i
DECLARATION	ii
ACKNOWLEDGEMENTS	iii-iv
TABLE OF CONTENTS	v-xii
LIST OF FIGURES	xiii-xxv
LIST OF TABLES	xxvi-xxix
LIST OF ABBREVIATIONS	xxx-xxxiii
CHAPTER 1	
1.1. General introduction	1-8
1.1.1. Introduction to Alzheimer’s disease (AD)	1
1.1.2. Different stages of Alzheimer’s disease	2
1.1.3. Different hypotheses of Alzheimer’s disease	2-4
1.1.3.1. Cholinergic hypothesis	2
1.1.3.2. Amyloid hypothesis	3
1.1.3.3. Tau hypothesis	3-4
1.1.4. Risk factors of Alzheimer’s disease	4-6
1.1.5. Treatment of Alzheimer’s disease	6-7
1.1.6. <i>Parkia timoriana</i> (Tree bean)	7-8
1.2. Objectives	8
CHAPTER 2	
GC-MS and LC-MS analysis of phytochemicals of <i>P. timoriana</i> and evaluation of phytochemicals toxicity using in silico tools.	
2.1. Introduction	9-15
2.1.1. Computational toxicology	9-10
2.1.2. GC-MS and LC-MS analyses	10-11
2.1.3. Polyphenols	11-12
2.1.4. Median lethal dose (LD₅₀), Median lethal concentration (LC₅₀), and IGC₅₀	12
2.1.5. Bioconcentration factor	12-13

2.1.6. Mutagenicity	13-14
2.1.7. Carcinogenicity	14
2.1.8. Reproductive and developmental toxicology	14
2.1.9. Biological activity prediction	15
2.2. Review of literature	15-19
2.2.1. Computational toxicology	15-16
2.2.2. Biological activity prediction	16-17
2.2.3. Phytochemical analysis	17-19
2.3. Materials and Methods	19-24
2.3.1. Collection, identification and extraction of <i>Parkia timoriana</i> seed pods	19
2.3.2. Total flavonoid content	19-20
2.3.3. Total phenol content	20
2.3.4. Gas chromatography-mass spectrometry analysis	20-21
2.3.5. Liquid chromatography-mass spectrometry analysis	21-22
2.3.6. Toxicity prediction by QSAR-TEST	22-23
2.3.7. Toxicity prediction by VEGA HUB, OECD QSAR and Toxtree	23
2.3.8. Biological activity prediction	24
2.4. Results	24-52
2.4.1. Gas chromatography-mass spectrometry and liquid chromatography-mass spectrometry analysis	24-25
2.4.2. Total flavonoid and phenol content	25
2.4.3. Toxicity prediction using QSAR-TEST	25-30
2.4.3.1. LC₅₀ 96-hr (Fathead minnow)	25-26
2.4.3.2. LC₅₀ 48-hr (<i>Daphnia magna</i>)	26-27
2.4.3.3. IGC₅₀ 48hr (<i>Tetrahymena pyriformis</i>)	27-28
2.4.3.4. LD₅₀ oral (rat)	28
2.4.3.5. Predicted toxicological hierarchy	28-29
2.4.3.6. Bioconcentration factor	29
2.4.3.7. Developmental toxicity	29-30

2.4.3.8. Mutagenicity	30
2.4.4. Toxicity prediction using VEGA HUB, Toxtree, and OECD QSAR tools	30-32
2.4.4.1. Oral toxicity (Cramer)	30
2.4.4.2. Carcinogenicity	31
2.4.4.3. Reproductive toxicity	31
2.4.4.4. NOAEL	31-32
2.4.4.5. Repeated dose (HESS)	32
2.4.4.6. Lipinski rule and cytochrome p450	32
2.4.5. PASS prediction for biological activities	32-33
FIGURES	34-38
TABLES	39-52
2.5. Discussions	53-58
2.5.1. GC-MS and LC-MS analyses	53
2.5.2. Total flavonoid and phenol content	54
2.5.3. Acute toxicity prediction for different species	54
2.5.4. Bioconcentration factor prediction	55
2.5.5. Developmental toxicity	55
2.5.6. Mutagenicity and carcinogenicity	55-56
2.5.7. Oral toxicity, reproductive toxicity, and NOAEL	56
2.5.8. Repeated dose toxicity, Lipinski rule, and cytochrome p450 metabolism	56-57
2.5.9. Biological activity prediction	57-58
2.6. Key findings	58-59
CHAPTER 3	
Molecular docking and molecular dynamics simulation of phytocompounds from <i>P. timoriana</i> to BACE1 and cholinesterase protein receptor: an in silico therapeutic intervention study on Alzheimer's disease.	
3.1. Introduction	60-67
3.1.1. β-site APP cleaving enzyme 1 (BACE1)	60-61
3.1.2. Acetylcholinesterase (AChE)	61-62

3.1.3. Molecular docking	62
3.1.4. Molecular dynamics simulation	63
3.1.5. Binding free energy	63
3.1.6. ADMET properties	64-65
3.1.7. In silico tools	65-67
3.1.7.1. Molinspiration Cheminformatics	65
3.1.7.2. SwissADME	65-66
3.1.7.3. PyRx and AutoDock Vina	66
3.1.7.4. GROMACS	66
3.1.7.5. MM/PBSA	66-67
3.2. Review of Literature	67-71
3.2.1. Molecular docking	67-69
3.2.2. Molecular dynamics simulation and MM/PBSA analyses	69-71
3.3. Material and methods	71-75
3.3.1. Retrieval of ligand and its preparation	71
3.3.2. ADMET	71-72
3.3.3. Retrieval of protein and its preparation	72
3.3.4. Predicting the active site of the protein receptor	72
3.3.5. Molecular docking	72-73
3.3.6. Molecular dynamics simulation	73-74
3.3.7. Free energy binding	74
3.3.8. Principal component analysis	74-75
3.4. Results	75-122
3.4.1. ADMET properties	75-77
3.4.2. Molecular docking	77-78
3.4.3. Hydrogen bonding and hydrophobic interaction	78-80
3.4.4. Molecular dynamics simulation	80
3.4.5. Free energy binding	81-82
3.4.6. Principal component analysis	82
FIGURES	83-100

TABLES	101-122
3.5. Discussion	123-128
3.5.1. ADMET	123-125
3.5.2. Molecular docking	125-126
3.5.3. Molecular dynamics simulation	126-127
3.5.4. Free energy binding	127
3.5.5. Principal component analysis	127-128
3.6. Key findings	128-130
CHAPTER 4	
Biological evaluation of <i>P. timoriana</i> in ameliorating learning and memory processes in an aluminum chloride induced Alzheimer's disease rat model.	
4.1. Introduction	131-139
4.1.1. Toxicity study	131-134
4.1.1.1. Acute toxicity test	131-132
4.1.1.2. Sub-acute toxicity	132
4.1.1.3. Liver function test	132-133
4.1.1.4. Kidney function test	133-134
4.1.1.5. Haematological parameters	134
4.1.2. Alzheimer's disease	135-139
4.1.2.1. Aluminum chloride-induced Alzheimer's disease	135
4.1.2.2. Alzheimer's disease pathology	136
4.1.2.3. Neuroinflammation	136-137
4.1.2.4. Oxidative stress	137
4.1.2.5. Apoptosis	138
4.1.2.5. Behavioural study	138-139
4.2. Review of Literature	139-144
4.2.1. Acute and sub-acute toxicity study	139-141
4.2.2. Alzheimer's disease treatment	141-144
4.3. Material and methods	145-153
4.3.1. Collection, identification and extraction of <i>Parkia timoriana</i> seed pods	145

4.3.2. Animal ethics	145
4.3.3. Experimental animals	145
4.3.4. Toxicity study	145-148
4.3.4.1. Acute toxicity study	145-146
4.3.4.2. Sub-acute toxicity study	146
4.3.4.3. Haematological parameters assessment	146-147
4.3.4.4. Serum biochemical parameters assessment	147-148
4.3.4.5. Relative organ weight measurement	148
4.3.4.6. Histopathological assessment	148
4.3.5. AlCl₃-mediated Alzheimer's disease treatment	148-153
4.3.5.1. Experimental design	148-149
4.3.5.2. Behavioural experiment	149-150
4.3.5.2.1. Novel object recognition (NOR) test	149-150
4.3.5.2.2. Y-maze test	150
4.3.5.4. Oxidative and anti-oxidant parameters assessment	150-151
4.3.5.4.1. Protein estimation	150
4.3.5.4.2. Lipid peroxidation (LPO)	150-151
4.3.5.4.3. Glutathione-S-transferase (GST)	151
4.3.5.4.4. Glutathione (GSH)	151
4.3.5.5. Enzyme-linked immunosorbent assay (ELISA)	152
4.3.5.6. Western blotting	152-153
4.3.5.7. Histopathological examination	153
4.3.6. Statistical analysis	153
4.4. Results	153-185
4.4.1. Acute toxicity study	153-155
4.4.1.1. Effect of single-dose PTME on morphological changes and mortality	153-154
4.4.1.2. Effect of single-dose PTME on feed and water intake	154
4.4.1.3. Effect of single-dose PTME on body weight and relative organ weight	154

4.4.1.4. Effect of single-dose PTME on haematological parameters	154
4.4.1.5. Effect of single-dose PTME on serum biochemical parameters	154
4.4.1.6. Effect of single-dose PTME on histological examination	154-155
4.4.2. Sub-acute toxicity study	155-156
4.4.2.1. Effect of repeated-dose PTME on morphological changes and mortality	155
4.4.2.2. Effect of repeated-dose PTME on feed and water intake	155
4.4.2.3. Effect of repeated-dose PTME on body weight and relative organ weight	155
4.4.2.4. Effect of repeated-dose PTME on haematological parameters	156
4.4.2.5. Effect of repeated-dose PTME on serum biochemical parameters	156
4.4.2.6. Effect of repeated-dose PTME on histological examination	156
4.4.3. AlCl₃-mediated Alzheimer's disease treatment	157-159
4.4.3.1. Effect of PTME on cognitive deficit in AlCl₃-mediated AD rats	157
4.4.3.2. Effect of PTME on oxidative stress in AlCl₃-mediated AD rats	157
4.4.3.3. Effect of PTME on anti-oxidant biomarkers in AlCl₃-mediated AD rats	157-158
4.4.3.4. Effect of PTME on acetylcholinesterase in AlCl₃-mediated AD rats	158
4.4.3.5. Effect of PTME on inflammatory biomarkers in AlCl₃-mediated AD rats	158
4.4.3.6. Effect of PTME on apoptotic biomarkers in AlCl₃-	158-159

mediated AD rats	
4.4.3.7. Effect of PTME on AD's pathological biomarkers in AlCl₃-mediated AD rats	159
4.4.3.7. Effect of PTME on hippocampal histology in AlCl₃-mediated AD rats	159
FIGURES	160-177
TABLES	178-185
4.5. Discussion	186-193
4.5.1. Acute and sub-acute toxicity study	186-189
4.5.2. AlCl₃-mediated Alzheimer's disease treatment	189-193
4.6. Key Finding	193-195
CHAPTER 5	
Summary	196-201
CHAPTER 6	
Conclusion	202-203
CHAPTER 7	
References	204-262
<i>Brief bio-data of the candidate</i>	263
<i>List of conference/workshop/seminar attended</i>	264-267
<i>List of Research Publications</i>	268-276
<i>Plagiarism Certificate</i>	277-278
<i>Particulars of the candidate</i>	279

LIST OF FIGURES

Figure No.	Figure caption	Page No.
Figure 1	<i>Parkia timoriana</i> (wild bean) tree and its green, soft, and processed pods. (A) A tree of <i>P. timoriana</i> located in Tanhril forest of Aizawl, Mizoram, India. (B) <i>P. timoriana</i> seed pods eaten as a vegetable, salad, or chutney. (C) <i>P. timoriana</i> seed pods that have been cleaned, cut, and allowed to air dry. (D) <i>P. timoriana</i> seed pods that have been processed for the process of methanolic extraction.	34
Figure 2	The chromatogram displays the results of the GC-MS (gas chromatography-mass spectrometry) examination of methanolic extract of <i>Parkia timoriana</i> seed pod.	35
Figure 3	The chromatogram displays the results for the positive ion mode of LC-MS (liquid chromatography-mass spectrometry) analysis of the methanolic extract of <i>Parkia timoriana</i> seed pod.	36
Figure 4	The chromatogram displays the results for the negative ion mode of LC-MS (liquid chromatography-mass spectrometry) analysis of the methanolic extract of <i>Parkia timoriana</i> seed pod.	37
Figure 5	Total flavonoid (measured in mg QE/g extract) and total phenolic (measured in mg GAE/g extract) were found in high concentrations in the methanolic extract of <i>Parkia timoriana</i> seed pod.	38
Figure 6	2D structures of phytocompounds, found in methanolic extract of <i>Parkia timoriana</i> seed pods, used as ligands for molecular docking studies against BACE1 and AChE.	83
Figure 7	2D structures of phytocompounds, found in methanolic extract of <i>Parkia timoriana</i> seed pods, used as ligands for	84

	molecular docking studies against BACE1 and AChE.	
Figure 8	Preparation of the target receptor (BACE1), and identification of its active site for molecular docking experiments. (A) The BACE1 receptor has been prepared for docking using UCSF Chimera software. This involved removing the multiple chains, co-crystallized ligand, metal ions, and water molecules from the target receptor. Additionally, polar hydrogen atoms and partial charges were added to the receptor. The truncated side chains were repaired, and Gasteiger charges were added using the Dock Prep function of the software. (B) The fpocket software was used to predict the active site of the BACE1. The colour grey indicates the BACE1's active site.	85
Figure 9	Preparation of the target receptor (AChE), and identification of its active site for molecular docking experiments. (A) The AChE receptor has been prepared for docking using UCSF Chimera software. This involved removing the multiple chains, co-crystallised ligand, metal ions, and water molecules from the target receptor. Additionally, polar hydrogen atoms and partial charges were added to the receptor. The truncated side chains were repaired, and Gasteiger charges were added using the Dock Prep function of the software. (B) The fpocket software was used to predict the active site of the AChE. The colour green indicates the AChE's active site.	86
Figure 10	2D (two-dimensional) and 3D (three-dimensional) docking poses demonstrate the interactions between the top-hit putative bioactive phytochemicals (ligands) from <i>Parkia timoriana</i> and the residues of BACE1's active site. (A, B) The binding affinity of BACE1-ergocristine	87

	complex is -10.3 kcal/mol. (C, D) The binding affinity of BACE1-nicotiflorin complex is -10.2 kcal/mol.	
Figure 11	2D (two-dimensional) and 3D (three-dimensional) docking poses demonstrate the interactions between the top-hit putative bioactive phytochemicals (ligands) from <i>Parkia timoriana</i> and the residues of BACE1's active site. (A, B) The binding affinity of BACE1-isorhamnetin-3-O-rutinoside complex is -10.1 kcal/mol. (C, D) The binding affinity of BACE1-voacamine complex is -10.1 kcal/mol.	88
Figure 12	2D (two-dimensional) and 3D (three-dimensional) docking poses demonstrate the interactions between the top-hit putative bioactive phytochemicals (ligands) from <i>Parkia timoriana</i> and the residues of AChE's active site. (A, B) The binding affinity of AChE-apiin complex is -10.3 kcal/mol. (C, D) The binding affinity of AChE-maritimetin-6-O-glucoside complex is -10.3 kcal/mol.	89
Figure 13	2D (two-dimensional) and 3D (three-dimensional) docking poses demonstrate the interactions between the top-hit putative bioactive phytochemicals (ligands) from <i>Parkia timoriana</i> and the residues of AChE's active site. (A, B) The binding affinity of AChE-paenoniflorin complex is -10.2 kcal/mol. (C, D) The binding affinity of AChE-silychrestin complex is -9.8 kcal/mol.	90
Figure 14	Evaluation of the compactness and stability of the docked complex (including BACE1-ergocristine, BACE1-nicotiflorin, BACE1-isorhamnetin-3-O-rutinoside, and BACE1-voacamine) by computing the deviation as a function of residue index and time from 100 ns of molecular dynamics (MD) simulation. (A) Stability of the receptor-ligand complex (BACE1-ergocristine, BACE1-	91

	<p>nicotiflorin, BACE1-isorhamnetin -3-O-rutinoside, and BACE1-voacamine) throughout the 100 ns MD simulation was shown by the root-mean square deviation (RMSD). (B) An analysis of the root mean square fluctuation (RMSF) revealed that the ligands (ergocristine, nicotiflorin, isorhamnetin-3-O-rutinoside, and voacamine) interacted with comparable residues of BACE1. (C) The number of hydrogen bonds established by the docked complex (BACE1-ergocristine, BACE1-nicotiflorin, BACE1-isorhamnetin -3-O-rutinoside, and BACE1-voacamine) throughout the 100 ns simulation, showing that BACE1-nicotiflorin complex creates the highest degree of stability with respect to hydrogen bond. (D) The measurement of the radius of gyration (Rg) reveals that the protein structure of BACE1 is compacted by each of the ligand (ergocristine, nicotiflorin, isorhamnetin-3-O-rutinoside, and voacamine).</p>	
Figure 15	<p>Evaluation of the compactness and stability of the docked complex (including AChE-apiin, AChE-maritimetin-6-O-glucoside, AChE-paenoniflorin, and AChE-silychrystin) by computing the deviation as a function of residue index and time from 100 ns of molecular dynamics (MD) simulation. (A) Stability of the receptor-ligand complex (AChE-apiin, AChE-maritimetin-6-O-glucoside, AChE-paenoniflorin, and AChE-silychrystin) throughout the 100 ns MD simulation was shown by the root-mean square deviation (RMSD). (B) An analysis of the root mean square fluctuation (RMSF) revealed that the ligands (apiin, maritimetin-6-O-glucoside, paenoniflorin, and silychrystin) interacted with comparable residues of AChE. (C) The number of hydrogen bonds established by</p>	92

	<p>the docked complex (AChE-apiin, AChE-maritimetin-6-O-glucoside, AChE-paenoniflorin, and AChE-silychrestin) throughout the 100 ns simulation, showing that AChE-maritimetin-6-O-glucoside complex creates the highest degree of stability with respect to hydrogen bond. (D) The measurement of the radius of gyration (Rg) reveals that the protein structure of AChE is compacted by each of the ligand (apiin, maritimetin-6-O-glucoside, paenoniflorin, and silychrestin).</p>	
Figure 16	<p>Molecular mechanics Poisson-Boltzmann surface area (MMPBSA) analysis for calculating the binding free energy of the receptor-ligand complex). (A) The binding free energy (kJ/mol) of the receptor-ligand complex (BACE1-ergocristine, BACE1-nicotiflorin, BACE1-isorhamnetin-3-O-rutinoside, and BACE1-voacamine) for the 100 ns of MD simulation trajectories, showing BACE1-voacamine complex as the strongest binding energy. (B) MMPBSA analysis revealed that comparable residues of BACE1 are implicated in ligand binding (ergocristine, nicotiflorin, isorhamnetin-3-O-rutinoside, and voacamine) by residue-wise breakdown of binding free energy. (C, D, E, and F) The individual residues of BACE1 contributing the highest energy when bound to the ligand (ergocristine, nicotiflorin, isorhamnetin-3-O-rutinoside, and voacamine, respectively). The breakdown of the binding free energy from MMPBSA analysis (van der Waals, electrostatic, nonpolar solvation energy, and polar solvation) is also displayed. A positive value destabilises the complex, while a negative value implies the formation of a stable complex.</p>	93-94
Figure 17	<p>Molecular mechanics Poisson-Boltzmann surface area</p>	95-96

	<p>(MMPBSA) analysis for calculating the binding free energy of the receptor-ligand complex). (A) The binding free energy (kJ/mol) of the receptor-ligand complex (AChE-apiin, AChE-maritimetin-6-O-glucoside, AChE-paenoniflorin, and AChE-silychrystin) for the 100 ns of MD simulation trajectories, showing AChE-silychrystin complex as the strongest binding energy. (B) MMPBSA analysis revealed that comparable residues of AChE are implicated in ligand binding (apiin, maritimetin-6-O-glucoside, paenoniflorin, and silychrystin) by residue-wise breakdown of binding free energy. (C, D, E, and F) The individual residues of AChE contributing the highest energy when bound to the ligand (apiin, maritimetin-6-O-glucoside, paenoniflorin, and silychrystin, respectively). The breakdown of the binding free energy from MMPBSA analysis (van der Waals, electrostatic, nonpolar solvation energy, and polar solvation) is also displayed. A positive value destabilises the complex, while a negative value implies the formation of a stable complex.</p>	
Figure 18	<p>Scatter plots derived from PCA (Principal Component Analysis) display the displacement of alpha carbon ($C\alpha$) atoms along the first and second eigenvectors of receptor-ligand complex. (A) BACE1-ergocristine. (B) BACE1-nicotiflorin. (C) BACE1-isorhamnetin-3-O-rutinoside. (D) BACE1-voacamine. These plots indicate that voacamine restricts the collective motion of the BACE1 receptor to a greater extent compared to the other compounds.</p>	97
Figure 19	<p>Scatter plots derived from PCA (Principal Component Analysis) display the displacement of alpha carbon ($C\alpha$)</p>	98

	atoms along the first and second eigenvectors of receptor-ligand complex. (A) AChE-apiin. (B) AChE-maritimetin-6-O-glucoside. (C) AChE-paenoniflorin. (D) AChE-silychrestin. These plots indicate that maritimetin-6-O-glucoside restricts the collective motion of the AChE receptor to a greater extent compared to the other compounds.	
Figure 20	Snapshot images depict the motion of top hit ligands inside the protein binding site of BACE1 at 20 ns intervals throughout a 100 ns period of molecular dynamics simulation.	99
Figure 21	Snapshot images depict the motion of top hit ligands inside the protein binding site of AChE at 20 ns intervals throughout a 100 ns period of molecular dynamics simulation.	100
Figure 22	The impact of the methanolic extract derived from the seed pod of <i>Parkia timoriana</i> on the body weight, feed, and water intake of the Wistar rats that were exposed to it in a single-dose acute toxicity study. (A) The impact on daily food consumption. (B) The impact on the volume of water consumed daily. (C) The impact on the body weight was measured every alternate day for a period of 14 days.	160
Figure 23	The effect of a single-dose of PTME on the liver (liver function test) of Wistar rats that were exposed to it in an acute toxicity study. (A) The level of AST (aspartate aminotransferase) showed no significant change between the treatment groups. (B) The level of ALT (alanine transaminase) showed no significant change between the treatment groups. (C) The level of ALP (alkaline phosphatase) was significantly high in 5000 mg/kg	161

	treatment group. All values are expressed as mean \pm SEM, n = 5. p < 0.05 shows a significant difference (one-way ANOVA/Tukey's multiple comparison). Statistically significant data are represented with different alphabetical letters.	
Figure 24	The effect of a single-dose of PTME on the kidney (kidney function test) of Wistar rats that were exposed to it in an acute toxicity study. (A) The level of creatinine was significantly high in the 5000 mg/kg treatment group. (B) The level of urea showed no significant change between the treatment groups. All values are expressed as mean \pm SEM, n = 5. p < 0.05 shows a significant difference (one-way ANOVA/Tukey's multiple comparison). Statistically significant data are represented with different alphabetical letters.	162
Figure 25	The effect of a single dose of PTME on the histopathological sections (40x magnification; H & E) of liver tissue of Wistar rats that were exposed to it in an acute toxicity study. (A) Control. (B) 1000 mg/kg treated group. (C) 3000 mg/kg treated group. (D) 5000 mg/kg treated group. The histopathological section of the 5000 mg/kg treated group showed alterations, with the central vein showing congestion, slight dilation in the sinusoids, and damaged hepatocytes. Whereas, the other groups showed normal liver architecture as the control. PV- portal vein, CV- central vein, H- hepatocyte, S- sinusoids, K- Kupffer's cell, and HA- hepatic artery.	163
Figure 26	The effect of a single dose of PTME on the histopathological sections (40x magnification; H & E) of kidney tissue of Wistar rats that were exposed to it in an acute toxicity study. (A) Control. (B) 1000 mg/kg treated	164

	<p>group. (C) 3000 mg/kg treated group. (D) 5000 mg/kg treated group. The histopathological section of the 5000 mg/kg treated group showed deteriorated alterations, with an enlarged Bowman's space around the glomerulus and an enlarged PCT. Whereas, the other groups showed normal structure of glomerulus, Bowman's capsule, DCT, and PCT. A slight enlargement in Bowman's capsule is seen in 3000 mg/kg treated group. G- glomerulus, B- Bowman's capsule, BS- Bowman's space, DCT- Distal convoluted tubule, and PCT- Proximal convoluted tubule.</p>	
Figure 27	<p>The impact of repeated-dose of the PTME on the body weight, feed and water intake by the Wistar rats that were exposed to it in a sub-acute toxicity study. (A) The impact on the food ingested was measured on an alternate day basis. (B) The impact on the volume of water consumed was recorded every other day. (C) The impact on the body weight was measured on a weekly basis for a period of 28 days.</p>	165
Figure 28	<p>The effect of a repeated-dose of PTME on the liver (liver function test) of Wistar rats that were exposed to it in a sub-acute toxicity study. (A) The level of AST (aspartate aminotransferase) showed no significant change between the treatment groups. (B) The level of ALT (alanine transaminase) showed no significant change between the treatment groups. (C) The level of ALP (alkaline phosphatase) showed no significant change between the treatment groups. All values are expressed as mean \pm SEM, n = 5. p < 0.05 shows a significant difference (one-way ANOVA/Tukey's multiple comparison). Statistically significant data are represented with different alphabetical letters.</p>	166

Figure 29	<p>The effect of a repeated-dose of PTME on the kidney (kidney function test) of Wistar rats that were exposed to it in a sub-acute toxicity study. (A) The level of creatinine showed no significant change between the treatment groups. (B) The level of urea showed no significant change between the treatment groups. All values are expressed as mean \pm SEM, n = 5. p < 0.05 shows a significant difference (one-way ANOVA/Tukey's multiple comparison). Statistically significant data are represented with different alphabetical letters.</p>	167
Figure 30	<p>The effect of a repeated-dose of PTME on the histopathological sections (40x magnification; H & E) of liver tissue of Wistar rats that were exposed to it in a sub-acute toxicity study. (A) Control. (B) 20 mg/kg treated group. (C) 50 mg/kg treated group. (D) 100 mg/kg treated group. (E) 300 mg/kg treated group. The 300 mg/kg treated group's histopathological section showed a liver with a skewed structure, a congested central vein, and damaged hepatocytes. Whereas, the other treated groups showed normal hepatocytes, portal vein, sinusoids, and hepatic artery, similar to the control group. PV- portal vein, CV- central vein, H- hepatocyte, S- sinusoids, K- Kupffer's cell, HA- hepatic artery, and BD- bile duct.</p>	168
Figure 31	<p>The effect of a repeated-dose of PTME on the histopathological sections (40x magnification; H & E) of kidney tissue of Wistar rats that were exposed to it in a sub-acute toxicity study. (A) Control. (B) 20 mg/kg treated group. (C) 50 mg/kg treated group. (D) 100 mg/kg treated group. (E) 300 mg/kg treated group. The histopathological section of the 300 mg/kg treated group showed significant damage. The kidney architecture of</p>	169

	the other treated groups, comparable to the control group, was normal. G- glomerulus, B- Bowman's capsule, BS- Bowman's space.	
Figure 32	The methanolic extract of <i>Parkia timoriana</i> seed pod improved the cognitive impairment in an aluminum chloride-mediated Alzheimer's disease rat. (A) The effect of PTME on the recognition index percentage in a novel object recognition (NOR) test. (B) The effect of PTME on the spontaneous alternation percentage (SAP) in a Y-maze test. All values are expressed as mean \pm SEM, n = 5. p < 0.05 shows a significant difference (one-way ANOVA/Tukey's multiple comparison). Statistically significant data are represented with different alphabetical letters.	170
Figure 33	The methanolic extract of <i>Parkia timoriana</i> seed pod lowered lipid peroxidation (measured as MDA level), a sign of oxidative stress, in the hippocampus of an aluminum chloride-mediated Alzheimer's disease rat. All values are expressed as mean \pm SEM, n = 5. p < 0.05 shows a significant difference (one-way ANOVA/Tukey's multiple comparison). Statistically significant data are represented with different alphabetical letters.	171
Figure 34	The methanolic extract of <i>Parkia timoriana</i> seed pod increased the anti-oxidant markers (glutathione, GSH; glutathione-S-transferase, GST) in the hippocampus of an aluminum chloride-mediated Alzheimer's disease rat. (A) The effect of PTME on the level of GSH in an AD rat. (B) The effect of PTME on GST levels in an AD rat. All values are expressed as mean \pm SEM, n = 5. p < 0.05 shows a significant difference (one-way	172

	ANOVA/Tukey's multiple comparison). Statistically significant data are represented with different alphabetical letters.	
Figure 35	PTME decreased the level of acetylcholinesterase (AChE) in an aluminum chloride-mediated Alzheimer's disease rat. All values are expressed as mean \pm SEM, n = 5. p < 0.05 shows a significant difference (one-way ANOVA/Tukey's multiple comparison). Statistically significant data are represented with different alphabetical letters.	173
Figure 36	Neuroprotective effect of PTME on neuroinflammation in the hippocampus of an aluminum chloride-mediated Alzheimer's disease rat. (A) NF-kB. (B) TNF- α . (C) IL-6. All values are expressed as mean \pm SEM, n = 5. p < 0.05 shows a significant difference (one-way ANOVA/Tukey's multiple comparison). Statistically significant data are represented with different alphabetical letters.	174
Figure 37	PTME treatment reduced apoptosis in the hippocampal region of an aluminum chloride-mediated Alzheimer's disease rat. (A) Active caspase-3. (B) BCL-2. (C) Bax. All values are expressed as mean \pm SEM, n = 5. p < 0.05 shows a significant difference (one-way ANOVA/Tukey's multiple comparison). Statistically significant data are represented with different alphabetical letters.	175
Figure 38	Ameliorative effect of PTME on the AD pathological markers in the hippocampal region of an aluminum chloride-mediated Alzheimer's disease rat. (A) BACE1. (B) A β . (C) Tau. All values are expressed as mean \pm SEM, n = 5. p < 0.05 shows a significant difference (one-	176

	way ANOVA/Tukey's multiple comparison). Statistically significant data are represented with different alphabetical letters.	
Figure 39	<p>PTME administration improved the histopathological alterations in the hippocampus of an aluminum chloride-mediated Alzheimer's disease rat. (A) Group 1, or the control group, showed viable, well-defined neuronal cells with a distinct nucleus (arrow). (B) Group 2 or AlCl_3 group showed a large number of damaged, distorted, irregular neuronal cells (arrowhead) with shrunken cytoplasm and dark pyknotic nuclei. (C) Group 3 or AlCl_3 + Pt_5 group showed a bit of improvement from damaged neurons (arrowhead), as a greater number of normal neurons (arrow) were seen compared to group 2. (D) Group 4 or AlCl_3 + Pt_{10} group showed a remarkable decrease in the number of injured or damaged cells and an increase in the number of viable neuronal cells. Arrow- viable and well-defined neuronal cells. Arrowhead- damaged, distorted, and irregular neuronal cells.</p>	177

LIST OF TABLES

Table No.	Table caption	Page No.
Table 1	The phytocompounds present in the methanolic extract of <i>Parkia timoriana</i> seed pod were identified using GC-MS (gas chromatography-mass spectrometry) and LC-MS (liquid chromatography-mass spectrometry) studies.	39-40
Table 2	The values of LD ₅₀ (<i>Rattus</i>), LC ₅₀ (<i>Pimephales promelas</i> ; <i>Daphnia magna</i>), and IGC ₅₀ (<i>Tetrahymena pyriformis</i>) of the phytocompounds found in the methanolic extract of <i>Parkia timoriana</i> seed pod were determined utilising the TEST software (Toxicity Estimation Software Tool) on the basis of a QSAR model (quantitative structure–activity relationship).	41-43
Table 3	The predicted values of bioaccumulation factor, mutagenicity, and developmental toxicity of the phytocompounds found in the methanolic extract of <i>Parkia timoriana</i> seed pod were derived utilising the TEST software (Toxicity Estimation Software Tool).	44-45
Table 4	Prediction of different toxicity parameters (oral toxicity, carcinogenicity, reproductive toxicity, NOAEL, and repeated dose toxicity) and drug-likeness properties (Lipinski rule of five and cytochrome-P450 Metabolism) on the basis of QSAR model (quantitative structure–activity relationship) utilising different software (Toxtree, VEGA HUB, and OECD QSAR).	46-49
Table 5	Prediction of different biological activities of the phytocompounds found in the methanolic extract of <i>Parkia timoriana</i> seed pod using PASS (way2drug).	50-52
Table 6	Phytocompounds, found in methanolic extract of <i>Parkia timoriana</i> seed pods, used as ligands for molecular docking	101-105

	analysis against BACE1 and AChE protein receptors.	
Table 7	Predicted ADMET (absorption, distribution, metabolism, excretion, and toxicity) properties of the phytochemicals found in the methanolic extract of <i>Parkia timoriana</i> seed pod using SwissADME and Molinspiration tools.	106-108
Table 8	Prediction of pharmacokinetic properties, water solubility, and lipophilicity of the phytochemicals from the methanolic extract of <i>Parkia timoriana</i> using SwissADME and Molinspiration tools.	109-111
Table 9	Predicted pharmacokinetic properties, medicinal chemistry, and drug-like qualities of the phytochemicals from the methanolic extract of <i>Parkia timoriana</i> using SwissADME and Molinspiration tools.	112-114
Table 10	The binding affinity values of each phytochemical (ligand) found in <i>Parkia timoriana</i> seed pods docked against BACE1 and AChE receptors acquired using the autodock vina tool.	115-116
Table 11	The predicted affinity for binding and interaction between the residues of the BACE1 receptor and the most potent phytochemicals (ligands) of <i>Parkia timoriana</i> seed pods.	117
Table 12	The predicted affinity for binding and interaction between the residues of the AChE receptor and the most potent phytochemicals (ligands) of <i>Parkia timoriana</i> seed pods.	118
Table 13	Examination of the stability, compactness, and fluctuation of the most potent phytochemicals found in methanolic extract of <i>Parkia timoriana</i> seed pods docked with the BACE1 receptor.	119
Table 14	Examination of the stability, compactness, and fluctuation of the most potent phytochemicals found in methanolic extract of <i>Parkia timoriana</i> seed pods docked with the AChE receptor.	120

Table 15	Total binding energy (kJ/mol) analysis by MMPBSA approach of the most potent phytocompounds found in methanolic extract of <i>Parkia timoriana</i> seed pods docked with the BACE1 receptor.	121
Table 16	Total binding energy (kJ/mol) analysis by MMPBSA approach of the most potent phytocompounds found in methanolic extract of <i>Parkia timoriana</i> seed pods docked with the AChE receptor.	122
Table 17	The effect of a single-dose methanolic extract of <i>Parkia timoriana</i> seed pod on the physical observations of Wistar albino rats exposed to it in an acute toxicity study.	178
Table 18	The impact of a single-dose methanolic extract of <i>Parkia timoriana</i> seed pod on the body weight and relative organ weight of Wistar albino rats exposed to it in an acute toxicity study.	179
Table 19	The impact of a single-dose methanolic extract of <i>Parkia timoriana</i> seed pod on the haematological parameters of Wistar albino rats exposed to it in an acute toxicity study. All values are expressed as mean \pm SEM, n = 5. *p < 0.05 shows a significant difference (one-way ANOVA/Tukey's multiple comparison). Statistically significant data are represented with different alphabetical letters.	180
Table 20	The impact of a single-dose methanolic extract of <i>Parkia timoriana</i> seed pod on the biochemical analysis of Wistar albino rats exposed to it in an acute toxicity study. All values are expressed as mean \pm SEM, n = 5. *p < 0.05 shows a significant difference (one-way ANOVA/Tukey's multiple comparison). Statistically significant data are represented with different alphabetical letters.	181
Table 21	The effect of a repeated-dose methanolic extract of <i>Parkia timoriana</i> seed pod on the physical observations of Wistar	182

	albino rats exposed to it in a 28 days sub-acute toxicity study.	
Table 22	The effect of a repeated-dose methanolic extract of <i>Parkia timoriana</i> seed pod on the body weight and relative organ weight of Wistar albino rats exposed to it in a sub-acute toxicity study.	183
Table 23	The effect of a repeated-dose methanolic extract of <i>Parkia timoriana</i> seed pod on the haematological parameters of Wistar albino rats exposed to it in a sub-acute toxicity study. All values are expressed as mean \pm SEM, n = 5. *p < 0.05 shows a significant difference (one-way ANOVA/Tukey's multiple comparison). Statistically significant data are represented with different alphabetical letters.	184
Table 24	The impact of a repeated-dose methanolic extract of <i>Parkia timoriana</i> seed pod on the biochemical analysis of Wistar albino rats exposed to it in a sub-acute toxicity study. All values are expressed as mean \pm SEM, n = 5. *p < 0.05 shows a significant difference (one-way ANOVA/Tukey's multiple comparison). Statistically significant data are represented with different alphabetical letters.	185

LIST OF ABBREVIATIONS

Ach	Acetylcholine
AD	Alzheimer's disease
ADMET	Absorption, distribution, metabolism, excretion, and toxicity
AlCl ₃	Aluminum chloride
ALP	Alkaline phosphatase
ALT	Alanine transaminase
APP	Amyloid precursor protein
ARIA	Amyloid-related imaging abnormalities
AST	Aspartate aminotransferase
ATSDR	Agency for toxic substances and disease registry
A β	Amyloid-beta
BACE1	Beta-site amyloid precursor protein cleaving enzyme 1
BBB	Blood brain barrier
BCF	Bioconcentration factor
Bcl-2	B cell leukemia/lymphoma-2
BDNF	Brain-derived neurotrophic factor
BSI	Botanical survey of India
BuChE	Butyrylcholinesterase
CADD	Computer-aided drug design
CCL	Chemokines like C-C motif chemokine ligand
CE-MS	Capillary electrophoresis–mass spectrometry
CNS	Central nervous system
CV	Central vein
CXCL	CXC motif chemokine ligand
DTNB	5,5'-dithiobis(2-nitrobenzoic acid)
ELISA	Enzyme-linked immunosorbant assay
ESOL	Estimated SOLubility
ETA	Expected time of arrival
FAD	Familial Alzheimer's disease

FTIR	Fourier-transform infrared spectroscopy
GAFF	General AMBER force field
GC-MS	Gas chromatography–mass spectrometry
GGT	Gamma-glutamyl transferase
GHS	Globally harmonised classification system
GI	Gastrointestinal absorption
GPX	Glutathione peroxidase
GR	Glutathione reductase
GSH	Glutathione
GSK-3 β	Glycogen synthase kinase 3 β
GST	Glutathione-S-transferase
H	Hepatocyte
HA	Hepatic artery
Hb-	Haemoglobin
HBA	Hydrogen bond acceptor
HBD	Hydrogen bond donor
HCT	Hematocrit
IGC ₅₀	Inhibition growth concentration 50%
iLOGP	Implicit log P
iNOS	Inducible nitric oxide synthase
Isaac	International serious adverse events consortium
K	Kupffer's cell
LC ₅₀	Lethal concentration 50%
LC-MS	Liquid chromatography–mass spectrometry
LD ₅₀	Lethal dose 50%
LINCS	LINEar constraint solver
LPO	Lipid peroxidation
MAPK	Mitogen-activated protein kinase
MCH	Mean corpuscular haemoglobin
MCHC	Mean corpuscular haemoglobin concentration

MCI	Moderate cognitive impairment
MCV	Mean cell volume
MDA	Malondialdehyde
MR	Molar refractivity
MW	Molecular weight
NCBI	National centre for biotechnology information
NCEs	New chemical entities
NFTs	Neurofibrillary tangles
NF- κ B	Nuclear factor-kappaB
NIST	National institute of standards and technology
NMDA	N-methyl-D-aspartate
NMR	Nuclear magnetic resonance
NO	Nitric oxide
NOAEL	No observed adverse effect level
NOR	Novel object recognition
OECD	Organisation for economic co-operation and development
OSDD	Open-source drug discovery
PAINS	Pan-assay interference compounds
PASS	Prediction of activity spectra for substances
PCA	Principal component analysis
PDB	Protein data bank
Pdbqt	Protein data bank, partial charge, and atom type
P-gp	Permeability glycoprotein
PHG	Polyherbal granules
PME	Particle mesh ewald
p-STAT3	Phosphorylated signal transducer and activator of transcription-3
PTME	Methanolic extract of <i>Parkia timoriana</i> see pod
PV	Portal vein
PyRx	Python prescription
QSAR	Quantitative structure activity relationship

RB	Rotatable bond
RBC	Red blood cells
RCSB	Research collaboratory for structural bioinformatics
RI	Recognition index
ROS	Reactive oxygen species
S	Sinusoids
SAP	Spontaneous alternation percentage
SAR	Structure activity relationship
SASA	Solvent accessible surface area
SBDD	Structure-based drug design
SDF	Structure-data file
SEM	Standard error of the mean
SMILES	Simplified molecular input line entry system
TBA	Thiobarbituric acid
TCA	Trichloroacetic acid
TERIS	Teratogen information system
TFAM	Mitochondrial transcription factor-A
TFC	Total flavonoid content
TLRs	Toll-like Receptors
TNF	Tumour necrosis factor
TPSA	Topological polar surface area
UFF-	Universal force field
UPLC	Ultra performance liquid chromatography
ULN	Upper limit of normal
WBC	White blood cells

CHAPTER-1

1.1. GENERAL INTRODUCTION

1.1.1. Introduction to Alzheimer's disease (AD)

Alzheimer's disease (AD) is a neurodegenerative disease that is the most prevalent and complex type of dementia, exhibiting a variety of cognitive deficits, altered personality traits, and aberrant behaviour (**Alzheimer's association, 2024; Ravi et al., 2018**). The World Health Organisation (WHO) projects that there will be 139 million dementia patients worldwide by 2050, up from 55 million in 2019 (**WHO, 2023**). Additionally, it is predicted that the expenses related to dementia would double, reaching \$2.8 trillion by 2030 from US\$1.3 trillion annually in 2019 (**Long et al., 2023**).

The two main pathogenic markers seen in AD are neurofibrillary tangles (NFTs) and senile plaques, although the precise processes causing these changes are yet unknown. Senile plaque is produced when extracellular A β peptide aggregate, while aberrant hyperphosphorylated tau protein deposits result in NFTs. In addition, AD has been associated with mitochondrial malfunction, neuroinflammatory, impaired neurotransmissions, hormonal changes, and cell cycle abnormalities (**Tarragon et al., 2013; Lam et al., 2016**).

Alois Alzheimer was the first to document AD in 1907. Despite the fact that the idea of dementia has been around for many years, the key clinical condition and related neurodegenerative alterations were first identified in the last century. In 1907, Alois Alzheimer meticulously documented the symptoms of Auguste Deter, a 51-year-old lady in his care at an asylum in Frankfurt, Germany (**Alzheimer et al., 1995**). The account of the symptoms by Alzheimer's is most likely the first neuropsychological description of AD. Alzheimer performed a microscopic examination of Auguste Deter's brain after her death using the novel silver staining histology method. He saw the amyloid angiopathy, NFTs, and senile plaques that are now recognised as the key markers of the disease (**Bondi et al., 2018**). By 1911, physicians in both Europe and the US were diagnosing patients based on Alzheimer's descriptions (**Mauer and Mauer, 2003**).

1.1.2. Different stages of Alzheimer's disease

Alzheimer's disease-related dementia is typified by AD's biomarker together with observable memory, language, cognitive, or behavioural symptoms that affect the ability of a person to function in everyday life (**Villemagne et al., 2013**). People with Alzheimer's disease often suffer a variety of symptoms that alter over time. The degree of neuronal loss in various brain regions is reflected in these symptoms. Alzheimer's disease has three stages: mild, moderate, and severe. The rate at which mild, moderate, and severe dementia symptoms progress varies from patient to patient (**Mahdi et al., 2019**). While most people with mild AD are able to operate independently in many fields, they will probably need assistance with certain activities in order to maintain their safety and maximise their independence. In addition to work, they might still be able to drive and engage in their favourite hobbies. It could take them longer to do everyday chores (**Alistair and Steve, 2009**). However, individuals with moderate AD struggle more with memory loss and language difficulties, are more prone to confusion, and find it more difficult to do multistep chores like getting dressed and taking a shower. They could sometimes lose their ability to urinate, start having trouble identifying loved ones, and exhibit behavioural and psychological changes, including anxiety and suspicion. As AD progresses to a severe degree, individuals lose their ability to accomplish everyday tasks like eating, walking around, dressing, and taking a shower on their own. Their verbal communication skills are significantly impaired, and they will probably need 24-hour care (**Alzheimer's Association, 2024; Alistair and Steve, 2009**).

1.1.3. Different hypotheses of Alzheimer's disease

1.1.3.1. Cholinergic hypothesis

The cholinergic hypothesis predates all of the other proposed explanations for AD aetiology (**Devi and Ohno, 2012**). This theory proposes that the deficiency of the neurotransmitter acetylcholine is the root cause of Alzheimer's disease. Researchers have proposed the cholinergic hypothesis for over 30 years, which states that the cognitive loss seen in Alzheimer's disease patients is caused by aberrant neurons that carry acetylcholine. Neurons essentially produce acetylcholine (ACh), which plays a

crucial role in transmitting sensory-related information and physiological functions like sleep, learning, stress response, alertness, memory, and attention. Researchers have identified cholinergic neuron damage as a significant pathogenic modification that correlates with AD's cognitive decline (**Francis et al., 1999; Terry et al., 2003**).

1.1.3.2. Amyloid hypothesis

The amyloid hypothesis is currently the most frequently recognized and researched theory in existence, despite the fact that the precise aetiology of AD is still up for debate (**Mohandas et al., 2009**). Among the most important features of AD pathophysiology is unquestionably the existence of amyloid plaques. This hypothesis states that APP's proteolytic cleavage forms amyloid plaques, which are essential to AD pathogenesis. Research indicates that the majority of the material in amyloid plaques in AD is polypeptides (about 4 kDa), typically synthesised in soluble form. Studies have shown that the A β protein has several isoforms, the majority of which are between amino acids 39 and 43. 56 amino acids make up the ectodomain of the two APP isoforms, APP751 and APP770 (**Hardy and Selkoe, 2002; Skovronsky et al., 2006**).

In addition, research has shown that the two most prevalent isoforms are A β 42 and A β 40 (**Golde et al., 2000**). It has been discovered that the abnormal processing of APP leads to the formation of imbalanced insoluble A β isoforms. Cluster formation forms amyloid protein aggregates, including oligomers and protofibrils. It has been proposed in earlier research that this is caused by the conversion of A β monomers to A β oligomers prior to accumulation (**Kayed et al., 2003**). Over time, the oligomers cause harm to neurons. Hence, in the early stages of Alzheimer's disease, substantial amounts of insoluble and probably A β 42 oligomers cause synaptic damage (**Sanchez-Varo et al., 2012**).

1.1.3.3. Tau hypothesis

The tau hypothesis states that when tau protein is overly phosphorylated, it changes from normal tau to PHF (paired helical filament) and NFTs (**Mohandas et al., 2009; Swerdlow et al., 2004**). At one point, research on AD concentrated on A β . Researchers have only just started to pay attention to tau proteins since several investigations have

demonstrated that tau proteins are among the important components of NFTs. Hyperphosphorylation is one of the post-translational modifications that tau undergoes; this process significantly affects the integrity of microtubules and contributes to tau protein buildup in Alzheimer's disease (**Duan et al., 2017**). According to previous research, the process of hyperphosphorylation involves changes in tau protein structure. The conversion of tau monomer to tau oligomer follows, resulting in the formation of paired helical filaments and NFTs (**Patterson et al., 2011; Lasagna-Reeves et al., 2010**).

1.1.4. Risk factors of Alzheimer's disease

Alzheimer's disease mostly affects those individuals who are typically aged 65 and above, known as late-onset Alzheimer's disease. It's believed by experts that Alzheimer's, similar to many other prevalent chronic illnesses, arises due to a combination of factors rather than a solitary cause. There are some exceptions, such as instances of Alzheimer's linked to trisomy 21 in Down syndrome and rare occurrences of the disease associated with particular genetic mutations (**Alzheimer's association, 2024**).

Age- The primary risk factors associated with Alzheimer's disease revolve around advancing age. The prevalence of Alzheimer's disease significantly rises as individuals grow older. Alzheimer's dementia specifically affects 5% of those aged 65 to 74, 13.2% of those aged 75 to 84, and 33.4% of those aged 85 or above (**Hebert et al., 2013**). However, it's crucial to understand that Alzheimer's disease is not a typical aspect of aging, and simply being older does not cause this condition (**Nelson et al., 2011**).

Genetics- Researchers have identified numerous genes that either raise or lower the risk of Alzheimer's disease. In 2022, they discovered 31 new genes that seem to influence biological processes associated with Alzheimer's disease (**Bellenguez et al., 2022**). Among the many genes that elevate the risk, APOE-e4 has the most significant impact on the likelihood of developing late-onset Alzheimer's disease. APOE encodes a protein responsible for transporting cholesterol in the blood. Every individual inherits one of the three APOE gene variants (e2, e3, or e4) from each parent, leading to six possible APOE pairings (e2/e2, e2/e3, e2/e4, e3/e3, e3/e4, and e4/e4). Carrying the e4

allele of the APOE gene heightens the risk of developing Alzheimer's disease compared to the e3 or e2 alleles, although it does not make the disease inevitable. In contrast, the e2 allele may lower the risk when compared to the e3 or e4 alleles. Persons with the e2 allele who develop Alzheimer's typically do so later in life than those lacking this allele. Experts believe that the e3 allele has no significant impact on the risk of Alzheimer's disease. Typically, the probability of developing Alzheimer's disease rises with inheriting a single copy of the e4 variant, and this risk escalates even more with inheriting two copies of the e4 variant, as opposed to inheriting only copies of the e2 or e3 variants (Nelson et al., 2011; Bellenguez et al., 2022; Loy et al., 2014).

According to estimates, mutations in any of three particular genes—the amyloid precursor protein, presenilin 1, and presenilin 2—cause Alzheimer's dementia in 1% or less of cases (Bekris et al., 2010). In this case, symptoms typically appear before age 65 and can sometimes emerge as early as age 30. Therefore, persons with these mutations may be described as having early-onset Alzheimer's disease. People who inherit a mutation in one of these specific genes are nearly certain to develop Alzheimer's if they live to a typical age (Goldman et al., 2011). Nonetheless, there have been rare instances where individuals with one of these mutations do not exhibit symptoms until much later in life (Lopera et al., 2023; Arboleda-Velasquez et al., 2019).

Family history- A family history of Alzheimer's disease is not required for someone to acquire the disease. However, persons with whose first-degree relative (a parent or sibling) who has or had Alzheimer's disease are at a higher risk of developing it compared to those without a first-degree relative with the disease (Green et al., 2002; Loy et al., 2014). The risk increases further for those with more than one first-degree relative affected by Alzheimer's disease (Lautenschlager et al., 1996).

Age, genetics, and family history are unchangeable risk factors, but we can alter certain other risk factors to decrease the likelihood of dementia. Modifiable risk factors include education, diet, physical activity, social and mental engagement, blood pressure, and smoking. The Lancet Commission report suggests that these modifiable risk factors could link to 40% of dementia cases (Livingston et al., 2020). In 2022, a

study linked eight modifiable risk factors to almost 37% of dementia cases in the US, with midlife obesity being the most prevalent, followed by a lack of physical activity and lower educational qualifications (Nianogo et al., 2022).

1.1.5. Treatment of Alzheimer's disease

Currently, Alzheimer's disease has no known treatment and no known means of prevention. Research centres worldwide are focusing on finding ways to cure or prevent dementia, given that over 55 million people worldwide suffer from Alzheimer's and other dementias, which have a terrible impact on people's lives (Alzheimer's association, 2024; WHO, 2023).

There are now eight medications on the market that can treat Alzheimer's disease (Alzheimer's association, 2024). Lecanemab and aducanumab alter the fundamental biology of AD and slow its progression. Their involvement in removing plaques and protofibrils, a kind of beta-amyloid that contributes to plaque formation, is crucial in this regard. The drug company of aducanumab has formally withdrawn the drug earlier this year (Bioten, 2024). Lecanemab is not a panacea for Alzheimer's disease and may not be suitable for every person with the illness. People with mild dementia or moderate cognitive impairment (MCI) as a result of Alzheimer's disease are the only ones for whom safety and efficacy have been shown (van Dyck et al., 2023). There are potential negative effects associated with anti-amyloid medications like lecanemab and aducanumab. Serious allergic reactions, infusion responses, headaches, falls, and ARIA (amyloid-related imaging abnormalities) are all possible side effects.

The cognitive symptoms may be alleviated by five of the eight medications: galantamine, rivastigmine, donepezil, memantine, and a combination of donepezil and memantine. Neither do they alter the fundamental brain alterations that lead to AD, nor do they mitigate or halt the progression of the illness. Increasing the number of neurotransmitters in the neurons is how they, except for memantine, cure the symptoms. Memantine prevents the overstimulation and potential harm to neurons caused by high amounts of the glutamate neurotransmitter. Nausea and headaches are among the possible adverse effects of these five medications. These aren't the only potential negative consequences (Alzheimer's association, 2024).

Brexpiprazole is one of the eight medications that have been authorised by the Food and Drug Administration (FDA) to treat agitation that may arise in Alzheimer's patients. Sixty percent of mild cognitive impairment patients and seventy-six percent of AD patients report agitation as a symptom of their condition (**Van der Mussele et al., 2015**). It is believed that brexpiprazole reduces agitation by acting on the brain's dopamine and serotonin protein receptors. These drugs have a reputation for increasing the risk of stroke and mortality in older patients suffering from dementia-related psychosis (**Ralph and Espinet, 2018; Maust et al., 2015**).

Apart from these eight medications, clinical studies have shown the effectiveness of suvorexant in treating sleep disorders, namely insomnia, which may affect individuals with mild to severe AD. Suvorexant inhibits orexin, a type of neurotransmitter involved in the sleep-wake cycle. Potential negative effects may include, but are not limited to, a decrease in mental clarity and impaired motor synchronization (including driving), an intensification of depression or thoughts of suicide, abnormalities in sleep patterns, paralysis during sleep, and altered breathing patterns (**Alzheimer's association, 2024**).

1.1.6. *Parkia timoriana* (Tree bean)

Parkia timoriana (DC.) Merr., also commonly known as tree bean, is a versatile tree belonging to the Leguminosae family and the Mimosoideae sub-family. This species is the most prevalent *Parkia* in the Indo-Pacific region, ranging from northeast India to Irian Jaya. It is a medium-height tree, reaching 10–12 meters, with numerous branches, and holds significant commercial and ecological value in the region (**Singha et al., 2021**). The indigenous people of northeast India use the pods and seeds of this tree as vegetables, chutneys, and salads at various stages of development or dry them in the sun for use during the off-season. It is a superior source of carbohydrates, proteins, minerals, and vitamins when compared to other legumes (**Saha et al., 2007; Seal, 2011**). The tree is well-suited to diverse agro-climatic regions, thriving in both cold hilly areas and hot plains. It typically grows wild in forests, Jhum fields, and backyards across northeast India without requiring special care. This tree is valued for its high medicinal and nutritional properties (**Thangjam, 2014**).

Tree bean can serve as an excellent source of a variety of nutrients and supplements. The seeds of *P. timoriana* are abundant in protein- globulins and albumins; minerals- phosphorus, manganese, magnesium, zinc, potassium, and iron; essential amino acids – tyrosine, phenylalanine, leucine, and isoleucine; and fatty acids- linoleic and oleic acids. The essential amino acid composition found in the kernel of *P. timoriana* is similar to the essential amino acid requirement pattern outlined by FAO/WHO/UNU (1985) for preschool children (Longvah and Deosthale, 1998; Angami et al., 2018).

Tree bean has demonstrated a wide range of medicinal properties, including antioxidant, antiviral, antidiabetic, insecticidal effects, antibacterial, immune-boosting, and antiproliferative. Additionally, it has been used in the treatment of colon cancer, skin and liver diseases, ulcers, eyes, hypertension, and leprosy. In addition to containing antioxidants that help prevent various diseases, tree bean can also enhance children's learning abilities (Sheikh et al., 2016; Tapan, 2011; Angami et al., 2018).

1.2. OBJECTIVES

- GC-MS and LC-MS analysis of phytochemicals of *P. timoriana* and evaluation of phytochemicals toxicity using in silico tools.
- Molecular docking and molecular dynamics simulation of phytochemicals from *P. timoriana* to BACE1 and cholinesterase protein receptor: an in silico therapeutic intervention study on Alzheimer's disease.
- Biological evaluation of *P. timoriana* in ameliorating learning and memory processes in an aluminum chloride induced Alzheimer's disease rat model.

CHAPTER-2

2.1. INTRODUCTION

2.1.1. Computational toxicology

Since time immemorial, plants have been widely recognised as a source of medicine for various human diseases (**Siddiqui et al., 2020**). Despite the discovery of numerous plant-derived drugs, the exploration of new bioactive compounds remains necessary to expand the range and find less toxic, more effective medications (**Noumi et al., 2020; Reddy et al., 2020**).

Herbal medications have recently garnered significant interest due to their safety and cost-effectiveness. Bioactive compounds, which are secondary metabolites of plants, can produce pharmacological and toxicological effects in living organisms (**López-Vallejo et al., 2011**). Additionally, the pharmaceutical industry utilises medicinal plants in drug manufacturing. However, safety and efficacy are the two primary issues that hinder the use of plants before commercialization (**van Wyk and Prinsloo, 2020**). Preclinical toxicity and adverse drug reactions account for approximately one-third of product failures (**Van Norman, 2020**). Screening each phytocompound for toxicity through *in vitro* and *in vivo* techniques is challenging. However, computational techniques are crucial for studying the toxicity and properties of both chemical and natural compounds, as they facilitate early drug development by enabling the early detection of substances lacking experimental data. These methodologies also provide a substitute for toxicity studies conducted on animal models (**Pognan et al., 2023**).

In silico prediction approaches use the physiochemical features of a substance to estimate its activity in a given biological system. QSAR (quantitative structure activity relationship) and SAR (structure activity relationship) are mathematical models that predict the relative structures' activities in a compound (**Kar and Leszczynski, 2019**). Various agencies, including those in the health care, agrochemical, food, and educational sectors, predominantly employ QSAR and SAR methods to assess the toxicity of a significant naturally occurring compound with clear annotation. QSAR and SAR programmes are considered to be efficient, significant, and enhanced prediction tools for studying biological systems. They have the potential to provide

valuable approaches for furthering our comprehension of the potentially detrimental effects of phytochemicals (Sripriya et al., 2021; Marak et al., 2023).

2.1.2. GC-MS and LC-MS analyses

Quantitative plant metabolomics is a technique that enhances our understanding of plant metabolism and biochemistry by providing precise measurements of known metabolite concentrations in plant samples. These measurements are then subjected to bioinformatics and statistical analysis (Fiehn et al., 2000). The primary analytical tools used in quantitative plant metabolomics investigations are MS (mass spectrometry) and NMR (nuclear magnetic resonance). Due to its superior sensitivity compared to NMR, MS is the preferred technology in most metabolomics research on plants. When combined with advanced chromatographic methods such as LC-MS, GC-MS, and CE-MS, it enables the separation and characterization of the vast array of compounds found in plants (Fernie et al., 2007; Jorge et al., 2016). These methods rely on a chromatograph to isolate the metabolites based on their distinct chromatographic characteristics (Theodoridis et al., 2011). This enables an expansion in the quantity of metabolites that may be analysed using an MS instrument while maintaining sensitivity. Metabolites' physicochemical characteristics and the nature of the stationary phase interact with the chromatograph to establish the elution order in the system. Typically, the examination of volatile organic chemicals, lipids, and molecules that may be modified is conducted with GC-MS analysis. Conversely, LC-MS is the method of choice for analysing most semi-polar metabolites. Consequently, the two methods are distinct in the kinds and quantities of metabolites that they can detect (Zhang et al., 2012).

The NMR approach is used more often as a specific tool for determining the structure in metabolomics investigations of plants (Kim et al., 2011). The primary drawback of the NMR apparatus is the restricted number of specified metabolites that can be detected in complicated biological samples, often ranging between 20 and 50. The GC-MS analysis may detect 100 metabolites, but in the case of the LC-MS analysis, the number of metabolites can reach up to 500 metabolites. Despite CE-MS having a better

separation efficiency than GC-MS and LC-MS, it is not often used in metabolomics research due to its limited reproducibility (**Williams et al., 2013**).

2.1.3. Polyphenols

Polyphenols are a significant category of bioactive plant compounds, encompassing various subgroups like flavonoids, phenolic acids, stilbenes, and lignans (**Manach et al., 2005**). In recent years, interest in dietary polyphenols has surged due to numerous epidemiological studies suggesting that diets abundant in plant-derived phytochemicals, especially polyphenols, confer significant health benefits to humans (**Pandey and Rizvi, 2009**). Among polyphenols, flavonoids are one of the most extensively researched groups. They are structured based on a 15-carbon skeleton consisting of a chromane ring connected to another aromatic ring. Flavonoids can be further classified into various subgroups, such as flavan-3-ols, flavanones, flavones, flavonols, isoflavones, and anthocyanins (**Corcoran et al., 2012; Butiuk et al., 2016**).

Polyphenols were initially believed to exert their primary effects through direct antioxidant activity. However, this isn't thought to be as important in real life because these compounds don't usually reach high enough levels in most tissues to have a big effect on free radical scavenging (**Forman et al., 2014; Fraga and Oteiza, 2011**). However, researchers have identified numerous other potential biochemical and molecular mechanisms. These include effects on various signalling pathways, such as regulating fat metabolism and nuclear transcription, and controlling the synthesis of inflammatory cytokines like interleukin-6, interleukin-1 β , and tumour necrosis factor α (**Kim et al., 2014; Fraga et al., 2018**).

Polyphenols can influence the assembly, structure, and function of the cell's protein. This can occur at three distinct levels: (i) by enhancing the transcription of protein encoded genes at the genomic level; (ii) by regulating protein translation, post-translational alterations, and their correct folding and assembly at the expression level; and (iii) by enhancing the activity of enzymatic reactions at the functional level (**Hajieva, 2017**).

The therapeutic effects of dietary polyphenols may also be attributed, at least partially, to a reciprocal interaction with the gut microbiome. Polyphenols have the ability to

influence the makeup of the gut microbiome, which is known to have positive effects on health. Additionally, the gut microbiome is able to break down polyphenols into bioactive molecules that have therapeutic advantages (Fraga et al., 2019).

2.1.4. Median lethal dose (LD₅₀), Median lethal concentration (LC₅₀), and IGC₅₀

J. W. Trevan developed the median lethal dose (LD₅₀) test in 1927 to determine the dosage of a chemical that causes 50% mortality in a certain animal species. Before proceeding with further toxicity testing, it often serves as the initial test for any chemical. It is used to assess the possible risks of substances to human health. Although death is the ultimate outcome, certain chemicals may exhibit non-lethal acute effects as indicators of toxicity (Erhirhie et al., 2018). Evaluating the acute toxicity of chemicals is necessary to determine the negative consequences that may arise from accidental or intentional contact. Long-term toxicity investigations and other animal-based research use the results of acute toxicity tests to determine doses (Clemmedson et al., 2000; Erhirhie et al., 2018).

An acute toxicity test can determine the toxicity of the test chemical. Compounds that have an LD₅₀ below 5 mg/kg are classified as very dangerous, while compounds with an LD₅₀ exceeding 15,000 mg/kg are considered generally safe (Loomis and Hayes, 1996).

Median lethal concentration (LC₅₀) is the concentration of a substance in water or air that is expected to cause the death of 50% of the test animals. LC₅₀ is a quantitative measure of the amount of a harmful substance in the environment that is required to cause death in 50% of the individuals being tested. The LD₅₀ number might vary based on the method of exposure (Michael et al., 2014).

The concentration of a chemical that, during a certain time frame, inhibits the growth of 50% of the test population (*Tetrahymena pyriformis*) predicted using the acute aquatic toxicity model is the IGC₅₀ (Piršelová et al., 1996).

2.1.5. Bioconcentration factor

The bioconcentration factor (BCF) measures the ability of environmental contaminants to accumulate via exposure to water (Wassenaar et al., 2020). Adequate

bioconcentration factor data is crucial for assessing the toxicological risk of environmental contaminants (**Arnot and Gobas, 2006**). The evaluation and understanding of the toxicity and mode of action of compounds are important. Field and laboratory tests are often carried out to gather BCF data on environmental contaminants (**Palladini et al., 2022**). Nevertheless, the data obtained from field research is unavoidably influenced by many biological and environmental variables, while the laboratory method is costly, time-consuming, and subject to growing ethical scrutiny. In addition, the experimental methods are insufficiently proactive in addressing the growing issue of swiftly addressing new emerging toxins. Hence, the use of computational methods is anticipated to be the preferred choice for addressing the lack of BCF and toxicological information regarding both existing and newly identified pollutants (**Pavan et al., 2008; Raies and Bajic, 2016**).

2.1.6. Mutagenicity

Currently, our immediate environment is marked by a multitude of natural and artificial substances that are foreign to our bodies, known as xenobiotics. Exposure of humans to environmental toxins by ingesting, inhalation, or dermal contact may lead to significant health repercussions. The manner in which a certain xenobiotic affects the body, especially DNA, is determined by the absorbed dosage and the biochemical features of the xenobiotic, including persistence, toxicity, and latency (**Baker, 2016**).

In the realm of current drug discovery, the mutagenicity of a compound is an important characteristic that might limit the development of a specific chemical at all phases of drug development owing to its strong association with carcinogenicity (**Custer and Sweder, 2008; Kramer et al., 2007**). Several studies have shown significant interest in using *in silico* prediction of compound mutagenicity to aid in the early discovery of possible mutagenic compounds. This approach aims to minimise the time and cost involved in hit to lead optimisation (**Xu et al., 2012; Kazius et al., 2005**).

The Ames test, developed by Bruce Ames in the early 1970s, is an extensively used assay for assessing the mutagenic properties of a chemical (**Ames et al., 1973; Ames et al., 1972**). The Ames test is a bacterial revertant mutation assay that simulates human metabolism. It is designed to detect compounds that have the potential to cause

genetic damage and frameshift mutations in the environment. The test is known for its high sensitivity to such substances (**Mortelmans and Zeiger, 2000**).

2.1.7. Carcinogenicity

The investigation into the processes of substance carcinogenesis and the assessment of the safety of both existing and novel chemicals are becoming more important and necessary in order to safeguard human health. Carcinogens are classified into two groups based on their mode of action: (a) genotoxic carcinogens, which damage DNA and are often the first step in cancer development; and (b) non-genotoxic carcinogens, which indirectly cause DNA damage and are generally negative in the standard testing assays (**Woo and Lai, 2003**).

Assessing the genotoxicity of a pharmaceutical medicine is an essential need throughout its development process. The Ames test, a technique for assessing inherited mutagenic events in bacterial DNA, is very prevalent for determining mutagenic activity and remains the most precise *in vitro* assay for predicting carcinogenicity in rats (**Kirkland et al., 2005**).

There is a collection of computational models that may be used to predict genotoxicity. These models are mostly built using data from *in vitro* tests that have been gathered over time. One kind of system, known as an expert system, uses human input (SAR) to build the model, while the other uses a computer algorithm to build the model, known as a QSAR (quantitative structure-activity relationship) (**Naven et al., 2010**).

2.1.8. Reproductive and developmental toxicology

The field of toxicology as a whole is beginning to acknowledge the significance of toxicity for reproduction and development. Evaluating the potential harm to development and reproduction is crucial for assessing the safety of novel pharmaceuticals and environmental substances. A considerable proportion of therapeutic candidates in the field of drug development have been unsuccessful in preclinical trials owing to their detrimental impact on embryonic development and reproductive capacity (**Boverhof and Zacharewski, 2006; Lhe et al., 2005**).

2.1.9. Biological activity prediction

Natural ingredients are extensively employed, particularly in China, India, and Russia, as medicines (Kong et al., 2009; Vaidya and Devasagayam, 2007). Naturally occurring substances are uniquely suited for their interactions with biological systems since they were generated by Mother Nature herself. Consequently, they are regarded as useful resources for the exploration of new drugs (Ertl et al., 2008). From 1981 to 2006, more than 70% of the NCEs (new chemical entities) that were brought in as drugs were derived from natural materials (Newman and Cragg, 2007). The intricate and varied structures of natural chemicals provide the foundation for altering many biological targets (Morphy and Rankovic, 2009). The simultaneous targeting of several activities by natural substances may result in either antagonistic or synergistic effects. Computer-aided approaches may prove to be very beneficial for the biological activity assessment of natural products since there are numerous recognised pharmacological targets and natural compounds may interact with many targets in a pleiotropic manner (Rollinger et al., 2006).

2.2. REVIEW OF LITERATURE

2.2.1. Computational toxicology

The study by Valerio et al. (2007) evaluated the effectiveness of a high-throughput QSAR prediction model in determining the cancer-causing potential of tiny, organic, naturally occurring compounds present in the human diet. This work showcases the effective use of QSAR predictive modelling to accurately anticipate the presence of natural carcinogens in the human diet. The accuracy of the predictions was confirmed by an external authentication test. The high-throughput method that utilises discriminant analysis is useful for evaluating the risk and determining the priority of food additives, untested natural products, and dietary constituents. This method is particularly effective when combined with experimental evidence of carcinogenic potential in rodents, structural-based alert classification, and other predictive toxicology approaches.

Sripriya et al. (2021) predicted the toxicity of three plant species using the QSAR prediction model. The study examined the methanolic extracts of *Carissa carandas*,

Epiphyllum oxypetalum, and *Canthium angustifolium* using GC-MS analysis. A total of 27 compounds were found, and their toxicity was assessed using the QSAR-TEST software. The toxicity ranking of the compounds, from highest to lowest, was as follows: *Daphnia magna* > *Tetrahymena pyriformis* > *Pimephales promelas* > Rat (oral). All chemicals exhibited non-bioaccumulative properties, with the majority demonstrating developmental toxicity. There was just one chemical that exhibited mutagenic properties. Chemicals are considered possible carcinogens if they show positive results in the Ames mutagenicity test (Griffiths et al., 2000).

Damayanti et al. (2015) used in silico toxicity prediction to predict the potential harmful effects of antioxidant food additives. Utilising programmes such as Toxtree, the OECD QSAR Toolbox, Admet Predictor, and TEST, it assessed the acute and chronic toxicity, carcinogenicity, ADI (acceptable daily intake), mutagenicity, and reproductive toxicity values of metabolites. Out of the forty-two antioxidant food additives that were evaluated, six were found to be carcinogens, two to be mutagens, eight to be hazardous to reproduction, and one to be both mutagen and reproductively toxic. The research used LD50 prediction to predict acute toxicity, with ethoxyquine exhibiting the lowest LD50 value (937.84 mg/kg) and dilauryl thiodipropionate demonstrating the highest (13367.79 mg/kg). The paired t-test approach was used to compare the prediction with the experimental data. The prediction of chronic toxicity was conducted by estimating the NOEL value, and the ADI value was then derived based on the NOEL value. The ADI values ranged from 0.38 mg/kg bw/day for carnosic acid to 1.35 mg/kg bw/day for calcium ascorbic acid and calcium disodium ethylene diamine tetraacetate. An early assessment of the safety of antioxidant food additives was given by the prediction techniques.

2.2.2. Biological activity prediction

Chuckles et al. (2022) studied the prediction of biological activity of compounds identified from *Cycas pectinata* Buch.-Ham using the PASS (Prediction of Activity Spectra for Substances) prediction tool. The analysis of *C. pectinata* phytochemicals using LC-MS, FTIR, and NMR revealed the existence of 32 significant phytochemicals with specific biological properties such as antioxidant, β -adrenergic

receptor kinase, anti-neoplastic, cholesterol antagonist, testosterone 17 β -dehydrogenase, and Cytochrome P450 enzyme digestion, as predicted by PASS analysis. The compounds showed a Pa (probable activity) value greater than a Pi (probable inactivity) value.

The study by Chy et al. (2019) conducted PASS prediction research to evaluate the biological activity of chemicals derived from *Piper sylvaticum* (Roxb.) leaves, namely as antibacterial, antiparasitic, and anthelmintic drugs. The PASS prediction examined six key compounds of *P. sylvaticum*, namely piperine, sylvone, piperlonguminine, sylvatine, sylvamide, and sylvatesmin. The results showed that all of these compounds had greater Pa values compared to Pi in terms of their antibacterial, antiparasitic, and anthelmintic properties. The discovery aligns with laboratory and animal research, which has shown that *P. sylvaticum* leaves have anthelmintic and antibacterial characteristics. Piperlonguminine and piperine are the most promising candidates for emerging as novel anthelmintic and antibacterial drugs, as shown by a prior study that attributed anthelmintic and antibacterial properties to these compounds (Naz et al., 2012).

Alam et al. (2021) evaluated the metabolites present in *Sterculia foetida* seeds using GC-MS analysis, and different experimental and computational analyses were performed to assess the antipyretic, anti-arthritic, thrombolytic, analgesic, and cytotoxic actions. The GC-MS analysis detected a total of 29 components, mostly including esters, terpenoids, phenols, and various other organic compounds. Seven specific compounds were examined to determine their antithrombotic, cytotoxic, anti-nociceptive, anti-inflammatory, antipyretic, and other biological actions. All of the potent activities had a greater active Pa value compared to the Pi value, as measured by the PASS online programme. Several other biological activities were also identified. The overall analyses revealed that using 1-azuleneethanol acetate in a comprehensive manner might be advantageous for the future advancement of therapeutic applications.

2.2.3. Phytochemical analysis

Fathalla et al. (2019) studied to identify and describe the active components present in the ethyl acetate fraction of *Senna tora* seeds, which are recognised for their biological

effects. The phenolic chemicals, mostly obtained from the ethyl acetate fraction, were verified by GC-MS and LC-MS analysis. The detected chemicals consist of 10-hydroxy-5-methoxy-2-methyl-1, Chrysarobin, Isotorachrysone, Parietin, Rubrofusarin, Cumbiasin B, Griseoxanthone-B, 4-anthracenedione, and Chrysophanol. GC-MS and LC-MS analyses are very sensitive techniques used to detect many components in plants. These approaches demonstrate that the ethyl acetate fraction includes the most potent ingredients. The presence of bioactive chemicals in seeds supports their use in folk and traditional medicine and verifies their ability to protect the liver (**Fathalla et al., 2015**).

Alencar Filho et al. (**2020**) studied the phytochemical analysis of *Alternanthera brasiliensis*, sometimes referred to as 'penicillin', used for its anti-inflammatory and wound curative properties. This work used LC-MS/MS and GC-MS analysis to detect the phytochemicals present in the species. A total of 27 chemicals were detected, with five identified using liquid chromatography-mass spectrometry (LC-MS), all of which were flavonoids. The other 22 compounds were identified using gas chromatography-mass spectrometry (GC-MS), and they included hydrocarbons, different types of terpenes, derivatives of vitamins, phytosterols, and carotenoids. Significantly, this work has identified 23 previously unreported chemicals for this species, therefore making a noteworthy addition to the understanding of its chemical composition.

Sen et al. (**2013**) estimated the total content of flavonoids, phenols, and anti-oxidant properties in *Meyna spinosa* leaves. The methanol extracts had the greatest polyphenolic concentration and demonstrated superior antioxidant activity compared to petroleum ether and ethyl acetate extracts. The methanol extract demonstrated significant reducing power and high antioxidant activity, successfully inhibiting LPO (lipid peroxidation) and hemolysis by oxidative stress, comparable to standard references. The findings demonstrated a clear and direct relationship between the polyphenolic content and the antioxidant activity, suggesting that the polyphenolic content is likely the primary factor contributing to the antioxidant properties of the plant. The current investigation has shown that the methanolic extract of *M. spinosa* has significant promise as a natural source of antioxidants.

Truong et al. (2019) assessed the effects of several solvents on the extraction efficiency, phytochemical composition, anti-inflammatory, and antioxidant properties of *Severinia buxifolia*. The study revealed that solvents have a substantial influence on the extraction yield, chemical constituents, and biological properties. The solvent methanol had the greatest efficacy, leading to the largest extraction yield and the highest concentrations of phenolic, flavonoid, terpenoid, and alkaloid compounds. The methanolic extract demonstrated significant anti-inflammatory and antioxidant properties, with antioxidant activity surpassing that of ascorbic acid by threefold and anti-inflammatory activity equivalent to that of aspirin. Thus, methanol is suggested as the ideal solvent for extracting abundant phytochemicals, anti-inflammatory, and antioxidant compounds.

2.3. MATERIALS AND METHODS

2.3.1. Collection, identification and extraction of *Parkia timoriana* seed pods

Seed pods of *Parkia timoriana* were obtained from Tanhril village in Aizawl, Mizoram. The species bearing the accession number 1016 was identified by the BSI (Botanical Survey of India), Eastern Regional Centre, Shillong. The seed pods were air-dried at normal room temperature and then crushed into a fine powder using an electric grinder (**Figure 1**). The powdered seed pod (100 g) was immersed in methanol (400 ml) at room temperature for at least 72 hours using a cold maceration process (**Kuete et al., 2006**). The mixture was occasionally shaken. The extract was filtered through Whatman filter paper No.1, then subjected to evaporation in an oven at a temperature of 40°C until all the liquid had evaporated. The resulting dry extract was then kept at a temperature of 4°C until used (**Sen et al., 2013**).

2.3.2. Total flavonoid content

The total flavonoid content was quantified using the method reported by Zhang et al. (2012), with minor adjustments. A volume of 2.5 mL of the extract was transferred into a 10 mL test tube, followed by the addition of 0.15 mL of a 5% NaNO₂ solution. The solution was well mixed and left undisturbed for 6 minutes at room temperature. Then, 0.15 mL of a 10% AlCl₃ solution was added to the test tube, thoroughly mixed, and left for another 6 minutes at room temperature. A volume of 2.2 millilitres of 1M

sodium hydroxide (NaOH) was added, well mixed, and left at room temperature for a duration of 12 minutes. A spectrophotometer was used to measure the absorbance at a wavelength of 510 nm. In order to generate a calibration curve, quercetin was used as the standard, with concentrations ranging from 0 to 400 µg/mL. The total flavonoid content (TFC) was quantified and reported as quercetin equivalents in mg QE/g (mg quercetin equivalent/g) of the dried extract.

2.3.3. Total phenol content

A solution was prepared by dissolving 0.2 g of extract in 10 mL of distilled water, using a ratio of 1:50 (w/v). This solution was then used to determine the total phenolic and flavonoid content. The Folin-Ciocalteu reagent technique (Sen et al., 2013) was used to quantify the total phenolic content in the extract of *P. timoriana* seed pod. 0.5 mL of the extract was added to a test tube containing 2.5 mL of Folin-Ciocalteu reagent (10% v/v) and 2.0 mL of Na₂CO₃ (2% w/v). The tubes were vigorously agitated. The solution was allowed to incubate for 60 minutes at ambient temperature. The spectrophotometer was used to measure the absorbance at a wavelength of 765 nm. To generate a calibration curve, gallic acid was used as the standard, with concentrations ranging from 0 to 450 µg/mL. The total phenolic content (TPC) was quantified as gallic acid equivalents in mg/g (mg GAE/g) of the dried extract.

2.3.4. Gas chromatography-mass spectrometry analysis

The PT seed pod extracts were analysed using the GC-MS-2010 (Shimadzu, Japan). The analysis was performed in EI mode at an electron ionisation energy of 70 eV. A Restek-5MS column with dimensions of 30 x 0.25 mm and a film thickness of 0.25 µm was used. The carrier gas used was pure helium gas with a purity of 99.99 percent, flowing at a constant rate of 1 mL/min. A high ionisation energy of 70 eV (electron volts), a scan period of 0.2 s, and fragments ranging from 40 to 650 m/z were chosen for the detection of the GC-MS spectrum using an electron ionisation energy technique. The injector temperature was maintained at a constant value of 260 °C, and a 2 µL injection volume was used with a split ratio of 10:1. The flow control mode exhibited linear behaviour at a pressure of 99.3 kPa. The flow rate is 1.21 mL/min in the column, with an overall flow rate of 16.3 mL/min. The initial temperature of the

column oven was set at 120 °C for a duration of two minutes. It was then increased by 10 °C each minute until it reached 280 °C. Finally, it was further raised to 300 °C and maintained at that temperature for 20 minutes. The chromatogram and mass spectra were analysed using the Xcalibur™ software integrated into the GC-MS/LC-MS equipment. The phytochemical contents of the test samples were determined by comparing their retention time (min), mass spectral patterns, peak height, and peak area with those compounds stored in the NIST library (National Institute of Standards and Technology), which contains over 62,000 patterns, and Dr. Duke's ethnobotanical phytochemical databases (Duke, 2000).

2.3.5. Liquid chromatography-mass spectrometry analysis

The Acquity UPLC H-Class (Acquity Ultra Performance Liquid Chromatography) equipment was used, consisting of an auto sampler and a binary pump (Waters, USA) equipped with a 10L loop. An investigation was conducted to separate phytochemicals using various chromatographic conditions, such as mobile phase composition, injection volume, flow rate, and gradient programmes. Various mobile phase combinations, such as methanol-water, acetonitrile-water, and acetonitrile-0.1% (v/v) formic acid aqueous solution, were tested in the gradient programme at a flow rate of 1.5 mL/min. The mobile phase consists of a 0.1% (v/v) aqueous solution of formic acid (A) and acetonitrile (B) at a flow rate of 1.5 mL/min. The ideal conditions for separation were determined to be a column pressure ranging from 0 to 300 bar and a column temperature of 30 °C. The compounds were separated at a temperature of 30 °C using an Acquity CSH C18 column with dimensions of 2.1 mm by 100 mm and a particle size of 1.7 μ m. Two solvents, namely 0.1% (v/v) formic acid in water (A) and methanol (B), were used to create a gradient elution at a flow rate of 1.5 ml/min.

The gradient programme started with an initial concentration of 5% (B) and remained constant for 1 minute. It then increased to 30% (B) from 6 to 12 minutes, 60% (B) from 12 to 16 minutes, and 80% (B) from 16 to 20 minutes. Finally, it returned to 5% (B) from 26 to 30 minutes. On the other hand, the concentration of component D started at 95% and remained constant for 1 minute. It then decreased to 70% from 6 to 12 minutes, 40% from 12 to 16 minutes, and 20% from 16 to 20 minutes. Finally, it

returned to 95% after 26 to 30 minutes. The sample injection volume was 10 μ L. The MS analysis was conducted on the Water UPLC-TQD Mass Spectrometer (XEVO TQD#QCA1232) using data-dependent automated switching between MS and MS/MS collection modes. The spectra were recorded using both positive and negative ionisation modes, with a mass acquisition range of 150–2000 m/z.

2.3.6. Toxicity prediction by QSAR-TEST

The toxicity of the phytochemicals found in *Parkia timoriana* seed pods was evaluated using QSAR-TEST (Version 5.1.2), a tool created by the US EPA (**Martin, 2020**). This programme uses many QSAR tactics, such as hierarchical, single-model, group contribution, nearest neighbour, and consensus mode of action approaches, to accurately assess the toxicity of a chemical for each specific endpoint (**Martin et al., 2008**). The TEST programme has models for predicting different toxicities: 96-hour fathead minnow and 48-hour *Daphnia magna* to test median lethal concentration (LC_{50}) (**Martin and Young, 2001; U.S.E.P.A., 2016**). *Tetrahymena pyriformis*, a single-celled organism, is to show a 50 percent growth inhibition concentration (IGC_{50}). Median lethal dose (LD_{50}) prediction using rats (**Zhu et al., 2009**). Also, bioconcentration factor (BCF), developmental toxicity (**Cassano et al., 2010**), and mutagenicity (Ames's test) (**Benfenati et al., 2009**).

The LC_{50} endpoint for fathead minnows (*Pimephales promelas*) is the concentration (mg/L) of a substance in water that results in the death of 50% of the exposed organisms after 96 h. The data set for the *D. magna* LC_{50} endpoint, which measures the amount of substance in water that causes the death of half of exposed *D. magna* after 48 hours, as well as the 96-hour fathead minnow LC_{50} , was retrieved from the ECOTOX aquatic toxicity database. The *D. magna* LC_{50} data set contained a total of 541 compounds. The model's endpoint was $-\log_{10} (LC_{50} \text{ mg/L})$. The *T. pyriformis* IGC_{50} endpoint refers to the concentration of a substance that inhibits 50% of the development of the protozoan ciliate after a duration of 40 hours. The IGC_{50} training set was obtained, and chemicals were included in the final *T. pyriformis* IGC_{50} dataset. The modelled endpoint was the negative logarithm of the IGC_{50} concentration in mg/L. The oral rat LD_{50} endpoint refers to the quantity of the chemical, measured in mg/kg

of rat body weight, that is fatal to 50% of the rats when ingested orally. The dataset for this endpoint was built by downloading data from the ChemIDplus database, resulting in the acquisition of 13548 items. The oral rat LD₅₀ data collection included a total of 7413 chemicals. The modelled endpoint was the LD₅₀ value expressed as -Log₁₀ (LD₅₀ mol/kg).

The criteria for mammalian and aquatic toxicity metrics, as established by ATSDR (the agency for toxic substances and disease registry), were associated with the predicted levels of toxicity for the chemical compounds. The toxicity metrics are classified into five categories: X (extreme toxicity), A (extremely high toxicity), B (high toxicity), C (moderate toxicity), and D (low toxicity). The BCF is a measure of the ratio between the concentration of a chemical in biota due to absorption via the respiratory surface and the concentration of the chemical in water in a stable state (Zhao et al., 2008). The data was compiled using many databases. Once the salts, mixtures, and ambiguous compounds have been removed by filtration, the resulting dataset consists of 676 chemicals. The modelled endpoint was the logarithm (base 10) of the bioconcentration factor (BCF). The EURAS BCF Gold Standard Database was used to forecast the bioaccumulation factor by applying QSAR-TEST. The developmental toxicity was anticipated based on the TERIS (Teratogen Information System), CAESAR project, and FDA rules. The mutagenicity of the substances was determined by analysing their response to the Ames test using a specific dataset.

2.3.7. Toxicity prediction by VEGA HUB, OECD QSAR and Toxtree

The toxicological properties, including repeated dose toxicity (HESS), oral toxicity, and Lipinski rule oasis, were predicted using the OECD QSAR toolbox (<https://qsartoolbox.org/download/>) (Suarez-Torres et al., 2020). The web programme VEGAHUB (www.vegahub.eu) was used to predict carcinogenicity, ADI, no observed adverse effect level (NOAEL), and developmental toxicity. The Toxtree platform, which is an open-source tool, was used to predict drug metabolism mediated by cytochrome P450.

2.3.8. Biological activity prediction

The PASS prediction online tool (<https://www.way2drug.com/passonline/>) was used to predict the different biological activities such as dementia treatment, cytochrome P450 stimulant, antioxidant, anti-inflammatory, neurotrophic factor enhancer, amyloid- β aggregation inhibitor, acetylcholine stimulant, and Alzheimer disease treatment. The PASS programme calculates the anticipated activity spectrum of a phytocompound, providing a prediction of likely activity (Pa) and probable inactivity (Pi). Pa and Pi have values that range from 0.000 to 1.000. Only the biological activities with a Pa value greater than the Pi value are considered for a specific phytocompound. $Pa \geq 0.7$ suggests a high probability of experimental pharmacological action, while values between 0.5 and 0.7 indicate a reduced probability. If the value of Pa is < 0.5 , it indicates a reduced probability of the activity being found via trials. However, it might also imply the possibility of detecting a completely new molecule (Goel et al., 2011).

2.4. RESULTS

2.4.1. Gas chromatography-mass spectrometry and liquid chromatography-mass spectrometry analysis

The GC-MS analysis identified nine phytocompounds from the methanolic extract of *Parkia timoriana* seed pod, namely, 3,7,11-Trimethyl-2,4-dodecadiene, 1,1,3,3,4-Pentamethyl-6-t-butyl-2,3-dihydroindene, Patchouli alcohol, 4-Isopropyl-3,4-dimethylcyclohexa-2,5-dienone, Bisabolene, 1H-Purin-6-amine,N-((3-fluorophenyl)methyl)-, 1-(4-Isopropylphenyl)-2-methylpropyl acetate, Tricyclo[4.3.0.0(7,9)]nonane,2,2,5,5,8,8-hexamethyl-, (1.alpha.,6.beta.,7.alpha.,9.alpha.)-, and 5-Ethyl-3-methyl-3,4-nonadien-6-yne (Table 1; Figure 2).

The LC-MS analysis revealed that the phytocompounds present in the methanolic extract of *Parkia timoriana* seed pod were mostly composed of flavonoids, alkaloids, and terpenoids. A total of fifty-two phytocompounds were detected in the LC-MS analysis in both positive (Figure 3) and negative (Figure 4) total ion modes. The identified phytocompounds using MS/MS parent ion fragmentation were twenty-nine from positive total ion mode and twenty-three from negative total ion mode. Sixteen

alkaloids were detected, including voacamine, guan-fu base Y, scopolamine, ergocristine, napelline, quinine, hydroxygardnutine, cycloheximide, isocorydine, speciosine, anabasamine, gardnerine, vincamine, rauwolscine, nantenine, and hirsutine. The methanolic extract of *Parkia timoriana* seed pod contained ten flavonoids, namely luteolin-8-C-glucoside, artocarpin, nicotiflorin, isoschaftoside, procyanidin B1, rotenone, isorhamnetin-3-o-rutinoside, silychrystin, apigenin, and apiin. Additionally, six terpenoids, namely azadirachtin, 4,4'-diaponeurosporene, ginkgolide C, paeoniflorin, loganin, and soyasapogenol B base, were also detected in the extract. In addition, the presence of several other phytochemicals such as demethoxycurcumin, maritimetin-6-O-glucoside (phenols); E-resveratrol trimethyl ether (polyphenols); ginsenoside F3, and alpha-hederin (saponins); linolenic acid, and 1-dodecanoyl-2-(11Z-eicosenoyl)-glycero-3-phospho-(1'-sn-glycerol) (fatty acids); taurodeoxycholate, lithocholenic acid, taurocholic acid (bile acids); phosphatidylcholine, phosphatidylethanolamine, 1,2-diarachidonoyl-sn-glycero-3-phosphoethanolamine (phospholipids); ouabain (cardiac glycoside); and 3-oxo-c8-homoserine lactone were also detected (Table 1).

2.4.2. Total flavonoid and phenol content

The methanolic extract of *P. timoriana* seed pods has a total phenol concentration of 421.64 ± 3.38 mg GAE/g of extract (gallic acid equivalent/gram). The plant's total flavonoid concentration was measured to be 280.893 ± 4.31 mg QE/g of extract (quercetin equivalent/gram). These measurements were determined using a standard curve with the equation $y = 0.0028x + 0.2331$ and a coefficient of determination (r^2) of 0.9756 for flavonoid, and $y = 0.0072x - 0.0035$ and r^2 for phenol.

2.4.3. Toxicity prediction using QSAR-TEST

2.4.3.1. LC₅₀ 96-hr (Fathead minnow)

Voacamine, isoschaftoside, speciosine, soyasapogenol B base + O-DDMP, O-HexA-HexA, artocarpin, apigenin glucoside arabinoside, nicotiflorin, 4,4'-diaponeurosporene, isorhamnetin-3-O-rutinoside, procyanidin B1, silychrystin, 1-dodecanoyl-2-(11Z-eicosenoyl)-glycero-3-phospho-(1'-sn-glycerol), ginsenoside F3, demethoxycurcumin, rotenone, and ergocristine all fall under the category of

extremely toxic (category X) because of their very low LC₅₀ values (0.0007-0.053 mg/L) against fathead minnow for 96 h. The following phytochemicals, namely, alpha-hederin, bisabolene, hirsutine, maritimetin-6-O-glucoside, E-resveratrol trimethyl ether, rauwolscline, 3,7,11-Trimethyl-2,4-dodecadiene, lithocholenic acid, gardnerine, linolenic acid, isocorydine, tricyclononane 2,2,5,5,8,8-hexamethyl (1.alpha., 6.beta.,7.alpha.,9.alpha.), azadirachtin, apiin, 1,1,3,3,4-pentamethyl-6-t-butyl-2,3-dihydroindene, nantenine, luteolin-8-C-glucoside, hydroxygardnutine, quinine, phosphatidylethanolamine (22:1/20:1), ouabain, napelline, and taurocholic acid have all been classified as category A due to their very high toxicity to fathead minnow. The LC₅₀ value for these compounds after 96 hours of exposure ranges from 0.16 to 4.61 mg/L. 1-(4-Isopropylphenyl)-2-methylpropyl acetate, Patchouli alcohol, Taurodeoxycholate, Guan-fu base Y, Anabasamine, Vincamine, Phosphatidylcholine(14:0/18:3n6), Taurochenodeoxycholate, and [3-hexadecoxy-2-[(9Z,11E)-13-hydroxy octadec a-9,11-dienoyl]oxypropyl] 2-(trimethylazanium yl) ethyl phosphate all fall under the category of high toxicity (category B). 4-Isopropyl-3,4-dimethylcyclohexa-2,5-dienone, 1H-Purin-6-amine,N-((3-fluorophenyl)methyl), Cycloheximide, and Phosphatidylethanolamine 18:0-22:6 were found to have moderate toxicity (category C). Only as few as three phytochemicals (3-oxo-C8-homoserine lactone, phosphatidylcholine 15:0/18:1(11Z), and loganin) were found to have low toxicity (category D) (Table 2).

2.4.3.2. LC₅₀ 48-hr (*Daphnia magna*)

Tricyclononane 2,2,5,5,8,8-hexamethyl(1.alpha.,6.beta.,7.alpha.,9.alpha.), 1-dodecanoyl-2-(11Z-eicosenoyl)-glycero-3-phospho-(1'-sn-glycerol)], Phosphatidyl ethanolamine (22:1/20:1), Phosphatidylethanolamine (18:0-22:6), 4,4'-diaponeurosporene1-(5Z,8Z,11Z,14Z, 17Z-eicosapentaenoyl)-2-(9 Z-nonadecenoyl)-glycero-3-phosphoserine, and 1,2-diarachidonoyl-sn-glycero-3-phosphoethanolamine showed extremely high toxicity (category X) on the basis of their LC₅₀ (0.0001-0.049 mg/L) against *D. magna* after 48 hr. Thirteen phytochemicals (3,7,11-trimethyl-2,4-dodecadiene, phosphatidylcholine (14:0/18:3n6), bisabolene, procyanidin B1, 1,1,3,3,4-Pentamethyl-6-t-butyl-2,3-dihydroindene, nantenine, voacamine, speciosine, artocarpin, silychrestin, rotenone, isocorydine, 3-hexadecoxy-2-

[(9Z,11E)-13-hydroxy octadeca-9,11-dienoyl]oxy propyl] 2-(trimethylazaniumyl) ethylphosphate, and phosphatidylcholine (15:0/18:1(11Z)) showed very high toxicity (category A), with their LC₅₀ ranging from 0.11-0.92 mg/L. On the other hand, the phytocompounds 4-isopropyl-3,4-dimethyl cyclohexa-2,5-dienone, patchouli alcohol, 1-(4-Isopropylphenyl)-2-methylpropyl acetate, 1H-purin-6-amine,N-((3-fluorophenyl)methyl), azadirachtin, taurodeoxycholate, quinine, E-resveratrol trimethyl ether, guan-fu base Y, ergocristine, vincamine, anabasamine, lithocholenic acid, rauwolscline, linolenic acid, hydroxygardnutine, hirsutine, gardnerine, taurocholic acid, and taurochenodeoxycholate were predicted to be highly toxic (category B) with LC50 value 1.12 – 6.76 mg/L against *D. magna* after 48 hr (**Table 2**).

2.4.3.3. IGC₅₀ 48hr (*Tetrahymena pyriformis*)

No phytocompounds of the methanolic extract of *Parkia timoriana* seed pod were predicted to have extreme toxicity (category X) against *T. pyriformis* for 48 h. Three compounds (bisabolene, 3,7,11-Trimethyl-2,4-dodecadiene, and linolenic acid) predicted very high toxicity (category A) against *T. pyriformis* (category A), having an IGC₅₀ value of 0.54, 0.33, and 0.43 mg/L, respectively. The majority of the phytocompounds, namely tricyclo[4.3.0.0(7,9)]nonane2,2,5,5,8,8-hexamethyl(1.alpha.,6.beta.,7.alpha.,9.alpha), 5-ethyl-3-methyl-3,4-nonadien-6-yne, 1,1,3,3,4-pentamethyl-6-t-butyl-2,3-dihydroindene, 4-isopropyl-3,4-dimethylcyclohexa-2,5-dienone 1-(4-Isopropylphenyl)-2-methylpropyl acetate, napelline, 1- dodecanoyl-2-(11Z-eicosenoyl)-glycero-3 phospho-(1'-sn-glycerol), ginsenoside F3, taurodeoxycholate, quinine, E-resveratrol trimethyl ether, demethoxycurcumin, ergocristine, artocarpin, guan-fu base Y, lithocholenic acid, rauwolscline, speciosine, rotenone, isocorydine, gardnerine, hydroxygardnutine, nantenine, ouabain, phophatidylethanolamine (22:1/20:1), 4,4'-diaponeurosporene, 1-(5Z,8Z,11Z,- 14Z,17Z-eicosapentaenoyl) -2-(9 Z-nonadecenoyl)- glycerol-3-phosphoserine, phophatidylethanolamine (18:0/22:6), 1,2- diarachidonoyl-sn-glycero-3-phosphoethanolamine, procyanidin B1, hirsutine, phosphatidylcholine (14:0/18:3n6), 3-hexadecoxy-2-[(9Z,11E)-13-hydroxy octadic a-9,11-dienoyl]oxy propyl] 2-(trimethylazaniumyl) ethyl phosphate, alpha-hederin, taurochenodeoxycholate, taurocholic acid, and soyasapogenol B base + O-DDMP, O-

HexA-HexA, had high toxicity (category B) with an estimated IGC₅₀ value between 2.37 and 9.64 mg/L (**Table 2**).

2.4.3.4. LD₅₀ oral (rat)

Phytocompounds from the methanolic extract of *P. timoriana* seed pod did not fall under the categories of either category X (extreme toxicity) or category A (severe toxicity) in the oral toxicity prediction in rats. Additionally, only two phytocompounds, including isocorydine and cycloheximide showed high toxicity (category B) in rats (oral), with predicted LD₅₀ values of 6.91 and 8.88 mg/kg, respectively. Among the 61 compounds identified from the methanolic extract of *P. timoriana* seed pod, 40 had LD₅₀ values greater than 500 mg/kg and were therefore classified as non-toxic to rats based on the toxicity scale (mammalian) of ATSDR, EPA. Napelline, quinine, voacamine, rotenone, rauwolscine, hirsutine, and gardnerine showed low toxicity (category D) with LD₅₀ values ranging between 180.63 mg/kg and 457.91 mg/kg. However, ginsenoside F3, ginkgolide C, azadirachtin, guan-fu base Y, ergocristine, anabasamine, ouabain, hydroxygardnutine, soyasapogenol B base + O-DDMP, O-HexA-HexA, and alpha-hederin fell under category C with moderate toxicity and LD₅₀ values ranging between 26.91 mg/kg and 61.21 mg/kg (**Table 2**).

2.4.3.5. Predicted toxicological hierarchy

Twenty phytocompounds from the methanolic extract of *Parkia timoriana* (napelline, ginsenoside F3, taurodeoxycholate, isoschaftoside, cycloheximide, demethoxycurcumin, apiin, lithocholenic acid, loganin, nantenine, apigenin glucoside arabinoside, nicotiflorin, luteolin-8-C-glucoside, ouabain, maritimetin-6-O-glucoside, hirsutine, isorhamnetin-3-O-rutinoside, alpha-hederin, taurochenodeoxycholate, and soyasapogenol B base + O-DDMP, O-HexA-HexA) had the same order of toxicity for different organisms as fathead minnow > *T. pyriformis* > *D. magna* > rat.

Nineteen phytocompounds from the methanolic extract of *Parkia timoriana* (3,7,11-trimethyl-2,4-dodecadiene, voacamine, 1-dodecanoyl-2- (11Z-eicosenoyl)-glycero-3 phospho-(1'-sn-glycerol), E-resveratrol trimethyl ether, azadirachtin, quinine, guan-fu base Y, ergocristine, artocarpin, vincamine, rotenone, rauwolscine, speciosine, silychrystin, linolenic acid, gardnerine, hydroxygardnutine, isocorydine, and

procyanidin B1) showed toxicity to mammalian and aquatic organisms in the given order: fathead minnow > *D. magna* > *T. pyriformis* > rat.

The toxicity order of *D. magna* > fathead minnow > *T. pyriformis* > rat was shown by fifteen phytocompounds from the methanolic extract of *Parkia timoriana*, including 4-isopropyl-3,4-dimethylcyclohexa-2,5-dienone, patchouli alcohol, 1-(4-isopropylphenyl)-2-methylpropyl acetate, 1H-purin-6-amine, N-((3-fluorophenyl)methyl), tricyclo[4.3.0.0(7,9)] nonane, 2,2,5,5, 8,8-hexa methyl-, (1.alpha.,6.beta.,7.alpha.,9.alpha.), 1,1,3,3,4-pentamethyl-6-t-butyl-2,3-dihydroindene, bisabolene, phosphatidylethanolamine (22:1/20:1), anabasamine, 4,4'-diaponeurosporene, phosphatidylethanolamine (18:0-22:6), 1-(5Z,8Z,11Z, 14Z,17Z-eicosapentaenoyl)-2-(9 Z-nonadecenoyl)- glycerol-3-phosphoserine, phosphatidylcholine (14:0/18:3n6), 1,2-diarachidonoyl-sn glycerol-3-phosphoethanolamine, and 3-hexadecyloxy-2-[(9Z,11E)-13-hydroxyoctadeca-9,11-dienoyl]oxy propyl]2-(trimethylazaniumyl) ethyl phosphate.

The toxicity order of two phytocompounds from the methanolic extract of *Parkia timoriana*, namely 3-oxo-C8-homoserine lactone, and taurocholic acid, showed the order *T. pyriformis* > fathead minnow > *D. magna* > rat.

2.4.3.6. Bioconcentration factor

The phytocompounds tricyclo[4.3.0.0(7,9)] nonane, 2,2,5,5,8,8-hexa-methyl-, (1.alpha.,6.beta.,7.alpha.,9.alpha.), and 1,1,3,3,4-pentamethyl-6-t-butyl-2,3-dihydroindene were predicted to have the highest bioconcentration factor, having a value of 16515.36, and 5726.79, respectively. This shows their high bioaccumulative character. No other phytocompounds from the methanolic extract of *Parkia timoriana* have a BCF value higher than 2000, therefore, it may be concluded that they do not have bioaccumulative characteristics (**Table 3**).

2.4.3.7. Developmental toxicity

A total of six compounds from PTME, including Isoschaftoside, apigenin glucoside arabinoside, apiin, ouabain, maritimetin-6-O-glucoside, and 3-oxo-C8-homoserine lactone, were predicted to be non-toxic in the development of an organism with a score

between 0.37 and 0.48. However, forty-six (out of sixty-one) showed toxicity to development, having a score between 0.53 and 1.38. Phytocompounds showing very high developmental toxicity were ergocristine (1.38), hydroxygardnutine (1.06), lithocholenic acid (1.00), and procyanidin B1 (1.00) (**Table 3**).

2.4.3.8. Mutagenicity

The phytocompounds from PTME, namely, 1H-purin-6-amine,N-((3-fluorophenyl)methyl), E-resveratrol trimethyl ether, taurodeoxycholate, gardnerine, anabasamine, luteolin-8-C-glucoside, nantenine, taurochenodeoxycholate, procyanidin B1, and taurocholic acid, are predicted to have a mutagenic score of above 0.5, therefore considered mutagens. Whereas, the other 51 phytocompounds of PTME were found to be non-mutagens, having scores below 0.5 (**Table 3**).

2.4.4. Toxicity prediction using VEGA HUB, Toxtree, and OECD QSAR tools

2.4.4.1. Oral toxicity (Cramer)

The Cramer classification approach is used to assess the toxicological profile of an orally taken chemical. Class I substances are considered to have low toxicity, Class II substances are considered to have intermediate toxicity, and Class III substances are considered to have high toxicity. Fourteen phytocompounds from PTME, namely, 3,7,11-trimethyl-2,4-dodecadiene, patchouli alcohol, 1-(4-Isopropylphenyl)-2-methylpropyl acetate, tricyclo[4.3.0.0(7,9)]nonane,2,2,5,5,8,8-hexamethyl,(1.alpha.,6.beta.,7.alpha.,9.alpha.), 1,1,3,3,4- penta methyl-6-t-butyl-2,3-dihydroindene, 1-methyl-4-(1,5-dimethyl-4hexenylidene)-1-cyclohexene, linolenic acid, 1-dodecanoyl-2-(11Z-eicosenoyl)-glycero-3-phospho-(1'-sn-glycerol), 4,4'-diaponeurosporene, phosphatidylethanolamine (22:1/20:1), phosphatidylethanolamine (18:0-22:6), 1,2-diarachidonoyl-sn-glycero-3-phosphoethanolamine, 1-(5Z,8Z,11Z,14Z,17Z-eicosapentaenoyl)-2-(9Z-nonadecenoyl)-glycero-3-phosphoserine, and phosphatidylcholine (14:0/18:3n6) showed low oral toxicity (category I) under Cramer's classification. 4-isopropyl-3,4-dimethylcyclohexa-2,5-dienone is the only phytocompound with intermediate toxicity (category II). The majority of the phytocompounds (i.e., forty-six) fall under high toxicity (category III) (**Table 4**).

2.4.4.2. Carcinogenicity

Most of the phytocompounds from PTME showed negative carcinogenicity, except ten, including 4-isopropyl-3,4-dimethylcyclohexa-2,5-dienone, scopolamine-N-butyl, 1H-purin-6-amine, N-((3-fluorophenyl)methyl), speciosine, azadirachtin, nantenine, isocorydine, isorhamnetin-3-O-rutinoside, hydroxygardnutine, and soyasapogenol B base + O-DDMP, O-HexA-HexA, which were predicted to be positive for carcinogenicity (Table 4).

2.4.4.3. Reproductive toxicity

Nineteen phytocompounds from PTME were predicted to be toxic reproductively. The phytocompounds include patchouli alcohol, scopolamine-N-butyl, 1,1,3,3,4-pentamethyl-6-t-butyl-2,3-dihydroindene, cycloheximide, 1-dodecanoyl -2-(11Z-eicosenoyl)-glycero-3-phospho-(1'-sn-glycerol), artocarpin, anabasamine, speciosine, rauwolscine, isocorydine, gardnerine, hydroxygardnutine, nantenine, phosphatidylethanolamine (22:1/20:1), phosphatidylethanolamine (18:0-22:6), 1,2-diarachidonoyl-sn-glycero-3-phosphoethanolamine, 1-(5Z,8Z,11Z,14Z,17Z-eicosapentaenoyl)-2-(9Znonadecenoyl)-glycero-3-phosphoserine, [3-hexadecoxy-2-[(9Z,11E)-13-hydroxyoctadeca-9,11-dienoyl]oxypropyl]2-(trimethylazaniumyl)ethyl phosphate, and phosphatidylcholine (14:0/18:3n6) (Table 4).

2.4.4.4. NOAEL

The NOAEL (no observable adverse effect level) is the dosage at which no effects are detected in repeated dose toxicity testing. This endpoint reflects the safety level of a chemical. The NOEL value is the level of exposure to a substance that does not cause any long-term toxicity. The phytocompounds (37.70 %) from PTME that had high NOAEL values suggest that these chemicals are safe and have not been associated with any adverse effects. However, the bulk of the phytocompounds (62.29 %) have low values for NOAEL. Among those phytocompounds, some of the lowest NOAEL include ergocristine (9.67 mg/kg), E-resveratrol trimethyl ether (9.67 mg/kg), phosphatidylethanolamine (22:1/20:1) (10.42 mg/kg), 5-ethyl-3-methyl-3,4-nonadien-6-yne (11.22 mg/kg), 1-methyl-4-(1,5-dimethyl-4-hexenyli dene)-1-cyclohexene

(10.65 mg/kg), and patchouli alcohol (15.86 mg/kg), suggesting their toxic effects in a repeated toxicity test (**Table 4**).

2.4.4.5. Repeated dose (HESS)

The majority of the phytochemicals (forty-eight out of sixty-one) were predicted to be harmless and did not cause any organ toxicity in a repeated toxicity test. Few of the phytochemicals, including 1,1,3,3,4-pentamethyl-6-*t*-butyl-2,3-dihydroindene, demethoxycurcumin, and quinine, showed both hepatotoxicity and nephrotoxicity in repeated toxicity tests. Cycloheximide is predicted to be hepatotoxic, while 5-ethyl-3-methyl-3,4-nonadien-6-yne, 3,7,11-trimethyl-2,4-dodecadiene, tricyclo[4.3.0.0(7,9)]nonane, 2,2,5,5,8,8-hexamethyl-(1.alpha.,6.beta.,7.alpha.,9.alpha.), E-resveratrol trimethyl ether, 1-methyl-4-(1,5-dimethyl-4-hexenyli dene)-1-cyclohexene, loganin, rauwolscine, and 4,4'-diaponeurosporene may show toxicity for kidney (**Table 4**).

2.4.4.6. Lipinski rule and cytochrome p450

Following the Lipinski rule, twenty-seven out of the sixty-one phytochemicals from PTME have been shown to be bioavailable. The phytochemicals include 1-(4-Isopropylphenyl)-2-methylpropyl acetate, patchouli alcohol, 4-isopropyl-3,4-dimethylcyclohexa-2,5-dienone, scopolamine-N-butyl, 1H-purin-6-amine, N-((3-fluorophenyl) methyl), taurodeoxycholate, napelline, E-resveratrol trimethyl ether, quinine, rauwolscine, ginkgolide C, guan-fu base Y, hydroxygardnutine, demethoxycurcumin, anabasamine, cycloheximide, rotenone, vincamine, gardnerine, speciosine, hirsutine, isocorydine, loganin, nantenine, 3-oxo-C8-homoserine lactone, and paeoniflorin (**Table 4**).

All the phytochemicals from PTME can be metabolised by the metabolic enzymes of cytochrome P450 into intermediates that may be more readily eliminated (**Table 4**).

2.4.5. PASS prediction for biological activities

Different phytochemicals from PTME exhibited different biological activities as per PASS (way2drug) prediction. Thirty-one phytochemicals had dementia treatment activity; seventeen phytochemicals can be metabolised by the cytochrome p450 enzyme complex; forty-one had anti-oxidant activity; forty-five showed anti-

inflammatory activity; twenty-three phytochemicals acted as neurotrophic factor enhancers; five can be used as an amyloid- β aggregation inhibitor; fifteen phytochemicals can stimulate the concentration of acetylcholine; and two phytochemicals can be used for treating Alzheimer's disease (**Table 5**). The phytochemicals exhibited a higher likelihood of activity (Pa) than inactivity (Pi) for all the activities predicted.

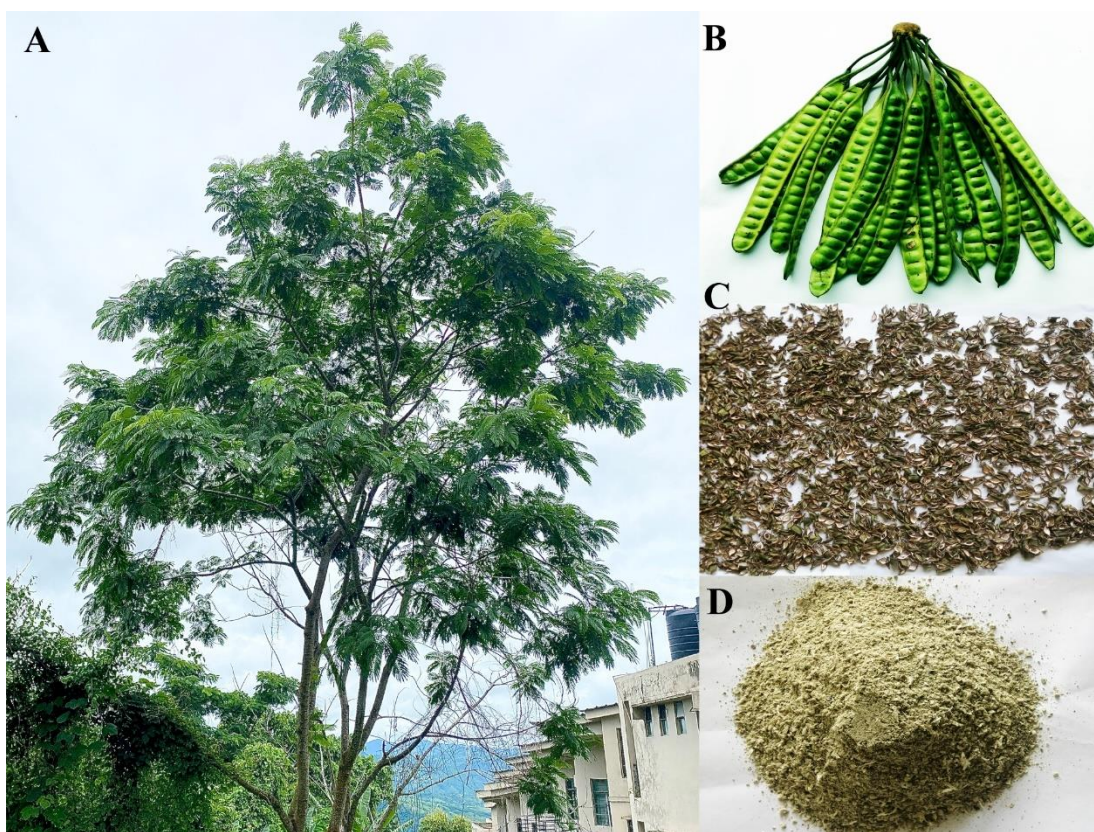


Figure 1. *Parkia timoriana* (wild bean) tree and its green, soft, and processed pods. (A) A tree of *P. timoriana* located in Tanhril forest of Aizawl, Mizoram, India. (B) *P. timoriana* seed pods eaten as a vegetable, salad, or chutney. (C) *P. timoriana* seed pods that have been cleaned, cut, and allowed to air dry. (D) *P. timoriana* seed pods that have been processed for the process of methanolic extraction.

Gas chromatography-mass spectrometry chromatogram of *Parkia timoriana* phytocompounds

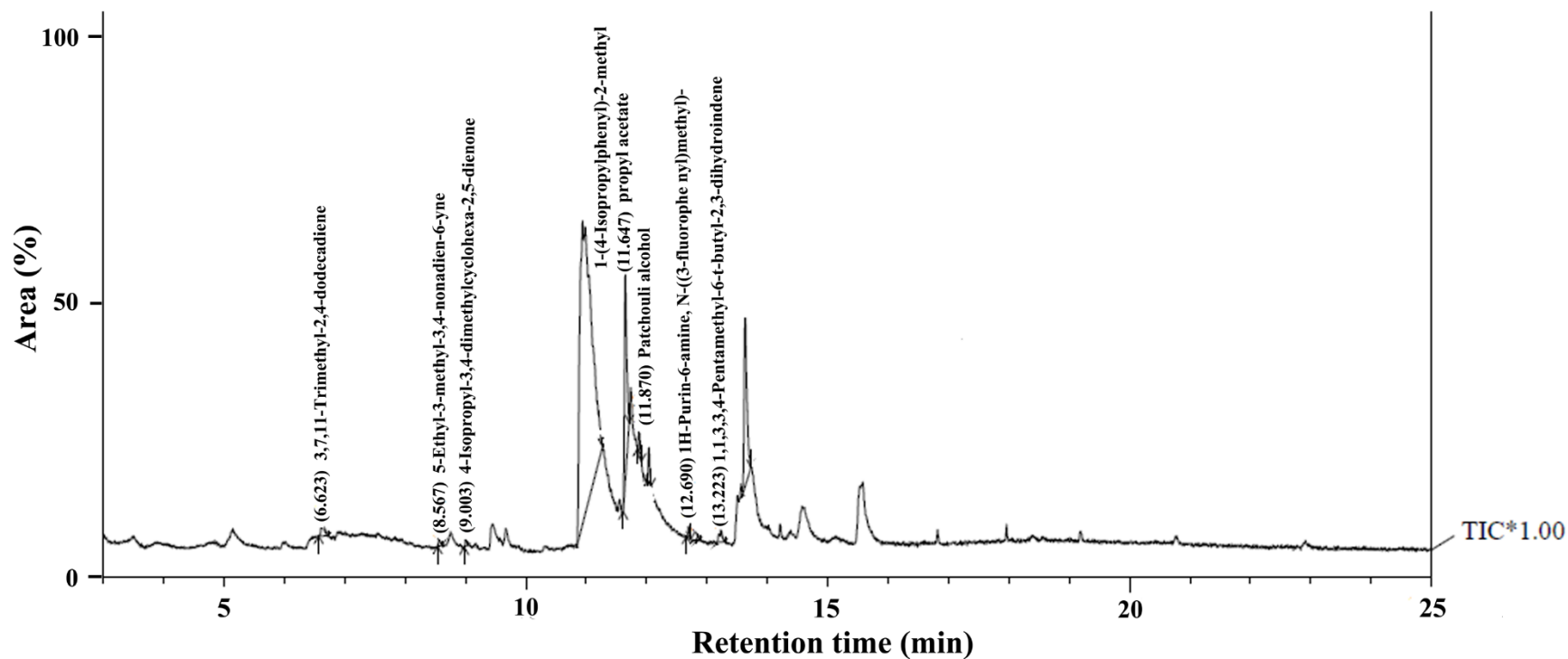


Figure 2. The chromatogram displays the results of the GC-MS (gas chromatography-mass spectrometry) examination of methanolic extract of *Parkia timoriana* seed pod.

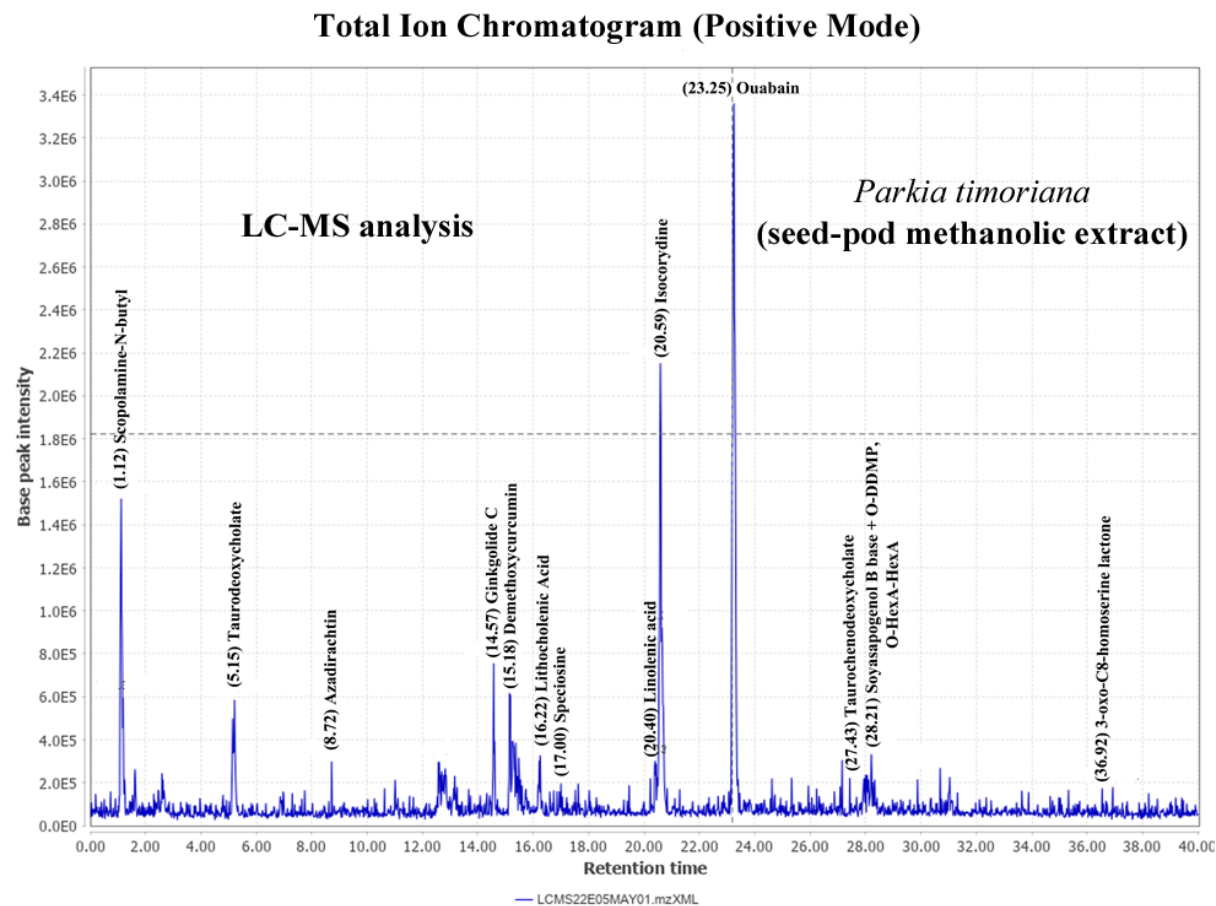


Figure 3. The chromatogram displays the results for the positive ion mode of LC-MS (liquid chromatography-mass spectrometry) analysis of the methanolic extract of *Parkia timoriana* seed pod.

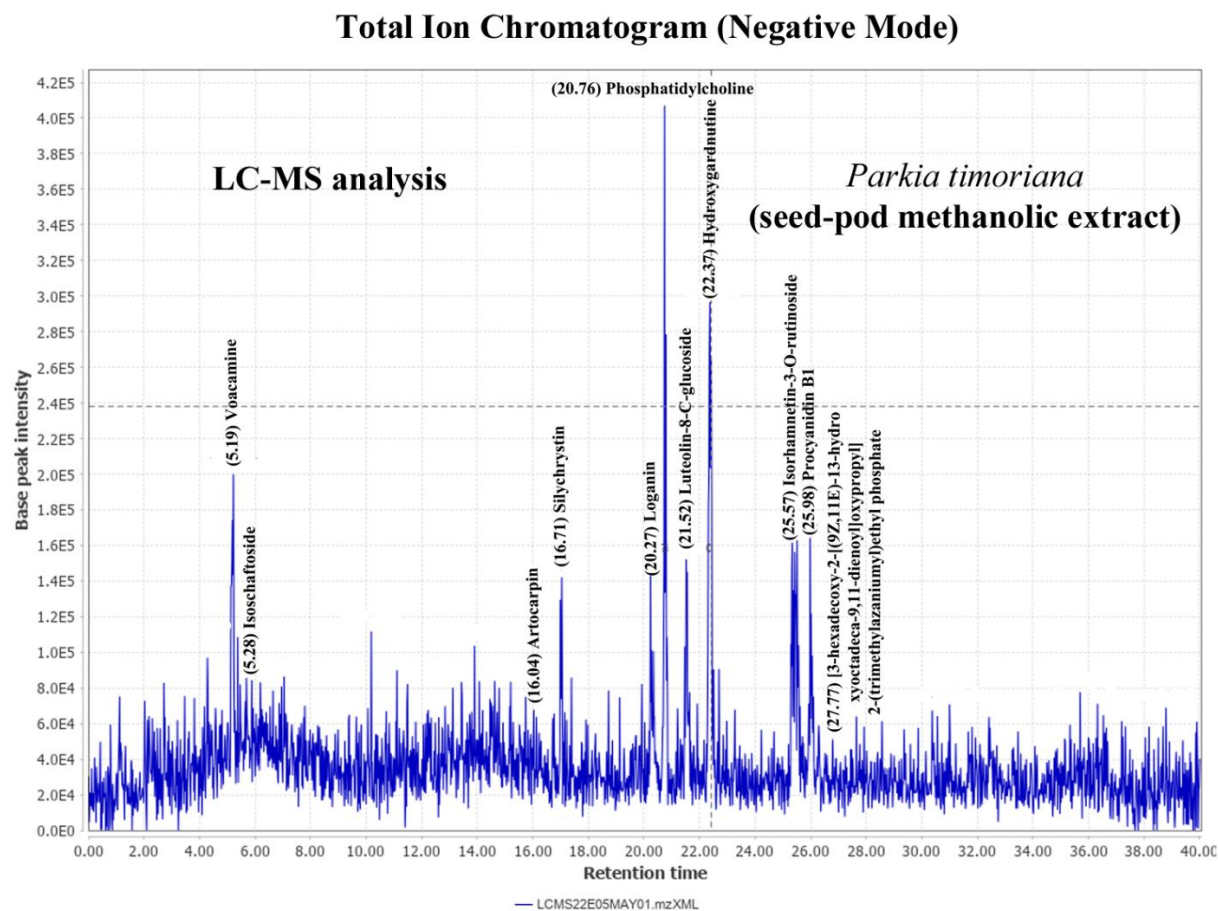


Figure 4. The chromatogram displays the results for the negative ion mode of LC-MS (liquid chromatography-mass spectrometry) analysis of the methanolic extract of *Parkia timoriana* seed pod.

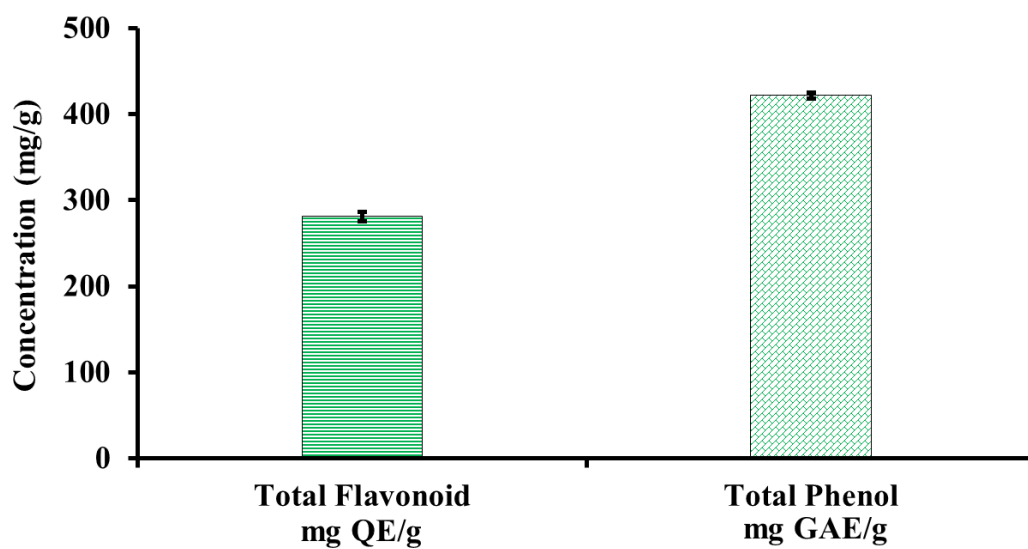


Figure 5. Total flavonoid (measured in mg QE/g extract) and total phenolic (measured in mg GAE/g extract) were found in high concentrations in the methanolic extract of *Parkia timoriana* seed pod.

Table 1. The phytochemicals present in the methanolic extract of *Parkia timoriana* seed pod were identified using GC-MS (gas chromatography-mass spectrometry) and LC-MS (liquid chromatography-mass spectrometry) studies.

Sl. no.	Compound	Formula	Retention time	Mass spectrum (m/z)	Molecular weight
GC-MS analysis					
1.	3,7,11-Trimethyl-2,4-dodecadiene	C ₁₅ H ₂₈	6.623	95.05	208.38
2.	5-Ethyl-3-methyl-3,4-nonadien-6-yne	C ₁₂ H ₁₈	8.567	133.20	162.27
3.	4-Isopropyl-3,4-dimethylcyclohexa-2,5-diene	C ₁₁ H ₁₆ O	9.003	122.10	164.24
4.	1-(4-Isopropylphenyl)-2-methylpropyl acetate	C ₁₅ H ₂₂ O ₂	11.647	191.15	234.33
5.	Patchouli alcohol	C ₁₅ H ₂₆ O	11.870	83.05	222.37
6.	Tricyclo[4.3.0.0(7,9)]nonane, 2,2,5,5,8,8-hexamethyl-, (1.alpha.,6.beta.,7.alpha.,9.alpha.)-	C ₁₅ H ₂₆	12.037	135.10	206.37
7.	1H-Purin-6-amine, N-((3-fluorophenyl)methyl)-	C ₁₂ H ₁₀ FN ₅	12.690	73.05	243.24
8.	Bisabolene	C ₁₅ H ₂₄	12.847	119.10	204.35
9.	1,1,3,3,4-Pentamethyl-6-tert-butyl-2,3-dihydro indene	C ₁₈ H ₂₈	13.223	229.15	244.42
LC-MS analysis					
10.	Scopolamine-N-butyl	C ₂₁ H ₃₀ NO ₄ ⁺	1.12	360.2690	360.5
11.	1-dodecanoyl-2-(11Z-eicosenoyl)-glycero-3-phospho-(1'-sn-glycerol)	C ₃₈ H ₇₃ O ₁₀ P	1.13	491.1929	721
12.	Napelline	C ₂₂ H ₃₃ NO ₃	1.19	360.3060	359.5
13.	Taurodeoxycholate	C ₂₆ H ₄₅ NO ₆ S	5.15	459.2112	499.7
14.	Voacamine	C ₄₃ H ₅₂ N ₄ O ₅	5.19	457.2131	704.9
15.	Ginsenoside F3	C ₄₁ H ₇₀ O ₁₃	5.22	459.2112	771.0
16.	Isoschaftoside	C ₂₆ H ₂₈ O ₁₄	5.28	457.1761	564.5
17.	Azadirachtin	C ₃₅ H ₄₄ O ₁₆	8.72	479.0069	720.7
18.	E-Resveratrol trimethyl ether	C ₁₇ H ₁₈ O ₃	11.01	225.1370	270.32
19.	Ginkgolide C	C ₂₀ H ₂₄ O ₁₁	14.57	325.3393	440.4
20.	Quinine	C ₂₀ H ₂₄ N ₂ O ₂	14.60	325.1912	324.4
21.	Ergocristine	C ₃₅ H ₃₉ N ₅ O ₅	15.14	223.1758	609.7
22.	Demethoxycurcumin	C ₂₀ H ₁₈ O ₅	15.18	223.1388	338.4
23.	Guan-fu base Y	C ₂₂ H ₂₉ NO ₅	15.25	264.3597	387.5
24.	Cycloheximide	C ₁₅ H ₂₃ NO ₄	15.37	264.3597	281.35
25.	Anabasamine	C ₁₆ H ₁₉ N ₃	15.42	264.3597	253.34
26.	Vincamine	C ₂₁ H ₂₆ N ₂ O ₃	15.47	264.3967	354.4
27.	Artocarpin	C ₂₆ H ₂₈ O ₆	16.04	325.4133	436.5
28.	Rauwolscine	C ₂₁ H ₂₆ N ₂ O ₃	16.12	293.2585	354.4
29.	Lithocholenic Acid	C ₂₄ H ₃₈ O ₃	16.22	241.2701	374.6
30.	Rotenone	C ₂₃ H ₂₂ O ₆	16.25	241.3441	394.4

31.	Silychrystin	C ₂₅ H ₂₂ O ₁₀	16.71	299.5488	482.4
32.	Speciosine	C ₂₈ H ₃₁ NO ₆	17.00	297.5137	477.5
33.	Apiin	C ₂₆ H ₂₈ O ₁₄	17.04	299.5118	564.5
34.	Gardnerine	C ₂₀ H ₂₄ N ₂ O ₂	20.23	325.2652	324.4
35.	Loganin	C ₁₇ H ₂₆ O ₁₀	20.27	227.2831	390.4
36.	Apigenin glucoside arabinoside	C ₂₆ H ₂₈ O ₁₄	20.34	227.0981	564.5
37.	Linolenic acid	C ₁₈ H ₃₀ O ₂	20.40	279.5306	278.4
38.	Isocorydine	C ₂₀ H ₂₃ NO ₄	20.59	279.3087	341.4
39.	Nantenine	C ₂₀ H ₂₁ NO ₄	20.64	279.2716	339.4
40.	Phosphatidylcholine 15:0/18:1(11Z)	C ₄₁ H ₈₀ NO ₈ P	20.76	205.3775	746.0
41.	Luteolin-8-C-glucoside	C ₂₁ H ₂₀ O ₁₁	21.52	253.3330	448.4
42.	Nicotiflorin	C ₂₇ H ₃₀ O ₁₅	21.56	253.4070	594.5
43.	Hydroxygardnutine	C ₂₀ H ₂₂ N ₂ O ₃	22.37	279.3826	338.4
44.	Phosphatidylethanolamine(22:1/20:1)	C ₄₇ H ₉₀ NO ₈ P	22.42	279.4566	828.2
45.	Phosphatidylethanolamine 18:0-22:6	C ₄₅ H ₇₈ NO ₈ P	22.51	279.4566	792.1
46.	Maritimetin-6-O-glucoside	C ₂₁ H ₂₀ O ₁₁	22.70	241.3071	448.4
47.	Ouabain	C ₂₉ H ₄₄ O ₁₂	23.25	403.3759	584.7
48.	4,4'-Diaponeurosporene	C ₃₀ H ₄₂	23.39	403.3389	402.7
49.	1-(5Z,8Z,11Z,14Z,17Z-eicosapenta enoyl)-2-(9Z-nonadecenoyl)-glycero-3-phosphoserine	C ₄₅ H ₇₆ NO ₁₀ P	25.43	255.4051	822.1
50.	Isorhamnetin-3-O-rutinoside	C ₂₈ H ₃₂ O ₁₆	25.57	255.2571	624.5
51.	Paeoniflorin	C ₂₃ H ₂₈ O ₁₁	25.62	255.3311	480.5
52.	Procyanidin B1	C ₃₀ H ₂₆ O ₁₂	25.98	281.3438	578.5
53.	1,2-diarachidonoyl-sn-glycero-3-phospho ethanolamine	C ₄₅ H ₇₄ NO ₈ P	26.02	281.3807	788.0
54.	Phosphatidylcholine(14:0/18:3n6)	C ₄₀ H ₇₄ NO ₈ P	26.10	281.4547	728.0
55.	Hirsutine	C ₂₂ H ₂₈ N ₂ O ₃	27.15	369.2234	368.5
56.	Taurochenodeoxycholate	C ₂₆ H ₄₅ NO ₆ S	27.43	465.5754	499.7
57.	[3-hexadecoxy-2-[(9Z,11E)-13-hydroxyoctadeca-9,11-dienoyl]oxypropyl] 2-(trimethyl azaniumyl)ethyl phosphate	C ₄₂ H ₈₂ NO ₈ P	27.77	610.8422	760.1
58.	Alpha-Hederin	C ₄₁ H ₆₆ O ₁₂	28.00	391.4244	751.0
59.	Soyasapogenol B base + O-DDMP, O-HexA -HexA	C ₄₈ H ₇₂ O ₁₈	28.21	391.4244	937.1
60.	Taurocholic acid	C ₂₆ H ₄₅ NO ₇ S	36.54	463.3923	515.7
61.	3-oxo-C8-homoserine lactone	C ₁₂ H ₁₉ NO ₄	36.92	214.3692	241.28

Table 2. The values of LD₅₀ (*Rattus*), LC₅₀ (*Pimephales promelas*; *Daphnia magna*), and IGC₅₀ (*Tetrahymena pyriformis*) of the phytocompounds found in the methanolic extract of *Parkia timoriana* seed pod were determined utilising the TEST software (Toxicity Estimation Software Tool) on the basis of a QSAR model (quantitative structure–activity relationship).

Sl. No.	Phytocompound (<i>Parkia timoriana</i>)	<i>Pimephales promelas</i> (Fathead minnow) (96 hr)		<i>Daphnia magna</i> (Giant water flea) (48 hr)		<i>Tetrahymena pyriformis</i> (Free living ciliate) (48 hr)		Rat (<i>Rattus norvegicus</i>) Oral	
		LC ₅₀ (mg/L)	Category	LC ₅₀ (mg/L)	Category	IGC ₅₀ (mg/L)	Category	LD ₅₀ (mg/kg)	Category
1.	3,7,11-Trimethyl-2,4-dodecadiene	0.19	A	0.25	A	0.33	A	5463.81	NT
2.	5-Ethyl-3-methyl-3,4-nonadien-6-yne	N/A	N/A	N/A	N/A	3.47	B	4365.01	NT
3.	4-Isopropyl-3,4-dimethylcyclohexa-2,5-dienone	10.15	C	4.65	B	9.32	B	4232.12	NT
4.	1-(4-Isopropylphenyl)-2-methylpropyl acetate	4.50	B	1.12	B	9.64	B	637.06	NT
5.	Patchouli alcohol	7.27	B	3.19	B	42.00	C	1368.51	NT
6.	Tricyclo[4.3.0.0(7,9)]nonane, 2,2,5,5,8,8-hexa methyl-, (1.alpha.,6.beta.,7.alpha.,9. alpha.)-	0.68	A	0.049	X	6.52	B	4193.31	NT
7.	1H-Purin-6-amine, N-((3-fluorophenyl)methyl)	12.39	C	3.14	B	48.51	C	2001.30	NT
8.	Bisabolene	0.23	A	0.13	A	0.54	A	4720.54	NT
9.	1,1,3,3,4-Pentamethyl-6-t-butyl-2,3-dihydroindene	0.87	A	0.11	A	2.20	B	1068.10	NT
10.	Scopolamine-N-butyl	N/A	N/A	N/A	N/A	N/A	N/A	N/A	N/A
11.	1-dodecanoyl-2-(11Z-eicosenoyl)-glycerol-3-phospho-(1'-sn-glycerol)	0.0029	X	0.011	X	7.55	B	21377.17	NT
12.	Napelline	0.62	A	15.86	C	4.91	B	233.91	D

13.	Taurodeoxycholate	1.94	B	4.26	B	2.37	B	1988.17	NT
14.	Voacamine	0.039	X	0.13	A	10.31	C	210.12	D
15.	Ginsenoside F3	0.043	X	46.74	C	3.24	B	36.52	C
16.	Isoschaftoside	0.035	X	122.66	D	18.09	C	1209.68	NT
17.	Azadirachtin	0.16	A	2.62	B	10.54	C	32.63	C
18.	E-Resveratrol trimethyl ether	0.17	A	2.53	B	5.05	B	1289.40	NT
19.	Ginkgolide C	N/A	N/A	19.95	C	11.28	C	30.32	C
20.	Quinine	0.61	A	6.64	B	7.58	B	430.63	D
21.	Ergocristine	0.0013	X	3.08	B	6.53	B	94.37	C
22.	Demethoxycurcumin	0.053	X	17.97	C	5.13	B	1747.94	NT
23.	Guan-fu base Y	2.37	B	4.49	B	5.29	B	36.06	C
24.	Cycloheximide	10.48	C	276.37	D	119.50	D	8.88	B
25.	Anabasamine	5.20	B	2.68	B	33.28	C	45.29	C
26.	Vincamine	1.42	B	3.98	B	7.96	C	996.51	NT
27.	Artocarpin	0.0003	X	0.62	A	2.73	B	2767.18	NT
28.	Rauwolscline	0.42	A	5.91	B	3.85	B	275.55	D
29.	Lithocholenic Acid	0.20	A	6.76	B	2.43	B	1936.85	NT
30.	Rotenone	0.0213	X	0.44	A	5.77	B	197.20	D
31.	Silychrystin	0.011	X	0.57	A	10.94	C	784.25	NT
32.	Speciosine	0.014	X	0.84	A	5.12	B	571.76	NT
33.	Apiin	0.23	A	177.95	D	37.59	C	1217.88	NT
34.	Gardnerine	0.44	A	3.71	B	4.41	B	457.91	D
35.	Loganin	143.94	D	1420.01	NT	25.40	C	3863.40	NT
36.	Apigenin glucoside arabinoside	0.035	X	87.89	C	18.09	C	712.93	NT
37.	Linolenic acid	0.35	A	2.01	B	0.43	A	10529.89	NT
38.	Isocorydine	0.57	A	0.92	A	5.77	B	6.91	B
39.	Nantenine	0.66	A	0.73	A	4.96	B	1849.47	NT
40.	Phosphatidylcholine 15:0/18:1(11Z)	124.19	D	0.62	A	N/A	N/A	2326.86	NT
41.	Luteolin-8-C-glucoside	0.26	A	31.54	C	24.64	C	1463.62	NT
42.	Nicotiflorin	0.0012	X	144.24	D	55.92	C	2154.77	NT
43.	Hydroxygardnutine	0.19	A	4.10	B	4.62	B	55.68	C

44.	Phosphatidylethanolamine(22:1/20:1)	4.61	A	0.0012	X	8.67	B	28810.26	NT
45.	Phosphatidylethanolamine 18:0-22:6	10.26	C	0.0008	X	8.30	B	20068.13	NT
46.	Maritimetin-6-O-glucoside	0.31	A	24.94	C	22.13	C	2110.06	NT
47.	Ouabain	0.45	A	352.41	D	6.27	B	26.91	C
48.	4,4'-Diaponeurosporene	0.0007	X	0.0001	X	4.22	B	8948.19	NT
49.	1-(5Z,8Z,11Z,14Z,17Z-eicosapentaenoyl)-2-(9 Z-nonadecenoyl)-glycerophosphoserine	0.87	A	0.0013	X	8.61	B	20827.58	NT
50.	Isorhamnetin-3-O-rutinoside	0.0013	X	143.13	D	58.74	C	1610.91	NT
51.	Paeoniflorin	N/A	N/A	N/A	N/A	N/A	N/A	N/A	N/A
52.	Procyanidin B1	0.0012	X	0.45	A	5.11	B	2248.22	NT
53.	1,2-diarachidonoyl-sn-glycero-3-phosphoethanolamine	0.83	A	0.0008	X	8.25	B	19965.79	NT
54.	Phosphatidylcholine(14:0/18:3n6)	3.20	B	0.60	A	7.63	B	530.65	NT
55.	Hirsutine	0.40	A	3.64	B	2.88	B	180.63	D
56.	Taurochenodeoxycholate	2.00	B	4.26	B	2.37	B	1988.17	NT
57.	[3-hexadecoxy-2-[(9Z,11E)-13-hydroxyoctadec-9,11-dienoyl]oxypropyl]2-(trimethylazaniumyl)ethylphosphate	3.34	B	0.63	A	7.97	B	554.01	NT
58.	Alpha-hederin	0.58	A	14.70	C	8.05	B	41.93	C
59.	Soyasapogenol B base + O-DDMP, O-HexA-HexA	0.0019	X	20.32	C	3.94	B	61.21	C
60.	Taurocholic acid	3.74	A	5.82	B	2.45	B	801.94	NT
61.	3-oxo-C8-homoserine lactone	267.39	D	488.36	D	189.82	D	995.41	NT

X: Extreme toxicity; A: very high toxicity; B: high toxicity; C: moderate toxicity; D: low toxicity; NT: nontoxic; T: Toxic; N/A: not applicable; LC_{50-96 h}: the amount of the test substance in water that, after 96 hours, is fatal to 50% of fathead minnows exposed in mg/L; LC_{50-48 h}: the amount of the test substance in water that, after 96 hours, is fatal to 50% of *Daphnia magna* exposed in mg/L; IGC_{50-48 h}: concentration of the test substance in water that, after 48 hours, inhibits *Tetrahymena pyriformis* development by 50%; LD₅₀ - chemical dose in mg/kg body weight that, when consumed orally, will cause death in 50% of rats.

Table 3. The predicted values of bioaccumulation factor, mutagenicity, and developmental toxicity of the phytocompounds found in the methanolic extract of *Parkia timoriana* seed pod were derived utilising the TEST software (Toxicity Estimation Software Tool).

Sl. No.	Phytocompound (<i>Parkia timoriana</i> seed pods)	BCF	Mutagenicity (Ames test)		Developmental toxicity	
			Value	Result	Value	Result
1.	3,7,11-Trimethyl-2,4-dodecadiene	1170.35	-0.02	-	0.79	T
2.	5-Ethyl-3-methyl-3,4-nonadien-6-yne	1905.46	0.19	-	0.81	T
3.	4-Isopropyl-3,4-dimethylcyclohexa-2,5-dienone	16.03	0.19	-	0.65	T
4.	1-(4-Isopropylphenyl)-2-methylpropyl acetate	187.91	0.21	-	0.64	T
5.	Patchouli alcohol	729.56	-0.09	-	0.63	T
6.	Tricyclo[4.3.0.0(7,9)]nonane, 2,2,5,5,8,8-hexa methyl-, (1.alpha.,6.beta.,7.alpha.,9.alpha.)-	16515.36	-0.06	-	0.79	T
7.	1H-Purin-6-amine,N-((3-fluorophenyl)methyl)	7.31	0.90	+	0.69	T
8.	Bisabolene	937.61	0.00	-	0.92	T
9.	1,1,3,3,4-Pentamethyl-6-t-butyl-2,3-dihydroindene	5726.79	-0.16	-	0.96	T
10.	Scopolamine-N-butyl	N/A	N/A	N/A	N/A	N/A
11.	1-dodecanoyl-2-(11Z-eicosenoyl)-glycerol-3-phospho-(1'-sn-glycerol)	2.37	0.22	-	N/A	N/A
12.	Napelline	81.13	0.05	-	0.88	T
13.	Taurodeoxycholate	3.91	0.60	+	0.87	T
14.	Voacamine	22.22	0.31	-	0.67	T
15.	Ginsenoside F3	48.49	-0.02	-	0.67	T
16.	Isoschaftoside	6.34	0.37	-	0.37	NT
17.	Azadirachtin	263.94	0.27	-	0.67	T
18.	E-Resveratrol trimethyl ether	87.43	0.82	+	0.67	T
19.	Ginkgolide C	N/A	-0.07	-	0.64	T
20.	Quinine	71.55	0.39	-	0.88	T
21.	Ergocristine	52.71	-0.03	-	1.38	T
22.	Demethoxycurcumin	10.12	0.10	-	0.97	T
23.	Guan-fu base Y	N/A	0.07	-	0.67	T
24.	Cycloheximide	1.39	-0.12	-	0.86	T
25.	Anabasamine	142.98	0.60	+	0.57	T
26.	Vincamine	67.55	0.27	-	0.81	T
27.	Artocarpin	60.14	0.22	-	0.76	T
28.	Rauwolfscine	17.31	0.42	-	0.97	T
29.	Lithocholenic Acid	42.03	0.26	-	1.00	T
30.	Rotenone	34.77	0.33	-	0.86	T
31.	Silychrystin	1.50	0.50	-	0.65	T
32.	Speciosine	N/A	-0.09	-	0.96	T
33.	Apiin	10.39	0.09	-	0.48	NT

34.	Gardnerine	44.17	0.55	+	0.92	T
35.	Loganin	5.90	0.24	-	0.57	T
36.	Apigenin glucoside arabinoside	6.34	0.38	-	0.38	NT
37.	Linolenic acid	9.93	0.24	-	0.72	T
38.	Isocorydine	103.38	0.42	-	0.92	T
39.	Nantenine	123.77	0.57	+	0.84	T
40.	Phosphatidylcholine 15:0/18:1(11Z)	10.52	0.19	-	N/A	N/A
41.	Luteolin-8-C-glucoside	7.46	0.53	+	0.57	T
42.	Nicotiflorin	16.32	0.02	-	0.53	T
43.	Hydroxygardnutine	30.15	0.34	-	1.06	T
44.	Phosphatidylethanolamine(22:1/20:1)	10.52	0.06	-	N/A	N/A
45.	Phosphatidylethanolamine 18:0-22:6	10.52	0.27	-	N/A	N/A
46.	Maritimetin-6-O-glucoside	0.30	0.47	-	0.46	NT
47.	Ouabain	27.93	0.02	-	0.37	NT
48.	4,4'-Diaponeurosporene	214.88	0.29	-	0.93	T
49.	1-(5Z,8Z,11Z,14Z,17Z-eicosapentaenoyl)-2-(9 Z-nonadecenoyl)-glycero-3-phosphoserine	10.52	0.28	-	N/A	N/A
50.	Isorhamnetin-3-O-rutinoside	3.86	0.02	-	0.54	T
51.	Paeoniflorin	N/A	0.13	-	0.70	T
52.	Procyanidin B1	23.17	0.64	+	1.00	T
53.	1,2-diarachidonoyl-sn-glycero-3-phosphoethanolamine	10.52	0.29	-	N/A	N/A
54.	Phosphatidylcholine(14:0/18:3n6)	10.52	0.39	-	N/A	N/A
55.	Hirsutine	355.88	0.43	-	0.91	T
56.	Taurochenodeoxycholate	4.00	0.60	+	0.89	T
57.	[3-hexadecoxy-2-[(9Z,11E)-13-hydroxyoctadec-9,11-dienoyl]oxypropyl] 2-(trimethylazanium yl) ethyl phosphate	10.52	0.37	-	N/A	N/A
58.	Alpha-hederin	48.49	-0.01	-	0.67	T
59.	Soyasapogenol B base + O-DDMP, O-HexA-HexA	6.79	-0.03	-	0.67	T
60.	Taurocholic acid	1.35	0.60	+	0.67	T
61.	3-oxo-C8-homoserine lactone	N/A	0.02	-	0.45	NT

BCF: bioconcentration factor; T: toxicant; NT: nontoxicant; N/A: not applicable; -: negative; +: positive.

Table 4. Prediction of different toxicity parameters (oral toxicity, carcinogenicity, reproductive toxicity, NOAEL, and repeated dose toxicity) and drug-likeness properties (Lipinski rule of five and cytochrome-P450 Metabolism) on the basis of QSAR model (quantitative structure–activity relationship) utilising different software (Toxtree, VEGA HUB, and OECD QSAR).

Sl. No.	Phytocompound (<i>Parkia timoriana</i>)	Oral Toxicity (Cramer)	Carcinogenicity	Reproductive toxicity	NOAEL		Repeated dose toxicity (HESS)	Lipinski Rule Oasis†	Cyt-P450 Metabolism
					mg/kg	ADI			
1.	3,7,11-Trimethyl-2,4-dodecadiene	Low	-	NT	24.99	0.7	Renal toxicity	Less bioavailable	Yes
2.	5-Ethyl-3-methyl-3,4-nonadien-6-yne	High	-	NT	11.22	0.438	Renal toxicity	Less bioavailable	Yes
3.	4-Isopropyl-3,4-dimethylcyclohexa-2,5-dienone	Intermediate	+	NT	49.18	0.85	-	Bioavailable	Yes
4.	1-(4-Isopropylphenyl)-2-methylpropyl acetate	Low	-	NT	160.36	0.85	-	Bioavailable	Yes
5.	Patchouli alcohol	Low	-	T	15.86	0.85	-	Bioavailable	Yes
6.	Tricyclo[4.3.0.0(7,9)]nonane, 2,2,5,5,8,8-hexamethyl-, (1.alpha.,6.beta.,7.alpha.,9.alpha.)-	Low	-	NT	1161.72	0.7	Renal toxicity	Less bioavailable	Yes
7.	1H-Purin-6-amine, N-((3-fluorophenyl)methyl)-	High	+	NT	24.9	0.85	-	Bioavailable	Yes
8.	1-Methyl-4-(1,5-dimethyl-4-hexenylidene)-1-cyclohexene	Low	-	NT	10.65	0.85	Renal toxicity	Less bioavailable	Yes
9.	1,1,3,3,4-Pentamethyl-6-t-butyl-2,3-dihydroindene	Low	-	T	19.84	0.85	Liver enzyme induction, Renal toxicity	Less bioavailable	Yes
10.	Scopolamine-N-butyl	High	+	T	28.67	0.85	-	Bioavailable	Yes
11.	1-dodecanoyl-2-(11Z-eicosenoyl)-glycero-3-phospho-(1'-sn-glycerol)	Low	-	T	66.74	0.85	-	Less bioavailable	Yes
12.	Napelline	High	-	NT	1097.23	0.7	-	Bioavailable	Yes
13.	Taurodeoxycholate	High	-	NT	171.95	0.625	-	Bioavailable	Yes

14.	Voacamine	High	-	NT	7346.83	0.585	-	Less bioavailable	Yes
15.	Ginsenoside F3	High	-	NT	2663790	0.7	-	Less bioavailable	Yes
16.	Isoschaftoside	High	-	NT	1734203	0.434	-	Less bioavailable	Yes
17.	Azadirachtin	High	+	NT	610379	0.476	-	Less bioavailable	Yes
18.	E-Resveratrol trimethyl ether	High	-	NT	9.67	0.85	Renal toxicity	Bioavailable	Yes
19.	Ginkgolide C	High	-	NT	8733.73	0.7	-	Bioavailable	Yes
20.	Quinine	High	-	NT	302.06	0.85	Hepatotoxicity, Renal toxicity	Bioavailable	Yes
21.	Ergocristine	High	-	NT	9.87	0.248	-	Less bioavailable	Yes
22.	Demethoxycurcumin	High	-	NT	74.44	0.85	Hepatotoxicity, Renal toxicity	Bioavailable	Yes
23.	Guan-fu base Y	High	-	NT	59.14	0.7	-	Bioavailable	Yes
24.	Cycloheximide	High	-	T	259.84	0.85	Hepatotoxicity	Bioavailable	Yes
25.	Anabasamine	High	-	T	25.62	0.85	Renal toxicity	Bioavailable	Yes
26.	Vincamine	High	-	NT	31.94	0.468	-	Bioavailable	Yes
27.	Artocarpin	High	-	T	2766.3	0.482	-	Less bioavailable	Yes
28.	Rauwolscline	High	-	T	714.99	0.85	Renal toxicity	Bioavailable	Yes
29.	Lithocholenic Acid	High	-	NT	396.83	0.7	-	Less bioavailable	Yes
30.	Rotenone	High	-	NT	381.59	0.85	-	Bioavailable	Yes
31.	Silychrystin	High	-	NT	26791	0.7	-	Less bioavailable	Yes
32.	Speciosine	High	+	T	301.23	0.642	-	Bioavailable	Yes
33.	Apiin	High	-	NT	3437.95	0.442	-	Less bioavailable	Yes
34.	Gardnerine	High	-	T	4298.33	0.7	-	Bioavailable	Yes
35.	Loganin	High	-	NT	5989.63	0.7	Renal toxicity	Bioavailable	Yes
36.	Apigenin glucoside arabinoside	High	-	NT	1029200	0.434	-	Less bioavailable	Yes
37.	Linolenic acid	Low	-	NT	268.29	0.7	-	Less bioavailable	Yes
38.	Isocorydine	High	+	T	3187.13	0.85	-	Bioavailable	Yes
39.	Nantenine	High	+	T	59.89	0.651	-	Bioavailable	Yes
40.	Phosphatidylcholine 15:0/18:1(11Z)	High	-	T	20.81	0.85	-	Less bioavailable	Yes
41.	Luteolin-8-C-glucoside	High	-	T	187154	0.466	-	Less bioavailable	Yes

42.	Nicotiflorin	High	-	NT	17607.6	0.433	-	Less bioavailable	Yes
43.	Hydroxygardnutine	High	+	T	187.72	0.85	-	Bioavailable	Yes
44.	Phosphatidylethanolamine(22:1/20:1)	Low	-	T	10.42	0.85	-	Less bioavailable	Yes
45.	Phosphatidylethanolamine 18:0-22:6	Low	-	T	70.79	0.85	-	Less bioavailable	Yes
46.	Maritimetin-6-O-glucoside	High	-	NT	35563	0.7	-	Less bioavailable	Yes
47.	Ouabain	High	-	NT	3180.53	0.7	-	Less bioavailable	Yes
48.	4,4'-Diaponeurosporene	Low	-	NT	14.02	0.699	Renal toxicity	Less bioavailable	Yes
49.	1-(5Z,8Z,11Z,14Z,17Z-eicosapentaenoyl)-2-(9Z-nonadecenoyl)-glycero-3-phosphoserine	Low	-	T	338.69	0.85	-	Less bioavailable	Yes
50.	Isorhamnetin-3-O-rutinoside	High	+	NT	50886.2	0.428	-	Less bioavailable	Yes
51.	Paeoniflorin	High	-	NT	3445.09	0.48	-	Bioavailable	Yes
52.	Procyanidin B1	High	-	NT	347456	0.625	-	Less bioavailable	Yes
53.	1,2-diarachidonoyl-sn-glycero-3-phosphoethanolamine	Low	-	T	172.19	0.85	-	Less bioavailable	Yes
54.	Phosphatidylcholine(14:0/18:3n6)	Low	-	T	54.24	0.85	-	Less bioavailable	Yes
55.	Hirsutine	High	-	T	854.28	0.85	-	Bioavailable	Yes
56.	Taurochenodeoxycholate	High	-	NT	127.15	0.625	-	Bioavailable	Yes
57.	[3-hexadecoxy-2-[(9Z,11E)-13-hydroxyoctadeca-9,11-dienoyl]oxypropyl]2-(trimethylazaniumyl)ethyl phosphate	High	-	T	92.62	0.85	-	Less bioavailable	Yes
58.	Alpha-Hederin	High	-	NT	15881.81	0.7	-	Less bioavailable	Yes
59.	Soyasapogenol B base + O-DDMP, O-HexA-HexA	High	+	NT	376530	0.7	-	Less bioavailable	Yes
60.	Taurocholic acid	High	-	NT	358.59	0.629	-	Less bioavailable	Yes
61.	3-oxo-C8-homoserine lactone	High	-	NT	31.52	0.85	-	Bioavailable	Yes

ADI: Acceptable daily intake; NOAEL: No-observed-adverse-effect-level; HESS: Hazard evaluation support system; NT: nontoxic; T: Toxic; -: negative; +: positive; Oral Toxicity (Cramer): the Cramer classification scheme is used for assessing the toxicological profile

of the chemicals, when administered orally, which places the compound in one of the three classes- Class I (Low toxicity), Class II (Intermediate toxicity), and Class III (High toxicity); Carcinogenicity: carcinogenicity is predicted based on a list of 55 structural alerts (SAs). The SAs for carcinogenicity are molecular functional groups or substructures known to be linked to the carcinogenic activity of chemicals. As one or more SAs embedded in a molecular structure are recognised, the system flags the potential carcinogenicity of the chemical; Reproductive toxicity: predicts the possible harm that a specific chemical agent will have on both male and female fertility as well as the development of the children; NOAEL: The highest concentration or amount of a chemical at which a population exposed to it experiences no discernible negative effects; Repeated dose (HESS): Predicts the possible organ toxicity for oral repeated dose base on test data in the database of Hazard Evaluation Support System (HESS); Lipinski Rule Oasis: Lipinski's Rule of Five is a rule of thumb to evaluate drug likeness. An orally active drug should have hydrogen bond donors < 5, hydrogen bond acceptors < 10, molecular weight < 500 Da, and octanol-water partition coefficient (log P) < 5; Cyt-P450 Metabolism: the enzymes of cytochrome P450 function to metabolize compounds that are possibly toxic, including drugs. The tool predicts the site of metabolism of chemicals by cyt-P450 enzymes; Toxtree: <https://toxtree.sourceforge.net/>; VEGA HUB: <https://www.vegahub.eu/>; OECD QSAR: <https://qsartoolbox.org/download/>

Table 5. Prediction of different biological activities of the phytochemicals found in the methanolic extract of *Parkia timoriana* seed pod using PASS (way2drug).

Sl. No.	Phytochemical (<i>P. timoriana</i>)	Dementia Treatment		Cytochrome P450 stimulant		Anti-oxidant		Anti-Inflammatory		Neurotrophic factor enhancer		Amyloid- β aggregation inhibitor		Acetylcholine stimulant		Alzheimer Disease treatment	
		Pa	Pi	Pa	Pi	Pa	Pi	Pa	Pi	Pa	Pi	Pa	Pi	Pa	Pi	Pa	Pi
1.	3,7,11-Trimethyl-2,4 -do decadiene	0.390	0.058	0.365	0.070	0.608	0.004	0.597	0.032	0.216	0.053	-	-	0.071	0.039	-	-
2.	5-Ethyl-3-methyl-3,4-no nadien-6-yne	0.451	0.028	0.402	0.054	-	-	-	-	0.206	0.062	-	-	0.098	0.085	-	-
3.	4-Isopropyl-3,4-dimethylcyclo hexa-2,5-dienone	0.452	0.028	0.508	0.026	0.173	0.076	0.704	0.015	0.278	0.019	-	-	0.613	0.018	-	-
4.	1-(4-Isopropylphenyl) -2-methylpropyl acetate	0.309	0.131	0.263	0.170	-	-	0.663	0.021	0.188	0.085	-	-	-	-	-	-
5.	Patchouli alcohol	0.608	0.004	0.243	0.210	-	-	0.314	0.060	0.207	0.061	-	-	-	-	0.394	0.118
6.	Tricyclo[4.3.0.0(7,9)]nonane, 2,2,5,5,8,8-hexamethyl-, (1.alpha.,6.beta.,7.alpha.,9.alpha.)-	0.598	0.004	0.501	0.028	0.165	0.085	0.347	0.030	0.281	0.018	-	-	0.110	0.053	0.443	0.087
7.	1,1,1,5,7,7-Heptamethyl-3,3-bis(trimethylsiloxy)tetrasiloxane	-	-	-	-	-	-	-	-	-	-	-	-	-	-	-	-
8.	Bisabolene	0.546	0.008	-	-	-	-	0.505	0.055	0.210	0.059	-	-	-	-	-	-
9.	1,1,3,3,4-Pentamethyl-6-ethyl-2,3-dihydroindene	-	-	-	-	-	-	-	-	-	-	-	-	-	-	-	-
10.	Scopolamine-N-butyl	-	-	-	-	-	-	-	-	-	-	-	-	-	-	-	-
11.	1-dodecanoyl-2-(11Z-eicosenoyl)-glycero-3-phospho-(1'-sn-glycerol)	-	-	-	-	0.235	0.040	0.550	0.043	-	-	-	-	-	-	-	-
12.	Napelline	0.292	0.153	-	-	-	-	0.302	0.158	-	-	-	-	-	-	-	-
13.	Taurodeoxycholate	-	-	-	-	0.167	0.082	0.493	0.059	-	-	-	-	-	-	-	-
14.	Voacamine	-	-	-	-	-	-	-	-	-	-	-	-	0.065	0.026	-	-

15.	Ginsenoside F3	0.947	0.000	-	-	0.862	0.003	0.794	0.007	-	-	-	-	-	-	-	-
16.	Isoschaftoside	0.309	0.131	-	-	0.829	0.003	0.530	0.048	0.161	0.128	-	-	-	-	-	-
17.	Azadirachtin	-	-	-	-	0.198	0.056	0.891	0.004	-	-	-	-	-	-	-	-
18.	E-Resveratrol trimethyl ether	-	-	0.522	0.024	0.388	0.013	0.494	0.059	0.219	0.050	0.258	0.010	0.133	0.019	-	-
19.	Ginkgolide C	0.245	0.233	-	-	0.971	0.002	-	-	-	-	-	-	-	-	-	-
20.	Quinine	-	-	0.693	0.005	-	-	-	-	-	-	-	-	0.066	0.025	-	-
21.	Ergocristine	-	-	0.763	0.004	-	-	-	-	-	-	-	-	-	-	-	-
22.	Demethoxycurcumin	0.329	0.109	0.326	0.095	0.624	0.004	0.667	0.020	-	-	0.145	0.031	-	-	-	-
23.	Guan-fu base Y	-	-	-	-	-	-	-	-	-	-	-	-	-	-	-	-
24.	Cycloheximide	-	-	-	-	-	-	0.246	0.186	-	-	-	-	-	-	-	-
25.	Anabasamine	0.509	0.013	-	-	-	-	-	-	-	-	-	-	0.193	0.004	-	-
26.	Vincamine	-	-	-	-	-	-	-	-	-	-	-	-	-	-	-	-
27.	Artocarpin	-	-	0.237	0.222	0.608	0.004	0.613	0.029	0.157	0.135	-	-	-	-	-	-
28.	Rauwolschine	-	-	-	-	-	-	-	-	-	-	-	-	0.187	0.014	-	-
29.	Lithocholenic Acid	0.496	0.016	-	-	0.170	0.079	0.459	0.070	-	-	-	-	0.248	0.031	-	-
30.	Rotenone	-	-	-	-	0.278	0.028	0.368	0.113	-	-	-	-	-	-	-	-
31.	Silychrestin	0.282	0.168	0.259	0.177	0.906	0.003	0.759	0.009	0.454	0.004	0.096	0.073	-	-	-	-
32.	Speciosine	-	-	0.242	0.212	0.182	0.067	0.293	0.089	-	-	-	-	0.105	0.067	-	-
33.	Apiin	0.477	0.020	-	-	0.765	0.004	0.743	0.011	0.252	0.029	-	-	-	-	-	-
34.	Gardnerine	-	-	-	-	-	-	-	-	-	-	-	-	-	-	-	-
35.	Loganin	0.695	0.002	-	-	0.647	0.004	0.738	0.012	-	-	-	-	-	-	-	-
36.	Apigenin glucoside arabinoside	0.366	0.074	-	-	0.837	0.003	0.510	0.054	0.207	0.062	-	-	-	-	-	-
37.	Linolenic acid	0.373	0.069	0.255	0.185	0.364	0.015	0.804	0.006	0.238	0.036	0.125	0.043	-	-	-	-
38.	Isocorydine	0.438	0.034	0.295	0.126	0.182	0.067	0.356	0.119	0.181	0.094	-	-	0.100	0.081	-	-
39.	Nantenine	0.303	0.139	0.234	0.231	-	-	-	-	0.222	0.048	-	-	-	-	-	-
40.	Phosphatidylcholine 15:0 /18:1(11Z)	-	-	-	-	0.138	0.118	0.766	0.009	-	-	-	-	-	-	-	-
41.	Luteolin-8-C-glucoside	0.384	0.062	-	-	0.828	0.003	0.626	0.027	-	-	-	-	-	-	-	-
42.	Nicotiflorin	0.583	0.005	-	-	0.924	0.003	0.743	0.011	-	-	-	-	-	-	-	-
43.	Hydroxygardnutine	-	-	-	-	-	-	-	-	-	-	-	-	0.093	0.090	-	-
44.	Phosphatidylethanolamine(22:1/20:1)	-	-	-	-	0.164	0.086	0.493	0.059	-	-	-	-	-	-	-	-

45.	Phosphatidylethanolamine 18:0-22:6	-	-	-	-	0.189	0.062	0.637	0.025	-	-	-	-	-	-	-	-
46.	Maritimetin-6-O-glucoside	0.558	0.006	-	-	0.750	0.004	0.566	0.039	0.348	0.008	-	-	-	-	-	-
47.	Ouabain	0.653	0.003	-	-	0.302	0.023	0.642	0.024	-	-	-	-	-	-	-	-
48.	4,4'-Diaponeurosporene	0.554	0.007	0.617	0.012	0.812	0.003	0.754	0.010	0.590	0.003	-	-	0.093	0.025	-	-
49.	1-(5Z,8Z,11Z,14Z,17Z-eicosa pentaenoyl)-2-(9Z-nonadece noyl)-glycero-3-phosphoserine	-	-	-	-	0.217	0.047	0.457	0.070	-	-	-	-	-	-	-	-
50.	Isorhamnetin-3-O-rutinoside	0.542	0.008	-	-	0.896	0.003	0.721	0.013	0.295	0.015	-	-	-	-	-	-
51.	Paeoniflorin	0.590	0.004	-	-	0.302	0.023	0.578	0.036	0.232	0.040	-	-	-	-	-	-
52.	Procyanidin B1	0.358	0.081	-	-	0.803	0.003	0.430	0.081	0.400	0.005	0.189	0.017	-	-	-	-
53.	1,2-diarachidonoyl-sn-glycero-3-phosphoethanolamine	-	-	-	-	0.176	0.073	0.570	0.038	-	-	-	-	-	-	-	-
54.	Phosphatidylcholine(14:0/18:3n6)	-	-	-	-	0.155	0.097	0.802	0.007	-	-	-	-	-	-	-	-
55.	Hirsutine	-	-	-	-	-	-	-	-	-	-	-	-	0.056	0.047	-	-
56.	Taurochenodeoxycholate	0.244	0.234	-	-	0.160	0.091	0.540	0.046	-	-	-	-	-	-	-	-
57.	[3-hexadecoxy-2-[(9Z,11 E)-13-hydroxyoctadeca-9,11-dien oyl]oxypropyl] 2-(trimethyl azaniumyl) ethyl phosphate	-	-	-	-	0.210	0.050	0.794	0.007	-	-	-	-	-	-	-	-
58.	Alpha-Hederin	-	-	-	-	0.575	0.005	0.839	0.005	0.168	0.115	-	-	-	-	-	-
59.	Soyasapogenol B base + O-DDMP, O-HexA-HexA	0.430	0.037	-	-	0.567	0.005	0.686	0.018	-	-	-	-	-	-	-	-
60.	Taurocholic acid	-	-	-	-	0.161	0.090	0.540	0.046	-	-	-	-	-	-	-	-
61.	3-oxo-C8-homoserine lactone	-	-	-	-	-	-	0.281	0.110	0.172	0.108	-	-	-	-	-	-

2.5. DISCUSSIONS

Individuals come into contact with phytochemicals daily, mostly via the food they consume. Knowledge of different dietary phytochemicals is necessary to understand possible toxicological issues due to the limited amount of research on the chronic toxicity of this group of chemicals. Therefore, it would be beneficial to have dependable approaches for assessing the hazards linked to these substances in order to ascertain their level of safety. The aim of the present study was to assess the suitability of utilising in silico QSAR-based tools (Toxtree, TEST, VEGA HUB, PASS, and OECD QSAR), employed by the US FDA and EPA, for predicting the toxicity of phytocompounds found in PTME across different endpoints (LD₅₀, LC₅₀, and IGC₅₀, bioconcentration factor, mutagenicity, developmental toxicity, oral toxicity, reproductive toxicity, carcinogenicity, repeated dose toxicity, NOAEL, Cyt-P450 metabolism, Lipinski rule oasis, and biological activity prediction). There is a very little knowledge about the toxicity of *Parkia timoriana*. Hence, assessing their toxicity might provide valuable information on the potential utilisation of the phytocompounds and their future uses in several innovative fields.

2.5.1. GC-MS and LC-MS analyses

The GC–MS analysis from previous study revealed the occurrence of forty-nine bioactive compounds of *P. timoriana* that are known to possess a variety of pharmacological activities (Ralte et al., 2022). However, in the present study only nine bioactive compounds were identified through GC-MS analysis and fifty-two bioactive compounds were identified through LC-MS analysis. The phytocompounds present in the methanolic extract of *P. timoriana* seed pod were mostly composed of flavonoids, alkaloids, and terpenoids. Similar bioactive compounds, including apigenin, isorhamnetin, and luteolin were identified in some previous studies on *Parkia* spp. (Kamishah et al., 2017; Loukrakpam et al., 2019). The variance in chemical composition may be attributed to species-specific differences in phytochemical substances or the difference may also be attributed to the method of extraction. It has been proposed that the chemical composition of plants exhibits considerable variability, even within the same species (Koutsoukis et al., 2019).

2.5.2. Total flavonoid and phenol content

The primary reason for the antioxidative efficacy of natural sources is the presence of phenolic and flavonoid components. Polyphenolic compounds have garnered significant interest due to their advantageous physiological function, which includes acting as antioxidants, antimutagenic agents, and combating illnesses induced by oxidative stress (Bacci et al., 2021; Del Rio, 2013). Phenolic chemicals are crucial components of plants owing to their scavenging activity, which is attributed to their hydroxyl groups (Tosun et al., 2009). Flavonoids are a diverse set of chemicals that are found everywhere and have antioxidant properties (Havsteen, 1983). Their flat arrangement, quantity, and arrangement of their hydroxyl groups, together with the existence of the C2-C3 double bond, play a crucial role in metal chelation, the capacity to scavenge free radicals, and the inhibition of enzymes that produce free radicals (Sharififar et al., 2008). In the present study, a high content of total flavonoid and total phenol was found to be present in the methanolic extract of *P. timoriana* seed pods. The biological activities, including antioxidant, antibacterial, antidiabetic, anti-proliferative, and insecticidal activities, of this plant may be attributed to its high content of polyphenolic compounds.

2.5.3. Acute toxicity prediction for different species

Prediction utilising QSAR techniques may significantly improve the accuracy of evaluating the toxicity of natural phytocompounds. The QSAR application specifies the structural, physicochemical, or biological characteristics of the phytocompound (Wu and Wang, 2018). The predicted toxicity of phytocompounds from PTME was detected in four distinct hierarchy for LD₅₀ (rat), LC₅₀ (fathead minnow), LC₅₀ (*Daphnia magna*), and IGC₅₀ (*Tetrahymena pyriformis*) which are as follows: a) fathead minnow > *T. pyriformis* > *D. magna* > rat (20 compounds), b) fathead minnow > *D. magna* > *T. pyriformis* > rat (19 compounds), c) *D. magna* > fathead minnow > *T. pyriformis* > rat (15 compounds), and d) *T. pyriformis* > fathead minnow > *D. magna* > rat (2 compounds). The phytocompounds showed a lesser toxicity for mammalian species (rat/LD₅₀) when compared to aquatic organisms (LC₅₀/fathead minnow and *D. magna*, IGC₅₀/ *T. pyriformis*).

2.5.4. Bioconcentration factor prediction

The phenomenon in which a chemical aggregate in organisms due to its presence in the environment is known as the bioconcentration factor. The bioaccumulation factor quantifies the ratio of a chemical's concentration in fish to that in water after equilibrium has been reached following absorption via the respiratory surface. A chemical is classified as bio-accumulative if its bioconcentration factor exceeds 2000, and it is regarded as highly bio-accumulative if its BCF exceeds 5000 (**Burden et al., 2014**). The phytocompounds found in PTME, except 1,1,3,3,4-pentamethyl-6-t-butyl-2,3-dihydroindene), and tricyclo[4.3.0.0(7,9)] nonane,2,2,5,5,8,8-hexamethyl-, (1.alpha.,6.beta., 7.alpha.,9.alpha.), had their value of bioconcentration factor under 2000, therefore considered non-bioaccumulative.

2.5.5. Developmental toxicity

Out of the sixty-one phytocompounds, the majority of it (forty-six) with a score ranging from 0.53 to 1.38 were deemed dangerous for the developmental stage. The phytocompounds, including procyanidin B1, ergocristine hydroxygardnutine, and lithocholenic acid, had scores greater than 1 out of the forty-six toxicants in the research. The phytocompounds that are safe for the developmental stage include apigenin glucoside arabinoside, isoschaftoside, maritimetin-6-O-glucoside, apiin, 3-oxo-C8-homoserine lactone, and ouabain. The low efficacy of in silico approaches may be partially ascribed to the multitude and heterogeneous nature of the systems that govern developmental toxicity, which are inherently understood very poorly (**Cendoya et al., 2020**).

2.5.6. Mutagenicity and carcinogenicity

The preclinical stages of drug discovery may aid in the creation of safe therapeutic substances by identifying mutagenicity at an initial stage and averting the manufacturing of potentially hazardous drugs. Different in silico prediction tools use structural warnings to make precise predictions about the mutagenicity of compounds (**Mostrag-Szlichtyng et al., 2010**). The majority of the phytocompounds (fifty-one out of sixty-one) from PTME showed negative carcinogenic and mutagenic properties. This indicates that the phytocompounds have potential for investigation in several

disciplines. However, it was predicted that taurodeoxycholate, 1H-purin-6-amine,N-((3-fluorophenyl)methyl), anabasamine, E-resveratrol trimethyl ether, nantenine, gardnerine, procyanidin B1, taurocholic acid, taurochenodeoxycholate, and luteolin-8-C-glucoside showed potential mutagens with a score > 0.5 for mutagenicity. The phytocompounds, including 1H-purin-6-amine,N-((3-fluorophenyl) methyl), scopolamine-N-butyl, 4-isopropyl-3,4-dimethylcyclohexa-2,5-dienone, speciosine, azadirachtin, nantenine, isocorydine, soyasapogenol B base + O-DDMP,O-HexA-HexA, isorhamnetin-3-O-rutinoside, and hydroxyl gardnutine were identified as potent carcinogens.

2.5.7. Oral toxicity, reproductive toxicity, and NOAEL

The oral toxicity test showed that forty-six phytocompounds (75% of the total phytocompounds from PTME) were predicted to be highly toxic, which falls under category III of Cramer's classification. These phytocompounds were proven to cause toxicity. Based on the findings of the predicted toxicity for reproduction, it was determined that 64% of the phytocompounds (thirty-nine out of sixty-one phytocompounds) did not have any adverse effects on the fertility of males and females or on reproduction. The No Observed Adverse Effect Level (NOAEL) is a measure of the toxicity caused by repeated doses. The predicted value obtained from the Acceptable Daily Intake (ADI) was used to get the predicted values for the No Observed Effect Level (NOEL). The acceptable concentration of the chemical compound in relation to its long-term toxicity is thus defined by this specific outcome (Pizzo et al., 2022). 37.70% of the phytocompounds (twenty-three out of sixty-one) showed high NOAEL values, indicating their safety and absence of negative toxic effects. Conversely, the other phytocompounds (62.29%) were determined to be toxic and had positive side effects.

2.5.8. Repeated dose toxicity, Lipinski rule, and cytochrome p450 metabolism

The Hazard Evaluation Assist System (HESS) was developed as a tool to aid in predicting toxicity using a category technique in relation to repeated-dose. It provides information on the toxicity, metabolism, and possible processes of analogue

pharmaceuticals. The toxicity database contains the NOAELs, chemical information, administration duration, purity of the investigated products, and over 400 test results.

The repeated dose toxicity analysis of the phytocompounds found in PTME (of the total components) showed that 78.68% (forty-eight out of sixty-one) are safe and do not cause any damage to organs. Based on analysis of Lipinski rule and cytochrome p450 metabolism, a considerable amount of phytocompounds were shown to be bioavailable, metabolised by the cytochrome P450 enzyme complex, and excreted from the body, which is an important characteristic of a drug candidate.

2.5.9. Biological activity prediction

The PASS programme was implemented for biological activity prediction, with the aim of expediting the process of identifying potent natural chemicals, mainly for treating Alzheimer's disease. PASS techniques for prediction were created using a total of 20,000 primary compounds. The prediction's result is presented as a list of potential biological activities, accompanied by the appropriate Pa and Pi ratios (**Khan et al., 2017**). The phytocompounds were studied for the following biological activities: dementia treatment, cytochrome P450 stimulant, anti-oxidant, anti-inflammatory, neurotrophic factor enhancer, amyloid- β aggregation inhibitor, acetylcholine stimulant, Alzheimer disease treatment, and neurodegenerative disease treatment. The majority of the phytocompounds possess anti-inflammatory, and antioxidant activities; therefore, the plant is expected to fight against oxidative and inflammatory reactions. Twenty-three phytocompounds had neurotrophic factor enhancer activity, therefore this could help in the development and survival of neurons, as well as the ability of synapses to change and strengthen over time in the central nervous system (**Di Carlo et al., 2019**). Seventeen phytocompounds can be metabolised by the cytochrome p450 enzyme complex, which is important for detoxifying xenobiotics, metabolism, and maintaining homeostasis (**Manikandan and Nagini, 2018**). Inhibiting the formation of A β (amyloid β) is a crucial therapeutic target in AD's treatment. The current study identified five phytocompounds as potent inhibitor of amyloid- β aggregation (**Lee et al., 2017**). Two phytocompounds, namely Patchouli alcohol, and Tricyclo[4.3.0.0(7,9)]nonane, 2,2,5,5,8,8-hexamethyl-, (1.alpha.,6.beta.,7. alpha.,9.alpha.)- showed potential Alzheimer's disease treatment. A similar finding showed that

patchouli alcohol improves cognitive impairments in TgCRND8 mice. Proposing that patchouli alcohol showed promise as a potential pharmacological therapy for AD and should be further developed (Xu et al., 2023).

2.6. KEY FINDINGS

- In the present study, nine bioactive compounds were identified through GC-MS analysis and fifty-two bioactive compounds were identified through LC-MS analysis. The phytochemicals present in the methanolic extract of *P. timoriana* seed pod were mostly composed of flavonoids, alkaloids, and terpenoids.
- The methanolic extract of *P. timoriana* seed pods has a total phenol concentration of 421.64 ± 3.38 mg GAE/g of extract and a total flavonoid concentration was measured to be 280.893 ± 4.31 mg QE/g of extract.
- The predicted acute toxicity of phytochemicals from PTME showed four distinct hierarchies. a) fathead minnow > *T. pyriformis* > *D. magna* > rat; b) fathead minnow > *D. magna* > *T. pyriformis* > rat; c) *D. magna* > fathead minnow > *T. pyriformis* > rat; and d) *T. pyriformis* > fathead minnow > *D. magna* > rat.
- The acute toxicity prediction revealed that phytochemicals from PTME had less toxicity for mammalian species (rat/LD₅₀) compared to aquatic organisms (LC₅₀/fathead minnow and *D. magna*, IGC₅₀/*T. pyriformis*).
- All of the phytochemicals found in PTME, except two, had a bioconcentration factor under 2000 and were therefore considered non-bioaccumulative.
- Forty-six out of sixty-one phytochemicals from PTME were considered toxic for the developmental stage, whereas apigenin glucoside arabinoside, isoschaftoside, maritimetin-6-O-glucoside, apiin, 3-oxo-C8-homoserine lactone, and ouabain were safe alternatives.
- The majority of the phytochemicals (fifty-one out of sixty-one) from PTME showed negative carcinogenic and mutagenic properties.

- The oral toxicity test revealed that 75% of the phytochemicals are highly toxic (Cramer/category III), while 64% do not affect fertility or possess reproductive toxicity.
- The study found that 37.70% of phytochemicals had a high NOAEL value, which indicated their safety and did not cause negative effects, while the remaining phytochemicals (62.29%) were toxic and had positive side effects.
- The repeated dose toxicity analysis of the phytochemicals showed forty-eight out of sixty-one are safe and do not cause any damage to organs, with a significant number of phytochemicals showing bioavailability, metabolized by cytochrome-P450 enzyme complex, and excreted from the body.
- The phytochemicals studied have properties for dementia treatment (thirty-one phytochemicals), cytochrome P450 stimulant (seventeen phytochemicals), anti-oxidant (forty-one phytochemicals), anti-inflammatory (forty-five phytochemicals), neurotrophic factor enhancer (twenty-three phytochemicals), amyloid- β aggregation inhibitor (five phytochemicals), acetylcholine stimulant (fifteen phytochemicals), and Alzheimer disease treatment (two phytochemicals).

CHAPTER-3

3.1. INTRODUCTION

3.1.1. β -site APP cleaving enzyme 1 (BACE1)

Beta-secretase 1 (BACE1, or beta-site amyloid precursor protein cleaving enzyme 1) was first identified in 1999. BACE1 is a newly discovered 501 amino acid enzyme that belongs to the type 1 transmembrane aspartic acid protease family. It has the characteristics of this protein family, with its active site having two aspartic acid residues. Primarily, BACE1 is expressed in the brain and throughout the early phases of postnatal development in the pancreas. Expression levels in other tissues are minimal. Neurons exhibit a rapid and intense expression of BACE1, particularly at the terminals where they communicate with other neurons. The amyloid-beta ($A\beta$) peptide is formed from the APP (amyloid precursor protein) by a sequence of proteolytic cleavages and subsequent post-translational modifications, resulting in the generation of amyloid plaque (**Hardy and Selkoe, 2002**). BACE1 is responsible for the crucial, or first, cleavage of APP at the β site. This cleavage is then followed by a series of processing events inside the cell membrane at various places by γ -secretase, resulting in the production of $A\beta$. Genetic polymorphisms that cause variances in amino acids at the β -cleavage region of APP lead to changes in BACE1 activity towards the APP substrate. These variations are linked to either early onset FAD (familial Alzheimer's disease) or protection against the illness, depending on the specific variation (**Koelsch, 2017**).

The cleavage of APP by BACE1 leads to a diversion from the normal non-amyloidogenic route, which is controlled by α secretase. This diversion results in the production of two peptides: APPs β (soluble ectodomain) and C99 (membrane-bound C terminus). γ -secretase further processes the C99 to produce $A\beta$ 40 and $A\beta$ 42 (**Golde et al., 2000; Suh and Checler, 2002**). $A\beta$ 42 is highly neurotoxic and is synthesised to generate the senile plaques, which are the pathological characteristics of Alzheimer's disease (**Sanchez-Varo et al., 2012**). According to the amyloid cascade hypothesis, the buildup of $A\beta$ 42 is a subsequent occurrence in AD. It occurs before and probably plays a role in triggering the excessive phosphorylation of tau, leading to the formation

of intracellular NFTs (neurofibrillary tangles). The presence of this secondary pathology, together with the buildup of A β , plays a role in a series of abnormal processes that result in the death of brain synapses and neurons (**Cervellati et al., 2021**).

Because of this factor, BACE1 has been extensively researched in relation to brain amyloidogenesis and has been shown to have a direct role in the generation of A β based on evidence from several mice knockout models. Pharmacological interventions have been used to target BACE1, resulting in the invention and testing of several inhibitory drugs. These compounds have effectively reduced the levels of A β in human subjects (**Park, 2010; Hampel et al., 2021**). The BACE1 level was discovered to be greatest in the postnatal brain of mice and in extracts from the brains of humans with AD. In both AD animal models and AD brains, there was a significant buildup of BACE1 in neuritic dystrophies around A β plaques. This accumulation is presumably due to a post-translational process. Inducing autophagy in mutated human neurons increases the accumulation of BACE1 in distant axons via autophagy, resulting in improved β -cleavage of APP (**Hampel et al., 2021**).

3.1.2. Acetylcholinesterase (AChE)

AChE plays a crucial role as an enzyme in the cholinergic nerve system. Throughout the course of Alzheimer's disease, several kinds of neurons deteriorate. There is a significant loss of cholinergic neurons in the brain of AD, which is followed by a gradual decrease in acetylcholine (**García-Ayllón et al., 2011**). In the brain tissue of people with AD, the enzyme acetylcholinesterase (AChE) is more prevalent than butyrylcholinesterase (BuChE). This abundance of AChE leads to the breakdown of acetylcholine (ACh) in the cerebral cortex and hippocampus (**Nordberg et al., 2013**). Currently, the improvement of cholinergic neurons remains a primary strategy in the symptomatic management of cognitive and behavioural symptoms in individuals with mild and moderate stages of AD. As part of this treatment approach, many substances were used which enhances the release of ACh in the hippocampus (**Lista et al., 2023; Nordberg et al., 2013**).

Cholinesterase inhibitors (ChE-Is) limit the breakdown of the neurotransmitter by raising the levels of ACh in the brain. This action improves the impaired neurotransmission of cholinergic neurons. ChE-Is were the first pharmaceuticals approved in both the United States and Europe for the explicit purpose of symptomatically treating AD (**Giacobini, 1998**). Four cholinesterase inhibitors: a) tacrine (**Watkins et al., 1994**); b) donepezil (**Sugimoto et al., 2002**); c) rivastigmine (**Grossberg and Desai, 2003**); and d) galantamine (**Amenta et al., 2001**) have been approved for the treatment of AD to manage the primary symptoms of memory loss and cognitive decline.

3.1.3. Molecular docking

Docking is essential in lead optimisation for conducting virtual screening on extensive chemical libraries, evaluating the outcomes, and generating structural hypotheses on how the ligands bind and inhibit the activity of the target (**Morris and Lim-Wilby, 2008**). Molecular docking is a commonly used technique in structure-based drug design (SBDD) because of its high accuracy in predicting the arrangement of ligands inside the protein binding site (**Meng et al., 2011**). In the 1980s, the algorithm was first created, and since then, molecular docking has emerged as a crucial tool in the field of drug discovery. In addition, the algorithms do precise calculations of binding energetics, ranking docked molecules according to the binding affinity of receptor-ligand complexes (**López-Vallejo et al., 2011; Huang and Zou, 2010**).

It takes two processes to find the most probable binding conformations: first, exploring a broad conformational space that represents several possible binding modes; and second, accurately predicting the binding conformations and their related interaction energies (**Kapetanovic, 2008**). Molecular docking programmes use a cyclical method to analyse the configuration of the ligand using specified scoring functions. This method is iteratively performed until reaching a solution with the lowest possible energy (**Yuriev et al., 2011; Huang and Zou, 2010**). Furthermore, a hydrogen bonding interaction is established between the protein's active site and the ligand to identify crucial residues and confine the ligand inside the pocket, restricting its mobility within the active site (**Ul Haq et al., 2017**).

3.1.4. Molecular dynamics simulation

Molecular dynamics (MD) simulation is used to investigate the dynamic aspects of the receptor-ligand complex in a real-life setting (**Amber et al., 1981**). MD simulation is very beneficial in comprehending the dynamic behaviour of proteins at different time scales, including rapid internal movements, slow structural alterations, and even the protein folding processes (**Snow et al., 2005**). noted that MD simulations have several applications, including protein structure optimisation before docking, preparing the receptor for protein flexibility, accounting for solvent effects, improving the fit of docked complexes, and calculating binding free energies to rank potential ligands accurately (**Alonso et al., 2006**).

MD simulations are widely used in computer-assisted drug development due to their ability to anticipate receptor-ligand molecular interactions. These simulations enable the rapid identification of potential novel drug candidates. These methods improve wet lab studies and reduce the cost of drug discovery by providing a well-informed list of candidates for testing (**Hollingsworth et al., 2022; Wu et al., 2018**).

3.1.5. Binding free energy

The combination of molecular mechanics (MM) energies with the PBSA (Poisson–Boltzmann surface area) or GBSA (generalised born surface area) continuum solvation techniques is widely used to quantify the free energy of small molecules binding to macromolecules. These approaches usually rely on MD simulations of the protein-ligand complex. As a result, they provide a balance between accuracy and computing effort, falling between experimental scoring and strict alchemical perturbation methods. They have been implemented in several systems with varied degrees of effectiveness (**Shirts et al., 2007; Homeyer et al., 2014**). The MM-PBSA approach accurately calculates the binding free energy of a protein-ligand complex by subtracting the free energies of the unbound receptor and ligand from the free energy of the complex (**Tuccinardi, 2009**).

3.1.6. ADMET properties

Absorption, distribution, metabolism, excretion, and toxicity (ADMET) of a chemical play a crucial role in the creation of novel pharmaceuticals. Specifically, an ideal medicine should be administered effectively, transported efficiently to different tissues and organs, metabolised in a manner that does not instantly diminish its effectiveness, removed correctly, and shown to be non-toxic (**Hodgson, 2001**). Traditionally, the evaluation of the ADMET qualities of a potential drug was often conducted after the determination of its effectiveness against a particular target (**Selick et al., 2002**). The predicted impact of ADMET inadequacies on attrition in drug discovery was as high as 50% in the 1990s (**Kola and Landis, 2004**). This served as a reminder of the significance of ADMET assessment in the transition from chemicals to pharmaceutical medications. Currently, the efficacy and pharmacokinetic properties of molecules are often assessed simultaneously, allowing for the early elimination of unwanted compounds throughout the drug discovery process (**Waring et al., 2015**). The primary reason for the lack of success of bioactive compounds as potential new drugs even in current years has been frequently ascribed to their ADME properties. Estimating pharmacokinetic characteristics during the early phases of drug development is crucial for effectively directing hit-to-lead and lead optimisation activities (**Ferreira and Andricopulo, 2019**).

Due to the ongoing collection of experimental ADMET data, several *in silico* tools have been created to aid in the efficient assessment of ADMET. Specifically, they may aid medicinal chemists in two ways: 1) by eliminating unwanted compounds during the drug design phase; 2) by providing prompt responses on ADMET data for lead optimisation (**Xiong et al., 2021**).

In 1997, Lipinski and colleagues introduced the "Rule of Five," which states that if a molecule fails to meet two or more of the following criteria, it is unlikely to be orally active: a) a molecular weight of 500 or greater; b) an octanol/water partition coefficient of 5 or greater; c) five or more hydrogen bond donors; and d) ten or more hydrogen bond acceptors. These criteria are widely recognised as the original and most

prominent rule-based filters for assessing the drug-likeness and oral absorption potential of a chemical (Guan et al., 2018).

3.1.7. In silico tools

Utilising in silico research is the optimal approach for initiating pharmacological target development. Traditional methods are insufficient for the timely discovery of drug targets. Attaining majority aims using considerably rapid methods is challenging. Computational methods, such as molecular docking, MD simulations, and MM/PBSA computations, are significantly contributing to the field of drug discovery (Hou et al., 2011; Keretsu et al., 2021).

3.1.7.1. Molinspiration Cheminformatics

Molinspiration provides a wide array of cheminformatics software tools that assist in the modification and processing of molecules. This programme utilises advanced algorithms to forecast the bioactivity and compute the molecular characteristics of chemical substances. This tool is used for the computation of molecular physicochemical parameters that are pertinent to drug design and QSAR. These properties include log P, PSA (molecule polar surface area), and the rule of 5 descriptors. The "Predict Bioactivity" option helps calculate the bioactivity score and drug-likeness properties, including GPCR ligands, ion channel modulators, kinase inhibitors, and nuclear receptor ligands (Molinspiration Cheminformatics, <https://www.molinspiration.com>).

3.1.7.2. SwissADME

This technique is used to forecast ADME characteristics for one or more small molecules. Its purpose is to assist in drug development. This tool provides the two-dimensional structure of the substance as well as its physiochemical characteristics, such as lipophilicity, pharmacokinetics, water solubility, medicinal chemistry, and druglikeness. The required input for this tool is the conventional simplified molecular input line entry system (SMILES) representation of compounds. The SwissADME online tool, available at <http://www.swissadme.ch>, allows users to easily submit and

analyse findings. It is designed to be user-friendly and accessible to both experts and non-experts in computer-aided drug design (CADD) (Daina et al., 2017).

3.1.7.3. PyRx and AutoDock Vina

PyRx (Python prescription) is a programme used for virtual screening in computational drug development. This may be used to evaluate collections of chemical compounds for their propensity to interact with certain therapeutic targets. PyRx enables medicinal chemists to do virtual screening on any platform and provides assistance throughout the whole process, including data preparation, job submission, and result analysis. PyRx has a docking wizard with a user-friendly interface, making it a powerful tool for computer-assisted drug development. PyRx utilises the AutoDock Vina function for the purpose of molecular docking. AutoDock Vina is a recently developed software platform used for molecular docking. Vina employs a powerful gradient optimisation technique in its local optimisation process. This approach successfully determines the gradient, providing the optimisation algorithm with a clear direction based on a single assessment (Trott and Olson, 2010).

3.1.7.4. GROMACS

GROMACS (GRoningen MACHine for Chemical Simulations) is a molecular dynamics platform specifically developed for conducting simulations of proteins, lipids, and nucleic acids. The software was first created inside the Biophysical Chemistry department at the University of Groningen. Currently, it is sustained by sponsors from many institutions and research institutes throughout the globe. GROMACS operates using a command-line interface and has the capability to use files for both input and output. The system offers feedback on the progress of calculations and gives expected time of arrival (ETA) information. The software is a tool for visualising trajectories and includes a comprehensive collection of methods for analysing trajectory data (Abraham et al., 2015; Berendsen et al., 1995).

3.1.7.5. MM/PBSA

The MM-PBSA method, which calculates binding free energies, has been widely used in the examination of biomolecular interactions. Recently, this technique has also been

used as a scoring function in the domain of computational drug discovery. *g_mmpbsa* was developed as a constituent of the OSDD (Open-Source Drug Discovery) effort. The goal is to integrate high-throughput molecular dynamics (MD) simulations with the calculation of binding energy. The programme provides options for choosing alternate atomic radii and other nonpolar solvation models. These models include those that are derived from SASA (solvent accessible surface area), SAV (solvent accessible volume), and a model that integrates both repulsive (SASA-SAV) and attractive components (Kumari et al., 2014).

3.2. REVIEW OF LITERATURE

3.2.1. Molecular docking

Choi et al. (2016) assessed the efficacy of certain ginsenosides in combating Alzheimer's disease by examining their ability to scavenge peroxynitrite and inhibit activity and by conducting molecular docking analysis to estimate their binding energies with BACE1. *In vitro* experiments conducted in a laboratory setting showed that ginsenosides had a notable ability to block the enzymes AChE, BChE, and BACE1, as well as the synthesis of ONOO⁻ and nitrotyrosine. Furthermore, molecular docking analyses demonstrated the ability of ginsenosides, particularly Rb1 and Rb2, to inhibit the activity of BACE1. These compounds displayed strong binding affinities for BACE1, as shown by a docking result of -10 kcal/mol. Rg1 and Rb1 are the primary bioactive compounds found in ginseng that have been scientifically proven to prevent Alzheimer's disease by inhibiting the buildup of amyloid beta (Xie et al., 2010; Chen et al., 2006). The results of this research indicate that ginsenosides have the potential to be used in the creation of treatments or preventative measures for Alzheimer's disease.

Youn et al. (2018) investigated the probability of isoflavones (genistein, formononetin, glycitein, daidzein, and puerarin) as potential inhibitors of BACE1 using molecular docking analysis and *in vitro* experiments. Genistein effectively inhibited BACE1 via a reversible non-competitive interaction, whereas the other isoflavones showed lower potency against BACE1. The docking investigation demonstrated that genistein had a strong binding affinity of -8.5 kcal/mol and was securely located inside the allosteric

regions of the BACE1 receptor. Through hydrogen bonding, it formed interactions with crucial amino acid residues in BACE1, including ASN37, TRP76, and GLN73. Similar findings also showed Genistein cell death suppression activity produced by A β in many neural cell lines, including C6, SHSY5Y, and human neuroblastoma cell lines. Furthermore, genistein also mitigated neuronal programmed cell death caused by A β in rodents (Vallés et al., 2008; Ma et al., 2015; Bagheri et al., 2011). Therefore, the findings indicated that genistein might potentially be advantageous in the prevention and/or treatment of AD. Moreover, it might provide valuable recommendations for the development of novel BACE1 inhibitors.

Ralte et al. (2022) analysed the phytochemicals of the underutilised plant *Parkia timoriana* using GC-MS analysis and investigated the potential anti-cancerous and anti-inflammatory compounds of the plant using molecular docking techniques. The GC-MS analysis detected the presence of 49 bioactive chemicals that are recognised for their diverse pharmacological actions. Following that, computational molecular docking investigations were conducted on the discovered compounds, which indicated potential anticancer and anti-inflammatory characteristics. This study provides a firsthand account of the bioactive chemicals found in extracts of the edible portions of *P. timoriana*. These compounds have significant antioxidant, antibacterial, and pharmacological properties. This work has the potential to facilitate the development of novel herbal remedies for a range of disorders using *P. timoriana*, and maybe contribute to the formulation of innovative drugs (Ralte et al., 2022).

Farihi et al. (2023) investigated the therapeutic capabilities of medicinal herbs and conducted molecular docking analysis to identify compounds that might potentially inhibit human AChE for the treatment of AD. This study systematically explored phytochemicals such as gedunin, curcumin, nobiletin, quercetin, fisetin, resveratrol, and berberine to investigate their potential as AChE inhibitors. A variety of bioinformatics tools were used to analyse molecular docking, ADMET properties, and compliance with Lipinski's rule of five. The results clearly highlighted the strong affinity of all phytochemicals for particular residues in AChE. Surprisingly, gedunin had a higher level of attraction (-8.7 kcal/mol) in comparison to the usual reference. These results highlight the possibility of these phytochemicals as suitable candidates

for oral medicine in the treatment of Alzheimer's disease. Both resveratrol and berberine have shown the ability to cross the blood-brain barrier (BBB), indicating their potential for targeting the CNS (central nervous system). Successfully addressing the obstacles presented by the blood-brain barrier (BBB) is crucial for the advancement of efficient central nervous system (CNS) medications. The capacity of the chosen compounds to penetrate the BBB is significant in the treatment of AD (**Pardridge, 2009**). Therefore, these seven compounds are deemed suitable for oral administration as drugs, with the potential to exceed the effectiveness of the traditional medicine, donepezil, in treating neurodegenerative illnesses.

A study on identifying potential cholinesterase inhibitors from phytochemicals of the apple for the treatment of AD was conducted using molecular docking by Jamal et al. (**2023**). The findings of the molecular docking analysis indicated that epicatechin gallate (-12.2 kcal/mol) had the most favourable interactions with AChE. Significantly, it was noted that the amino acid Trp286 of AChE played a role in the formation of hydrogen bonds, Van Der Waals contacts, and hydrophobic interactions in the examined complexes. Furthermore, the findings of the MD simulation investigation demonstrated the presence of stable interactions.

3.2.2. Molecular dynamics simulation and MM/PBSA analyses

Kumar et al. (**2019**) investigated the potential BACE1 and GSK-3 β inhibitors of additional naphthofuran derivatives using molecular docking, MD simulation, and free energy analysis. In the docking result, NS7 and NS9 exhibited superior binding affinity in comparison to previously documented inhibitors. The hydrogen bond interactions of NS7 and NS9 demonstrated strong contact with BACE1 through residues Gln73 and Thr72, as well as GSK-3 β through Arg141 and Thr138 residues. The analysis of MM-PBSA and energy breakdown per residue provided distinct components of binding energy and a relative assessment of the significance of amino acids in the binding process. The findings indicated that the binding was mostly influenced by hydrophobic interactions, implying that hydrophobic interactions might be crucial in developing inhibitors that simultaneously inhibit BACE1 and GSK-3 β . The findings

indicated that naphthofuran derivatives have the potential to function as a dual inhibitor targeting both BACE-1 and GSK-3 β .

Ghosh et al. (2021) have determined the binding attractions and binding mechanisms of various polyphenols towards Mpro using Autodock Vina for molecular docking, GROMACS for MD simulation, and MM/GBSA for binding free energy calculations. The polyphenols demonstrate strong binding affinity towards Mpro, ranging from -7.1 to -9.0 kcal/mol. However, only epicatechin gallate, epigallocatechin gallate, and gallocatechin-3-gallate, exhibit substantial interactions with one or both His41 and Cys145 (catalytic residues) of Mpro. The molecular dynamics simulations, lasting 100 nanoseconds, demonstrate that these three protein-ligand complexes are very stable, exhibit minimal conformational variations, and possess a comparable level of compactness. The stability of these three Mpro-ligand complexes is confirmed by estimating the high number of H-bonds and conducting MM-GBSA examination. Both MM/PBSA and MM/GBSA approaches are equally effective in predicting the accurate binding free energies (Venugopal et al., 2020; Chen et al., 2015). Furthermore, the pharmacokinetic research indicated that these polyphenols have desirable drug-like properties. In summary, our investigation demonstrates that these three polyphenols have the ability to act as inhibitors against Mpro and might be interesting options for the therapy of COVID-19.

Ahmad et al. (2023) evaluated the pharmacological properties of *Nyctanthes arbor-tristis* to confirm its traditional medicinal use for treating numerous diseases. This study assessed the anti-inflammatory properties of twenty-six phytochemicals by using AutoDock tool for molecular docking, GROMACS programme for MD simulation, MM/PBSA analysis for free energy calculations and SwissADME assessed the ADME characteristics. Arb-E and β -sito, which are natural chemicals derived from the plant, exhibited notable binding affinity towards a variety of inflammatory markers. The control medicine celecoxib had a binding energy of -9.29 kcal/mol. Among the phytochemicals examined, Arb-E had the highest significance with a binding affinity of -10.26 kcal/mol. The β -sito compound exhibited a significant binding affinity of -8.86 kcal/mol when interacting with the COX-2 receptor. The COX-2 MD simulation, conducted with both Arb-E and the control medication

celecoxib, had a root mean square deviation ranging from 0.15-0.25 nm. This indicates that the MD simulation remained stable throughout its duration. Furthermore, the MM-PBSA study revealed that the binding energy of COX-2-Arb_E complex was the most favourable (-277.602 kJ/mol). Arb-E and β -sito exhibited noteworthy ADME physicochemical properties and druglikeness features, resulting in considerable drug-like properties. Hence, this in silico study revealed the anti-inflammatory properties of these phytochemicals and may be tested in vitro/in vivo experiments to create innovative anti-inflammatory medications.

3.3. MATERIALS AND METHODS

3.3.1. Retrieval of ligand and its preparation

A total of sixty-one phytochemicals, obtained from the methanolic extract of *Parkia timoriana* seed pods using LC-MS and GC-MS analyses, were subjected to molecular docking analysis against BACE1 and AChE protein receptors (**Table 6; Figure 6, 7**). The 2D and 3D structures of each ligand were obtained from the NCBI (National Centre for Biotechnology Information) PubChem (<https://pubchem.ncbi.nlm.nih.gov/>). The 3D structures were saved in sdf (structure-data file) format, and the phytochemicals whose 3D structure were not available in PubChem were drawn using Chemdraw software (ChemBioOffice 2010). The PyRx 0.8 programme was used to import ligands via the Open Babel plug-in tool. In order to achieve a stable arrangement of the ligands, they underwent energy reduction using the UFF (universal force field) energy minimization parameter, in combination with the conjugate gradient descent optimisation technique. Prior to conducting molecular docking, the ligands were transformed into pdbqt (protein data bank, partial charge, and atom type) forms (**Dallakyan and Olson, 2015**).

3.3.2. ADMET

The canonical Simplified Molecular Input Line Entry System (SMILES) format of the sixty-one compounds found in PTME was obtained from PubChem and used as inputs for the ADMET webservers. The determination of physicochemical and molecular characteristics was conducted using the Molinspiration Cheminformatics Software (<http://www.molinspiration.com>) (**Kolodziejczyk-Czepas et al., 2018**). The ADMET

properties, including water solubility, lipophilicity, and pharmacokinetic bioactivity score, as well as the pharmacokinetics, medicinal chemistry, drug likeness, and bioavailability score of the ligands, were assessed using the SwissADME server (<http://www.swissadme.ch/>) (Daina et al., 2017).

3.3.3. Retrieval of protein and its preparation

The 3D structures of BACE1 (PDB ID: 5I3V) and AChE (PDB ID: 7E3D) were obtained from the PDB (Protein Data Bank) under RCSB (Research Collaboratory for Structural Bioinformatics). The resolution of the BACE1 structure is 1.62 Å, while the resolution of the AChE structure is 2.5 Å. The BACE1 and AChE receptors' structures were constructed prior to docking using UCSF Chimera 1.15 (Figure 8A and 9A) (Pettersen et al., 2004). The ligand, solvent, and metal ions that were co-crystallised with the protein receptors were eliminated. Structures have been modified by introducing polar hydrogen atoms and partial charges. The shortened side chains were restored, and gasteiger charges were added to the protein receptors using the integrated dock prep programme (Opo et al., 2021).

3.3.4. Predicting the active site of the protein receptor

An essential step in a molecular docking investigation is the discovery and characterization of pockets within a protein structure (Le Guilloux et al., 2009). The fpocket web server, available at <https://bioserv.rpbs.univ-paris-diderot.fr/services/fpocket/>, was used to identify the active sites of the BACE1 and AChE receptors. This tool utilises Voronoi tessellation and α -spheres to detect the active site of a protein. The fpocket accurately detected 94% and 92% of known protein binding sites from the top three ranked pockets (Schmidtke et al., 2010). The highest rated pocket (Pocket 0) was chosen for the receptor (Figure 8B and 9B). The findings were visualised using Schrödinger's Pymol 2.4.0 software.

3.3.5. Molecular docking

The molecular docking was conducted using the Autodock Vina plug-in tool in PyRx 0.8 (Trott and Olson, 2010). The receptors and the ligands were loaded into the programme using the "Vina Wizard" feature. The PyRx programme was used to

identify, analyse, and classify the residue of the active pocket of the receptor. This was done by selecting the "molecules" option in order to conduct point-specific molecular docking. Following classification, a grid box was positioned on the receptor and adjusted to include the whole active pocket of the receptor. The dimensions of the grid box were set at $x=30.000$, $y=30.000$, $z=30.000$ for both receptors. Following the production of the grid mapping, the AutoDock Vina programme was developed and executed to perform molecular docking. The conformation with the most negative value for binding affinity (kcal/mol) was chosen as the optimal interaction for each ligand. The most significant protein-ligand complexes were selected for further investigation. The chosen complexes were visualised using BIOVIA Discovery Studio Visualizer v21.1.0.20298 and Schrödinger's Pymol 2.4.0 software.

3.3.6. Molecular dynamics simulation

The findings from the molecular docking investigations were then examined by MD simulations using GROMACS v5.1.5 (Abraham et al., 2015; Berendsen et al., 1995). The GAFF (General AMBER Force Field) and AMBER99SB were used to create force field and parameter files for the ligand and protein, respectively (Hornak et al., 2006). A cubic box with periodic boundaries was placed around the complex, ensuring a minimum distance of 10 Å from the box edges. The box was then filled with solvent using a three-point water model known as TIP3P. In order to nullify the system, Na⁺ and Cl⁻ ions were introduced as counter ions (Sharma et al., 2022). Subsequent to the execution of energy minimization and equilibrating the system, the genuine MD simulation was conducted. The system was subjected to energy reduction using the steepest descent minimization technique for 1000 steps. This was done to prevent steric conflicts, with a tolerance of 10 kJ/mol/nm (Selvaraj et al., 2021). An equilibration process was conducted for 500 ps at 300 K using the Berendsen Thermostat coupling in the NVT ensemble, where the number of particles, volume, and temperature were kept constant (Berendsen et al., 1984). The NPT ensemble equilibration, which included a constant number of particles, pressure, and temperature, was conducted for a duration of 1000 picoseconds (1 nanosecond). The Parrinello-Rahman barostat was used to couple the pressure at 1 bar (Parrinello and Rahman, 1981). The Particle Mesh Ewald (PME) method was used to compute long-

range electrostatic interactions. The LINear Constraint Solver (LINCS) method (**Hess et al., 1998; Sharma et al., 2022**) was used to limit all bond lengths. Subsequently, the system, which had undergone energy minimization and equilibration, was then exposed to unconstrained production molecular dynamics (MD) simulations lasting 100 nanoseconds while maintaining a goal temperature of 300 Kelvin and a pressure of 1 bar. The trajectories obtained from a 100 ns MD simulation were used for conducting many dynamic studies, including RMSD (root mean square deviation), RMSF (root mean square fluctuation), Rg (radius of gyration), and determination of the amount of hydrogen bonds. These analyses were performed using the built-in scripts of GROMACS.

3.3.7. Free energy binding

The complex's binding free energy was determined by the use of the MM-PBSA technique. The concept of free energy is denoted by the equation $G_X = E_{MM} + G_P + G_{NP}$, where X represents the complex. E_{MM} refers to the average potential energy of the molecules in a vacuum (van der Waal's energy (E_v) + electrostatics energy (E_e)), while G_P and G_{NP} reflect the solvation energies associated with the polar and non-polar components, respectively. The MM-PBSA calculation used the MD trajectory data, which was recorded at intervals of 500 picoseconds. The energies obtained from the MD simulation trajectories were computed using the default settings of the `g_mmpbsa` programme (**Baker et al., 2001; Kumari et al., 2014**). The non-polar solvation energy was calculated using the SASA (solvent accessible surface area) model. The 'MmPbSaDecomp.py' script of `g_mmpbsa` programme was used to calculate the energy contributed by individual residues to the overall binding energy.

3.3.8. Principal component analysis

Principal component analysis (PCA) is a statistical method that simplifies a complex data and identifies the combined and connected movements of atoms in biological macromolecules. PCA was conducted on snapshots taken every 2 picoseconds from the 100 nanosecond simulations. The important collective movements of the protein receptor with ligands were captured by constructing covariance matrices of C α atoms (**Amadei et al., 1993; Prakash et al., 2019**). A positive value in the covariance matrix

implies associated motion, whereas a negative value shows anti-correlated motion between two C α atoms. The covariance matrices were diagonalized, resulting in a collection of eigenvectors and their equivalent eigenvalues. The eigenvalues indicate the importance of their equivalent eigenvectors in the behaviour of the system, with the eigenvector associated with the highest eigenvalue representing the most significant movements. Principal components (PCs) are derived by projecting the movement of the C α atoms at each period onto the eigenvectors. The covariance matrices, eigenvectors, and two-dimensional graphs of PC1 vs PC2 were generated using the built-in tools 'gmx covar' and 'gmx anaeig' in Gromacs (Taidi, 2022).

3.4. RESULTS

3.4.1. ADMET properties

The analysis of drug-likeness and pharmacokinetic parameters revealed that forty out of sixty-one phytocompounds concurred with Lipinski's rule of five. No violation of the rules was observed on 3-oxo-C8-homoserine lactone, taurochenodeoxycholate, hirsutine, hydroxygardnutine, nantenine, isocorydine, loganin, gardnerine, speciosine, demethoxycurcumin, guan-fu base Y, cycloheximide, anabasamine, vincamine, rauwolscine, lithocholenic acid, rotenone, quinine, E-resveratrol trimethyl ether, napelline, taurodeoxycholate, scopolamine-N-butyl, 1H-purin-6-amine, N-((3-fluorophenyl)methyl)-, 5-ethyl-3-methyl-3,4-nonadien-6-yne, 4-isopropyl-3,4-dimethylcyclohexa-2,5-dienone, 1-(4-Isopropylphenyl)-2-methylpropyl acetate, and patchouli alcohol. Whereas, 3,7,11-Trimethyl-2,4-dodecadiene, Tricyclo[4.3.0.0(7,9)]nonane, 2,2,5,5, 8,8-hexamethyl-, (1.alpha.,6.beta.,7.alpha.,9.alpha.)-, Bisabolene, 1,1,3,3,4-Pentamethyl-6-t-butyl-2,3-dihydroindene, Ginkgolide C, Ergocristine, Artocarpin, Silychrystin, Linolenic acid, 4,4'-Diaponeurosporene, Paeoniflorin, Phosphatidylcholine(14:0/18:3n6), Taurocholic acid showed 1 violation of the rule. Whereas, the other compounds violate two or more parameters of the Lipinski rule of five. Thirty-one compounds have an octanol-water partition coefficient (log P) value between 0.7 and 5.0. The majority of the compounds (63.93 %, or thirty-nine out of sixty-one) have a molecular weight (MW) below 500. According to the SwissADME parameters, thirty out of the sixty-one selected

compounds did not meet the TPSA (topological polar surface area) range, seventeen compounds exceeded the limit of the number of H-bond acceptors, and thirteen compounds exceed the number of H-bond donor limit. Except for thirteen compounds, the others fall under the acceptable range of heavy atoms. Thirty-two phytocompounds meet the acceptable range of rotatable bonds. Sixteen phytocompounds were under the acceptable range of molar volumn. Except for twenty-five phytocompounds, the others were in the acceptable range of molar refractivity (**Table 7**). Twenty-seven out of sixty-one phytocompounds revealed high absorption in the gastrointestinal tract. Among the phytocompounds, 5-Ethyl-3-methyl-3,4-nonadien-6-yne, 4-isopropyl-3,4-dimethylcyclohexa-2,5-dienone, 1-(4-Isopropylphenyl)-2-methylpropyl acetate, patchouli alcohol, 1H-purin-6-amine, N-((3-fluoropheny l)methyl)-, scopolamine-N-butyl, napelline, E-resveratrol trimethyl ether, quinine, anabasamine, vincamine, rauwolscine, lithocholenic acid, rotenone, gardnerine, linolenic acid, isocorydine, nantenine, hydroxygardnutine, and hirsutine showed blood-brain barrier permeation. No compound had solubility value (Log S) > 0. However, six compounds had LogS value between 0 and -2, twenty compounds between -2 and -4, and thirty-five compounds had LogS value > -4. The majority of the phytocompounds (thirty-eight) passed the P-gp (P-Glycoprotein) substrate criterion. For the GPCR ligand, thirty-one compounds have scored > 0.0, and thirty compounds scored between 0.0 and -5.0. With respect to the ion channel modulator, the values of twenty-eight compounds were > 0.0, and thirty-three compounds had values between 0.0 and -5.0. For the kinase inhibitor, five compounds had values > 0.0, and the others between 0.0 and -5.0. For the nuclear receptor ligand, twenty-nine compounds had values > 0.0, and thirty-two compounds scored between 0.0 and -5.0. For the protease inhibitor, twenty-one compounds had values > 0.0, and forty compounds had values between 0.0 and -5.0. For the enzyme inhibitor, forty-four compounds had values > 0.0, and the others between 0.0 and -5.0 (**Table 8**). Isoschaftoside had the lowest log Kp of -11.30 cm/s, followed by ouabain (-11.07 cm/s), apigenin glucoside arabinoside (-10.91 cm/s), and isorhamnetin-3-O-rutinoside (-10.12 cm/s). Thirty-eight compounds had log Kp values between -5.0 and -10.0 cm/s, and nineteen compounds had log Kp values between 0.0 and -5.0 cm/s. Rauwolscine, speciosine, gardnerine, luteolin-8-C-glucoside, hydroxygardnutine, maritimetin-6-O-glucoside, procyanidin B1, and

hirsutine were alert for PAINS filters. On the other hand, 4-Isopropyl-3,4-dimethylcyclohexa-2,5-dienone, 1-(4-Isopropylphenyl)-2-methylpropyl acetate, patchouli alcohol, tricyclo[4.3.0.0(7,9)]nonane, 2,2,5,5,8,8-hexamethyl-, (1.alpha.,6.beta.,7.alpha.,9.alpha.)-, 1H-purin-6-amine, N-((3-fluorophenyl) methyl)-, 1,1,3,3,4-pentamethyl-6-t-butyl-2,3-dihydroindene, isoschaftoside, ergocristine, anabasamine, vincamine, rauwolscline, silychrystin, speciosine, apiin, loganin, apigenin glucoside arabinoside, isocorydine, nantenine, and nicotiflorin did not show any alert for BRENK. The majority of the phytochemicals (thirty-nine out of sixty-one) inhibited one or the other cytochrome p450 enzyme complex (CYP1A2, CYP2C19, CYP2C9, CYP2D6 and CYP3A4). Twenty-eight compounds had a synthetic accessibility score < 5.0, while the other thirty-three compounds had a synthetic accessibility score > 5.0. Forty-one had bioavailability scores ≥ 0.55 , while the other twenty phytochemicals had a bioavailability score < 0.55 (**Table 9**).

3.4.2. Molecular docking

3.4.2.1. BACE1

For each ligand, a total of eight potential binding sites were determined as the output of the docking tool. We determined the ligand with the strongest binding affinity by identifying the lowest value (most negative) binding energy. According to the docking results of sixty-one phytochemicals from *P. timoriana* against BACE1, ergocristine was the best-ranked ligand with a binding affinity of -10.3 kcal/mol, followed by nicotiflorin, voacamine, and isorhamnetin-3-O-rutinoside with binding affinity of -10.2 kcal/mol, -10.1 kcal/mol and -10.1 kcal/mol, respectively (**Table 10**). Subsequently, these compounds underwent MD simulation to confirm the compactness and stability of the complex. The docked complex may be visualised using the Pymol programme. As many as twelve compounds have a binding affinity between -9.9 kcal/mol and -9.0 kcal/mol (apiin, apigenin glucoside arabinoside, ginsenoside F3, isoschaftoside, silychrystin, procyanidin B1, maritimetin-6-O-glucoside, rauwolscline, luteolin-8-C-glucoside, paeoniflorin, soyasapogenol B base + O-DDMP, O-HexA-HexA, and ouabain). Eighteen compounds were found to have binding affinity between -8.9 kcal/mol and -8.0 kcal/mol (taurochenodeoxycholate,

rotenone, alpha-hederin, taurodeoxycholate, vincamine, artocarpin, azadirachtin, gardnerine, taurocholic acid, napelline, demethoxycurcumin, lithocholenic acid, nantenine, ginkgolide C, Guan-fu base Y, hirsutine, quinine, and hydroxygardnutine). The other twenty-seven compounds showed a binding affinity between -7.9 kcal/mol and -5.3 kcal/mol (**Table 10**).

3.4.2.2. AChE

Similar to BACE1, a total of eight potential binding sites were determined as the output for each ligand by the docking tool. We determined the ligand with the strongest binding affinity by identifying the lowest value (most negative) binding energy. The docking results of the sixty-one compounds against the AChE receptor showed that apiin and maritimetin-6-O-glucoside were the best binding ligands with binding affinity of -10.3 kcal/mol each, followed by paeoniflorin and silychrystin with binding affinity of -10.2 kcal/mol and 9.8 kcal/mol, respectively (**Table 10**). To study the stability of these four compounds with AChE, they were subjected to molecular dynamic simulation. Eleven compounds were found to have binding affinity between -9.7 kcal/mol and -9.0 kcal/mol (1H-Purin-6-amine, N-((3 fluorophenyl) methyl), taurodeoxycholate, isoschaftoside, demethoxycurcumin, cycloheximide, ergocristine, artocarpin, taurochenodeoxycholate, loganin, taurocholic acid, and rotenone). Eighteen compounds have been shown to have binding affinity between -8.9 kcal/mol and -8.0 kcal/mol (bisabolene, napelline, ginsenoside F3, voacamine, E-resveratrol trimethyl ether, quinine, anabasamine, rauwolscine, lithocholenic acid, speciosine, gardnerine, isocorydine, luteolin-8-C-glucoside, nicotiflorin, hydroxygardnutine, 4,4'-diaponeurosporene, isorhamnetin-3-O-rutinoside, and procyanidin B1), and the other twenty-eight compounds showed binding affinity between -7.9 kcal/mol and -6.2 kcal/mol (**Table 10**).

3.4.3. Hydrogen bonding and hydrophobic interaction

3.4.3.1. BACE1

The amino acid interactions of the BACE1 receptor with the best hit ligands (binding \leq -10.0 kcal/mol) were analysed in 2D conformation using BIOVIA Discovery Studio Visualizer v21.1.0.20298. Ergocristine was found to have hydrophobic bonds with

TRP76, PRO70, PHE108, LYS107, and TYR71 residues of BACE1 at distances of 7.03 Å, 7.97 Å, 5.87 Å, 6.58 Å, and (3.99 Å, 4.47 Å, and 4.26 Å), respectively. Additionally, the residues TYR71 and ASP32 also interacted with ergocristine through hydrogen bonding at a distance of 6.42 Å and 5.95 Å, respectively (**Table 11; Figure 10A, 10B**). Nicotiflorin was found to have hydrophobic bonds with TYR 71 (5.42 Å, 5.07 Å, and 4.22 Å) and PHE 108 (5.07 Å, and 6.74 Å) residues of BACE1. Also, LYS107 (4.93 Å), ILE126 (4.57 Å), THR231 (3.34 Å), GLY74 (3.73 Å), VAL69 (3.25 Å), and TRP76 (3.85 Å, and 5.02 Å) also interacted through the Hydrogen bond (**Table 11; Figure 10C, 10D**). Isorhamnetin-3-O-rutinoside was found to have a hydrophobic bond with TYR71 and PHE108 residues of BACE1 at distances of (6.79 Å, 5.42 Å, 4.94 Å, and 4.16 Å) and (6.86 Å, and 5.14 Å), respectively. Also, THR231 (4.84 Å, and 3.21 Å), LYS107 (4.81 Å), GLN73 (6.01 Å), ILE126 (4.15 Å) and ARG128 (6.32 Å) interacted through the hydrogen bond (**Table 11; Figure 11A, 11B**). Voacamine was found to have a hydrophobic bond with PHE108, LEU30, VAL69, TYR198, ILE126, ILE118, TRP76, and TYR71 residues of BACE1 at distances of 5.07 Å, 5.72 Å, 5.43 Å, 6.32 Å, 3.76 Å, 6.64 Å, (6.27 Å & 5.79 Å) and (5.41 Å, 4.70 Å, 5.36 Å, & 5.91 Å), respectively. Hydrogen bonding was also found between Voacamine and TRP76 (6.27 Å), TYR71 (5.91 Å), ILE126 (3.76 Å), and PRO70 (5.15 Å) of BACE1 (**Table 11; Figure 11C, 11D**).

3.4.3.2. AChE

Similarly, the amino acid interactions of the AChE receptor with the best hit ligands (binding ≤ -9.8 kcal/mol) were analyzed in 2D conformation using BIOVIA Discovery Studio Visualizer v21.1.0.20298. Apiin was found to have bound with AChE through hydrogen bonding by GLU202, SER125, ASN87, TYR341, and TYR124 at a distance of 5.66 Å, 4.43 Å, 5.00 Å, 4.89 Å, and 5.80 Å, respectively, and by hydrophobic bonds through TRP86 (4.10 Å), TYR124 (6.15 Å), and TYR341 (4.14 Å) (**Table 12; Figure 12A, 12B**). Maritimetin-6-O glucoside interacted with AChE through hydrogen bonds by PHE295 (4.22 Å), TYR72 (5.59 Å), and SER125 (4.12 Å) and hydrophobic bonds by TRP86, TYR337, and TYR124 at a distance of 4.85 Å, 5.92 Å, and 6.83 Å & 6.47 Å, respectively (**Table 12; Figure 12C, 12D**). ASN87 (3.83 Å, and 4.11 Å), SER125 (4.42 Å, and 4.22 Å), PHE295 (4.11 Å), GLY122 (3.62 Å), TYR341 (5.71 Å), and

HIS447 (5.05 Å) of AChE interacted with paeoniflorin through hydrogen bonds, and TRP286 (7.35 Å) and TRP86 (4.86 Å) through hydrophobic bond (**Table 12; Figure 13A, 13B**). Silychrystin interacted with AChE through hydrogen bonding by TYR341 (6.56 Å) and TYR124 (6.42 Å). It also interacted with AChE through hydrophobic bonds with TYR341 (4.85 Å, and 5.33 Å), TYR124 (6.42 Å), TYR72 (5.64 Å), TRP286 (6.14 Å, 6.68 Å, 3.95 Å, and 5.41 Å), and LEU76 (6.62 Å) (**Table 12; Figure 13C, 13D**).

3.4.4. Molecular dynamics simulation

3.4.4.1. BACE1

BACE1-ligand complexes of the best hit ligands (ergocristine, nicotiflorin, isorhamnetin-3-O rutinose, and voacamine) were found to have an average RMSD of 0.184 nm, 0.215 nm, 0.226 nm, and 0.217 nm, respectively (**Table 13; Figure 14A**). The average RMSF of the BACE1 ligand complexes was 0.103 nm (BACE1-ergocristine complex), 0.117 nm (BACE1-icotiflorin complex), 0.130 nm (BACE1-Isorhamnetin-3-O-rutinose complex), and 0.117 nm (BACE1-voacamine complex) (**Table 13; Figure 14B**). The number of hydrogen bonds formed between BACE1 and ligands, namely ergocristine, nicotiflorin, isorhamnetin-3-O-rutinose, and voacamine, was 0.666, 4.940, 3.880, and 0.173, respectively (**Table 13; Figure 14C**). The average radius of gyration (Rg) of the BACE1-ligand complexes was 2.114 nm (BACE1-ergocristine complex), 2.142 nm (BACE1-nicotiflorin complex), 2.144 nm (BACE1-isorhamnetin-3-O-rutinose complex), and 2.144 nm (BACE1-voacamine complex) (**Table 13; Figure 14D**).

3.4.4.2. AChE

The average RMSD of AChE-ligand complexes of the best hit ligands (apiin, maritimetin-6-O glucoside, paeoniflorin, and silychrystin) were found to be 0.25 nm, 0.24 nm, 0.24 nm, and 0.24 nm, respectively (**Table 14; Figure 15A**). The average RMSF of all the AChE-ligand complexes was found to be ~0.11 nm (**Table 14; Figure 15B**). The number of hydrogen bonds formed between AChE and ligands, namely apiin, maritimetin-6-O glucoside, paeoniflorin, and silychrystin, was 1.88, 3.27, 2.76,

and 0.23, respectively (**Table 14; Figure 15C**). The average radius of gyration (R_g) of all the AChE-ligand complexes was found to be ~ 2.3 nm (**Table 14; Figure 15D**).

3.4.5. Free energy binding

3.4.5.1. BACE1

The total binding energy (sum total of van der Waals energy, electrostatic energy, polar solvation energy, and SASA energy) between BACE1 receptor and the best hit ligands was -288.631 ± 16.489 kJ/mol (BACE1-ergocristine complex), -102.789 ± 17.818 kJ/mol (BACE1-nicotiflorin complex), -107.567 ± 23.195 kJ/mol (BACE1-isorhamnetin-3-O-rutinoside complex), and -417.951 ± 31.736 kJ/mol (BACE1-voacamine complex) (**Table 15; Figure 16A**). The analysis of the energy contribution by an individual residue showed that ASP106, ASP228, TYR71, GLU77, and GLU104 contributed approximately -20 kJ/mol of energy each in the BACE1-ergocristine complex (**Figure 16C**). In the BACE1-nicotiflorin complex, the top energy-contributing residues were TYR71, PHE108, and SER35 (**Figure 16D**). TYR71, PHE108, and ASP106 contributed the maximum energy to the BACE1-isorhamnetin-3-O-rutinoside complex (**Figure 16E**). The number of residues contributing maximum energy is significantly high in the BACE1-voacamine complex, namely, ASP228, ASP32, ASP106, ASP223, GLU77, GLU265, GLU104, GLU125, ASP131, GLU339, and GLU116, all generating above -30 kJ/mol each (**Figure 16F**).

3.4.5.2. AChE

The total binding energies of AChE-apiin complex, AChE-maritimetin-6-O glucoside complex, AChE-paeoniflorin complex, and AChE-silychrystin complex were -93.705 ± 19.494 kJ/mol, -68.854 ± 24.995 kJ/mol, -110.015 ± 20.417 kJ/mol, and -385.386 ± 18.965 kJ/mol, respectively (**Table 16; Figure 17A**). The analysis of the energy contribution by an individual residue showed that TRP286, TYR341, and LEU36 were the maximum energy contributors in the AChE-apiin complex (**Figure 17C**). In the AChE-maritimetin-6-O-glucoside complex, ARG3 contributed energy significantly. Additionally, GLU4, ASP5, ALA6, and GLU7 were also major energy contributors (**Figure 17D**). ASP74, TYR341, TRP86, and GLU285 contributed the most energy to the AChE-paeoniflorin complex (**Figure 17E**). In the AChE-silychrystin complex,

ASP-74 and GLU-292 contributed approximately -30 kJ/mol energy, whereas GLU285, GLU243, ASP349, GLU84, GLU202, GLU358, GLU334, GLU81, ASP374, and GLU351 contributed approximately -20 kJ/mol each (**Figure 17F**).

3.4.6. Principal component analysis

3.4.6.1. BACE1

The 2D projections revealed that the BACE1-nicotiflorin complex had the smallest occupied phase space with PCA1-66.784% and PCA2-33.215% (**Figure 18B**), followed by the BACE1-isorhamnetin-3-O-rutinoside complex with PCA1-71.811% and PCA2-28.189% (**Figure 18C**). Among the others, the BACE1-voacamine complex had a lesser occupied phase area with PCA1-69.642% and PCA2-30.358% (**Figure 18D**) compared to the BACE1-ergocristine complex, which occupied the most space out of the four complexes with PCA1-59.956% and PCA2-40.044% (**Figure 18A**).

3.4.6.2. AChE

The 2D projections showed that the AChE-maritimetin-6-O-glucoside complex had the smallest occupied phase area with PCA1-73.688% and PCA2-26.312% (**Figure 19B**), followed by the AChE-apiin complex with PCA1-74.124% and PCA2-25.876% (**Figure 19A**). Comparing the others, the AChE-paeoniflorin complex appeared to occupy a lesser phase area with PCA1-62.356% and PCA2-37.644% (**Figure 19C**) compared to the AChE-silychrystin complex, which occupied the maximum area with PCA1-71.75% and PCA2-28.25% (**Figure 19D**).

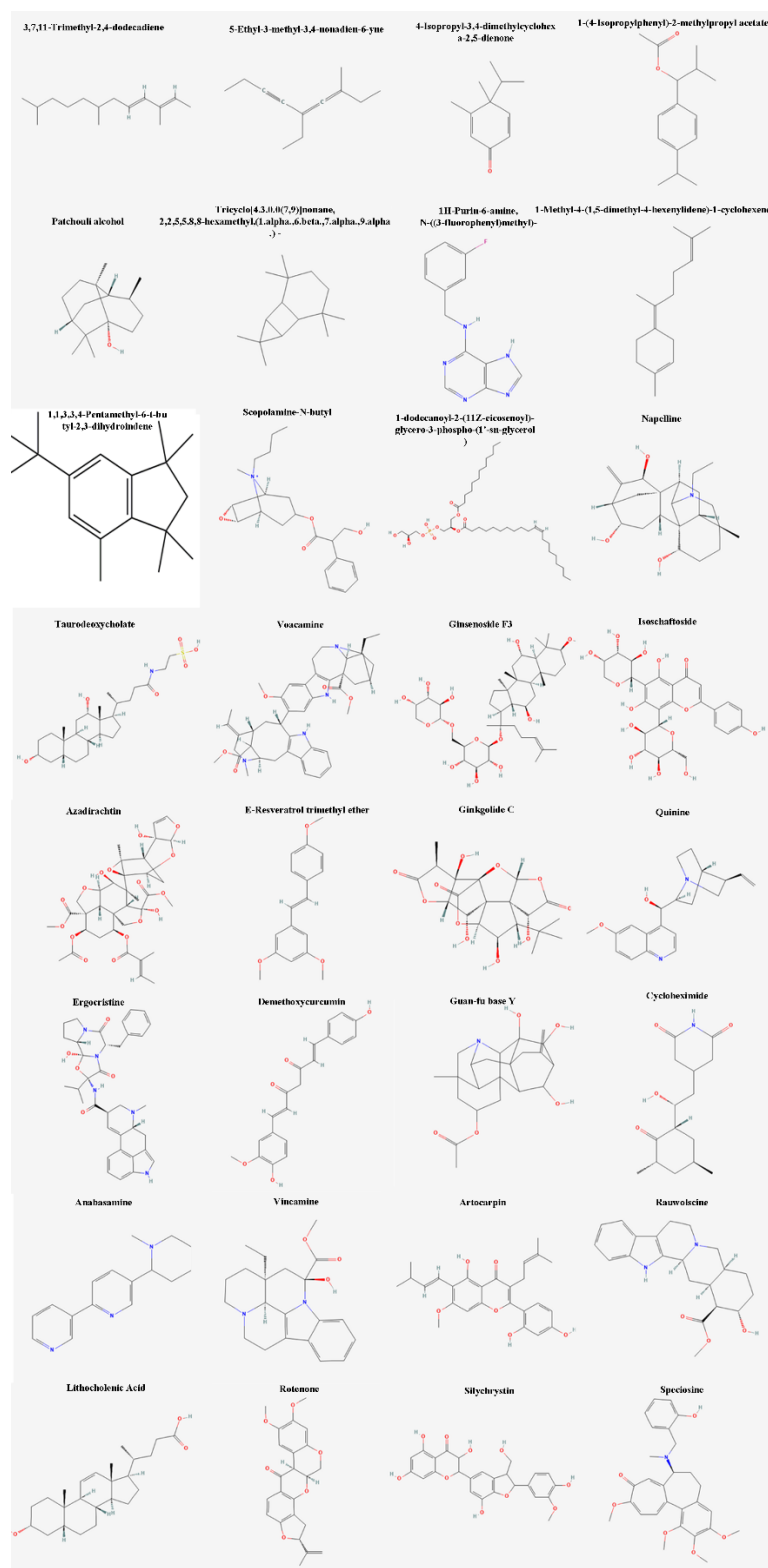


Figure 6. 2D structures of phytocompounds, found in methanolic extract of *Parkia timoriana* seed pods, used as ligands for molecular docking studies against BACE1 and AChE.

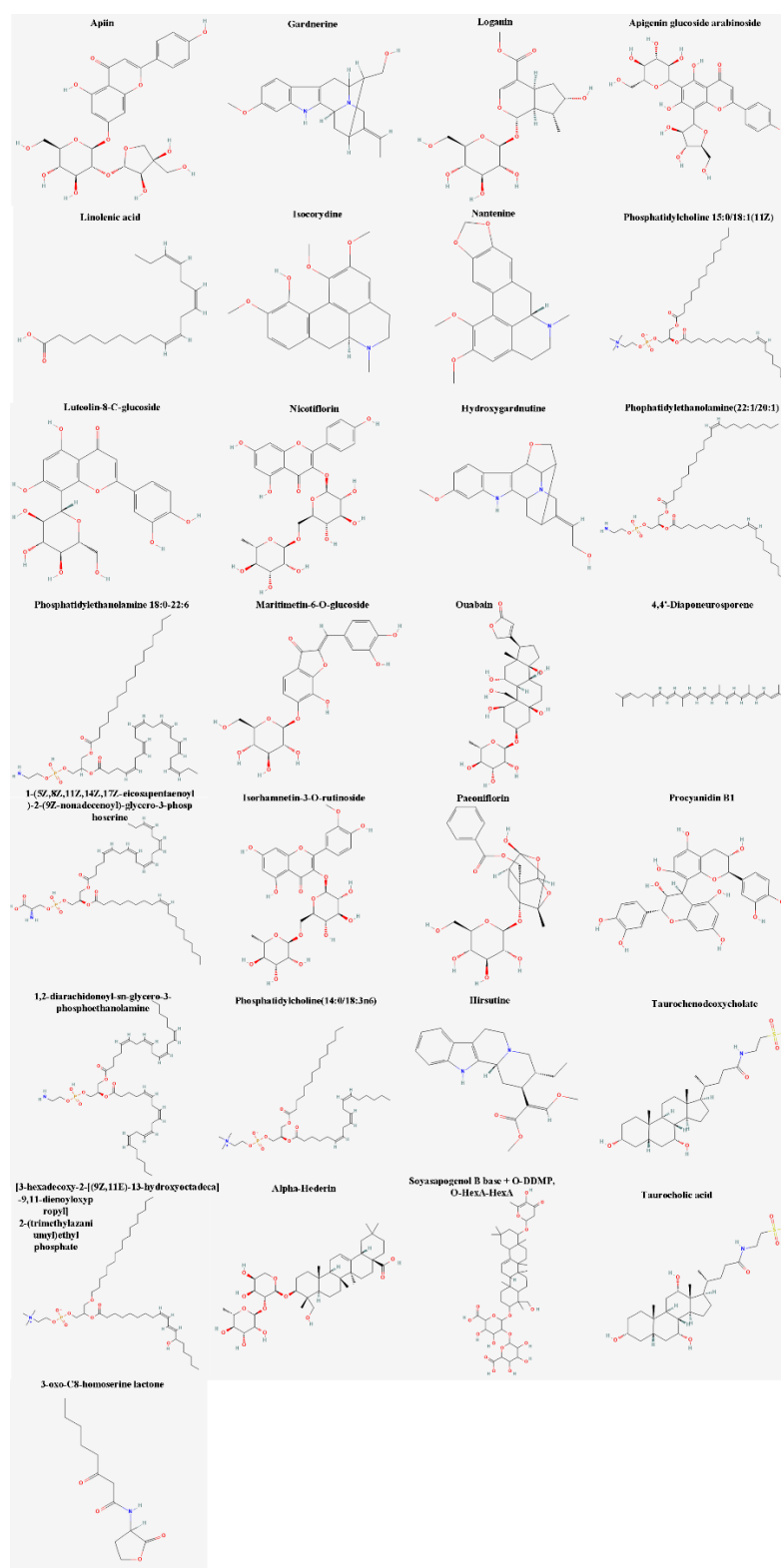


Figure 7. 2D structures of phytocompounds, found in methanolic extract of *Parkia timoriana* seed pods, used as ligands for molecular docking studies against BACE1 and AChE.

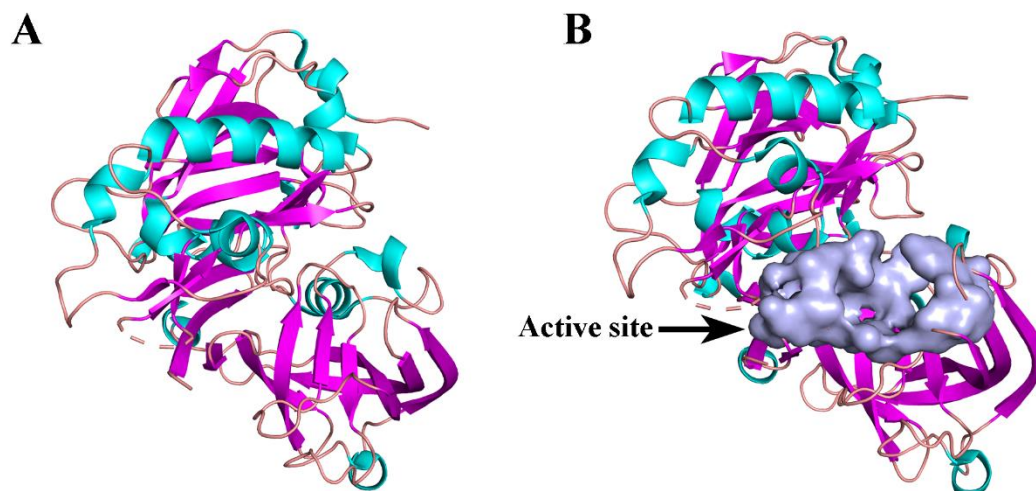


Figure 8. Preparation of the target receptor (BACE1), and identification of its active site for molecular docking experiments. (A) The BACE1 receptor has been prepared for docking using UCSF Chimera software. This involved removing the multiple chains, co-crystallized ligand, metal ions, and water molecules from the target receptor. Additionally, polar hydrogen atoms and partial charges were added to the receptor. The truncated side chains were repaired, and Gasteiger charges were added using the Dock Prep function of the software. (B) The fpocket software was used to predict the active site of the BACE1. The colour grey indicates the BACE1's active site.

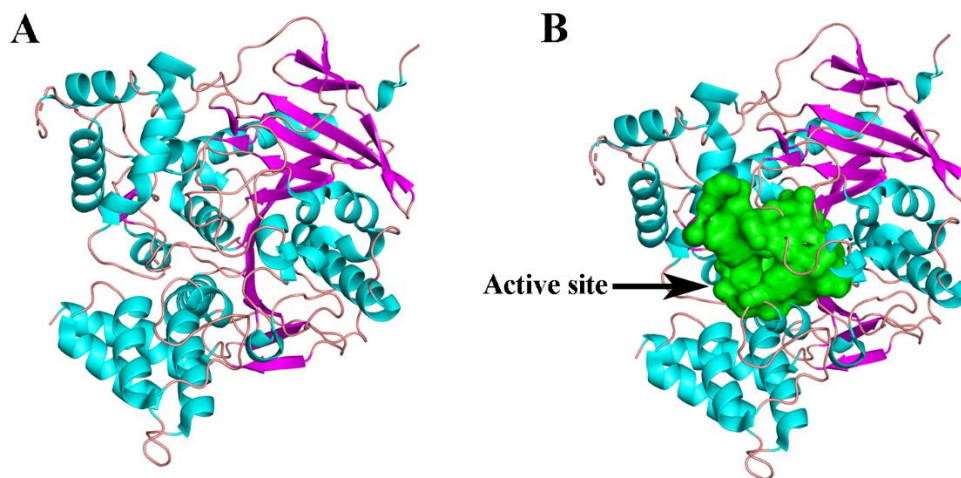


Figure 9. Preparation of the target receptor (AChE), and identification of its active site for molecular docking experiments. (A) The AChE receptor has been prepared for docking using UCSF Chimera software. This involved removing the multiple chains, co-crystallised ligand, metal ions, and water molecules from the target receptor. Additionally, polar hydrogen atoms and partial charges were added to the receptor. The truncated side chains were repaired, and Gasteiger charges were added using the Dock Prep function of the software. (B) The fpocket software was used to predict the active site of the AChE. The colour green indicates the AChE's active site.

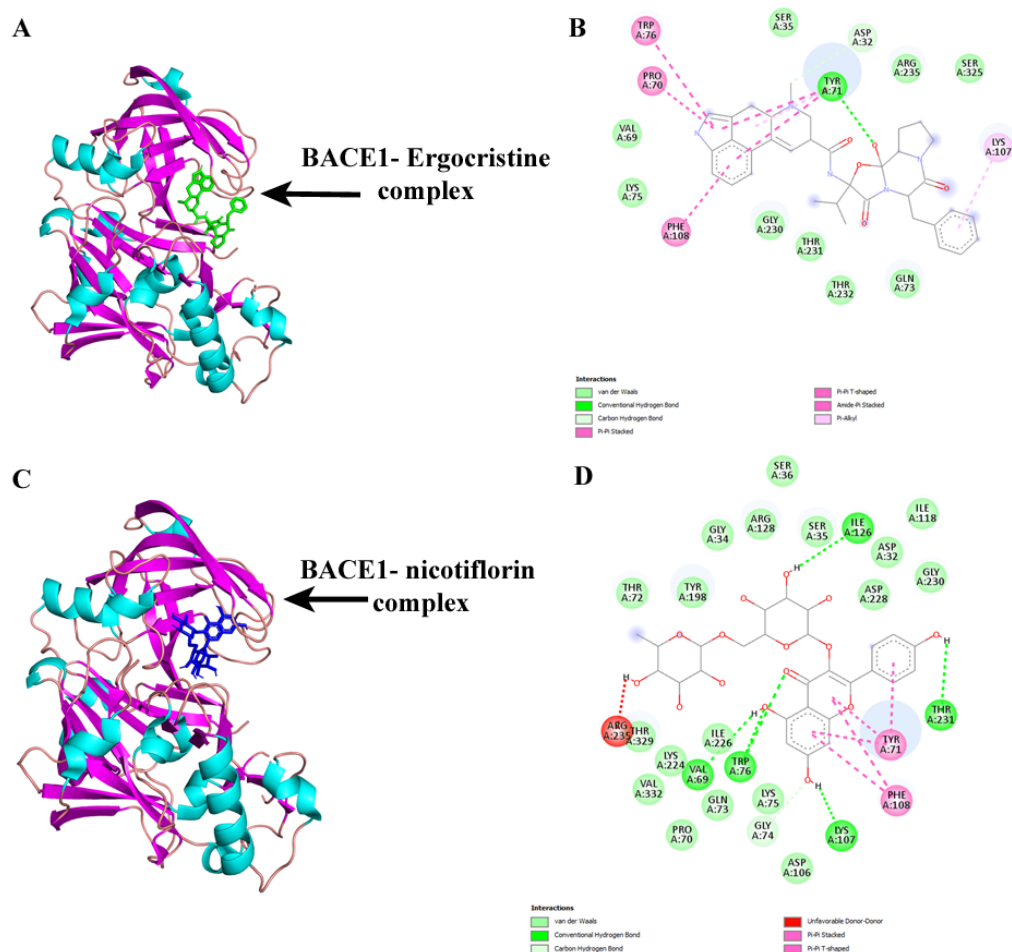


Figure 10. 2D (two-dimensional) and 3D (three-dimensional) docking poses demonstrate the interactions between the top-hit putative bioactive phytochemicals (ligands) from *Parkia timoriana* and the residues of BACE1's active site. (A, B) The binding affinity of BACE1-ergocristine complex is -10.3 kcal/mol. (C, D) The binding affinity of BACE1-nicotiflorin complex is -10.2 kcal/mol.

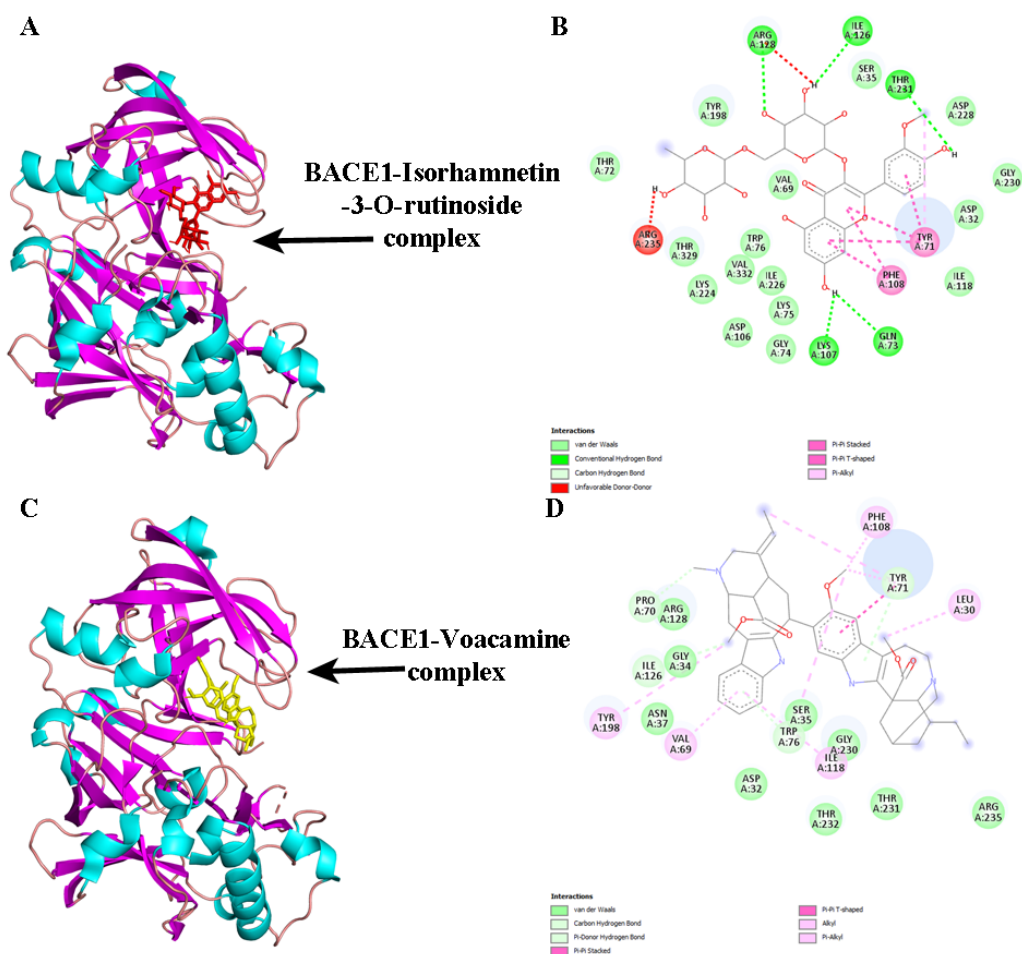


Figure 11. 2D (two-dimensional) and 3D (three-dimensional) docking poses demonstrate the interactions between the top-hit putative bioactive phytochemicals (ligands) from *Parkia timoriana* and the residues of BACE1's active site. (A, B) The binding affinity of BACE1-isorhamnetin -3-O-rutinoside complex is -10.1 kcal/mol. (C, D) The binding affinity of BACE1-voacamine complex is -10.1 kcal/mol.

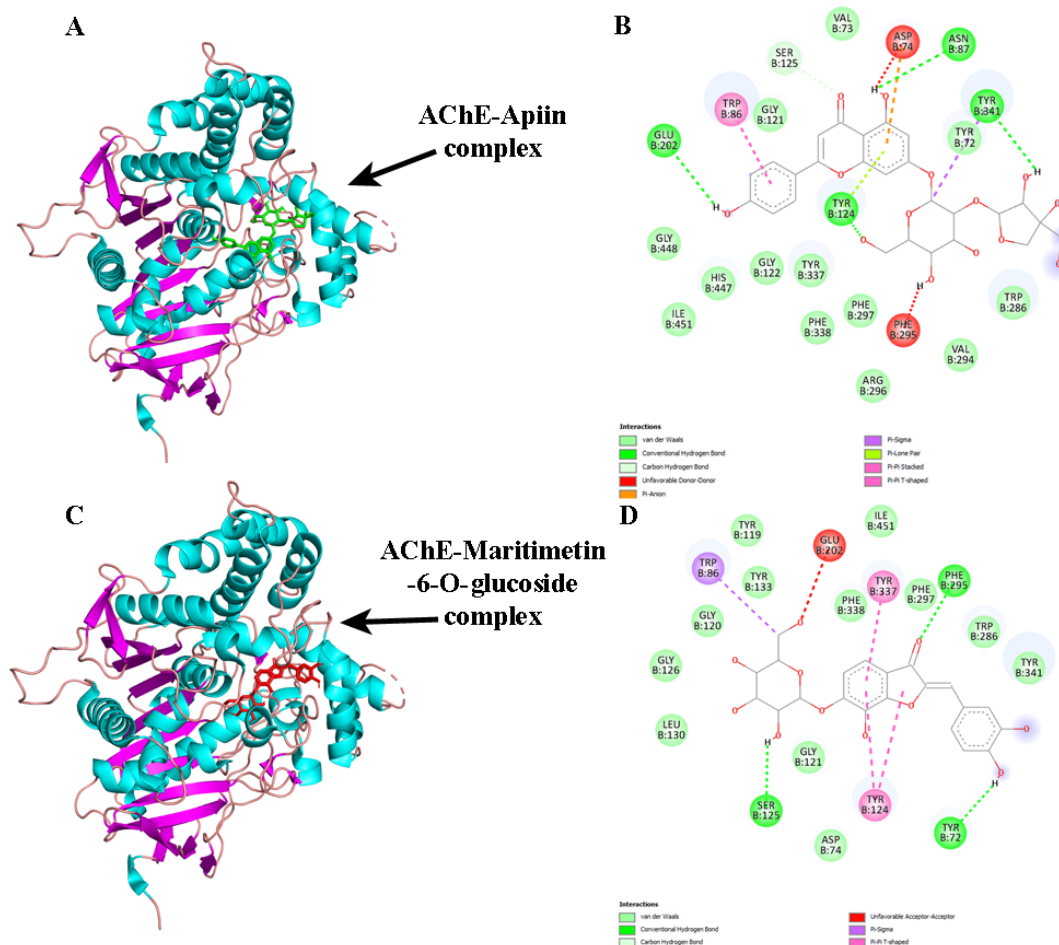


Figure 12. 2D (two-dimensional) and 3D (three-dimensional) docking poses demonstrate the interactions between the top-hit putative bioactive phytocompounds (ligands) from *Parkia timoriana* and the residues of AChE's active site. (A, B) The binding affinity of AChE-apiin complex is -10.3 kcal/mol. (C, D) The binding affinity of AChE-maritimetin-6-O-glucoside complex is -10.3 kcal/mol.

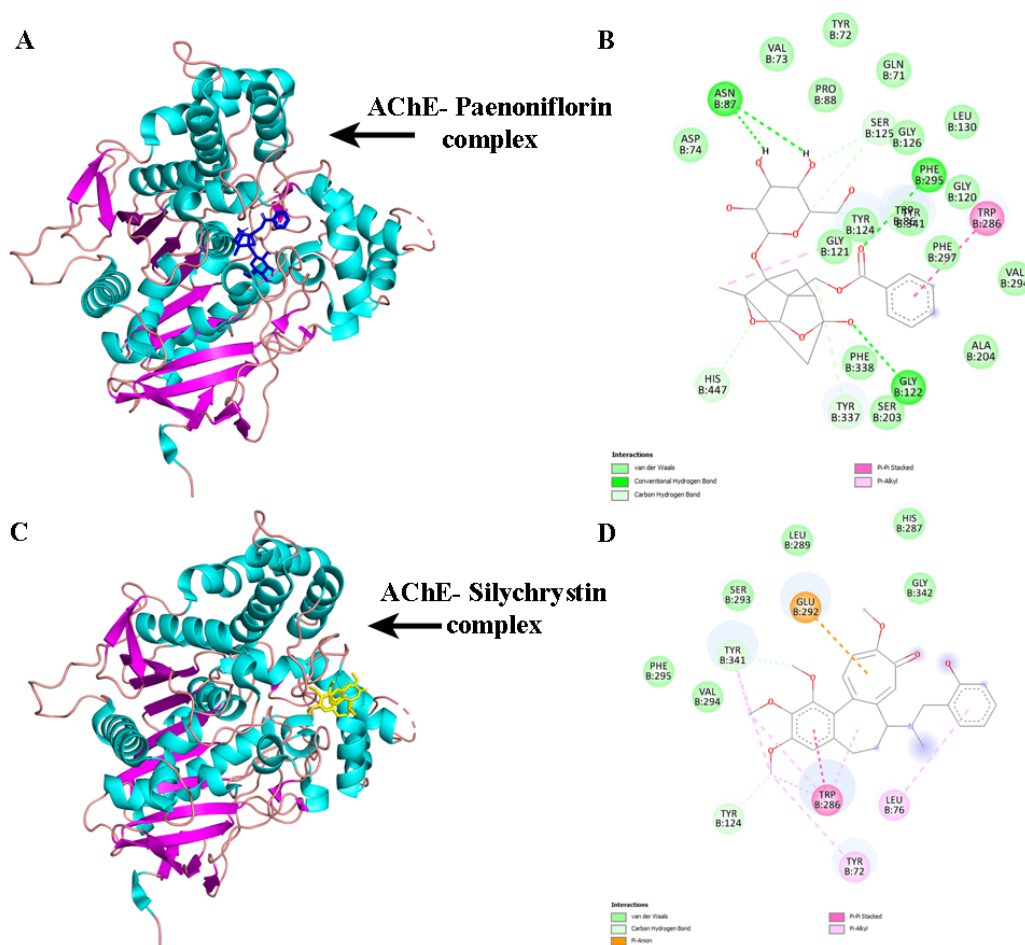


Figure 13. 2D (two-dimensional) and 3D (three-dimensional) docking poses demonstrate the interactions between the top-hit putative bioactive phytochemicals (ligands) from *Parkia timoriana* and the residues of AChE's active site. (A, B) The binding affinity of AChE-paenoniflorin complex is -10.2 kcal/mol. (C, D) The binding affinity of AChE-silychrystin complex is -9.8 kcal/mol.

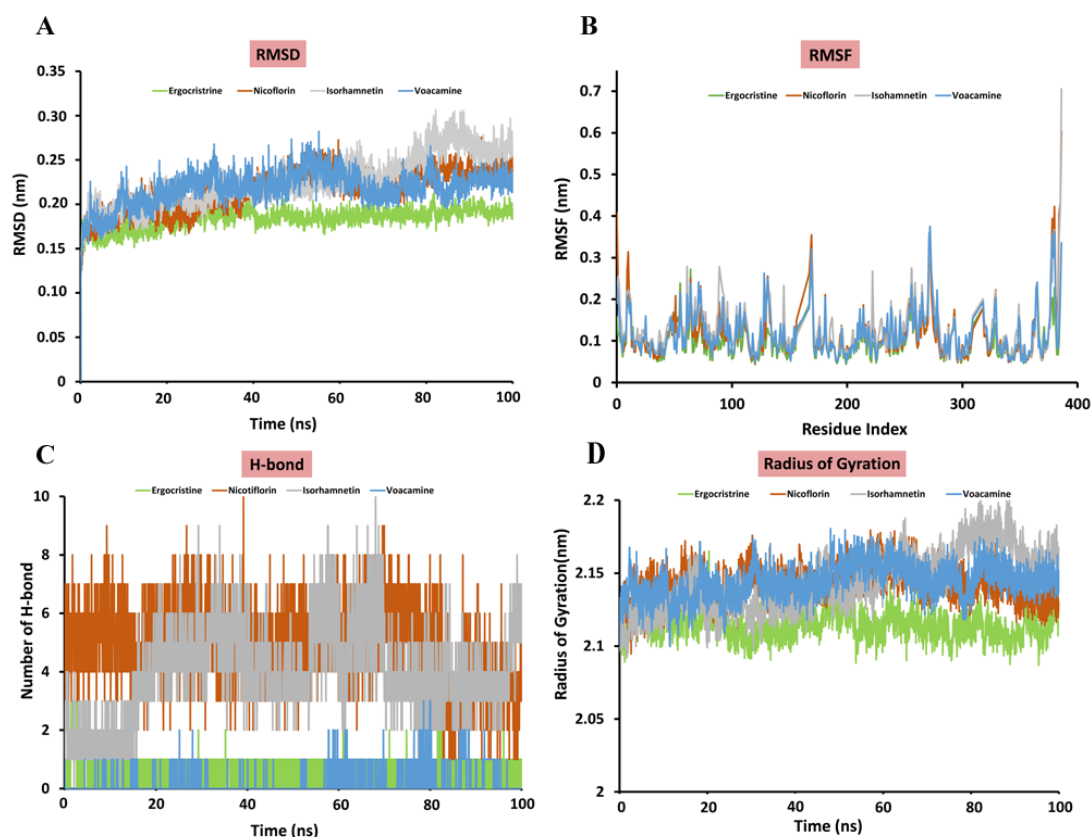


Figure 14. Evaluation of the compactness and stability of the docked complex (including BACE1-ergocristine, BACE1-nicotiflorin, BACE1-isorhamnetin-3-O-rutinoside, and BACE1-voacamine) by computing the deviation as a function of residue index and time from 100 ns of molecular dynamics (MD) simulation. (A) Stability of the receptor-ligand complex (BACE1-ergocristine, BACE1-nicotiflorin, BACE1-isorhamnetin -3-O-rutinoside, and BACE1-voacamine) throughout the 100 ns MD simulation was shown by the root-mean square deviation (RMSD). (B) An analysis of the root mean square fluctuation (RMSF) revealed that the ligands (ergocristine, nicotiflorin, isorhamnetin-3-O-rutinoside, and voacamine) interacted with comparable residues of BACE1. (C) The number of hydrogen bonds established by the docked complex (BACE1-ergocristine, BACE1-nicotiflorin, BACE1-isorhamnetin -3-O-rutinoside, and BACE1-voacamine) throughout the 100 ns simulation, showing that BACE1-nicotiflorin complex creates the highest degree of stability with respect to hydrogen bond. (D) The measurement of the radius of gyration (Rg) reveals that the protein structure of BACE1 is compacted by each of the ligand (ergocristine, nicotiflorin, isorhamnetin-3-O-rutinoside, and voacamine).

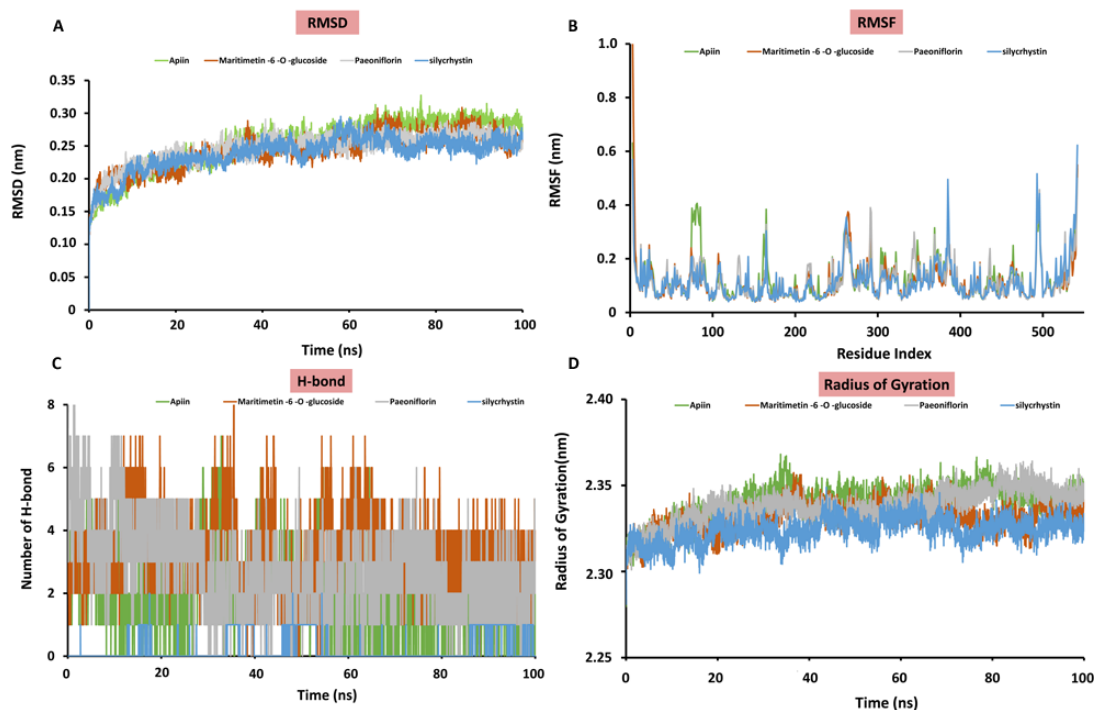


Figure 15. Evaluation of the compactness and stability of the docked complex (including AChE-apiin, AChE-maritimetin-6-O-glucoside, AChE-paenoniflorin, and AChE-silychrystin) by computing the deviation as a function of residue index and time from 100 ns of molecular dynamics (MD) simulation. (A) Stability of the receptor-ligand complex (AChE-apiin, AChE-maritimetin-6-O-glucoside, AChE-paenoniflorin, and AChE-silychrystin) throughout the 100 ns MD simulation was shown by the root-mean square deviation (RMSD). (B) An analysis of the root mean square fluctuation (RMSF) revealed that the ligands (apiin, maritimetin-6-O-glucoside, paenoniflorin, and silychrystin) interacted with comparable residues of AChE. (C) The number of hydrogen bonds established by the docked complex (AChE-apiin, AChE-maritimetin-6-O-glucoside, AChE-paenoniflorin, and AChE-silychrystin) throughout the 100 ns simulation, showing that AChE-maritimetin-6-O-glucoside complex creates the highest degree of stability with respect to hydrogen bond. (D) The measurement of the radius of gyration (Rg) reveals that the protein structure of AChE is compacted by each of the ligand (apiin, maritimetin-6-O-glucoside, paenoniflorin, and silychrystin).

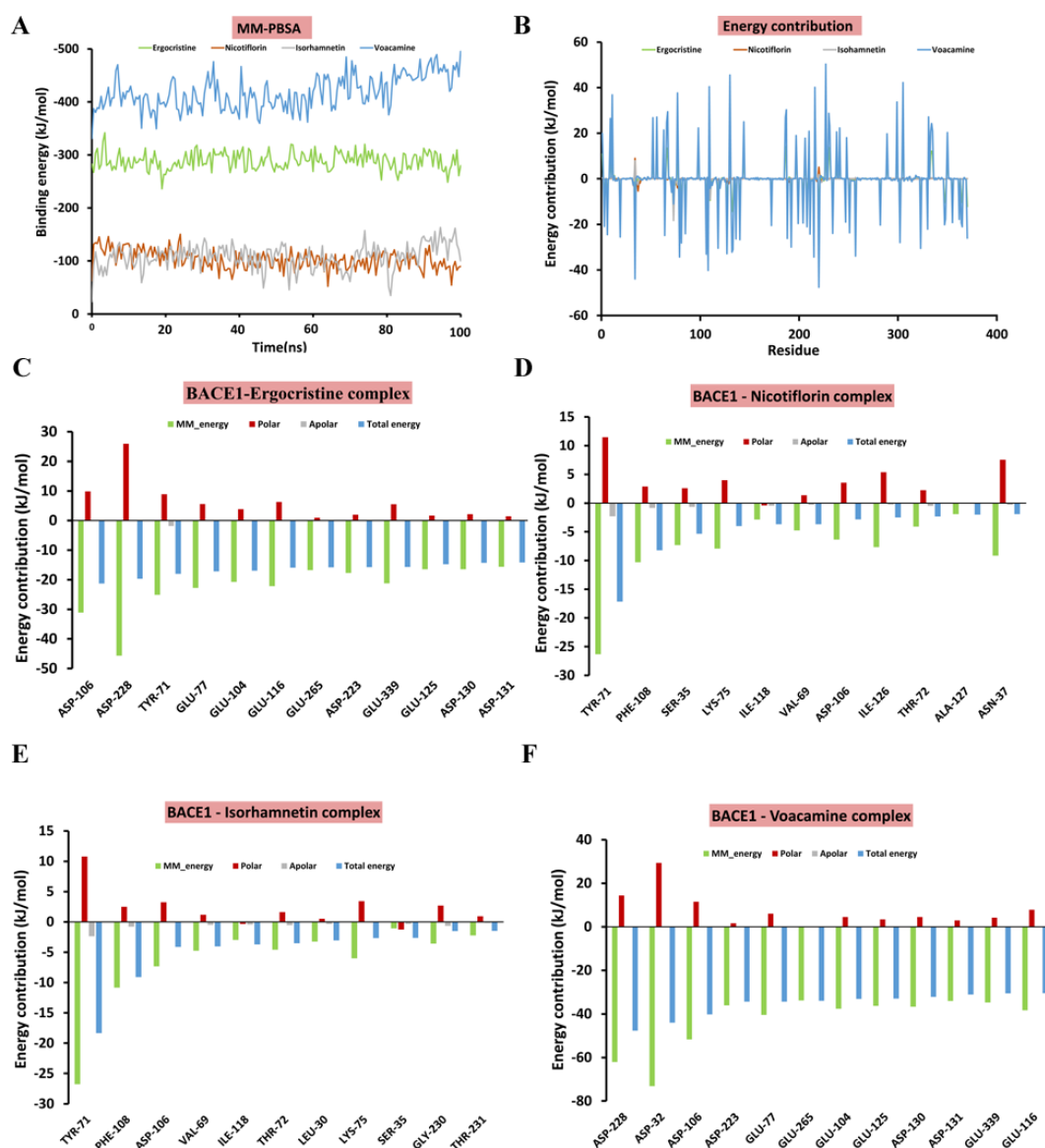


Figure 16. Molecular mechanics Poisson-Boltzmann surface area (MMPBSA) analysis for calculating the binding free energy of the receptor-ligand complex). (A) The binding free energy (kJ/mol) of the receptor-ligand complex (BACE1-ergocristine, BACE1-nicotiflorin, BACE1-isorhamnetin-3-O-rutinoside, and BACE1-voacamine) for the 100 ns of MD simulation trajectories, showing BACE1-voacamine complex as the strongest binding energy. (B) MMPBSA analysis revealed that comparable residues of BACE1 are implicated in ligand binding (ergocristine, nicotiflorin, isorhamnetin-3-O-rutinoside, and voacamine) by residue-wise breakdown of binding free energy. (C, D, E, and F) The individual residues of BACE1 contributing the highest energy when bound to the ligand (ergocristine, nicotiflorin,

isorhamnetin-3-O-rutinoside, and voacamine, respectively). The breakdown of the binding free energy from MMPBSA analysis (van der Waals, electrostatic, nonpolar solvation energy, and polar solvation) is also displayed. A positive value destabilises the complex, while a negative value implies the formation of a stable complex.

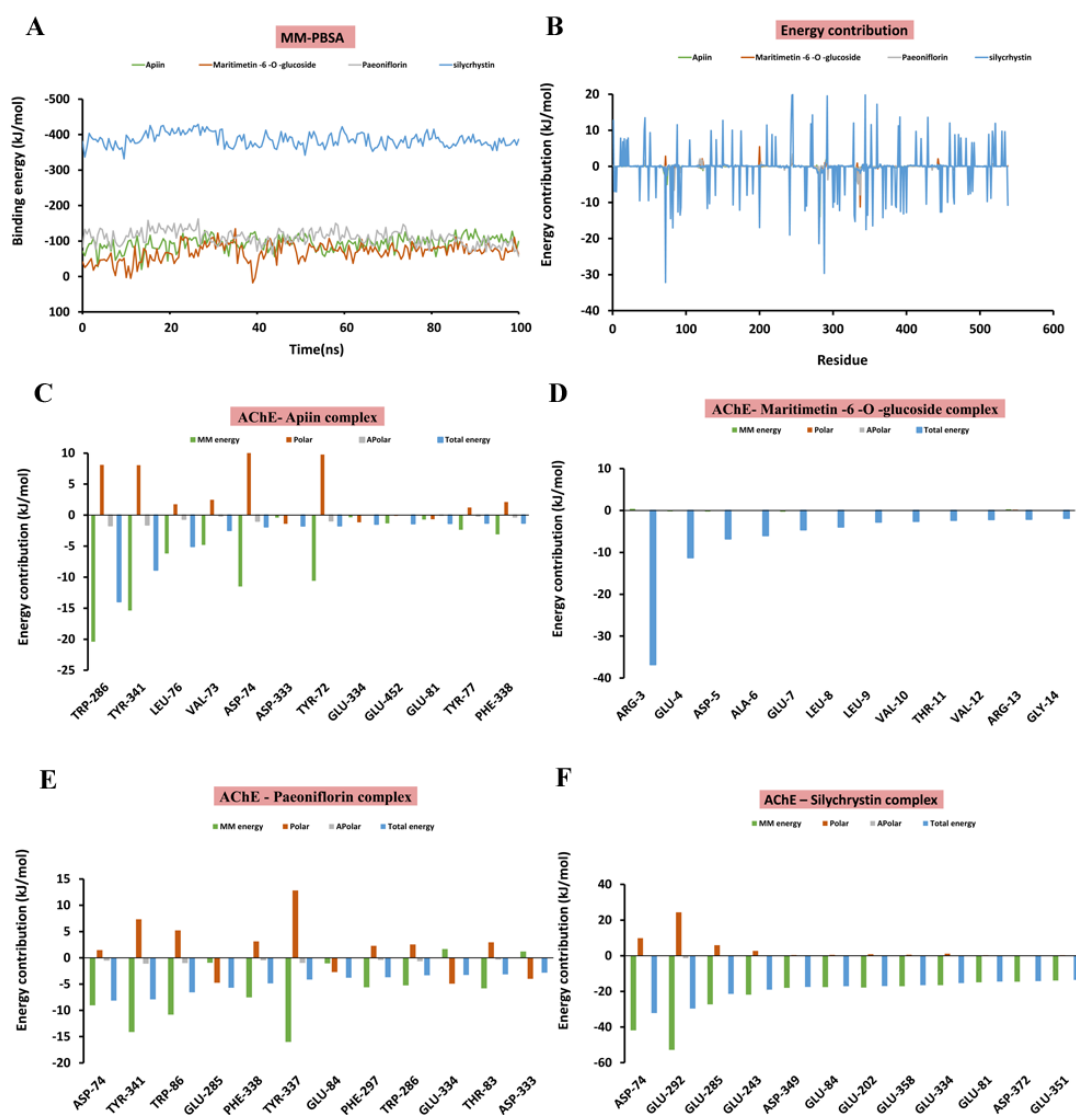


Figure 17. Molecular mechanics Poisson-Boltzmann surface area (MMPBSA) analysis for calculating the binding free energy of the receptor-ligand complex). (A) The binding free energy (kJ/mol) of the receptor-ligand complex (AChE-apiin, AChE-maritimetin-6-O-glucoside, AChE-paenoniflorin, and AChE-silychrystin) for the 100 ns of MD simulation trajectories, showing AChE-silychrystin complex as the strongest binding energy. (B) MMPBSA analysis revealed that comparable residues of AChE are implicated in ligand binding (apiin, maritimetin-6-O-glucoside, paenoniflorin, and silychrystin) by residue-wise breakdown of binding free energy. (C, D, E, and F) The individual residues of AChE contributing the highest energy when bound to the ligand (apiin, maritimetin-6-O-glucoside, paenoniflorin, and silychrystin, respectively). The

breakdown of the binding free energy from MMPBSA analysis (van der Waals, electrostatic, nonpolar solvation energy, and polar solvation) is also displayed. A positive value destabilises the complex, while a negative value implies the formation of a stable complex.

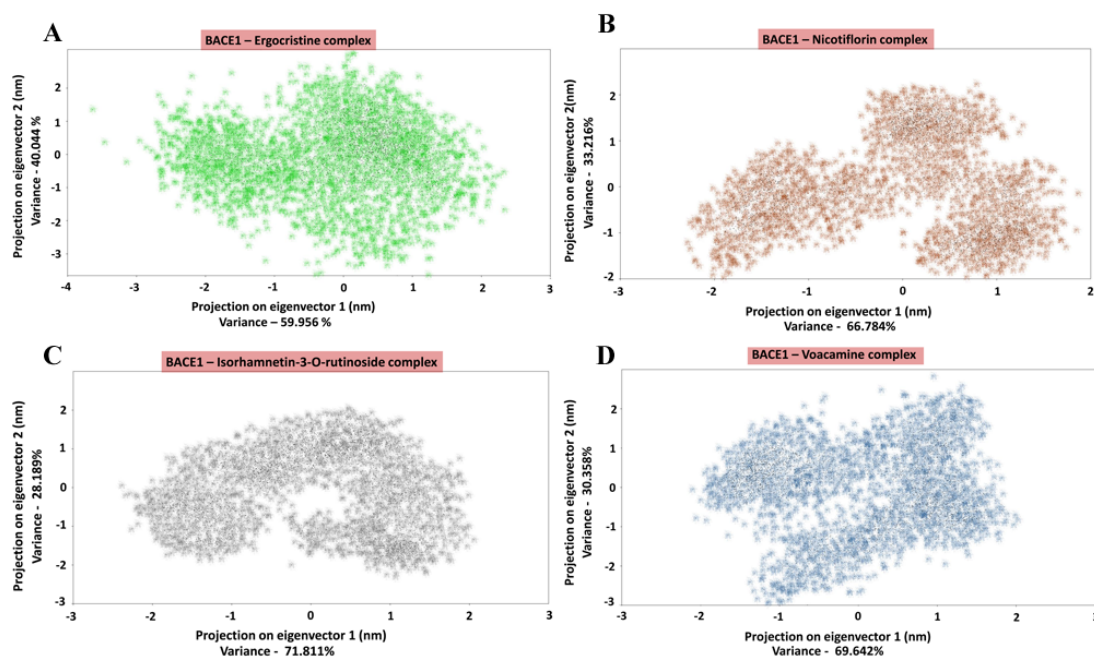


Figure 18. Scatter plots derived from PCA (Principal Component Analysis) display the displacement of alpha carbon ($C\alpha$) atoms along the first and second eigenvectors of receptor-ligand complex. (A) BACE1-ergocristine. (B) BACE1-nicotiflorin. (C) BACE1-isorhamnetin-3-O-rutinoside. (D) BACE1-voacamine. These plots indicate that voacamine restricts the collective motion of the BACE1 receptor to a greater extent compared to the other compounds.

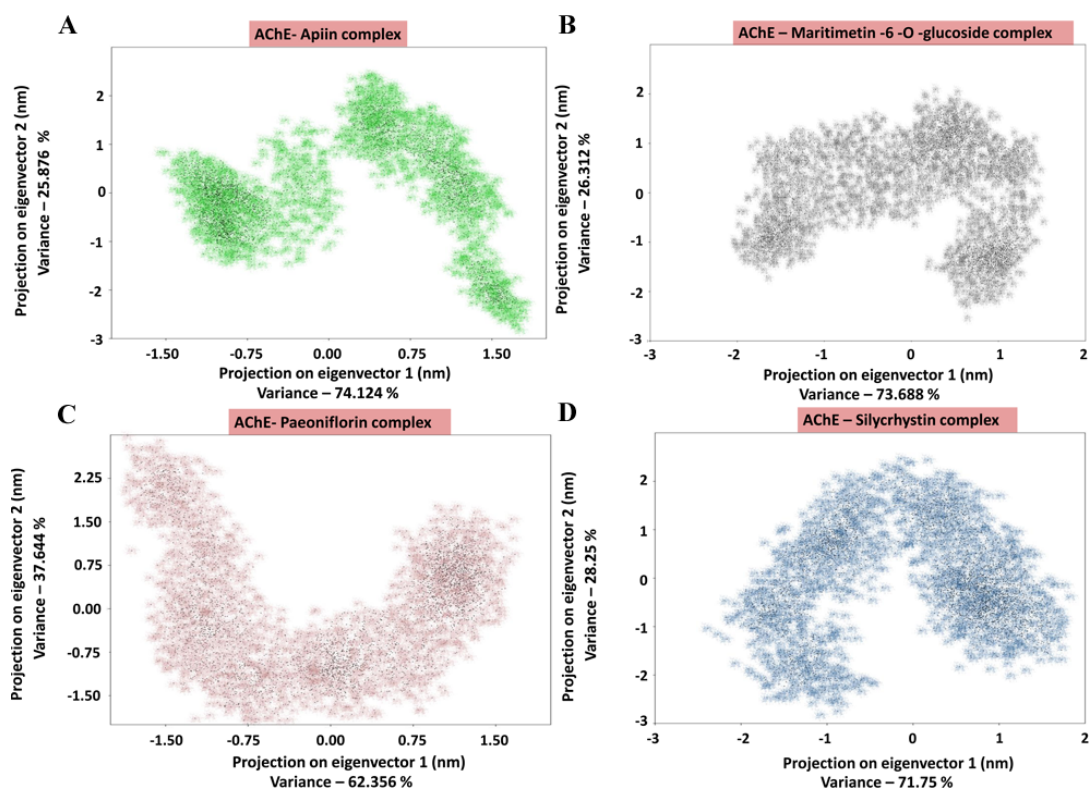


Figure 19. Scatter plots derived from PCA (Principal Component Analysis) display the displacement of alpha carbon ($C\alpha$) atoms along the first and second eigenvectors of receptor-ligand complex. (A) AChE-apiin. (B) AChE-maritimetin-6-O-glucoside. (C) AChE-paenoniflorin. (D) AChE-silychrystin. These plots indicate that maritimetin-6-O-glucoside restricts the collective motion of the AChE receptor to a greater extent compared to the other compounds.

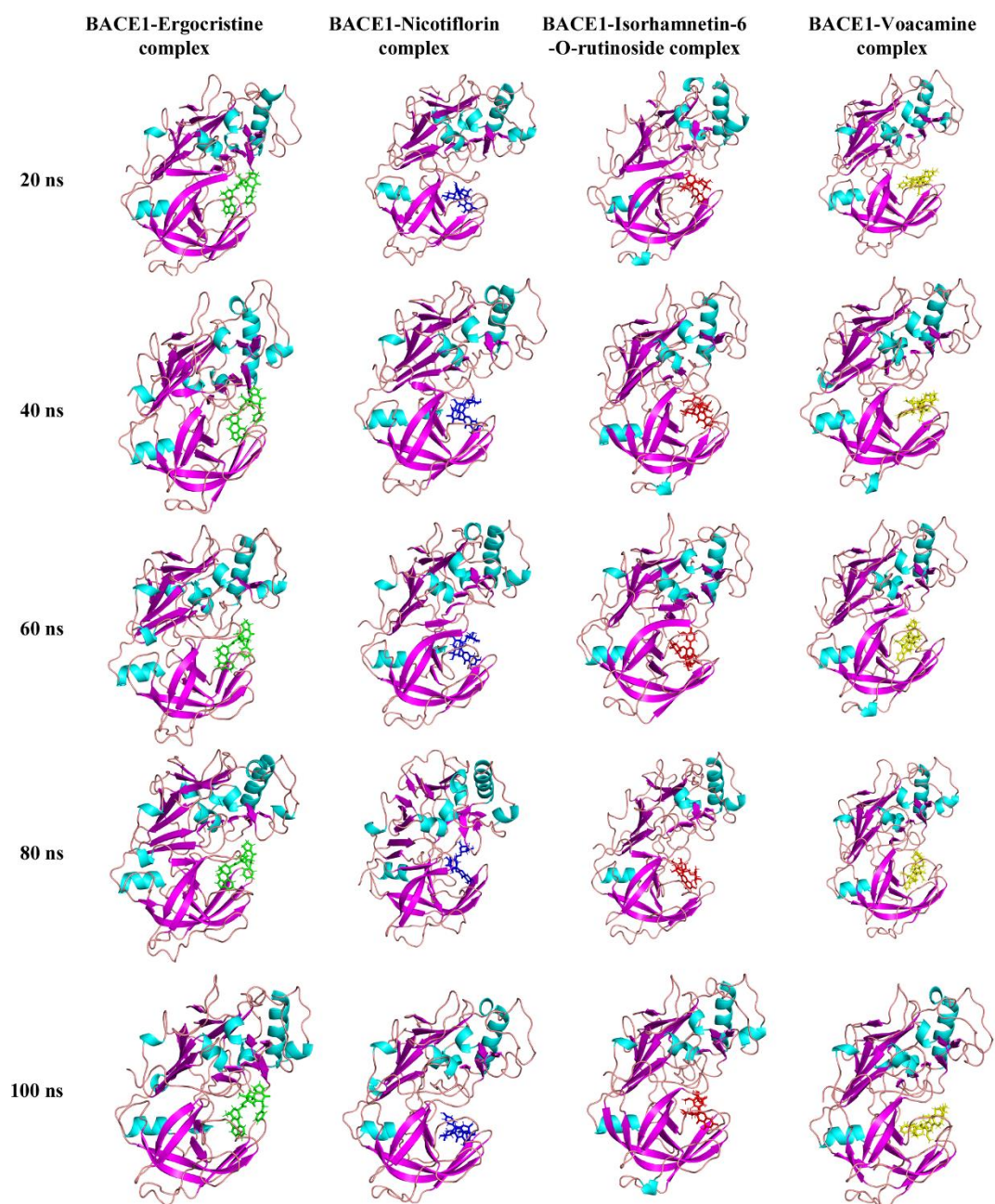


Figure 20. Snapshot images depict the motion of top hit ligands inside the protein binding site of BACE1 at 20 ns intervals throughout a 100 ns period of molecular dynamics simulation.

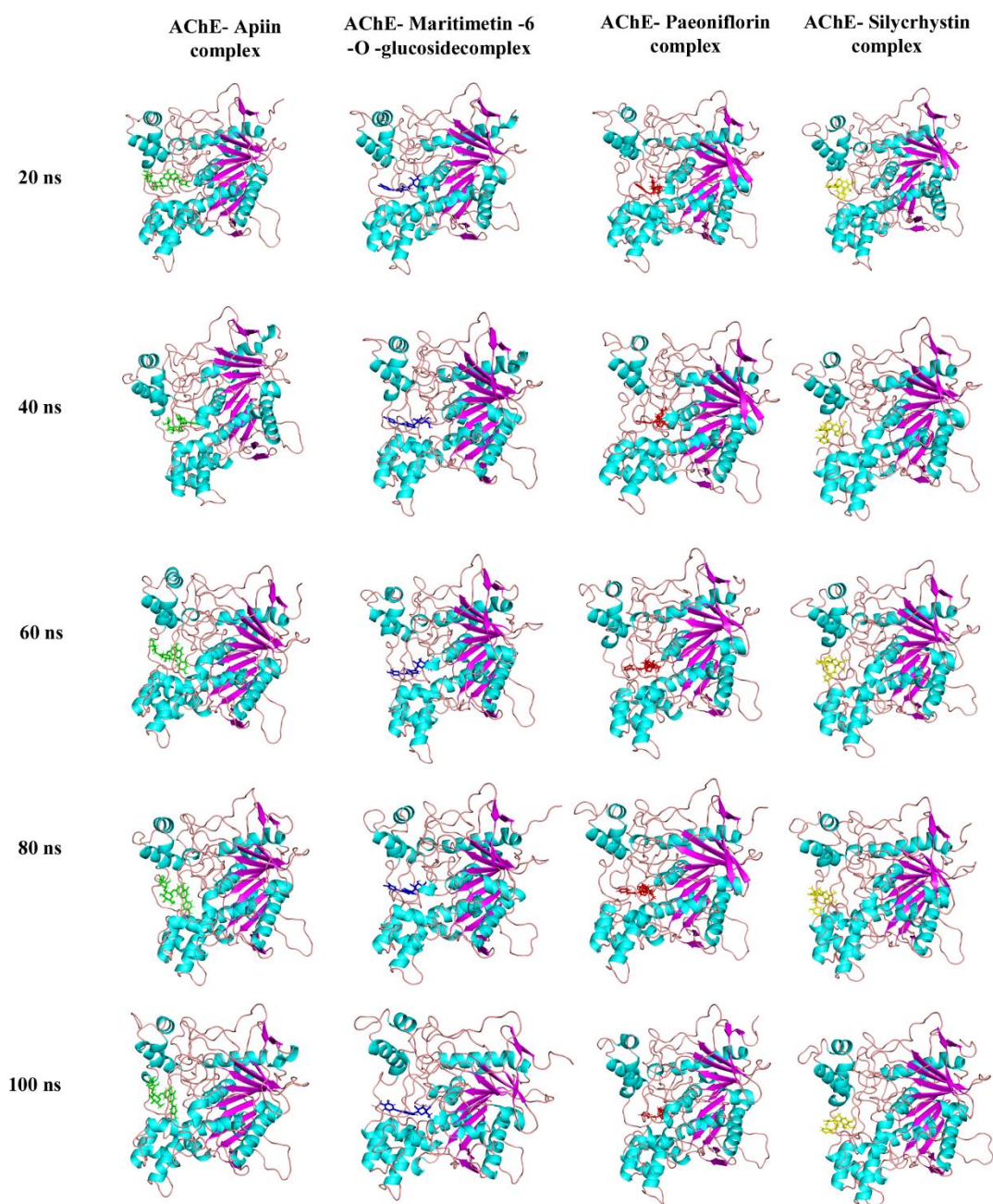


Figure 21. Snapshot images depict the motion of top hit ligands inside the protein binding site of AChE at 20 ns intervals throughout a 100 ns period of molecular dynamics simulation.

Table 6. Phytochemicals, found in methanolic extract of *Parkia timoriana* seed pods, used as ligands for molecular docking analysis against BACE1 and AChE protein receptors.

Sl. no.	Compound	Formula	Molecular weight	Compound ID	SMILES
1.	3,7,11-Trimethyl-2,4-dodecadiene	C ₁₅ H ₂₈	208.38	21599893	<chem>CC=C(C)C=CCC(C)CCCC(C)C</chem>
2.	5-Ethyl-3-methyl-3,4-nonadien-6-yne	C ₁₂ H ₁₈	162.27	535138	<chem>CCC#CC(=C=C(C)CC)CC</chem>
3.	4-Isopropyl-3,4-dimethylcyclohexa-2,5-dienone	C ₁₁ H ₁₆ O	164.24	578926	<chem>CC1=CC(=O)C=CC1(C)C(C)C</chem>
4.	1-(4-Isopropylphenyl)-2-methylpropyl acetate	C ₁₅ H ₂₂ O ₂	234.33	154574010	<chem>CC(C)C1=CC=C(C=C1)C(C(C)C)OC(=O)C</chem>
5.	Patchouli alcohol	C ₁₅ H ₂₆ O	222.37	10955174	<chem>CC1CCC2(C(C3CCC2(C1C3)C)(C)C)O</chem>
6.	Tricyclo[4.3.0.0(7,9)]nonane, 2,2,5,5,8,8-hexamethyl-, (1.alpha.,6.beta.,7.alpha.,9.alpha.)-	C ₁₅ H ₂₆	206.37	549738	<chem>CC1(CCC(C2C1C3C2C3(C)C)(C)C)C</chem>
7.	1H-Purin-6-amine, N-((3-fluorophenyl)methyl)-	C ₁₂ H ₁₀ FN ₅	243.24	6455415	<chem>C1=CC(=CC(=C1)F)CNC2=NC=NC3=C2N=C=N3</chem>
8.	Bisabolene	C ₁₅ H ₂₄	204.35	3033866	<chem>CC1=CCC(=C(C)CCC=C(C)C)CC1</chem>
9.	1,1,3,3,4-Pentamethyl-6-t-butyl-2,3-dihydroindene	C ₁₈ H ₂₈	244.42	1FVnmyl G7Pj	<chem>CC1=CC(C(C)(C)C)=CC2=C1C(C)(CC(C)2)C</chem>
10.	Scopolamine-N-butyl	C ₂₁ H ₃₀ NO ₄ ⁺	360.5	9004	<chem>CCCC[N+](C2CC(C(C1C3C2O3)OC(=O)C(CO)C4=CC=CC=C4)C</chem>
11.	1-dodecanoyl-2-(11Z-eicosenoyl)-glycero-3-phospho-(1'-sn-glycerol)	C ₃₈ H ₇₃ O ₁₀ P	721	52926324	<chem>CCCCCCCCCCCC(=O)OCC(COP(=O)(O)OCC(CO)O)OC(=O)CCCCCCCCCCC=CCCCCCCCC</chem>
12.	Napelline	C ₂₂ H ₃₃ NO ₃	359.5	441749	<chem>CCN1CC2(CCC(C34C2CC(C31)C56C4CC(C(C5)C(=C)C6O)O)O)C</chem>
13.	Taurodeoxycholate	C ₂₆ H ₄₅ NO ₆ S	499.7	2733768	<chem>CC(CCC(=O)NCCS(=O)(=O)O)C1CCC2C1(C(C3C2CCC4C3(CCC(C4)O)C)O)C</chem>
14.	Voacamine	C ₄₃ H ₅₂ N ₄ O ₅	704.9	11953931	<chem>CCC1CC2CC3(C1N(C2)CCC4=C3NC5=CC(=C(C=C45)OC)C6CC7C(C(C8=C6NC9=CC=CC=C89)N(CC7=CC)C)C(=O)OC)C(=O)OC</chem>

15.	Ginsenoside F3	C ₄₁ H ₇₀ O ₁₃	771.0	46887678	<chem>CC(=CCCC(C)(C1CCC2(C1C(CC3C2(CC(C4C3(CCC(C4(C(C)O)C)O)C)O)C)OC5C(C(C(C(O5)COC6C(C(C(CO6)O)O)O)O)O)O)C</chem>
16.	Isoschaftoside	C ₂₆ H ₂₈ O ₁₄	564.5	3084995	<chem>C1C(C(C(C(O1)C2=C(C(=C3C(=C2O)C(=O)C=C(O3)C4=CC=C(C=C4)O)C5C(C(C(C(O5)CO)O)O)O)O)O)O)O</chem>
17.	Azadirachtin	C ₃₅ H ₄₄ O ₁₆	720.7	5281303	<chem>CC=C(C)C(=O)OC1CC(C2(COC3C2C14COC4C(C3O)(C)C56C7CC(C5(O6)C)C8(C=CO8O7)O)(C(=O)OC)O)C(=O)OC(=O)C</chem>
18.	E-Resveratrol trimethyl ether	C ₁₇ H ₁₈ O ₃	270.32	5388063	<chem>COC1=CC=C(C=C1)C=CC2=CC(=CC(=C2)OC)OC</chem>
19.	Ginkgolide C	C ₂₀ H ₂₄ O ₁₁	440.4	24721502	<chem>CC1C(=O)OC2C1(C34C(=O)OC5C3(C2O)C6(C(C5O)C(C)(C)C)C(C(=O)OC6O4)O)O</chem>
20.	Quinine	C ₂₀ H ₂₄ N ₂ O ₂	324.4	3034034	<chem>COC1=CC2=C(C=CN=C2C=C1)C(C3CC4CCN3CC4C=C)O</chem>
21.	Ergocristine	C ₃₅ H ₃₉ N ₅ O ₅	609.7	31116	<chem>CC(C)C1(C(=O)N2C(C(=O)N3CCCC3C2(O1)O)CC4=CC=CC=C4)NC(=O)C5CN(C6CC7=CNC8=CC=CC(=C78)C6=C5)C</chem>
22.	Demethoxycurcumin	C ₂₀ H ₁₈ O ₅	338.4	5469424	<chem>COC1=C(C=CC(=C1)C=CC(=O)CC(=O)C=CC2=CC=C(C=C2)O)O</chem>
23.	Guan-fu base Y	C ₂₂ H ₂₉ NO ₅	387.5	3101182	<chem>CC(=O)OC1CC2(CN3C4C2C5(C1)C3C6(C(C7C(C5C6(C4)CC7=C)O)O)O)C</chem>
24.	Cycloheximide	C ₁₅ H ₂₃ NO ₄	281.35	6197	<chem>CC1CC(C(=O)C(C1)C(CC2CC(=O)NC(=O)C2)O)C</chem>
25.	Anabasamine	C ₁₆ H ₁₉ N ₃	253.34	161313	<chem>CN1CCCCC1C2=CN=C(C=C2)C3=CN=CC=C3</chem>
26.	Vincamine	C ₂₁ H ₂₆ N ₂ O ₃	354.4	15376	<chem>CCC12CCCN3C1C4=C(CC3)C5=CC=CC=C5N4C(C2)(C(=O)OC)O</chem>
27.	Artocarpin	C ₂₆ H ₂₈ O ₆	436.5	5458461	<chem>CC(C)C=CC1=C(C=C2C(=C1O)C(=O)C(=C(O2)C3=C(C=C(C=C3)O)O)CC=C(C)C)OC</chem>

28.	Rauwolscline	C ₂₁ H ₂₆ N ₂ O ₃	354.4	643606	<chem>COC(=O)C1C(CCC2C1CC3C4=C(CCN3C2)C5=CC=CC=C5N4)O</chem>
29.	Lithocholenic Acid	C ₂₄ H ₃₈ O ₃	374.6	5283972	<chem>CC(CCC(=O)O)C1CCC2C1(C=CC3C2CCC4C3(CCC(C4)O)C)C</chem>
30.	Rotenone	C ₂₃ H ₂₂ O ₆	394.4	6758	<chem>CC(=C)C1CC2=C(O1)C=CC3=C2OC4COC5=CC(=C(C=C5C4C3=O)OC)OC</chem>
31.	Silychrystin	C ₂₅ H ₂₂ O ₁₀	482.4	4481797	<chem>COC1=C(C=CC(=C1)C2C(C3=C(O2)C(=C(C(=C3)C4C(C(=O)C5=C(C=C(C=C5O4)O)O)O)CO)O</chem>
32.	Speciosine	C ₂₈ H ₃₁ NO ₆	477.5	330188	<chem>CN(CC1=CC=CC=C1O)C2CCC3=CC(=C(C(=C3C4=CC=C(C(=O)C=C24)OC)OC)OC</chem>
33.	Apiin	C ₂₆ H ₂₈ O ₁₄	564.5	5280746	<chem>C1C(C(C(O1)OC2C(C(C(OC2OC3=CC(=C4C(=C3)OC(=CC4=O)C5=CC=C(C=C5)O)O)CO)O)O)O)(CO)O</chem>
34.	Gardnerine	C ₂₀ H ₂₄ N ₂ O ₂	324.4	6445140	<chem>CC=C1CN2C3CC1C(C2CC4=C3NC5=C4C=CC(=C5)OC)CO</chem>
35.	Loganin	C ₁₇ H ₂₆ O ₁₀	390.4	87691	<chem>CC1C(CC2C1C(OC=C2C(=O)OC)OC3C(C(C(C(O3)CO)O)O)O)O</chem>
36.	Apigenin glucoside arabinoside	C ₂₆ H ₂₈ O ₁₄	564.5	131750832	<chem>C1=CC(=CC=C1C2=CC(=O)C3=C(C(=C(C(=C3O2)C4C(C(C(O4)CO)O)O)O)C5C(C(C(C(O5)CO)O)O)O)O)O</chem>
37.	Linolenic acid	C ₁₈ H ₃₀ O ₂	278.4	5280934	<chem>CCC=CCC=CCC=CCCCCCCCC(=O)O</chem>
38.	Isocorydine	C ₂₀ H ₂₃ NO ₄	341.4	10143	<chem>CN1CCC2=CC(=C(C3=C2C1CC4=C3C(=C(C=C4)OC)O)OC)OC</chem>
39.	Nantenine	C ₂₀ H ₂₁ NO ₄	339.4	197001	<chem>CN1CCC2=CC(=C(C3=C2C1CC4=CC5=C(C=C43)OCO5)OC)OC</chem>
40.	Phosphatidylcholine 15:0/18:1(11Z)	C ₄₁ H ₈₀ NO ₈ P	746.0	24778662	<chem>CCCCCCCCCCCCCCCC(=O)OCC(COP(=O)([O])OCC[N+](C)(C)C)OC(=O)CCCCCCC</chem> <chem>CCC=CCCCCCC</chem>
41.	Luteolin-8-C-glucoside	C ₂₁ H ₂₀ O ₁₁	448.4	5281675	<chem>C1=CC(=C(C=C1C2=CC(=O)C3=C(O2)C(=C(C=C3O)O)C4C(C(C(C(O4)CO)O)O)O)O)O</chem>

42.	Nicotiflorin	C ₂₇ H ₃₀ O ₁₅	594.5	5318767	CC1C(C(C(C(O1)OCC2C(C(C(C(O2)OC3=C(OC4=CC(=CC(=C4C3=O)O)O)C5=CC=C(C=C5)O)O)O)O)O)O)O
43.	Hydroxygardnutine	C ₂₀ H ₂₂ N ₂ O ₃	338.4	12310668	COC1=CC2=C(C=C1)C3=C(N2)C4CC5C6COC3C6N4CC5=CCO
44.	Phophatidylethanolamine(22:1/20:1)	C ₄₇ H ₉₀ NO ₈ P	828.2	53479865	CCCCCCCCC=CCCCCCCCCCCCC(=O)OCC(COP(=O)(O)OCCN)OC(=O)CCCCCCC=CCCCCCCCC
45.	Phosphatidylethanolamine 18:0-22:6	C ₄₅ H ₇₈ NO ₈ P	792.1	6426737	CCCCCCCCCCCCCCCCCCCC(=O)OCC(COP(=O)(O)OCCN)OC(=O)CCC=CCC=CCC=CCC=CCC=CCC=CCC
46.	Maritimetin-6-O-glucoside	C ₂₁ H ₂₀ O ₁₁	448.4	6450184	C1=CC(=C(C=C1C=C2C(=O)C3=C(O2)C(=C(C=C3)OC4C(C(C(C(O4)CO)O)O)O)O)O)O
47.	Ouabain	C ₂₉ H ₄₄ O ₁₂	584.7	439501	CC1C(C(C(C(O1)OC2CC(C3(C4C(CCC3(C2)O)C5(CCC(C5(CC4O)C)C6=CC(=O)OC6)O)CO)O)O)O)O
48.	4,4'-Diaponeurosporene	C ₃₀ H ₄₂	402.7	6443791	CC(=CCCC(=CC=CC(=CC=CC=C(C)C=CC=C(C)C=CC=C(C)C)C)C)C
49.	1-(5Z,8Z,11Z,14Z,17Z-eicosapentaenoyl)-2-(9Z-nonadecenoyl)-glycero-3-phosphoserine	C ₄₅ H ₇₆ NO ₁₀ P	822.1	52925775	CCCCCCCCC=CCCCCCCCC(=O)OC(CO C(=O)CCCC=CCC=CCC=CCC=CCC=CCC)COP(=O)(O)OCC(C(=O)O)N
50.	Isorhamnetin-3-O-rutinoside	C ₂₈ H ₃₂ O ₁₆	624.5	5481663	CC1C(C(C(C(O1)OCC2C(C(C(C(O2)OC3=C(OC4=CC(=CC(=C4C3=O)O)O)C5=CC(=C(C=C5)O)OC)O)O)O)O)O
51.	Paeoniflorin	C ₂₃ H ₂₈ O ₁₁	480.5	442534	CC12CC3(C4CC1(C4(C(O2)O3)COC(=O)C5=CC=CC=C5)OC6C(C(C(C(O6)CO)O)O)O)O
52.	Procyanidin B1	C ₃₀ H ₂₆ O ₁₂	578.5	11250133	C1C(C(OC2=C1C(=CC(=C2C3C(C(OC4=CC(=CC(=C34)O)O)C5=CC(=C(C=C5)O)O)O)O)O)C6=CC(=C(C=C6)O)O)O

53.	1,2-diarachidonoyl-sn-glycero-3-phosphoethanolamine	C ₄₅ H ₇₄ NO ₈ P	788.0	52924874	CCCCC=CCC=CCC=CCC=CCCC(=O)OCC(COP(=O)(O)OCCN)OC(=O)CCCC=CC=C=CCC=CCC=CCCCC
54.	Phosphatidylcholine(14:0/18:3n6)	C ₄₀ H ₇₄ NO ₈ P	728.0	52922220	CCCCCCCCCCCCC(=O)OCC(COP(=O)([O])OCC[N+](C)(C)C)OC(=O)CCCC=CCC=CCC=CCCCC
55.	Hirsutine	C ₂₂ H ₂₈ N ₂ O ₃	368.5	3037884	CCC1CN2CCC3=C(C2CC1C(=COC)C(=O)OC)NC4=CC=CC=C34
56.	Taurochenodeoxycholate	C ₂₆ H ₄₅ NO ₆ S	499.7	387316	CC(CCC(=O)NCCS(=O)(=O)O)C1CCC2C1(CCC3C2C(CC4C3(CCC(C4)O)C)O)C
57.	[3-hexadecoxy-2-[(9Z,11E)-13-hydroxyoctadeca-9,11-dienyl]oxypropyl] 2-(trimethylazaniumyl)ethyl phosphate	C ₄₂ H ₈₂ NO ₈ P	760.1	134778782	CCCCCCCCCCCCCCCCOCC(COP(=O)([O])OCC[N+](C)(C)C)OC(=O)CCCCCCCC=CC=CC(CCCCC)O
58..	Alpha-Hederin	C ₄₁ H ₆₆ O ₁₂	751.0	73296	CC1C(C(C(C(O1)OC2C(C(COC2OC3CCC4(C(C3(C)CO)CCC5(C4CC=C6C5(CCC7(C6CC(CC7)(C)C)C(=O)O)C)C)O)O)O)O)O)O
59.	Soyasapogenol B base + O-DDMP, O-HexA-HexA	C ₄₈ H ₇₂ O ₁₈	937.1	139292121	CC1=C(C(=O)CC(O1)OC2CC(CC3C2(CCC4(C3=CCC5C4(CCC6C5(CCC(C6(C)CO)OC7C(C(C(C(O7)C(=O)O)O)O)OC8C(C(C(C(O8)C(=O)O)O)O)O)C)C)C)C)C)O
60.	Taurocholic acid	C ₂₆ H ₄₅ NO ₇ S	515.7	6675	CC(CCC(=O)NCCS(=O)(=O)O)C1CCC2C1(C(CC3C2C(CC4C3(CCC(C4)O)C)O)O)C
61.	3-oxo-C8-homoserine lactone	C ₁₂ H ₁₉ NO ₄	241.28	4476497	CCCCC(=O)CC(=O)NC1CCOC1=O

Table 7. Predicted ADMET (absorption, distribution, metabolism, excretion, and toxicity) properties of the phytocompounds found in the methanolic extract of *Parkia timoriana* seed pod using Molinspiration and SwissADME tools.

Calculated ADMET properties of the phytocompounds from <i>P. timoriana</i> †											
Sl. No.	Phytocompound (<i>P. timoriana</i>)	iLOGP*	TPSA*	nheavy atoms*	MW*	HBA*	HBD*	LR5*	RB*	MV*	MR*
1.	3,7,11-Trimethyl-2,4-dodecadiene	5.72	0.00	15	208.39	0	0	1	7	251.14	73.27
2.	5-Ethyl-3-methyl-3,4-nonadien-6-yne	4.48	0.00	12	162.28	0	0	0	2	189.92	56.19
3.	4-Isopropyl-3,4-dimethylcyclohexa-2,5-dienone	2.67	17.07	12	164.25	1	0	0	1	175.19	51.87
4.	1-(4-Isopropylphenyl)-2-methylpropyl acetate	4.60	26.30	17	234.34	2	0	0	5	245.30	71.31
5.	Patchouli alcohol	3.94	20.23	16	222.37	1	1	0	0	238.37	68.56
6.	Tricyclo[4.3.0.0(7,9)]nonane, 2,2,5,5, 8,8-hexamethyl-, (1.alpha.,6.beta.,7.alpha.,9. alpha.)-	5.30	0.00	15	206.37	0	0	1	0	229.90	67.10
7.	1H-Purin-6-amine, N-((3-fluorophenyl)methyl)-	2.15	66.49	18	243.25	4	2	0	3	206.10	65.43
8.	Bisabolene	5.51	0.00	15	204.36	0	0	1	3	234.30	70.68
9.	1,1,3,3,4-Pentamethyl-6- <i>t</i> -butyl-2,3-dihydroindene	6.38	0.00	18	244.42	0	0	1	1	272.00	82.30
10.	Scopolamine-N-butyl	-1.49	59.06	26	360.47	4	1	0	8	347.61	103.76
11.	1-dodecanoyl-2-(11 <i>Z</i> -eicosenoyl)-glycerol-3-phospho-(1'-sn-glycerol)	9.53	148.83	49	720.97	10	3	2	39	737.19	201.19
12.	Napelline	2.11	63.92	26	359.51	4	3	0	1	347.02	104.23
13.	Taurodeoxycholate	1.19	123.92	34	499.71	6	4	0	8	475.07	133.98
14.	Voacamine	7.71	99.90	52	704.91	7	2	2	7	661.98	211.78
15.	Ginsenoside F3	3.20	218.99	54	771.00	13	9	3	9	735.37	199.84
16.	Isoschaftoside	-1.68	250.96	40	564.50	14	10	3	4	461.51	133.26
17.	Azadirachtin	1.42	215.37	51	720.72	16	3	2	10	611.69	165.92
18.	E-Resveratrol trimethyl ether	4.59	27.70	20	270.33	3	0	0	5	259.51	81.29
19.	Ginkgolide C	-3.29	169.06	31	440.40	11	4	1	1	355.93	94.45
20.	Quinine	3.06	45.59	24	324.42	4	1	0	4	310.79	99.73
21.	Ergocristine	2.82	118.21	45	609.73	6	3	1	6	549.98	179.96
22.	Demethoxycurcumin	2.48	83.83	25	338.36	5	2	0	7	306.64	96.31

23.	Guan-fu base Y	1.07	90.23	28	387.48	6	3	0	2	347.05	103.44
24.	Cycloheximide	0.76	83.47	20	281.35	4	2	0	3	269.59	78.47
25.	Anabasamine	2.42	29.02	19	253.35	3	0	0	2	249.68	81.17
26.	Vincamine	3.18	54.70	26	354.45	4	1	0	3	330.22	103.74
27.	Artocarpin	6.09	100.13	32	436.50	6	3	1	6	404.30	128.71
28.	Rauwolscine	3.22	65.56	26	354.45	4	2	0	2	330.78	104.02
29.	Lithocholenic Acid	4.66	57.53	27	374.56	3	2	0	4	383.40	110.97
30.	Rotenone	3.58	63.24	29	394.42	6	0	0	3	348.33	106.15
31.	Silychrestin	1.26	166.14	35	482.44	10	6	1	4	399.89	121.05
32.	Speciosine	4.23	77.47	35	477.56	7	1	0	7	441.78	135.76
33.	Apiin	-0.74	228.97	40	564.50	14	8	3	7	463.10	132.56
34.	Gardnerine	3.31	48.49	24	324.42	3	2	0	2	305.34	99.14
35.	Loganin	-1.25	155.15	27	390.38	10	5	0	5	337.54	87.37
36.	Apigenin glucoside arabinoside	-0.94	250.96	40	564.50	14	10	3	5	461.51	133.26
37.	Linolenic acid	5.84	37.30	20	278.44	2	1	1	13	306.47	88.99
38.	Isocorydine	3.00	51.17	25	341.41	5	1	0	3	315.00	100.47
39.	Nantenine	3.32	40.17	25	339.39	5	0	0	2	305.37	98.20
40.	Phosphatidylcholine 15:0/18:1(11Z)	6.40	111.21	51	746.06	8	0	2	40	784.29	214.13
41.	Luteolin-8-C-glucoside	0.03	201.27	32	448.38	11	8	2	3	363.22	108.63
42.	Nicotiflorin	-0.57	249.20	42	594.52	15	9	3	6	488.05	139.36
43.	Hydroxygardnutine	2.56	57.73	25	338.41	4	2	0	2	303.75	98.11
44.	Phosphatidylethanolamine(22:1/20:1)	10.23	134.40	57	828.21	9	2	2	47	877.45	244.37
45.	Phosphatidylethanolamine 18:0-22:6	9.57	134.40	55	792.09	9	2	2	41	819.10	232.86
46.	Maritimetin-6-O-glucoside	-0.51	190.28	32	448.38	11	7	2	4	364.19	106.03
47.	Ouabain	-2.18	206.60	41	584.66	12	8	3	4	520.54	140.66
48.	4,4'-Diaponeurosporene	9.33	0.00	30	402.67	0	0	1	11	452.89	141.58
49.	1-(5Z,8Z,11Z,14Z,17Z-eicosapentaen oyl) -2-(9Z-nonadecenoyl)-glyce ro-3-phospho serine	8.88	171.70	57	822.07	11	3	3	41	829.32	234.63
50.	Isorhamnetin-3-O-rutinoside	-0.76	258.43	44	624.55	16	9	3	7	513.60	145.85
51.	Paeoniflorin	0.04	164.38	34	480.47	11	5	1	7	401.41	109.26
52.	Procyanidin B1	2.58	220.75	42	578.53	12	10	3	3	475.67	146.71

53.	1,2-diarachidonoyl-sn-glycero-3-phosphoethanolamine	9.36	134.40	55	788.06	9	2	2	39	806.72	231.91
54.	Phosphatidylcholine(14:0/18:3n6)	4.45	111.21	50	728.00	8	0	1	37	755.11	208.38
55.	Hirsutine	4.07	54.57	27	368.48	4	1	0	5	352.67	110.39
56.	Taurochenodeoxycholate	1.19	123.92	34	499.71	6	4	0	8	475.07	133.98
57.	[3-hexadecoxy-2-[(9Z,11E)-13-hydroxy octadeca-9,11-dienoyl]oxy propyl] 2-(tri methylazaniumyl) ethyl phosphate	5.46	114.36	52	760.09	8	1	2	40	800.76	219.43
58.	Alpha-hederin	3.57	195.60	53	750.97	12	7	3	6	710.54	195.45
59.	Soyasapogenol B base + O-DDMP, O-HexA-HexA	3.01	288.67	66	937.09	18	9	3	9	849.33	232.23
60.	Taurocholic acid	0.28	144.15	35	515.71	7	5	1	8	483.12	135.14
61.	β-oxo-C8-homoserine lactone	0.14	72.47	17	241.29	4	1	0	8	231.13	62.17

* iLOGP: octanol-water partition coefficient; TPSA: topological Polar surface area; nheavy atoms: number of heavy atoms; MW: molecular weight; HBA: number of H-bond acceptors; HBD: number of H-bond donors; LR5: number of violations to Lipinski's rule of five; RB: number of rotatable bonds; MV: molecular volume; MR: molar refractivity.

† ADMET Default range: MW- 50–500; iLOGP- 2–10; TPSA- 20–130; HBA- 0–10; HBD- 0–5; RB- 0–5; nheavy atoms- 15–50; logP- 0.7–5.0; MR- 40–130; MV- 500–2000.

Table 8. Prediction of pharmacokinetics properties, water solubility, and lipophilicity of the phytocompounds from the methanolic extract of *Parkia timoriana* using Molinspiration and SwissADME tools.

Sl. No.	Phytocompounds (<i>P. timoriana</i>)	Log S*	Pharmacokinetics - Bioactivity								
			GPCR*	Ion channel modulator	Kinase inhibitor	Nuclear receptor ligand	Protease inhibitor	Enzyme inhibitor	GI*	BBB*	P-gp*
1.	3,7,11-Trimethyl-2,4-dodecadiene	-6.38	-0.36	0.07	-0.81	0.14	-0.67	0.25	Low	no	no
2.	5-Ethyl-3-methyl-3,4-nonadien-6-yne	-3.9	-0.49	0.15	-0.75	-0.16	-0.83	0.14	Low	yes	no
3.	4-Isopropyl-3,4-dimethylcyclohexa-2,5-dienone	-2.69	-0.65	-0.36	-1.75	0.14	-0.65	0.25	High	yes	no
4.	1-(4-Isopropylphenyl)-2-methylpropyl acetate	-3.81	-0.07	-0.12	-0.60	-0.03	-0.31	0.07	High	yes	no
5.	Patchouli alcohol	-4.18	-0.12	0.37	-0.88	0.55	-0.32	0.40	High	Yes	no
6.	Tricyclo[4.3.0.0(7,9)]nonane, 2,2,5,5, 8,8-hexamethyl-, (1.alpha.,6.beta.,7.alpha.,9. alpha.)-	-4.98	-0.32	-0.03	-0.65	-0.26	-0.52	-0.06	Low	no	no
7.	1H-Purin-6-amine, N-((3-fluorophenyl)methyl)-	-3.03	0.35	0.29	0.69	-1.39	-0.30	0.46	High	yes	yes
8.	Bisabolene	-6.12	-0.39	0.12	-0.84	0.11	-0.74	0.25	Low	no	no
9.	1,1,3,3,4-Pentamethyl-6-tert-butyl-2,3-dihydroindene	-6.34	-0.10	0.00	-0.34	0.10	-0.31	-0.08	Low	no	no
10.	Scopolamine-N-butyl	-3.13	0.71	0.40	-0.10	-0.28	0.15	0.48	High	yes	yes
11.	1-dodecanoyl-2-(11Z-eicosenoyl)-glycerol-3-phospho-(1'-sn-glycerol)	-14.56	-0.11	-0.97	-0.59	-0.72	-0.01	-0.29	Low	no	yes
12.	Napelline	-2.16	0.32	0.35	-0.29	0.57	0.16	0.41	High	yes	yes
13.	Taurodeoxycholate	-4.55	0.16	0.09	-0.42	0.42	0.30	0.56	Low	no	yes
14.	Voacamine	-7.95	-0.51	-1.59	-1.57	-1.46	-0.58	-1.23	High	no	no
15.	Ginsenoside F3	-6.41	-1.00	-2.10	-1.94	-1.56	-0.65	-0.95	Low	no	yes
16.	Isoschaftoside	-2.55	0.10	-0.33	0.00	0.02	-0.00	0.33	Low	no	yes
17.	Azadirachtin	-5.20	-0.71	-1.51	-1.46	-0.67	-0.35	-0.71	Low	no	yes
18.	E-Resveratrol trimethyl ether	-4.22	-0.14	-0.12	-0.13	-0.02	-0.29	-0.05	High	yes	no
19.	Ginkgolide C	-1.69	1.16	0.04	-0.23	0.07	0.26	0.28	Low	no	yes
20.	Quinine	-3.50	0.39	0.37	-0.05	0.10	0.18	0.11	High	yes	no
21.	Ergocristine	-6.21	0.62	-0.53	-0.44	-0.60	0.20	-0.26	high	no	yes

22.	Demethoxycurcumin	-4.76	-0.04	-0.20	-0.26	0.18	-0.14	0.10	High	no	no
23.	Guan-fu base Y	-1.44	0.08	0.01	-0.39	0.36	0.20	0.34	High	no	yes
24.	Cycloheximide	-1.87	-0.04	-0.21	-0.64	-0.03	0.40	0.26	High	no	no
25.	Anabasamine	-1.77	0.31	0.44	0.13	-0.35	-0.12	0.22	High	yes	yes
26.	Vincamine	-3.67	0.25	0.06	-0.22	0.06	0.03	0.10	High	yes	yes
27.	Artocarpin	-7.59	-0.01	-0.16	-0.09	0.41	-0.22	0.32	High	no	no
28.	Rauwolscine	-3.98	0.47	0.36	-0.14	-0.03	0.11	0.16	High	yes	yes
29.	Lithocholenic Acid	-6.76	0.35	0.33	-0.34	0.80	0.33	0.68	High	yes	no
30.	Rotenone	-5.13	-0.07	-0.37	-0.53	0.21	-0.41	0.28	High	yes	no
31.	Silychrystin	-4.66	0.25	-0.12	-0.10	0.04	-0.06	0.41	Low	no	no
32.	Speciosine	-4.52	-0.02	-0.04	-0.06	-0.13	-0.15	0.07	high	no	yes
33.	Apiin	-3.99	0.18	-0.17	0.09	0.18	0.17	0.42	Low	no	yes
34.	Gardnerine	-2.71	0.61	0.38	-0.01	0.04	-0.15	0.13	High	yes	yes
35.	Loganin	-1.37	0.28	0.10	-0.25	0.14	0.13	0.47	Low	no	yes
36.	Apigenin glucoside arabinoside	-3.12	0.31	-0.23	0.13	-0.03	0.03	0.57	Low	no	yes
37.	Linolenic acid	-7.04	0.33	0.23	-0.19	0.35	0.13	0.42	High	yes	no
38.	Isocorydine	-3.29	0.41	0.18	-0.13	-0.15	-0.06	0.15	High	yes	yes
39.	Nantenine	-3.76	0.39	0.20	-0.14	-0.22	-0.13	0.12	High	yes	yes
40.	Phosphatidylcholine 15:0/18:1(11Z)	-15.74	-0.51	-1.44	-1.20	-1.45	-0.42	-0.76	Low	no	yes
41.	Luteolin-8-C-glucoside	-3.62	0.12	-0.14	0.20	0.20	0.01	0.45	Low	no	no
42.	Nicotiflorin	-4.81	-0.01	-0.43	-0.09	-0.17	-0.04	0.18	Low	no	yes
43.	Hydroxygardnutine	-1.48	0.54	0.31	-0.03	0.06	-0.14	0.18	High	yes	yes
44.	Phosphatidylethanolamine(22:1/20:1)	-16.91	-1.37	-2.58	-2.15	-2.45	-0.95	-1.72	Low	no	yes
45.	Phosphatidylethanolamine 18:0-22:6	-13.39	-0.92	-2.11	-1.67	-1.92	-0.61	-1.23	Low	no	yes
46.	Maritimetin-6-O-glucoside	-3.85	-0.62	-0.72	-0.28	-0.32	-0.65	0.28	Low	no	yes
47.	Ouabain	-2.13	0.14	-0.26	-0.39	0.30	0.09	0.65	Low	no	no
48.	4,4'-Diaponeurosporene	-11.79	0.10	0.14	-0.01	0.48	-0.08	0.32	Low	no	yes
49.	1-(5Z,8Z,11Z,14Z,17Z-eicosapentaen oyl)-2-(9Z-nonadecenoyl)-glycero-3-phosphoserine	-12.77	-1.24	-2.48	-2.20	-2.35	-0.88	-1.61	Low	no	yes
50.	Isorhamnetin-3-O-rutinoside	-4.97	-0.12	-0.66	-0.23	-0.36	-0.13	0.02	Low	no	yes
51.	Paeoniflorin	-1.94	0.24	0.16	-0.03	0.15	0.14	0.44	Low	no	yes

52.	Procyanidin B1	-6.65	0.20	-0.33	-0.12	0.16	0.17	0.09	Low	no	no
53.	1,2-diarachidonoyl-sn-glycero-3-phospho ethanolamine	-11.51	-0.94	-2.13	-1.65	-1.94	-0.62	-1.25	Low	no	yes
54.	Phosphatidylcholine(14:0/18:3n6)	-13.75	-0.33	-1.21	-1.01	-1.25	-0.30	-0.56	Low	no	yes
55.	Hirsutine	-4.27	0.42	0.31	-0.27	-0.16	-0.09	0.01	High	yes	yes
56.	Taurochenodeoxycholate	-4.11	0.21	0.11	-0.48	0.53	0.33	0.57	Low	no	yes
57.	[3-hexadecoxy-2-[(9Z,11E)-13-hydroxy octadeca-9,11-dienoyl]oxy propyl] 2-(trimethylazanium) ethyl phosphate	-14.77	-0.52	-1.53	-1.31	-1.51	-0.42	-0.76	Low	no	yes
58.	Alpha-hederin	-7.44	-0.91	-2.12	-1.89	-1.38	-0.56	-0.90	Low	no	yes
59.	Soyasapogenol B base + O-DDMP, O-HexA-HexA	-10.15	-3.30	-3.68	-3.72	-3.55	-2.89	-3.18	Low	no	yes
60.	Taurocholic acid	-3.44	0.20	0.07	-0.42	0.50	0.32	0.62	Low	no	no
61.	3-oxo-C8-homoserine lactone	-3.09	-0.30	-0.37	-1.01	-0.47	-0.08	0.08	High	no	no

*Log S- water solubility (ESOL); GPCR: G-Protein coupled receptor ligand; GI: Gastrointestinal absorption; BBB: Blood brain barrier permeability; P-gp: P-glycoprotein substrate.

Table 9. Predicted pharmacokinetic properties, medicinal chemistry, and drug-like qualities of the phytochemicals from the methanolic extract of *Parkia timoriana* using SwissADME and Molinspiration tools.

Sl. No.	Phytochemical (<i>P. timoriana</i>)	CYP1A2 inhibitor*	CYP2C19 inhibitor*	CYP2C9 inhibitor*	CYP2D6 inhibitor*	CYP3A4 inhibitor*	Log Kp (cm/s)*	PAINS (alert)	Brenk (alert)	SAS*	BAS*
1.	3,7,11-Trimethyl-2,4-dodecadiene	no	no	no	no	no	-2.90	0	1	4.12	0.55
2.	5-Ethyl-3-methyl-3,4-nonadien-6-yne	no	no	no	no	no	-4.30	0	1	4.09	0.55
3.	4-Isopropyl-3,4-dimethylcyclohexa-2,5-dienone	no	no	no	no	no	-5.40	0	0	3.53	0.55
4.	1-(4-Isopropylphenyl)-2-methylpro pylacetate	no	no	no	no	no	-4.82	0	0	2.28	0.55
5.	Patchouli alcohol	no	no	yes	no	no	-4.78	0	0	3.73	0.55
6.	Tricyclo[4.3.0.0(7,9)]nonane, 2,2,5,5,8,8 -hexa methyl-, (1.alpha.,6.beta.,7.alpha.,9. alpha.)-	no	yes	yes	no	no	-3.85	0	0	4.13	0.55
7.	1H-Purin-6-amine, N-((3-fluorophenyl) methyl)-	yes	no	no	no	no	-6.36	0	0	2.03	0.55
8.	Bisabolene	yes	no	yes	no	no	-3.05	0	1	3.46	0.55
9.	1,1,3,3,4-Pentamethyl-6-t-butyl-2,3-dihy - droindene	no	no	no	no	no	-3.15	0	0	2.22	0.55
10.	Scopolamine-N-butyl	no	no	no	no	no	-6.90	0	2	4.61	0.55
11.	1-dodecanoyl-2-(11Z-eicosenoyl)-gly ce-ro-3-phospho-(1'-sn-glycerol)	no	no	no	no	yes	-2.71	0	3	7.82	0.11
12.	Napelline	no	no	no	no	no	-7.63	0	1	6.16	0.55
13.	Taurodeoxycholate	no	no	no	no	yes	-7.83	0	1	5.78	0.56
14.	Voacamine	no	no	no	no	yes	-6.29	0	2	7.99	0.55
15.	Ginsenoside F3	no	no	no	no	no	-9.46	0	1	9.04	0.17
16.	Isoschaftoside	no	no	no	no	no	-11.30	0	0	6.18	0.17
17.	Azadirachtin	no	no	no	no	no	-9.92	0	3	8.11	0.17
18.	E-Resveratrol trimethyl ether	yes	yes	yes	yes	no	-5.03	0	1	2.40	0.55
19.	Ginkgolide C	no	no	no	no	no	-9.95	0	1	6.48	0.55
20.	Quinine	no	no	no	yes	no	-6.23	0	1	4.34	0.55
21.	Ergocristine	no	no	yes	yes	yes	-7.17	0	0	6.36	0.55
22.	Demethoxycurcumin	yes	no	yes	no	yes	-6.01	0	2	2.82	0.55

23.	Guan-fu base Y	no	no	no	no	no	-8.67	0	1	6.23	0.55
24.	Cycloheximide	no	no	no	no	no	-7.63	0	1	3.17	0.55
25.	Anabasamine	no	no	no	yes	yes	-6.74	0	0	3.06	0.55
26.	Vincamine	no	no	no	yes	no	-6.43	0	0	4.49	0.55
27.	Artocarpin	no	yes	no	no	no	-4.90	0	1	4.43	0.55
28.	Rauwolfscine	no	no	no	yes	no	-6.37	1	0	4.21	0.55
29.	Lithocholenic Acid	no	no	yes	no	no	-4.48	0	1	5.31	0.85
30.	Rotenone	no	yes	yes	yes	yes	-5.79	0	1	4.52	0.55
31.	Silychrystin	no	no	no	no	yes	-8.14	0	0	4.88	0.55
32.	Speciosine	no	no	no	yes	yes	-6.93	1	0	4.41	0.55
33.	Apiin	no	no	no	no	no	-10.00	0	0	6.08	0.17
34.	Gardnerine	no	no	no	yes	no	-6.82	1	1	4.64	0.55
35.	Loganin	no	no	no	no	no	-9.67	0	0	5.77	0.11
36.	Apigenin glucoside arabinoside	no	no	no	no	no	-10.91	0	0	6.18	0.17
37.	Linolenic acid	yes	no	yes	no	no	-3.41	0	1	3.03	0.85
38.	Isocorydine	yes	no	no	yes	yes	-6.56	0	0	3.80	0.55
39.	Nantenine	yes	yes	yes	yes	yes	-6.07	0	0	3.75	0.55
40.	Phosphatidylcholine 15:0/18:1(11Z)	no	no	yes	no	yes	-1.51	0	4	7.91	0.55
41.	Luteolin-8-C-glucoside	no	no	no	no	no	-9.14	1	1	5.17	0.17
42.	Nicotiflorin	no	no	no	no	no	-9.91	0	0	6.48	0.17
43.	Hydroxygardnutine	no	no	no	yes	no	-7.87	1	1	4.42	0.55
44.	Phosphatidylethanolamine(22:1/20:1)	no	no	no	no	no	-1.55	0	3	8.70	0.17
45.	Phosphatidylethanolamine 18:0-22:6	no	no	no	no	no	-3.73	0	3	8.16	0.17
46.	Maritimetin-6-O-glucoside	no	no	no	no	no	-8.77	1	2	5.12	0.17
47.	Ouabain	no	no	no	no	no	-11.07	0	1	7.13	0.17
48.	4,4'-Diaponeurosporene	no	no	yes	no	no	-0.39	0	2	5.22	0.55
49.	1-(5Z,8Z,11Z,14Z,17Z-eicosapentaenoyl) -2-(9Z-nonadecenoyl)-glycero-3-phosphoserine	no	no	yes	no	no	-4.87	0	3	8.36	0.11
50.	Isorhamnetin-3-O-rutinoside	no	no	no	no	no	-10.12	0	0	6.64	0.17
51.	Paeoniflorin	no	no	no	no	yes	-9.96	0	0	5.51	0.55
52.	Procyanidin B1	no	no	no	no	yes	-8.15	1	1	5.32	0.17

53.	1,2-diarachidonoyl-sn-glycero-3-phospho ethanol amine	no	no	yes	no	no	-4.99	0	3	7.93	0.17
54.	Phosphatidylcholine(14:0/18:3n6)	no	no	yes	no	yes	-2.77	0	4	7.60	0.55
55.	Hirsutine	no	no	no	yes	yes	-6.11	1	2	4.27	0.55
56.	Taurochenodeoxycholate	no	no	no	no	yes	-8.13	0	1	5.83	0.56
57.	[3-hexadecoxy-2-[(9Z,11E)-13-hydroxy octadeca -9,11-dienoyl]oxy propyl] 2-(tri methylazaniumyl) ethyl phosphate	no	no	no	no	yes	-2.31	0	3	8.37	0.55
58.	Alpha-hederin	no	no	no	no	no	-8.30	0	2	8.75	0.11
59.	Soyasapogenol B base + O-DDMP, O-HexA-HexA	no	no	no	no	no	-8.91	0	2	9.92	0.11
60.	Taurocholic acid	no	no	no	no	yes	-8.98	0	1	5.93	0.11
61.	3-oxo-C8-homoserine lactone	no	no	no	no	no	-6.39	0	1	2.62	0.55

*CYP1A2 inhibitor: cytochrome P450 1A2 inhibitor; CYP2C19 inhibitor: cytochrome P450 2C19 inhibitor; CYP2C9 inhibitor: cytochrome P450 2C9 inhibitor; CYP2D6 inhibitor: cytochrome P450 2D6 inhibitor; CYP3A4 inhibitor: cytochrome P450 3A4 inhibitor; Log Kp(cm/s): Skin Permeation; SAS: synthetic accessibility score; BAS: bio-availability score.

Table 10. The binding affinity values of each phytocompound (ligand) found in *Parkia timoriana* seed pods docked against BACE1 and AChE receptors acquired using the autodock vina tool.

Sl. No.	Phytocompound (Ligand) (<i>P. timoriana</i>)	Compound ID	BACE1 (kcal/mol)	AChE (kcal/mol)
1.	3,7,11-Trimethyl-2,4-dodecadiene	21599893	-5.3	-7.3
2.	5-Ethyl-3-methyl-3,4-nonadien-6-yne	535138	-5.3	-6.2
3.	4-Isopropyl-3,4-dimethylcyclohexa-2,5-dienone	578926	-6.5	-7.0
4.	1-(4-Isopropylphenyl)-2-methylpropyl acetate	154574010	-7.2	-7.8
5.	Patchouli alcohol	10955174	-6.7	-6.5
6.	Tricyclo[4.3.0.0(7,9)]nonane, 2,2,5,5,8,8-hexamethyl-, (1.alpha.,6.beta.,7.alpha.,9.alpha.)-	549738	-6.9	-7.3
7.	1H-Purin-6-amine, N-((3-fluorophenyl)methyl)-	6455415	-7.8	-9.1
8.	Bisabolene	3033866	-7.3	-8.2
9.	1,1,3,3,4-Pentamethyl-6-t-butyl-2,3-dihydroindene	1FVnmylG7Pj	-7.8	-7.9
10.	Scopolamine-N-butyl	9004	-7.9	-7.1
11.	1-dodecanoyl-2-(11Z-eicosenoyl)-glycero-3-phospho-(1'-sn-glycerol)	52926324	-6.0	-6.9
12.	Napelline	441749	-8.5	-8.2
13.	Taurodeoxycholate	2733768	-8.7	-9.1
14.	Voacamine	11953931	-10.1	-8.0
15.	Ginsenoside F3	46887678	-9.7	-8.3
16.	Isoschaftoside	3084995	-9.7	-9.6
17.	Azadirachtin	5281303	-8.6	-6.8
18.	E-Resveratrol trimethyl ether	5388063	-7.2	-8.3
19.	Ginkgolide C	24721502	-8.2	-6.5
20.	Quinine	3034034	-8.0	-8.0
21.	Ergocristine	31116	-10.3	-9.2
22.	Demethoxycurcumin	5469424	-8.3	-9.4
23.	Guan-fu base Y	3101182	-8.2	-7.8
24.	Cycloheximide	6197	-7.7	-9.1
25.	Anabasamine	161313	-7.6	-8.8
26.	Vincamine	15376	-8.7	-7.1
27.	Artocarpin	5458461	-8.7	-9.0
28.	Rauwolfscine	643606	-9.3	-8.6
29.	Lithocholenic Acid	5283972	-8.3	-8.5
30.	Rotenone	6758	-8.8	-9.4
31.	Silychrestin	4481797	-9.7	-9.8
32.	Speciosine	330188	-7.9	-8.2

33.	Apiin	5280746	-9.9	-10.3
34.	Gardnerine	6445140	-8.6	-8.4
35.	Loganin	87691	-7.5	-9.8
36.	Apigenin glucoside arabinoside	131750832	-9.8	-7.4
37.	Linolenic acid	5280934	-5.7	-7.4
38.	Isocorydine	10143	-7.7	-8.5
39.	Nantenine	197001	-8.3	-7.9
40.	Phosphatidylcholine 15:0/18:1(11Z)	24778662	-6.6	-6.6
41.	Luteolin-8-C-glucoside	5281675	-9.3	-8.8
42.	Nicotiflorin	5318767	-10.2	-8.1
43.	Hydroxygardnutine	12310668	-8.0	-8.4
44.	Phosphatidylethanolamine(22:1/20:1)	53479865	-6.2	-6.0
45.	Phosphatidylethanolamine 18:0-22:6	6426737	-6.4	-6.3
46.	Maritimetin-6-O-glucoside	6450184	-9.4	-10.3
47.	Ouabain	439501	-9.0	-7.2
48.	4,4'-Diaponeurosporene	6443791	-7.5	-8.8
49.	1-(5Z,8Z,11Z,14Z,17Z-eicosapentaenoyl)-2-(9Z-nonadecenoyl)-glycero-3-phosphoserine	52925775	-6.6	-7.1
50.	Isorhamnetin-3-O-rutinoside	5481663	-10.1	-8.1
51.	Paeoniflorin	442534	-9.1	-10.2
52.	Procyanidin B1	11250133	-9.7	-8.6
53.	1,2-diarachidonoyl-sn-glycero-3-phosphoethanolamine	52924874	-6.9	-6.0
54.	Phosphatidylcholine(14:0/18:3n6)	52922220	-6.6	-6.8
55.	Hirsutine	3037884	-8.1	-7.6
56.	Taurochenodeoxycholate	387316	-8.9	-9.2
57.	[3-hexadecoxy-2-[(9Z,11E)-13-hydroxyoctadeca-9,11-dienoyl]oxypropyl] 2-(trimethylazaniumyl)ethyl phosphate	134778782	-5.8	-6.7
58.	Alpha-hederin	73296	-8.8	-7.2
59.	Soyasapogenol B base + O-DDMP, O-HexA-HexA	139292121	-9.1	-7.7
60.	Taurocholic acid	6675	-8.6	-9.1
61.	3-oxo-C8-homoserine lactone	4476497	-5.9	-7.4

Table 11. The predicted affinity for binding and interaction between the residues of the BACE1 receptor and the most potent phytochemicals of *Parkia timoriana* seed pods.

Ligand	Binding affinity (kcal/mol)	Docked complex (BACE1-ligand) interactions			
		Hydrogen bond	Distance(Å)	Hydrophobic bond	Distance(Å)
Ergocristine	-10.3	TYR 71	6.42	TRP 76	7.03
		ASP 32	5.95	PRO 70	7.97
				PHE 108	5.87
				LYS 107	6.58
				TYR 71	3.99,4.47,4.26
Nicotiflorin	-10.2	LYS 107	4.93	TYR 71	5.42,5.07,4.22
		ILE 126	4.57	PHE 108	5.07,6.74
		THR 231	3.34		
		GLY 74	3.73		
		VAL 69	3.25		
		TRP 76	3.85,5.02		
Isorhamnetin - 3-O – rutinoside	-10.1	THR 231	4.84,3.21	TYR 71	6.79,5.42,4.94,4.16
		LYS 107	4.81	PHE 108	6.86,5.14
		GLN 73	6.01		
		ILE 126	4.15		
		ARG 128	6.32		
Voacamine	-10.1	TRP 76	6.27	PHE 108	5.07
		TYR 71	5.91	LEU 30	5.72
		ILE 126	3.76	VAL 69	5.43
		PRO 70	5.15	TYR 198	6.32
				ILE 126	3.76
				ILE 118	6.64
				TRP 76	6.27,5.79
				TYR 71	5.41,4.70,5.36,5.91

Table 12. The predicted affinity for binding and interaction between the residues of the AChE receptor and the most potent phytocompounds (ligands) of *Parkia timoriana* seed pods.

Ligand	Binding affinity (kcal/mol)	Docked complex (AChE-ligand) interactions			
		Hydrogen bond	Distance(Å)	Hydrophobic bond	Distance(Å)
Apiin	-10.3	GLU 202	5.66	TRP 86	4.10
		SER 125	4.43	TYR 124	6.15
		ASN 87	5.00	TYR 341	4.14
		TYR 341	4.89		
		TYR 124	5.80		
Maritimetin-6-O-glucoside	-10.3	PHE 295	4.22	TRP 86	4.85
		TYR 72	5.59	TYR 337	5.92
		SER 125	4.12	TYR 124	6.83, 6.47
Paenoniflorin	-10.2	ASN 87	3.83, 4.11	TRP 286	7.35
		SER 125	4.42, 4.22	TRP 86	4.86
		PHE 295	4.11		
		GLY 122	3.62		
		TYR 341	5.71		
		HIS 447	5.05		
Silychrystin	-9.8	TYR 341	6.56	TYR 341	4.85, 5.33
		TYR 124	6.42	TYR 124	6.42
				TYR 72	5.64
				TRP 286	6.14, 6.68, 3.95, 5.41
				LEU 76	6.62

Table 13. Examination of the stability, compactness, and fluctuation of the most potent phytochemicals found in methanolic extract of *Parkia timoriana* seed pods docked with the BACE1 receptor.

Sl. No.	Compounds	RMSD (nm)	RMSF (nm)	Rg (nm)	H-bond
1	Ergocristine	0.184045229	0.103447970	2.114483547	0.666066787
2	Nicotiflorin	0.215964255	0.117904600	2.142448600	4.940011998
3	Isorhamnetin-3-O-rutinoside	0.226005947	0.130892683	2.144187091	3.880823840
4	Voacamine	0.217927569	0.117304070	2.144168660	0.173165370

Table 14. Examination of the stability, compactness, and fluctuation of the most potent phytochemicals found in methanolic extract of *Parkia timoriana* seed pods docked with the AChE receptor.

Sl. No.	Compounds	RMSD (nm)	RMSF (nm)	Rg (nm)	H-bond
1	Apiin	0.2530555	0.1235134	2.339719684	1.881223755
2	Maritimetin-6-O-glucoside	0.243552702	0.115025279	2.33141063	3.271545691
3	Paeoniflorin	0.246054716	0.114932528	2.337643277	2.769246151
4	Silychrystin	0.23892445	0.11436375	2.32408877	0.23515297

Table 15. Total binding energy (kJ/mol) analysis by MMPBSA approach of the most potent phytocompounds found in methanolic extract of *Parkia timoriana* seed pods docked with the BACE1 receptor.

Sl. No.	Compounds	Van der Waals energy (kJ/mol)	Electrostatic energy (kJ/mol)	Polar solvation energy (kJ/mol)	SASA energy (kJ/mol)	Total binding energy (kJ/mol)
1	Ergocristine	-228.468 ± 19.339	-262.208 ± 19.448	225.008 ± 30.094	-22.963 ± 1.515	-288.631 ± 16.489
2	Nicotiflorin	-231.022 ± 16.521	-120.005 ± 24.740	272.354 ± 31.907	-24.116 ± 1.263	-102.789 ± 17.818
3	Isorhamnetin-3-O-rutinoside	-204.563 ± 23.170	-122.670 ± 35.580	242.760 ± 34.343	-23.093 ± 1.688	-107.567 ± 23.195
4	Voacamine	-227.962 ± 32.054	-383.451 ± 47.688	219.879 ± 46.000	-26.418 ± 2.029	-417.951 ± 31.736

Table 16. Total binding energy (kJ/mol) analysis by MMPBSA approach of the most potent phytochemicals found in methanolic extract of *Parkia timoriana* seed pods docked with the AChE receptor.

Sl. No.	Compounds	Van der Waals energy (kJ/mol)	Electrostatic energy (kJ/mol)	Polar solvation energy (kJ/mol)	SASA energy (kJ/mol)	Total binding energy (kJ/mol)
1	Apiin	-226.555 ± 16.657	-43.483 ± 21.363	200.269 ± 31.647	-23.937 ± 1.655	-93.705 ± 19.494
2	Maritimetin-6-O-glucoside	-199.870 ± 18.260	-91.140 ± 28.849	244.650 ± 32.811	-22.494 ± 1.121	-68.854 ± 24.995
3	Paeoniflorin	-220.420 ± 18.719	-55.838 ± 24.255	188.791 ± 31.768	-22.549 ± 1.301	-110.015 ± 20.417
4	Silychrystin	-151.640 ± 20.690	-388.413 ± 33.453	172.585 ± 38.116	-17.917 ± 1.684	-385.386 ± 18.965

3.5. DISCUSSIONS

3.5.1. ADMET

The primary and difficult stage in the process of discovering and developing drugs is evaluating the ADMET characteristics of a compound. These factors describe how a drug is absorbed, digested, metabolised, distributed, and excreted out from the body (**Daina et al., 2017; Egbuna et al., 2021**). It is necessary to screen the ADMET characteristics of a compound in order to find the lead compounds for drug development, in order to prevent the medicine from failing during clinical trials. Consequently, computational approaches continue to be the most efficient and economical methods for screening medicinal compounds (**Omoboyowa et al., 2021**). Forty compounds showed drug-likeness properties as indicated by Lipinski's rule of five. The acceptable range for the Lipinski rule of five parameters are as follows: a) molecular weight= 50 to 500; b) number of H-bond acceptors= 0 to 10; c) number of H-bond donors= 0 to 5; d) number of rotatable bonds= 0 to 5. Any compound that violates two or more of these parameters are said to fail as a drug candidate (**Lipinski, 2004**). Thirty-two compounds were considered to have a good affinity for a lipophilic environment (lipophilicity/iLogP). There are thirty-one chemicals that have the capacity to be absorbed by the body when taken orally and have the ability to reach certain target areas inside the body as per their TPSA values. Forty-eight compounds have non-hydrogen atoms that falls under the acceptable range. Sixteen compounds possess an acceptable molar volume that influences the transport properties of a molecule. Thirty-six compounds were in the acceptable range of molar refractivity. In addition to the molecular volume, molar refractivity is also correlated with the London dispersive forces involved in the interaction between drug and receptor (**Padrón et al., 2002**). No compound was found highly soluble as per LogS value. However, six compounds showed solubility, twenty compounds slightly soluble, and thirty-five compounds lack solubility. The acceptable range for the above criteria of drug-likeness are; a) number of heavy atoms= 15-50; b) molecular volume= 500-2000; c) iLogP= 0.7-5.0; d) TPSA= 20-130; e) Log S= > 0 highly soluble, 0 to -2 soluble, -2 to -4 slightly soluble, and < -4 insoluble; f) molar refractivity= 40-130 (**Veber et al., 2002; Ertl and Schuffenhauer, 2009; Daina et al., 2014**).

Twenty-seven out of sixty-one phytocompounds revealed high absorption in the gastrointestinal tract. The limited absorption of drugs in the gastrointestinal (GI) tract often restricts their delivery to parenteral methods (**Abramson et al., 2019**). Twenty compounds showed blood-brain barrier permeation. Blood-brain barrier permeation is important for efficient development of central nervous system (CNS) drugs as it relies heavily on effectively overcoming the challenges posed by the blood-brain barrier (BBB) (**Pardridge, 2009**). With respect to G-protein coupled receptor ligand, ion channel modulator, kinase inhibitor, nuclear receptor ligand, protease inhibitor, and enzyme inhibitor, all the sixty-one phytocompounds of *Parkia timoriana* fall under the category of active and moderately active drugs. The mentioned parameters with scores > 0 was deemed indicative of an active drug, while scores ranging from -5.0 to -0.0 were regarded moderately active medications, and scores < -5.0 were classified as inactive pharmaceuticals (**Molinspiration cheminformatics, 2022; Daina and Zoete, 2016**). Thirty-eight phytocompounds successfully met the P-gp (P-Glycoprotein) substrate criteria. P-glycoprotein (Pgp) is an exemplary drug transporter that is clinically significant owing to its wide-ranging specificity and its impact on the absorption, distribution, metabolism, excretion, and toxicity (ADMET) characteristics of medicines (**Prachayasittikul and Prachayasittikul, 2016**). Rauwolfscine, speciosine, gardnerine, luteolin-8-C-glucoside, hydroxygardnutine, maritimetin-6-O-glucoside, procyanidin B1, and hirsutine were alert for PAINS filters, which means they have the probability of giving false positive results (**Baell and Holloway, 2010**). Nineteen phytocompounds did not show alert for BRENK, therefore considered to have good pharmacokinetics (**Brenk et al., 2008**). The majority of the phytocompounds had lesser skin permeability, with isoschaftoside considered the least skin permeability, followed by ouabain, apigenin glucoside arabinoside, and isorhamnetin-3-O-rutinoside since a more negative value indicate a lesser permeability to the skin (**Potts and Guy, 1992**). The synthetic accessibility score showed that the ease of synthesis of majority of the phytocompounds is moderate as the score 1 indicate easy to synthesize, while a score of 10 is very difficult to be synthesize as a drug (**Ertl and Schuffenhauer, 2009**). The majority of the compounds indicated good oral bioavailability, as a score ≥ 0.55 shows good bioavailability (**Khalifaoui et al., 2021**). The majority (thirty-nine) of the phytocompounds inhibited one or the other enzyme

of the cytochrome p450 enzyme complex. This inhibition leads to reduced metabolism of the compounds. In the case of most medications, this may result in higher amounts of the unchanged substance in the blood, which increases the risk of toxicity (**Ogu and Maxa, 2000**). Several lead ligand compounds in this research failed to meet the criteria for ADMET properties. Nevertheless, research has shown that there are some constraints when it comes to accurately forecasting the drug-like properties and physicochemical characteristics of ligand molecules (**Neidle, 2012; Schneider, 2013**).

3.5.2. Molecular docking

The current study aims to identify novel inhibitors of BACE1 and AChE protein receptors from phytochemicals found in the methanolic extract of *P. timoriana* seed pods, with the purpose of assisting in the treatment of Alzheimer's disease. BACE1 is the primary receptor that has to be targeted in order to stop the harmful effects of A β , which ultimately leads to the development of toxic amyloids and the death of neurons (**Moussa-Pacha et al., 2020; Machauer et al., 2021**). The cholinergic hypothesis of Alzheimer's disease states that the destruction of cholinergic neurons in the brain and the decrease in cholinergic transmission (resulting in a deficiency of acetylcholine, serotonin, and noradrenaline) are responsible for the development of cognitive and non-cognitive symptoms in patients with Alzheimer's disease (**Lunardi, 2010; Marucci et al., 2021**).

Based on the findings of molecular docking, the majority of ligands exhibited a strong binding affinity for both BACE1 and AChE receptors. The analysis of the findings revealed that the compounds exhibit binding affinities ranging from -5.3 kcal/mol to -10.3 kcal/mol for BACE1, and from -6.0 kcal/mol to -10.3 kcal/mol for AChE. Among the sixty-one compounds, sixteen compounds, including ergocristine, nicotiflorin, voacamine, isorhamnetin-3-O rutinoside, apiin, apigenin glucoside arabinoside, ginsenoside F3, isoschaftoside, silychrystin, procyanidin B1, maritimetin-6-O-glucoside, rauwolscine, luteolin-8-C-glucoside, paeoniflorin, soyasapogenol B base + O-DDMP, O-HexA-HexA, and ouabain exhibited a binding affinity of ≤ -9.0 kcal/mol for BACE1. Additionally, fifteen compounds, including 1H-Purin-6-amine, N-((3-fluorophenyl) methyl)-, taurodeoxycholate, isoschaftoside, silychrystin, ergocristine,

demethoxycurcumin, cycloheximide, artocarpin, rotenone, apiin, loganin, maritimetin-6-O-glucoside, paeoniflorin, taurochenodeoxycholate, and taurocholic acid) for AChE showed a binding affinity of ≤ -9.0 kcal/mol. The compounds that had a binding energy value of ≤ -9.0 kcal/mol being chosen to identify the highest rated compounds for inhibiting the target receptors (Ul Haq et al., 2017). Different studies have shown that ouabain (Song et al., 2019), voacamine (Currais et al., 2014), isorhamnetin-3-O rutinoside (Mahnashi et al., 2023), apigenin (Venigalla et al., 2015), isoschaftoside (Madi et al., 2020), procyanidin B1 (Qian et al., 2022), luteolin (Choi et al., 2014), paeoniflorin (Meng et al., 2022), taurodeoxycholate (Elhabak et al., 2023), demethoxycurcumin (Villaflares et al., 2012), cycloheximide (Zhong et al., 2021), and loganin (Nie et al., 2021) have ameliorative effects of cognitive impairments and pathogenic burden in Alzheimer's disease treatment.

3.5.3. Molecular dynamics simulation

A molecular dynamics (MD) simulation study was performed on the most significant protein-ligand complexes. These complexes have a strong binding affinity (≤ -10.1 kcal/mol for BACE1 and ≤ -9.8 kcal/mol for AChE) to the active site of the receptors, which aids in evaluating their docking. Various parameters, including RMSD, RMSF, H-bonds, Rg, non-bonded interactions, and hydrophobic interactions, were analysed to assess the stability, compactness, and folding of the structures. The study's findings revealed that the lead ligands formed stable complexes with the BACE1 and AChE receptors, as evidenced by their low RMSD values. This indicates the structural stability and low mobility of the ligand-receptor during simulation. Additionally, the low RMSF value suggests the compactness and stability of the amino acid residues of the BACE1 and AChE receptors throughout the simulation process. In addition, the stability of the bound complexes (BACE1-ligand and AChE-ligand complexes) was evaluated using the Radius of Gyration (Rg). The findings indicated a low Rg value, which corroborated the great compactness and proper folding of the protein receptors when complexed with the lead ligands. The number of H-bonds between the ligand and receptor within the complex further proved the stability of the complex, as a decent number of hydrogen bonds were formed throughout the simulation for almost all the receptor-ligand complexes (Majumder et al., 2022). However, despite the fact that

the complexes formed have almost identical binding affinities, there was a notable disparity in the formation of hydrogen bonds in the solvent environment among the complexes formed in both the receptors for the lead ligands. This might be attributed to the strong influence of the solvent on the binding of the ligand (Rafi et al., 2022).

3.5.4. Free energy binding

The total binding free energy of the receptor-ligand complex for the top lead ligands was calculated for the 100 ns MD simulation trajectories using the MM-PBSA method. This calculation took into account the non-bonded interaction energies, specifically the E_v (van der Waal's energy), E_e (electrostatics energy), and the G_p (polar energy) and G_{np} (nonpolar solvation energy, SASA). According to the outcome, all of the bound complexes exhibited a very favourable total binding energy, thereby providing more evidence of the complexes' stability. The transition states of all the complexed structure, as seen in terms of E_X , exhibited reduced fluctuations. This suggests that there were consistent and enduring interactions between the receptor and ligand complex throughout the 100 ns simulation period. Residual disintegration analysis reveals that the lead ligands are coupled to the BACE1 receptor via identical amino acid residues (**Figure 16B**). Similarly, identical amino acid residues of AChE were involved in binding with the lead ligands (**Figure 17B**). The study also examined the main energy contribution of the BACE1 receptor's amino acids in the binding of lead ligands (ergocristine, nicotiflorin, isorhamnetin-3-O-rutinoside, and voacamine) at the active site. The residues TYR 71, ASP 106, ASP 228, PHE 108, SER 35, ASP 32, and ASP 223 of the BACE1 receptor played a significant role in the intermolecular interaction and the binding of the ligands. However, in complexes involving AChE and ligands, distinct amino acid residues played a role in contributing to the binding energy for each of the lead ligands. Low E_X values were reported in the docked complexes, indicating strong and stable protein-ligand complex binding, which is mainly contributed by E_v , E_e , and E_{np} intermolecular interactions (Sharma et al., 2020).

3.5.5. Principal component analysis

Principal Component Analysis was used to assess the structural phase space and transition dynamics of the principal components, namely PCA1 and PCA2, in order to

determine the stability of the receptor-ligand complexes. The analysis focused on the C α atoms. The PCA plots illustrate the positive (C α atoms moving in the same direction) and negative (C α atoms moving in the opposite direction) extremes of eigenvector 1 and eigenvector 2. The motion of C α atoms in the receptor, when interacting with different ligands, exhibited consistent, parallel, and comparable movement. The receptor-ligand complexes were examined and their eigenvector values were determined using a diagonalized covariance matrix. The first and second principal components (PCA1 and PCA2) of the BACE1 and AChE complexes, when bound to their ligands, exhibited less pronounced conformational changes. This suggests that the movements of the carbon atoms were more restricted, perhaps owing to the formation of intermolecular interactions, namely hydrogen bonds, between the receptor and the ligands (**Macalalad and Gonzales, 2022**). Moreover, it is evident that the ligands stay consistently bound to the active site of the BACE1 and AChE receptors without undergoing any structural alterations, suggesting that the ligand molecules are in harmony with the target receptor.

3.6. KEY FINDINGS

- From the ADMET studies, forty compounds showed drug-likeness properties as indicated by Lipinski's rule of five, thirty-two compounds were considered to have a good affinity for a lipophilic environment, thirty-one compounds that have the capacity to be absorbed by the body when taken orally and have the ability to reach certain target areas inside the body as per their TPSA value, forty-eight compounds have non-hydrogen atoms that falls under the acceptable range, sixteen compounds possess an acceptable molar volume, and thirty-six compounds were in the acceptable range of molar refractivity. No compound was found highly soluble as per LogS value. However, six compounds showed solubility, twenty compounds slightly soluble, and thirty-five compounds lack solubility.
- Additionally, twenty-seven phytocompounds revealed high absorption in the gastrointestinal tract, and twenty compounds showed blood-brain barrier permeation. With respect to GPCR, ion channel modulator, kinase inhibitor, nuclear receptor ligand, protease inhibitor, and enzyme inhibitor, all the sixty-

one phytocompounds of *Parkia timoriana* fall under the category of active and moderately active drugs. Thirty-eight phytocompounds successfully met the P-gp substrate criteria, fifty-three showed no alert for PAINS filters, and nineteen phytocompounds did not show alert for BRENK. The majority of the phytocompounds had lesser skin permeability. Similarly, the majority of the compounds indicated good oral bioavailability and can be moderately synthesize. Thirty-nine compounds inhibited one or the other enzyme of the cytochrome p450 enzyme complex.

- The molecular docking analysis revealed that the phytocompounds from the methanolic extract of *Parkia timoriana* seed pods strongly bind to BACE1 and AChE receptors, with binding affinities ranging from -5.3 kcal/mol to -10.3 kcal/mol against the BACE1 receptor and from -6.0 kcal/mol to -10.3 kcal/mol against the AChE receptor. Sixteen and fifteen phytocompounds had binding affinity \leq -9.0 kcal/mol against BACE1 and AChE, respectively.
- The selected top hit ligands for the BACE1 receptor include ergocristine as the best-ranked ligand with a binding affinity of -10.3 kcal/mol, followed by nicotiflorin, voacamine, and isorhamnetin-3-O-rutinoside with binding affinity of -10.2 kcal/mol, -10.1 kcal/mol, and -10.1 kcal/mol, respectively.
- The top hit ligands for the AChE receptor include apiin and maritimetin-6-O-glucoside as the best binding ligands with binding affinity of -10.3 kcal/mol each, followed by paeoniflorin and silychrystin with binding affinity of -10.2 kcal/mol and 9.8 kcal/mol, respectively.
- TRP76, PHE108, TYR71, LYS107, and ILE126 were the most common residues of BACE1, among the other interacting residues, that were interacting with the top hit ligands through hydrogen and hydrophobic bonds and therefore may be important in ligand binding.
- SER125, TYR341, TYR124, and TRP86 were the most common residues of AChE, among the other interacting residues, that were interacting with the top hit ligands through hydrogen and hydrophobic bonds and therefore may be important in ligand binding.

- The MD simulation studies confirmed that the top hit ligands formed a stable complex with BACE1 having RMSD, RMSF, and Rg values of ~0.2 nm, ~0.1 nm, and ~2.0 nm, respectively. However, the BACE1-nicotiflorin and BACE1-isorhamnetin-3-O-rutinoside complexes formed a significantly higher number of H-bonds of 4.94 and 3.88, respectively, compared to the other complexes.
- Similarly, the MD simulation studies confirmed that the top hit ligands formed a stable complex with AChE having RMSD, RMSF, and Rg values as ~0.24 nm, ~0.11, and ~2.3 nm, respectively. On the other hand, the AChE-maritimetin-6-O glucoside and AChE-paeoniflorin complexes formed a higher number of H-bond of 3.27 and 2.76, respectively, compared to the other complexes.
- The binding free energy calculation for BACE1 by MM/PBSA method showed that all the simulated complexes formed a strong bonding complex, with BACE1-voacamine complex showing exceptionally high binding free energy of -417.951 ± 31.736 kJ/mol.
- Similarly, the binding free energy calculation for AChE by MM/PBSA method showed that all the simulated complexes aslo formed a strong bonding complex, with AChE-silychristin complex showing exceptionally high binding free energy of -385.386 ± 18.965 kJ/mol.
- The main energy contribution of the BACE1 receptor's amino acids in the binding of lead ligands at the active site indicated that residues TYR 71, ASP 106, ASP 228, PHE 108, SER 35, ASP 32, and ASP 223 of the BACE1 receptor played a significant role in the intermolecular interaction and the binding of the ligands. However, in complexes involving AChE and ligands, distinct amino acid residues played a role in contributing to the binding energy for each of the lead ligands.
- The principal component analysis showed that the C α of both BACE1 and AChE when complexed with the top hit ligands occupied very less phase space further confirming the stability of the complex formed.

CHAPTER-4

4.1. INTRODUCTION

4.1.1. Toxicity study

4.1.1.1. Acute toxicity test

Acute toxicity is commonly defined as the negative changes that occur immediately or shortly after being exposed to a substance or substances. It can also refer to the adverse effects that happen shortly after taking a single dose of a substance or multiple doses within a 24-hour period. An adverse effect refers to any outcome that causes functional impairment and/or biochemical damage, which might impact the overall performance of an organism or hinder its capacity to adapt to further challenges (**Sass, 2000; Rhodes, 1993**). Therefore, a substance that enters the body via the mouth within a certain timeframe and causes any harmful effects with little delay is considered orally and acutely hazardous. Nevertheless, the phrase acute oral toxicity is mostly used in relation to lethality and the measurement of LD₅₀. Chemicals are classified based on their LD₅₀ value, which is the dosage of a drug that is statistically likely to cause death in 50% of the animals in an experimental group (**Gribaldo et al., 2005; Walum, 1998**).

The primary objectives of acute toxicity testing are to gather data on the biological activity of a chemical and to get a deeper understanding of its mechanism of action. Moreover, the data obtained from the test about acute systemic toxicity is used for the purpose of identifying potential hazards and managing risks associated with the manufacture, handling, and utilisation of chemicals (**Gribaldo et al., 2005**). The LD₅₀ value, whether accurate or approximate, serves as the foundation for the toxicological categorization of chemicals. Consequently, it is often unnecessary to get an accurate LD₅₀ value in the research. Therefore, testing is conducted at the highest thresholds of danger categorization levels (**Schrage, 2011**).

Currently, it is mandated by government bodies in many circumstances for the study of acute toxicity. Consequently, the evaluation of chemicals and agrochemicals globally still necessitates the study of acute oral toxicity (**Schrage, 2011**). The Organisation for Economic Co-operation and Development (OECD) recommends the

use of oral LD₅₀ values. The OECD classifies substances based on their toxicity levels: very toxic, < 5 mg/kg body weight; toxic, > 5 < 50 mg/kg; harmful, >50<500 mg/kg; and no label, > 500 < 2000 mg/kg (Walum, 1998).

4.1.1.2. Sub-acute toxicity

Subacute toxicity studies are performed to assess the possible negative effects of a new medicine after a treatment period of 2-4 weeks. This study presents details on the potential health risks that may occur as a result of frequent and limited-term exposure (OECD, 2008). Subacute toxicity studies are performed as preliminary investigations to determine appropriate dose levels for further sub-chronic and chronic toxicity studies. Furthermore, subacute toxicity studies might provide further evidence for the first clinical trials, during which the treatment period may extend up to 4 weeks. These studies aim to evaluate the advancement and reversal of drug-induced damage (Colerangle, 2017). The test substance is supplied on a daily basis for a predetermined period of time. Dosages are often determined based on data gathered from acute toxicity studies, which include the use of LD₅₀ and the slope of the dose response curve (Agrawal and Paridhavi, 2007). It is important to accurately identify the target organs affected by toxicity and assess the potential reversibility of the toxic effects. The maximum dosage used in these experiments is intentionally chosen to elicit toxicity. A minimal dosage is used in order to determine the No Observed Adverse Effect Level (NOAEL). Whenever feasible, the NOAEL (No Observed Adverse Effect Level) dosage should be chosen to be a sufficient multiple of the anticipated maximum clinical dose (Colerangle, 2017).

4.1.1.3. Liver function test

The liver is the primary site of metabolism and drug biotransformation, making liver cells a suitable option for toxicological and pharmacological testing (Soldatow et al., 2013). Chemical-induced liver toxicity often occurs due to the combined effects of general cell type-nonspecific cytotoxicity and liver tissue-specific toxicity (Tabernilla et al., 2021). Drug-induced liver damage is a significant contributor to liver dysfunction. It may result in a variety of symptoms, ranging from mild, non-specific symptoms such as asymptomatic transaminitis, acute hepatitis, chronic hepatitis, and

cholestasis to liver failure (**Alempijevic et al., 2017**). It may be triggered by a wide range of prescription medicines, natural remedies, and nutritional supplements (**Holt and Ju, 2010**).

Typically, drug-induced liver damage results in a mild to moderate increase in liver tests. However, in exceptional circumstances, it might result in deadly consequences (**García Rodríguez et al., 1997**). It may lead to an increase in liver enzymes such as alanine aminotransferase (ALT), aspartate aminotransferase (AST), alkaline phosphatase (ALP), gamma-glutamyl transferase (GGT), and total bilirubin (**Ye et al., 2018**). Signs of severe liver damage include increased levels of bilirubin in the blood, decreased albumin levels, and impaired blood coagulation (**Yu et al., 2017**). In hepatocellular drug-induced liver damage, the level of ALT is higher compared to ALP. Conversely, in cholestatic liver injury, the level of ALP is higher compared to ALT (**Katarey and Verma, 2016**). In 2011, the International Serious Adverse Events Consortium (iSAEC) proposed revised biochemical criteria for detecting drug-induced liver damage, which include meeting any of the following criteria: a) Elevated alanine transferase levels equal to or above 5 times the upper limit of normal (ULN); b) Alkaline phosphatase levels equal to or higher than twice the ULN, particularly in patients with increased 5'-nucleotidase or GGT, and without elevation of ALP due to bone diseases; c) Alanine transferase levels equal to or higher than three times the ULN and total bilirubin levels equal to or higher than twice the ULN (**Aithal et al., 2011**).

4.1.1.4. Kidney function test

The kidneys have a crucial function in eliminating waste products and toxins, such as creatinine, urea, and uric acid. They also regulate the volume of fluid outside the cells, the concentration of electrolytes, and the osmolality of the blood serum. Additionally, the kidneys produce hormones like erythropoietin, 1,25 dihydroxy vitamin D, and renin (**Okoro and Farate, 2019; Damiasi, 2019**). Various clinical laboratory tests are valuable for exploring and assessing kidney function. Creatinine is the most often used endogenous marker for evaluating glomerular function. Creatinine is a metabolic waste product derived from creatine phosphate in muscle tissue, and it is generated by the body at a consistent pace. The kidney is primarily responsible for completely

removing creatinine from the bloodstream. Reduced renal clearance leads to elevated levels of creatinine in the bloodstream (**Gounden et al., 2023**).

Urea, also known as BUN (blood urea nitrogen), is a nitrogenous substance that is produced in the liver as the final result of protein metabolism and the urea cycle. Approximately 85% of urea is excreted via the renal system, while the remaining portion is removed through the gastrointestinal (GI) tract. Conditions characterised by reduced renal clearance led to an elevation in serum urea levels (**Kamianowska et al., 2019**).

4.1.1.5. Haematological parameters

The evaluation of haematological parameters may be used to diagnose the harmful effects of foreign substances on the blood components of an animal (**Ashafa et al., 2012**). Administering chemical substances at dangerous dosages sometimes leads to alterations in blood parameters that are symptomatic of haematological illnesses, such as anaemia, which is characterised by a low level of haemoglobin (**Price and Schrier, 2008**). Neutropenia is a condition characterised by a decrease in the production of white blood cells or an increase in their utilisation and destruction, or both (**Bodey et al., 1982**). Thrombocytopenia is a condition where there is a decrease in the number of platelets due to reduced platelet production, shorter platelet survival, and dilution of platelet numbers resulting from the transfusion of blood with a low platelet count. Malignancies such as leukaemia, lymphoma, and myeloma are also associated with these conditions (**Bradbury and Murray, 2013; Izak and Bussel, 2014**).

Blood parameters are crucial indications for determining the true physiological condition of an organism. In order to operate effectively, an organism must maintain a consistent and stable composition of its blood and its contents in normal settings (**Pankaj and Varma, 2013**). Haematological changes are more reliable indicators of human toxicity (**Yakubu et al., 2007**).

4.1.2. Alzheimer's disease

4.1.2.1. Aluminum chloride-induced Alzheimer's disease

Environmental heavy metals are well-known agents that have a proven influence on brain development via their neurotoxic effects. There is increasing evidence suggesting a link between heavy metals and neurodegenerative disorders such as Alzheimer's disease (AD) and Parkinson's disease (**Nallagouni and Reddy, 2017**). Heavy metals are well recognised for their ability to harm the neurological system. Among all the heavy metals, the impact of aluminum (Al) on biological systems has been well documented (**Chiroma et al., 2018; Exley, 2013; Mujika et al., 2014**).

The brains of individuals with AD have been shown to have a significant concentration of Al, which leads to toxicological consequences such as encephalopathy, bone disease, and anaemia. The accumulation of aluminum in aged neurons is likely mostly due to dietary intake, since the ingestion of aluminum additions is the primary way the general population is exposed to aluminum (**Walton, 2007**). Recently, it was observed that orally administering Al (300 mg/kg body weight) caused oxidative stress, cholinergic deficiency, and the buildup of A β and NFTs in the brains of rats (**Chiroma et al., 2018**). Several other laboratory animal investigations have also shown that aluminum-induced neuropathological, neurochemical, and neurobehavioral alterations are comparable to those seen in Alzheimer's disease (AD) (**Justin Thenmozhi et al., 2017; Alawdi et al., 2017; Yin et al., 2020**).

Furthermore, the Al-treated group exhibits significant histological alterations, including widespread gliosis accompanied by pericellular oedema in the brain area. Additionally, there is evidence of neuronophagia and neuronal death. Multiple studies have shown a strong correlation between aluminum neurotoxicity and cognitive impairment in Alzheimer's disease. This connection is mostly attributed to oxidative stress and disruption in the cholinergic system (**Willhite et al., 2014**). The results have shown an increase in the expression and activity of acetylcholinesterase (AChE) and malondialdehyde (MDA), but a notable reduction in the expression and activity of glutathione-s-transferase (GST), glutathione peroxides (GPX), and glutathione reductase (GR) (**Attia and Ahmed, 2020**).

4.1.2.2. Alzheimer's disease pathology

The main structural pathologies of Alzheimer's disease are the buildup of extracellular amyloid- β (A β) protein as senile plaques, the formation of neurofibrillary tangles within neurons due to aberrant hyperphosphorylation of tau protein in the cytoskeleton, and extensive neuronal death (**Selkoe, 2001**). The hippocampus is among the first brain regions to be impacted by these disorders (**Braak et al., 1993; Mu and Gage, 2011**).

The APP is normally cleaved by α -secretase and improperly processed by β - and γ -secretases, leading to an imbalance in the generation and removal of A β peptide (**Salomone et al., 2012**). Therefore, A β peptides naturally come together to form soluble oligomers and then combine to create insoluble fibrils with a β -sheet shape. These fibrils are ultimately deposited in widespread senile plaques (**Hardy, 2009**).

Kinase enzymes, such as glycogen synthase kinase 3 β (GSK-3 β), and phosphatases have a role in regulating tau (**Mi and Johnson, 2006**). Accumulation of A β in the brain of individuals with Alzheimer's disease triggers the activation of kinases, such as GSK-3 β , which then phosphorylate tau NFTs (**Cho and Johnson, 2004**).

4.1.2.3. Neuroinflammation

Alzheimer's disease is characterised by neuroinflammation and abnormal gliosis, as shown by recent investigations (**Salter and Stevens, 2017**). Genetic and transcriptome investigations have also validated the inflammatory theory (**Zhang et al., 2013; Bolós et al., 2017; Guerreiro et al., 2013**). Microglia-associated pathways were identified as significant risk factors for Alzheimer's disease and its development. Abundant evidence has revealed that microglia play a vital role. During the early stage of AD, microglia and its associated proteins might impact the decrease in synaptic connections (**Paolicelli et al., 2011; Hong et al., 2016**).

The production of pro-inflammatory cytokines, such as IL-1 β , IL-6, IL-18, and tumour necrosis factor (TNF), chemokines like C-C motif chemokine ligand 1 (CCL1), CCL5, and C-X-C motif chemokine ligand 1 (CXCL1), small-molecule messengers like prostaglandins and nitric oxide (NO), and reactive oxygen species by innate immune cells in the central nervous system (CNS) can lead to synaptic dysfunction, neural cell

death, and destruction of neurogenesis (**DiSabato et al., 2016**). The primary intrinsic immune cells involved in this process are mostly microglia and astrocytes. Capillary endothelial cells and infiltrating blood cells contribute to neuroinflammation, especially in cases when there is pharmacological or mechanical disruption of the blood-brain barrier (BBB) (**DiSabato et al., 2016; Heneka et al., 2014**).

NF- κ B's significant role in cellular inflammatory responses has garnered attention as a promising subject for research on inflammatory illnesses. Toll-like receptors (TLRs) are excessively produced on microglia and neurons in the AD brain. Toll-like receptors (TLRs) primarily stimulate the canonical NF- κ B signalling pathway, resulting in the production of proinflammatory molecules (**Chiarini et al., 2020**). Therefore, the initiation of NF- κ B signalling and subsequent secretion of cytokines and chemokines by microglia leads to the persistent inflammation that is found in Alzheimer's disease (**Thawkar and Kaur, 2019**).

4.1.2.4. Oxidative stress

Oxidative stress is considered to be crucial in the development of Alzheimer's disease (**Manoharan et al., 2016**). The brain is recognised for its higher energy consumption and greater functional demands compared to other organs during mitochondrial respiration. This also leads to an increased chance of exposure to reactive oxygen species (ROS) (**Chen et al., 2018**). Moreover, AD is intricately associated with molecular oxidative stress, protein nitration, increased protein oxidation, lipid peroxidation, and glycooxidation. Furthermore, AD is strongly associated with the accumulation of A β , which has been shown to induce oxidative stress (**Butterfield et al., 2002; Gibson et al., 2004; Mohammad Abdul et al., 2006**). Therefore, antioxidant substances are promising candidates for providing protection against oxidative stress and A β toxicity, to some degree. While oxidative stress is a factor in Alzheimer's disease (AD), the effectiveness of the antioxidant strategy in slowing down the progression of AD has been questioned. It has been recommended that antioxidant therapy should be used in tandem with other treatments (**Teixeira et al., 2013; Persson et al., 2014**).

4.1.2.5. Apoptosis

In Alzheimer's disease, there is a significant amount of neuronal death seen in many regions of the brain. The degeneration of neurons in Alzheimer's disease starts in the preclinical stage and continues to worsen during the prodromal phase, or mild cognitive impairment (MCI) and AD dementia. Initially, there may be a loss of neurons in specific regions, such as the entorhinal cortex, basal nucleus of Meynert, and locus coeruleus. However, as the disease progresses, neuronal loss becomes more widespread and affects multiple areas of the brain, including the hippocampus, amygdala, temporal lobe, frontal cortex, and parietal cortex (**Serrano-Pozo et al., 2011; Arendt et al., 2015; DeTure and Dickson, 2019**). Apoptosis, a programmed cell death process, is triggered by various factors such as p21, p38, mitogen-activated protein kinase (MAPK), c-Jun-NH2-terminal protein kinase, p53, caspases 2, 3, 8, and 9, BCL-XS, Bax, apoptosis-inducing factor, and Par-4 (**Lauterbach et al., 2010; Friedlander, 2003; Zhang et al., 2003; El-Guendy and Rangnekar, 2003**). On the other hand, B cell lymphoma/leukemia-2 protein (Bcl-2), Bcl-XL, and other factors act as inhibitors of apoptosis (**Kim, 2005**).

4.1.2.5. Behavioural study

Several behavioural tests have been developed to assess the cognitive impairments associated with Alzheimer's disease pathology in mouse models. The Morris water maze is the predominant approach used to assess spatial memory in rats (**D'Hooge and De Deyn, 2001**). Contextual memory tests, such as fear conditioning, are often used to assess hippocampal functioning (**Dineley et al., 2002**) and may also be utilised in animal models of Alzheimer's disease (**Comery et al., 2005**). The Y-maze and T-maze, when combined with positive or negative stimuli, are used to determine particular information that animals use to choose between response possibilities. These mazes are often used to assess working memory in animal models of Alzheimer's disease. The Ennaceur and Delacour study in 1988 introduced the novel object recognition test. This test relies on the innate tendency of rats to exhibit more interaction with a new item compared to a known one (**Ennaceur and Delacour, 1988**). This test does not assess the animals' spatial reference memory, unlike the Morris water maze. However, the

novel object recognition experiment yielded comparable findings to those of the Morris water maze. The novel object recognition is a simple and stress-free test for mice, making it an appropriate first screening assay to assess cognitive function in an Alzheimer's disease model (Zhang et al., 2012).

4.2. REVIEW OF LITERATURE

4.2.1. Acute and sub-acute toxicity study

Upadhyay et al. (2019) assessed the harmful effects of a hydroalcoholic extract of *Reinwardtia indica* leaves in Charles Foster rats, using both acute and sub-acute experiments. In the acute toxicity test, rats were administered a single dosage orally, but in the sub-acute phase, they were given varying doses orally for 28 consecutive days. The satellite group was administered a dosage of 2000 mg/kg for a duration of 6 weeks, following the standards set by OECD-407. The acute toxicity study evaluated general behavioural indicators and saw no deaths or visible symptoms of harm. During the sub-acute investigation, the animals were examined for biochemical, haematological, and histopathological markers, as well as for body weight, food intake, and water consumption, after 14 and 28 days. The research indicates a statistically insignificant ($P < 0.05$) difference in the treatment group compared to the control group. The hydroalcoholic extract of *Reinwardtia indica* leaves was determined to be non-toxic in acute studies at a dosage of up to 5000 mg/kg and in sub-acute studies at a dosage of up to 2000 mg/kg.

Marak et al. (2023) conducted an assessment of the acute and sub-acute toxicity of the methanolic extract of *Cycas pectinate* fruit (CPFE) on mice by administering it orally. The examination of phytochemicals was conducted using LC-MS, NMR, and FTIR. The research on acute toxicity was conducted using a single dosage of 1000, 3000, and 5000 mg/kg, whereas the study on sub-acute toxicity included daily administration of doses of 100, 300, and 500 mg/kg over a period of 28 days. The LD₅₀ of CPFE was determined to be 4000 mg/kg. The levels of AST, ALT, ALP, and bilirubin were tested, and the findings indicated that ALT, ALP, and direct bilirubin were reduced in the groups receiving 1000 and 3000 mg/kg compared to the control group. However, these changes were not statistically significant. The liver is a crucial organ that is susceptible

to xenobiotics (**Bariweni et al., 2018**). AST, ALT, and bilirubin are biomarkers that may detect hepatocellular toxicity, and their increased levels signal liver damage (**Ramaiah, 2011**). Both the acute and sub-acute investigations indicated that a dosage of 5000 mg/kg and 500 mg/kg was hazardous to the mice. The acute toxicity findings demonstrated that CPFE had a minor toxic impact on the kidney at doses of 3000 and 5000 mg/kg. This was evident from the observed deteriorating alterations in the kidney as well as a rise in creatinine levels. At a dosage of 3000 mg/kg, acute toxicity resulted in an elevation of white blood cells (WBC). Nevertheless, sub-acute toxicity tests indicate no adverse impact on liver, renal, or haematological markers. Therefore, it may be inferred that CPFE administered at a dosage of 100 and 300 mg/kg would be considered safe for ingestion.

Patel et al. (**2022**) assessed the short-term and long-term oral toxicity of anti-obesity polyherbal granules (PHG) in Sprague Dawley rats, following the recommendations provided by the OECD in documents No. 425 and 407. The use of herbal medicines is increasing annually in many nations, driven by a misguided perception that ayurvedic preparations are devoid of any negative consequences, without taking into account the documented instances of pharmacovigilance (**Leenaars et al., 2019**). However, toxicological investigations are crucial for the development of new pharmaceuticals in pharmaceutical businesses, including the manufacturing of ayurvedic drugs. The purpose of this research is to assess the acute oral toxicity of PHG in rats. A single dosage of 2 g/kg of PHG was given to the rats, and their mortality, body weight, and clinical observations were recorded for a period of fourteen days. Nevertheless, in the subacute oral toxicity trial, the PHG was delivered orally at dosages of 0.3, 0.5, and 1 g/kg per day for a duration of 28 days to rats. The consumption of food and the measurement of body weight were recorded on a weekly basis. On the 29th day, rats were euthanized, and their blood, biochemistry, urine, organs, and tissues were analysed for haematological, biochemical, necropsy, and histological purposes. No treatment-related mortality, behavioural abnormalities, or toxicity were seen in an acute oral toxicity trial conducted over a period of fourteen days. In the sub-acute toxicity investigation, no deaths or harmful effects were seen in the examination of blood, biochemistry, urine, necropsy, and histopathology in rats treated with PHG for

28 days. The findings indicate that the LD₅₀ of PHG is higher than 2 g/kg and the no-observed-adverse-effect limit (NOAEL) of PHG for rats is 0.5 g/kg/day. Therefore, based on the results of animal research, it can be concluded that anti-obesity polyherbal granules have a favourable safety profile and may be regarded as a significant treatment option for managing obesity in clinical settings.

Jegnie et al. (2023) assessed the acute and sub-acute toxicity of 80% methanolic extracts from the leaves of *Justicia schimperiana* in Wistar albino rats, following the guidelines set by the OECD for acute toxicity testing, guideline 423, and guideline 407 for sub-acute toxicity testing. *J. schimperiana* has been historically used for treating several ailments such as jaundice, rabies, anthrax, asthma, common cold, stomachache, diarrhoea, tapeworm infestation, wounds, external parasites, and skin irritation in several parts of Ethiopia (Abera, 2014; Chekole et al., 2015). For the acute toxicity research, three female rats were orally given a single dosage of 5000 mg/kg of extract. For the sub-acute research, the plant extract was given orally for 28 consecutive days at daily doses of 250, 500, and 1000 mg/kg. No fatalities or major morbidities occurred as a consequence of administering the plant orally in a single dosage. The LD₅₀ was more than 5000 mg/kg. The 28-day oral administration of the plant extract did not have a notable impact on overall behaviour, food consumption, organ weight, biochemical parameters, or most of the haematological markers. However, there was a reduction in haemoglobin and hematocrit levels in the groups treated with 1000 mg/kg of the extract, compared to the control group. Both genders exhibited substantial weight gains at all dose levels. No major histological change was seen. The study concludes that the methanolic leaf extract of *J. schimperiana*, whether administered orally in a single dosage or in repeated doses over a period of 28 days, is considered to be reasonably safe.

4.2.2. Alzheimer's disease treatment

Alawdi et al. (2017) sought to examine the neuroprotective properties of nanodiamond (ND), which are nanoparticles based on adamantine, in rats with aluminum-induced cognitive impairment. Alzheimer's disease was induced by the administration of aluminum chloride at a dosage of 17 mg/kg orally for a duration of 6 weeks. Elevated

concentrations of aluminum in the brain may hinder long-term potentiation, which is believed to be the primary physiological mechanism underlying learning and memory (Shuchang et al., 2008; Llansola et al., 1999). The presence of AD was established by the use of Morris water maze and Y-maze behavioural tests. These behavioural experiments are often used to evaluate the impact of different treatments on spatial recognition learning and memory (Morris, 1984; Hidaka et al., 2011). Additionally, biochemical and histological investigations were conducted on the hippocampus. Rats treated with aluminum exhibited behavioural, biochemical, and histological alterations that resembled those linked to AD. ND enhanced cognitive abilities and restored structural changes in the tissues. ND at the molecular level reduced the rise of hippocampal A β 42 and BACE1, while also decreasing the amounts of phosphorylated tau protein. Additionally, it regulated the amount of the excitatory neurotransmitter glutamate. In addition, ND increased the levels of BDNF and mitochondrial transcription factor-A (TFAM), while reducing the levels of the proinflammatory cytokines TNF- α and IL-6. It also mitigated oxidative stress by inhibiting the activity of iNOS. In addition, ND increased the levels of p-STAT3 and Bcl-2 anti-apoptotic protein in the hippocampus, while reducing the expression of NF- κ B and caspase-3. The production of TNF- α and IL-6 in the hippocampus is likely associated with the accumulation of A β , phosphorylation of tau, activation of NF- κ B and reduced phosphorylation of STAT3 (Rubio-Perez and Morillaz-Ruiz, 2012; de Jonge et al., 2005). The results suggest that ND has a protective impact against memory impairments and Alzheimer's disease-like pathological abnormalities. This effect is likely achieved via regulating NF- κ B and STAT3 signalling pathways, perhaps through the modulation of N-methyl-D-aspartate (NMDA) receptors.

Cao et al. (2017) determined the neuroprotective effects of *Hypericum perforatum* extract (HPE) on rats with Alzheimer's disease caused by AlCl₃. *H. perforatum* has gained significant attention over the last twenty years for its strong antioxidant, anti-inflammatory, antibacterial properties, as well as its ability to enhance memory (Hasler, 2002; Butterweck et al., 2003). Rats were administered AlCl₃ over a period of 90 days in order to elicit behavioural, biochemical, and neurochemical changes comparable to those seen in Alzheimer's disease (AD). Starting from the 31st day, the

rats received HPE treatment for a duration of 60 days. The findings of our study shown that HPE effectively enhanced cognitive performance in rats with Alzheimer's disease produced by AlCl_3 . Additionally, HPE mitigated the rise in acetylcholinesterase activity and glutamic acid level caused by AlCl_3 , while also reducing noradrenaline and dopamine levels. The increase in AChE activity leads to enhanced breakdown of acetylcholine, causing a subsequent decrease in cholinergic neurotransmission, which is directly associated with AD (**Francis et al., 1999**). Furthermore, HPE effectively counteracted the hippocampal damage caused by AlCl_3 . This included reducing the accumulation of $\text{A}\beta$, such as elevated $\text{A}\beta_{42}$ levels and the presence of amyloid plaques. HPE also mitigated oxidative stress by decreasing reactive oxygen species levels and thiobarbituric acid reactive substances levels, while increasing glutathione levels and superoxide dismutase activity. Additionally, HPE suppressed neuroinflammation by reducing the mRNA expressions of IL-1b, IL-6, TNF- α , and MHC-II in the hippocampus of rats. Several studies propose that a reciprocal activation of $\text{A}\beta$, oxidative stress, and neuroinflammation may form a harmful loop, ultimately resulting in the onset and advancement of AD (**Daulatzai, 2016; Zhou et al., 2016**). Therefore, HPE provides neuroprotection against the Alzheimer's disease-like pathology produced by AlCl_3 .

Khalifa et al. (**2020**) investigated the neuroprotective impact of telmisartan in rats with aluminum-induced cognitive impairment. Telmisartan, an angiotensin II type 1 receptor (AT1R) antagonist (ARB), shown a prophylactic benefit in a mouse model of ischemia/reperfusion by inhibiting the AT1R. Furthermore, it had a defensive impact against oxidative stress, inflammation, and apoptosis in a rat model of intracerebral haemorrhage (**Wincewicz and Braszko, 2014**). Aluminum chloride was supplied intraperitoneally at a dosage of 10 mg/kg for a duration of 2 months. Subsequently, behavioural tests, namely the Y-maze and Morris water maze, were conducted. Subsequent to that, an examination of the biochemical and histological aspects of the hippocampus was conducted. The hippocampus is one of the first and most seriously affected regions in Alzheimer's disease (**Bingman, 1992**). The hippocampus is more vulnerable to oxidative stress compared to other parts of the brain (**Miller and O'Callaghan, 2005; Yargicoglu et al., 2007**). Rats treated with aluminum exhibited

histological, biochemical, and behavioural changes similar to those seen in Alzheimer's disease. Telmisartan enhanced the well-being of the rats both in terms of their behaviour and histological characteristics. The intervention caused a decrease in the levels of hippocampal amyloid beta protein and phosphorylated tau protein, while increasing the level of neprilysin. Additionally, it reduced the levels of NF- κ B, FAS ligand, TNF- α , malondialdehyde, and AChE content.

Zhao et al. (2020) studied the neuroprotective effects of syringic acid (SA) on behavioural impairments and neuroinflammation induced by aluminum chloride in rats with Alzheimer's disease (AD). Syringic acid is a compound derived from benzoic acid and phenolic compounds found in plants and fruits. It has been demonstrated to possess various biological advantages, such as potent immunomodulatory and hepatoprotective effects, as well as the ability to scavenge free radicals and act as an antioxidant, and anti-inflammatory (Gheena and Ezhilarasan, 2019; Rekha et al., 2014). An intraperitoneal injection of AlCl₃ at a dosage of 100 mg/kg of body weight was administered for a duration of 60 days to induce the stimulation of AD. The rats were administered low and high dosages of SA (25 & 50 mg/kg.b.wt) for a duration of 30 days. Following the conclusion of the experiment, behavioural assessments including the Morris water maze, Y-maze, elevated plus maze, and open field test were conducted. After the activity of acetylcholinesterase (AChE), the levels of biochemical measurement and the expression of inflammatory proteins were analysed using western blotting. The AD rats exhibited decreased cognitive function and impaired learning abilities, increased short-term memory loss, and decreased locomotor activity. Remarkably, the neurobehavioral deficits in the AD rats were significantly improved by the addition of SA supplementation. The expressions of NF- κ B, IL-1 β , IL-6, and TNF- α were reduced by the addition of SA to rats with AD. IL-1 β , IL-6, and TNF- α have been widely studied as pro-inflammatory mediators in the brain, and they play a vital role in the pathological progression of memory and learning impairments in Alzheimer's disease (Akiyama et al., 2000). This study showed that the application of SA improved the symptoms of AD induced by AlCl₃.

4.3. MATERIALS AND METHODS

4.3.1. Collection, identification and extraction of *Parkia timoriana* seed pods

Seed pods of *Parkia timoriana* were obtained from Tanhril village in Aizawl, Mizoram. The species bearing the accession number 1016 was identified by the BSI (Botanical Survey of India), Eastern Regional Centre, Shillong. The seed pods were air-dried at normal room temperature and then crushed into a fine powder using an electric grinder (**Figure 1**). The powdered seed pod (100 g) was immersed in methanol (400 ml) at room temperature for at least 72 hours using a cold maceration process (**Kuete et al., 2006**). The mixture was occasionally shaken. The extract was filtered through Whatman filter paper No.1, then subjected to evaporation in an oven at a temperature of 40°C until all the liquid had evaporated. The resulting dry extract was then kept at a temperature of 4°C until used (**Sen et al., 2013**).

4.3.2. Animal ethics

The animal experiments were carried out in compliance with the ethical guidelines for the maintenance and usage of laboratory animals and were authorised by the Mizoram University Institutional Animal Ethics Committee, situated in Aizawl, Mizoram, India (approval no. **MZU/IAEC/2021-22/09**).

4.3.3. Experimental animals

Adult Wistar albino rats weighing 130-160 g were used for the experiment. Animals were housed in polypropylene rat cages (421 × 290 × 190 mm) and kept under controlled environmental conditions: room temperature (25 ± 2 °C), constant humidity (60 ± 10 %), and constant photoperiodic conditions (12:12 h day light/darkness cycles) in the animal facility of the Department of Zoology, Mizoram University, Aizawl. The standard pellet diet and water were allowed ad libitum.

4.3.4. Toxicity study

4.3.4.1. Acute toxicity study

The acute toxicity of *P. timoriana* methanolic extract (PTME) was tested on male adult Wistar albino rats, following the guidelines outlined in the Organisation of Economic

Cooperation and Development (OECD) guideline no. 423. The animals were allocated into four groups using a random process, with each group consisting of five animals ($n = 5$). A single dosage of 1000 mg/kg, 3000 mg/kg, and 5000 mg/kg of PTME dissolved in distilled H₂O was given orally to the rats that had fasted overnight. Control animals were orally given distilled water. Each rat was individually observed for symptoms of acute toxicity for the first 4 hours, followed by 8 hours, and then once daily for a period of 14 days to detect any delayed toxicity indicators. Recorded observations included morphological changes such as alterations in rectal temperature, skin and eye colour, food intake, overall physique, presence of diarrhoea, coma, sleepiness, breathing problems, tremors, fur condition, salivation, red tear production, and mortality. The initial body weight was measured before the administration of PTME, and the final body weight was measured at the conclusion of the experiment.

4.3.4.2. Sub-acute toxicity study

A set of male Wistar albino rats was randomly assigned to four groups, with five rats in each group ($n = 5$), in order to investigate the sub-acute toxicity of PTME. Four groups were administered PTME orally, dissolved in distilled water, at concentrations of 20 mg/kg, 50 mg/kg, 100 mg/kg, and 300 mg/kg for 28 consecutive days. The control group was administered distilled water. Throughout the investigation, we observed all the common indicators of toxicity in animals. The initial body weight of all the experimental animals was recorded before the administration of PTME and thereafter at the end of each week.

4.3.4.3. Haematological parameters assessment

Haematological assays were conducted on all surviving animals at the end of the toxicity experiment, namely on the 15th day for acute toxicity and the 29th day for sub-acute toxicity. Animals were sacrificed, and their blood was collected in tubes. The haematological parameters, such as red blood cells (RBC), white blood cells (WBC), haemoglobin (Hb), haematocrit (HCT), mean cell volume (MCV), mean corpuscular haemoglobin (MCH), and mean corpuscular haemoglobin concentration (MCHC), were measured (Thrall and Weiser, 2002; Higgins et al., 2008; Feldman et al., 2000).

The red blood cells (RBC) were counted using a haemocytometer or Neubauer's chamber by diluting the blood with RBC diluting fluid (1:200) and counting the number of cells present inside the five small squares.

$$\text{Total RBC} = \text{No. of RBC} \times 10,000/\mu\text{L}$$

Similarly, white blood cells (WBC) were counted with the help of a haemocytometer or Neubauer's chamber. However, it was diluted with WBC diluting fluid (1:20), and counting of the cells was done in the four bigger squares of the chamber.

$$\text{Total WBC} = \text{No. of WBC} \times 50/\mu\text{L}$$

Haemoglobin (Hb) was estimated by Sahli's method. The blood is taken in a haemoglobinometer tube, and 0.1N HCl was added up to mark 2, and it was allowed to stand for ten minutes to enable the maximum conversion of haemoglobin to acid haematin. The haemoglobinometer is then placed in the comparator, and distilled water is added until the colour matches with the comparator.

The estimation of haematocrit (HCT) was performed by centrifugation of a blood sample in a tube at high velocity. This results in the separation of plasma and blood cells, with the denser red blood cells settling at the bottom of the tube.

$$\text{HCT (\%)} = (\text{Height of the packed RBC column} / \text{total height of the blood column}) \times 100$$

$$\text{MCV (fl)} = (\text{HCT \%} / \text{RBC}) \times 10$$

$$\text{MCH (pg)} = (\text{Hb} / \text{RBC}) \times 10$$

$$\text{MCHC (g/dl)} = (\text{Hb} / \text{HCT \%}) \times 100$$

4.3.4.4. Serum biochemical parameters assessment

At the end of the experiment, a biochemical analysis was conducted on all the surviving rats. The blood was collected in the tubes and then subjected to centrifugation at a speed of 3500 revolutions per minute for a duration of 30 minutes. The serum from each sample was collected and kept at a temperature of -20 °C until it was analysed. The levels of serum alanine aminotransferase (ALT, EC.2.6.1.2,

Reitman and Frankel, 1957), aspartate aminotransferase (AST, EC.2.6.1.1, **Reitman and Frankel, 1957**), alkaline phosphatase (ALP, EC.3.1.3.1, **Kind and King, 1954**), creatinine (**Bonsnes and Taussky, 1945**), urea (**Fawcett and Scott, 1960**), cholesterol, triglycerides, high-density lipoprotein (HDL), and low-density lipoprotein (LDL) (**Trinder, 1969**) were measured using a diagnostic kit from Coral Clinical Systems, Goa, India.

4.3.4.5. Relative organ weight measurement

Following the sacrifice of the rats on the 15th day for the acute toxicity test and the 29th day for sub-acute toxicity, the crucial organs, including the liver, kidney, lungs, heart, and spleen, were removed, body fats were carefully removed from the organs and dried using absorbent tissue paper before being measured for weight. The relative organ's weight was determined and documented as a ratio to the bodyweight using the following equation:

$$\text{Relative organ weight} = (\text{Absolute organ weight/body weight}) \times 100$$

4.3.4.6. Histopathological assessment

The liver and kidney samples from both acute and sub-acute cases were analysed using histological testing. Following the retrieval of the organs, they were immersed in Bouin's fixative for 24 hours. Subsequently, they were moved into a solution of 70% ethanol until they underwent standard processing. The organs were immersed in paraffin wax and then sliced with a thickness of 7 μm using a Leica rotary microtome (RM2125 RTS). The slices were placed onto glass slides, treated with xylene to remove paraffin, and then stained with haematoxylin and eosin for general histology. The histopathology of organs was analysed using an Olympus CX41 microscope (Model CX41RF, Olympus Corporation, Tokyo, Japan), and images were captured for further examination (**Bancroft and Gamble, 2002**).

4.3.5. AlCl_3 -mediated Alzheimer's disease treatment

4.3.5.1. Experimental design

Wistar adult rats were randomly divided into four groups ($n = 5$) as follows:

- a) Group I: Rat administered saline water (0.5 ml, i.p) daily once for 42 days.
- b) Group II: Rat intraperitoneally treated with AlCl₃ (17 mg/kg b.w., i.p) (Sigma-Aldrich) for 42 days. The dose of AlCl₃ used is according to the previous study by Alawdi et al. (2017).
- c) Group III: Rat administered orally using intragastric tubes with PTME (5 mg/kg b.w., p.o.) dissolved in saline (1 h prior to AlCl₃ administration) and intraperitoneally treated with AlCl₃ as in group II for 42 days.
- d) Group IV: Rat administered orally using intragastric tubes with PTME (10 mg/kg b.w., p.o.) dissolved in saline (1 h prior to AlCl₃) and intraperitoneally treated with AlCl₃ as in group II for 42 days.

4.3.5.2. Behavioural experiment

4.3.5.2.1. Novel object recognition (NOR) test

The NOR test strategy was derived from the methodology proposed by Ennaceur and Delacour (1988). The equipment was a rectangular open box with dimensions of 65 cm x 45 cm x 45 cm. There were two distinct stages: the habituation phase and the test phase. Each rat was given unrestricted access to the vacant apparatus for a duration of three days, with a time limit of ten minutes each day. On the fourth day, the testing phase commenced. During the testing phase, two trials were conducted: a familiarisation trial lasting ten minutes and a test trial lasting five minutes. During the familiarisation experiment, each rat was introduced to the apparatus containing two similar items. The rats were released oriented towards the wall, with their backs turned towards the items. Following a period of 10 minutes of unrestricted exploration, each individual rat was promptly returned to its own cage. After an hour, each rat was placed back in the apparatus. During this time, one of the two familiar items was replaced with a new one. This marked the beginning of a five-minute testing session. The animal's exploration time was recorded when it approached an item with its snout within a distance of 2 cm or when it pawed or smelled the object. The act of standing or sitting on an item during exploration was not taken into consideration. The

recognition index (RI) of the testing trial was calculated using the formula (**Zhang et al., 2012**):

$$\text{RI (\%)} = \frac{\text{Time exploring novel object}}{(\text{time exploring novel object} + \text{time exploring familiar object})} \times 100$$

4.3.5.2.2. Y-maze test

The assessment of spontaneous alteration behaviour for short-term memory was evaluated using the Y-maze test. The Y-maze apparatus consisted of three arms, each labelled with the letters A, B, and C, measuring 40 cm x 35 cm x 12 cm. These arms were arranged perpendicular to each other. Each rat was given a five-minute period of unrestricted movement in the labyrinth, starting at the end of one arm. An arm entrance will only be permitted once both hind paws are fully within the arm. An alternation is the act of entering three different arms in a row inside a set of overlapping triplets. All arm entries and alternations were recorded (**Alawdi et al., 2017**). Every instance of arm entries and alternations was documented, and the spontaneous alternation percentage (SAP) was computed.

$$\text{SAP (\%)} = \frac{\text{Number of alternations}}{(\text{total arm entries} - 2)} \times 100$$

4.3.5.4. Oxidative and anti-oxidant parameters assessment

4.3.5.4.1. Protein estimation

The Bradford method was used for protein estimation (**Bradford, 1976**). 10% of hippocampus tissue was homogenised in phosphate buffered saline, centrifuged, and the supernatant was recovered. 0.1 mL of protein sample was taken in a test tube, and 0.5 mL of Bradford reagent was added to it. The contents were mixed either by inversion or vortexing. The absorbance at 595 nm was measured spectrophotometrically after 2 minutes against a reagent blank prepared from 0.1 ml of distilled water and 0.5 ml of Bradford reagent.

4.3.5.4.2. Lipid peroxidation (LPO)

Lipid peroxidation was quantified spectrophotometrically by using the thiobarbiturate test to measure malonaldehyde (MDA) levels (**Ohkawa et al., 1979**). 10% of

hippocampus tissue was homogenised in phosphate-buffered saline, centrifuged, and the supernatant recovered. A total of 200 μ L of supernatant was combined with an equal volume of 15% trichloroacetic acid (TCA). Following the process of centrifugation, the supernatant was collected. The supernatant was mixed with an equal amount of 8% thiobarbituric acid (TBA). After vortex mixing, the sample was incubated at a temperature of 95 °C in a water bath for a duration of 25 minutes. Subsequently, the sample was analysed using spectrophotometry at a wavelength of 540 nm. The LPO was expressed as the level of MDA in nmol/mg of protein.

4.3.5.4.3. Glutathione-S-transferase (GST)

GST was assayed spectrophotometrically by the principal of conjugation of 1-chloro-2,4-dinitrobenzene (CDNB) with glutathione (GSH) at 340 nm at 37 °C (**Habig et al., 1974**). The test combination consisted of a 3 mL volume containing 0.5 nM CDNB, 1 mM GSH, and 100 nM phosphate buffer at pH 6.5. Prior to use, the CDNB was dissolved in 95 % ethanol and thereafter introduced into the phosphate buffer. The phosphate buffer-CDNB combination was allowed to incubate for 10 minutes at a temperature of 37 °C. The reaction was initiated by adding GSH, followed immediately by a 0.15 mL portion of the 10% tissue homogenate. The spectrophotometer was used to quantify the rate of rise in absorbance at 340 nm against a blank containing the reaction mixture without homogenate. The level of GST was expressed as U/mg of protein.

4.3.5.4.4. Glutathione (GSH)

The concentration of reduced glutathione (GSH) was determined by reacting it with 5,5'-dithiobis(2-nitrobenzoic acid) (DTNB) to form a product that can be detected at 412 nm (**Moron et al., 1979**). Each sample tube consisted of 2 ml of 0.6 mM DTNB, 0.2 M sodium phosphate with a pH of 8.0, 0.1-0.2 ml of 10 % tissue homogenate and 0.2 M phosphate buffer, resulting in a total volume of 3 ml. The reference tube was filled with 0.1-0.2 ml of GSH solution instead of the sample. The reaction was initiated by adding the supernatant to the sample tube. The level of GSH was expressed as nmol/mg of protein.

4.3.5.5. Enzyme-linked immunosorbent assay (ELISA)

The activity of acetylcholinesterase (AChE) in the hippocampus was measured using commercially available ELISA kit from Elabscience, USA (Rat AChE ELISA Kit; Catalog No.: E-EL-R0355). The manufacturer's instructions were followed for the detection process. A spectrophotometer was used to detect the change in absorbance at 450 nm.

4.3.5.6. Western blotting

The western blotting was performed to study the expression of NF- κ B, TNF- α , IL-6, active caspase-3, BCL-2, Bax, A β , BACE1, and Tau protein in the hippocampus. The western blot technique was similar to the one previously described by Annie et al. (2020). A tissue homogenate (50 μ g) of the hippocampus was separated on a 10% sodium dodecyl sulphate (SDS)–polyacrylamide gel. The gel was then transferred to a polyvinylidene difluoride membrane (PVDF, Millipore, India) using a semi-dry apparatus for a duration of 30 minutes. In order to avoid non-specific binding, the membranes were treated with a blocking agent (5% skim milk, Sigma-Aldrich, USA) for 30 minutes. Subsequently, the membranes were incubated overnight at 4 °C with the primary antibodies, namely NF- κ B (1:2000, E-AB-22066, mouse monoclonal antibody, Elabscience, Texas, USA), TNF- α (1:1000, BS-2081R, rabbit polyclonal antibody, Bioss, Massachusetts, USA), IL-6 (1:1000, BS-0782R, rabbit polyclonal antibody, Bioss, Massachusetts, USA), active caspase-3 (1:1000, E-AB-22115, mouse monoclonal antibody, Elabscience, Texas, USA), BCL-2 (1:2000, sc-7382, mouse polyclonal antibody, Santa Cruz Biotechnology, Texas, USA), Bax (1:1000, sc-7480, mouse monoclonal antibody, Santa Cruz Biotechnology, Texas, USA), A β (1:500, BS-0107R, rabbit polyclonal antibody, Bioss, Massachusetts, USA), BACE1 (1:3000, BS-0164R, rabbit polyclonal antibody, Bioss, Massachusetts, USA), and Tau (1:1000, BS-8453R, rabbit polyclonal antibody, Bioss, Massachusetts, USA). Subsequently, the membranes were exposed to the suitable HRP-conjugated secondary antibody (goat anti-mouse, 1:4000, E-AB-1001, Elabscience, Texas, USA; goat anti-rabbit, 1:4000, A-AB-1003, Elabscience, Texas, USA) and incubated for 3 hours at room temperature. The visualisation was performed using the ECL detection technique (BIO-RAD,

Clarity Western ECL Substrate; Catalog No. 170-5061). The internal control used was β -tubulin (1:1000, E-AB-20070, rabbit polyclonal antibody, Elabscience, Texas, USA), and β -actin (1:1000, E-AB-20058, rabbit, Elabscience, Texas, USA). The levels of the proteins were calculated using densitometric analysis using ImageJ.

4.3.5.7. Histopathological examination

The brains were dissected quickly after the rats were sacrificed, followed by washing with isotonic saline solution and then drying on filter paper. The brains were bisected sagittally into two hemispheres, and the hippocampus was dissected out for histological examination. Following the retrieval of the tissue, it was immersed in Bouin's fixative for a duration of 24 hours. Subsequently, it was moved into a solution of 70% ethanol until it underwent standard processing. The tissue was immersed in paraffin wax and then sliced with a thickness of 7 μ m using a Leica rotary microtome (RM2125 RTS). The slices were placed onto glass slides, treated with xylene to remove paraffin, and then stained with haematoxylin and eosin for general histology. The histopathology of the hippocampus was analysed using an Olympus CX41 microscope (Model CX41RF, Olympus Corporation, Tokyo, Japan), and images were captured for further examination (**Bancroft and Gamble, 2002**).

4.3.6. Statistical analysis

The data were reported as the mean value \pm the standard error of the mean (SEM). The criterion for determining statistical significance was set at a p-value < 0.05 . The data were examined using a one-way analysis of variance (ANOVA) to compare means. The significant differences were evaluated using Tukey's multiple comparisons in GraphPad Prism.

4.4. RESULTS

4.4.1. Acute toxicity study

4.4.1.1. Effect of single-dose PTME on morphological changes and mortality

The single dose oral administration of PTME at various concentrations (1000 mg/kg, 3000 mg/kg, and 5000 mg/kg) resulted in death in treated rats at a dose of 5000 mg/kg during a 14-day period. Out of the five rats treated, two rats died within a week of

receiving the 5000 mg/kg dosage. The group administered at dosages of 1000 mg/kg and 3000 mg/kg did not exhibit any indications of death. There were no observable morphological changes, except a red tear in one rat from the group that received a dosage of 5000 mg/kg (**Table 17**).

4.4.1.2. Effect of single-dose PTME on feed and water intake

The single dose oral administration of PTME did not have any significant effect on the intake of feed and water at all doses (**Figure 22B, 22C**).

4.4.1.3. Effect of single-dose PTME on body weight and relative organ weight

The single dose oral administration of PTME did not show any significant change on the relative organ weight of the vital organs, including kidney, liver, lungs, spleen, brain, and heart, at all doses (**Table 18**). Similarly, the body weight was not affected by the single dose oral administration of PTME (**Table 18; Figure 22A**).

4.4.1.4. Effect of single-dose PTME on haematological parameters

Although slight increase was seen in the WBC at a dose of 5000 mg/kg, the haematological parameters revealed no significantly change in WBC, RBC, Hb, haematocrit, MCV, MCH, and MCHC at all doses (**Table 19**).

4.4.1.5. Effect of single-dose PTME on serum biochemical parameters

The single dose oral administration of PTME did not show any significant change on serum biochemical parameters, including AST, ALT, urea, cholesterol, triglycerides, HDL, and LDL, at all doses. However, a significant increase in serum ALP and creatinine was observed at 5000 mg/kg dosage (**Table 20; Figure 23, 24**).

4.4.1.6. Effect of single-dose PTME on histological examination

The liver histological examinations in the control, 1000 mg/kg, and 3000 mg/kg dosages revealed the presence of normal hepatocytes displaying no apparent alterations in the morphological features (**Figure 25A, 25B, 25C**). However, the 5000 mg/kg treated group showed deteriorated changes with constricted central vein and dilated sinusoids in the liver tissue (**Figure 25D**).

The kidney histopathological section of the 5000 mg/kg treated group showed deteriorated alterations, with an enlarged Bowman's space around the glomerulus, an enlarged PCT, and necrosis (**Figure 26D**). A slight enlargement in Bowman's capsule is seen in 3000 mg/kg treated group (**Figure 26C**). Whereas, the renal histopathology of the control and 1000 mg/kg groups displayed normal-sized renal structures, including the PCT, DCT, Bowman's capsule, Bowman's space, and glomeruli (G) (**Figure 26 A, 26B**).

4.4.2. Sub-acute toxicity study

4.4.2.1. Effect of repeated-dose PTME on morphological changes and mortality

The repeated-dose oral administration of PTME at various concentrations (20 mg/kg, 50 mg/kg, 100 mg/kg, and 300 mg/kg) for 28 days resulted in death in four treated rats at a dose of 300 mg/kg. However, no mortality was observed in control, 20 mg/kg, 50 mg/kg, and 100 mg/kg dosage. There were no observable morphological changes at all doses (**Table 21**). As a result, it was not possible to gather data from the group that received a dosage of 300 mg/kg for the examination of haematological and serum biochemical parameters because of statistical requirements. However, the analysis of kidney and liver histopathology was conducted.

4.4.2.2. Effect of repeated-dose PTME on feed and water intake

Administering PTME orally for 28 consecutive days did not result in any notable impact on the consumption of food and water at any of the given dosages (**Figure 27B, 27C**).

4.4.2.3. Effect of repeated-dose PTME on body weight and relative organ weight

The repeated-dose oral administration of PTME did not have a significant effect on the relative weight of important organs such as the kidney, liver, lungs, spleen, brain, and heart, across all dosages (**Table 22**). Furthermore, the repeated oral administration of PTME did not have any impact on the body weight (**Table 22; Figure 27A**).

4.4.2.4. Effect of repeated-dose PTME on haematological parameters

There were no significant changes in the haematological parameters, such as white blood cell count (WBC), red blood cell count (RBC), haemoglobin (Hb), hematocrit, mean corpuscular volume (MCV), mean corpuscular haemoglobin (MCH), and mean corpuscular haemoglobin concentration (MCHC), after administering PTME orally for 28 days at various dosages (**Table 23**).

4.4.2.5. Effect of repeated-dose PTME on serum biochemical parameters

The serum biochemical analysis for liver function test, including AST, ALT, and ALP, were not affected by the repeated-dose administration of PTME for 28-days (**Table 24**; **Figure 28**). Similarly, the kidney function test, including creatinine and urea, showed normal functioning of the kidney at all doses (**Table 24**; **Figure 29**). Additionally, the other biochemical analysis, including cholesterol, triglycerides, HDL, and LDL did not change significantly at all doses after the repeated-dose administration of PTME for 28-days (**Table 24**).

4.4.2.6. Effect of repeated-dose PTME on histological examination

The liver histological investigations at the control, 20 mg/kg, 50 mg/kg, and 100 mg/kg doses showed the existence of normal architecture of the liver tissue with normal hepatocytes, portal vein, sinusoids, and hepatic artery, and with no observable changes in their morphological characteristics (**Figure 30A-30D**). However, the group treated with a dosage of 300 mg/kg had showed a liver with a skewed structure. The presence of minor inflammation in the lobules of the liver was observed, with a congested central vein, and damaged hepatocytes (**Figure 30E**).

The kidney architecture of the the control, 20 mg/kg, 50 mg/kg, and 100 mg/kg doses showed the existence of normal architecture (**Figure 31A-31D**). However, the histopathological section of the 300 mg/kg treated group showed significant damage (**Figure 31E**).

4.4.3. AlCl₃-mediated Alzheimer's disease treatment

4.4.3.1. Effect of PTME on cognitive deficit in AlCl₃-mediated AD rats

In the Y-maze task, we observed a statistically significant decrease in spatial memory in the groups treated with AlCl₃. This decrease was indicated by a lower percentage (44.64 %) of spontaneous alternation (SAP) compared to the control group (80.30 %), suggesting an impact on short-term memory. Nonetheless, the administration of PTME (5 mg/kg and 10 mg/kg) for a period of 42 days demonstrated a noteworthy and statistically significant increase (66.89 % and 75.86 %, respectively) in the SAP of rats with AD (**Figure 32A**).

The novel object recognition test demonstrated a significant decline in short-term memory in the AlCl₃-mediated AD rats. The rats in the control group spent a longer time exploring the new object, showing that they remembered the familiar object with a recognition index (RI) of 80.26 %. On the other hand, rats with AD had a significantly reduced RI of 33.45 %, which aligns with their compromised cognitive ability. However, when administered daily for a period of 42 days, both the dosages of PTME (5 mg/kg and 10 mg/kg) resulted in a considerable rise in the RI in rats with AD. The RI values reached 66.26 % for 5 mg/kg and 77.87 % for 10 mg/kg, indicating the therapeutic impact of PTME on the AD animals (**Figure 32B**).

4.4.3.2. Effect of PTME on oxidative stress in AlCl₃-mediated AD rats

The level of MDA resulting from LPO (lipid peroxidation) in the hippocampus showed a significant rise in AlCl₃-mediated AD rat models (14.83 ± 0.303 nmol/mg protein) compared to the control (8.89 ± 0.277 nmol/mg protein). However, the levels of MDA reduced significantly to 11.12 ± 0.293 nmol/mg protein in AD rats when treated with PTME at a dose of 5 mg/kg. Further treatment with PTME at a dose of 10 mg/kg significantly reduces the level of MDA (9.94 ± 0.291 nmol/mg protein), similar to the control group (**Figure 33**).

4.4.3.3. Effect of PTME on anti-oxidant biomarkers in AlCl₃-mediated AD rats

Exposure to AlCl₃ resulted in a significant decrease in the levels of reduced glutathione (GSH) and glutathione-S-transferase (GST) activity in the hippocampus compared to

the normal control group (2.098 ± 0.078 nmol/g protein for GSH; 1.73 ± 0.061 U/mg protein). While the level of GSH was reduced to 0.76 ± 0.033 nmol/mg protein, the administration of PTME in AD rats at doses of 5 mg/kg and 10 mg/kg significantly increased it to 1.22 ± 0.069 nmol/mg protein and 1.99 ± 0.039 nmol/mg protein, respectively (**Figure 34A**). Similarly, the level of GST was reduced to 1.032 ± 0.057 U/mg protein in AlCl_3 -mediated AD rats. However, the administration of PTME in AD rats at doses of 5 mg/kg and 10 mg/kg significantly increased it to 1.46 ± 0.052 U/mg protein and 1.6 ± 0.05 U/mg protein, respectively (**Figure 34B**).

4.4.3.4. Effect of PTME on acetylcholinesterase in AlCl_3 -mediated AD rats

The ELISA analysis showed that the AChE level in the AlCl_3 -mediated AD group was significantly increased in the hippocampus (124.21 ± 6.065 ng/ml) compared to its control level in the hippocampus (53.58 ± 2.15 ng/ml). Administration of 5 mg/kg PTME to AD rats for 42 days significantly reduced the level of AChE in the hippocampus (97.45 ± 2.51 ng/ml) compared to the AD group. Administration of PTME at a dose of 10 mg/kg further reduces the level of AChE in the hippocampus of AD rats to 64.38 ± 1.36 ng/ml (**Figure 35**).

4.4.3.5. Effect of PTME on inflammatory biomarkers in AlCl_3 -mediated AD rats

Western blot analysis revealed that the expression levels of pro-inflammatory markers, including NF- κ B, TNF- α , and IL-6 were significantly high in the hippocampus of AlCl_3 -mediated AD rats when compared to the control group. However, the administration of PTME at two different doses, namely 5 mg/kg and 10 mg/kg, for 42 days significantly reduced the expression level of these pro-inflammatory markers in the hippocampus of AD rats (**Figure 36A-36C**).

4.4.3.6. Effect of PTME on apoptotic biomarkers in AlCl_3 -mediated AD rats

Rats that were administered AlCl_3 over a period of 42 days had a significant increase in bax and active caspase-3 levels in the hippocampus, while BCL-2 level was significantly lower than the control group. However, administration of PTME to AlCl_3 treated rats significant drop the expression levels of bax and active caspase-3 in the

hippocampus, and significantly increase the expression level of BCL-2 (**Figure 37A-37C**).

4.4.3.7. Effect of PTME on AD's pathological biomarkers in AlCl₃-mediated AD rats

The administration of AlCl₃ resulted in a 2.14-fold increase in the hippocampus content of BACE1, 1.43-fold increase in A β protein, and a 2.46-fold rise in the hippocampal content of tau protein compared to the normal control group. However, when PTME was administered at a dose of 5 mg/kg to the AD rats, it significantly reduced the levels of BACE1 to 49.6 %, A β protein to 68.82 %, and p-tau to 58 %, compared to the AlCl₃ treated group. The administration of PTME at a dose of 10 mg/kg further reduces significantly the levels of BACE1 to 46.73 %, A β protein to 56.72 %, and p-tau to 38.52 %, compared to the AlCl₃ treated group (**Figure 38A-38C**).

4.4.3.7. Effect of PTME on hippocampal histology in AlCl₃-mediated AD rats

The histopathological examination of the hippocampus sections obtained from the control group showed a normal architecture of the hippocampus, exhibiting a regular, healthy, and normal distribution of the neuronal cells (**Figure 39A**). In contrast, the hippocampus of the group treated with aluminum exhibited degenerative alterations, with a large number of damaged, distorted, irregular neuronal cells with shrunken cytoplasm and dark pyknotic nuclei (**Figure 39B**). The administration of PTME at a dose of 5 mg/kg to the AD rats mitigated the histological alterations in the hippocampus to some extent (**Figure 39C**). In addition, the administration of PTME at a dose of 10 mg/kg further improved the histological alterations of the hippocampus, similar to the control group, with normal and healthy neuronal cells (**Figure 39D**).

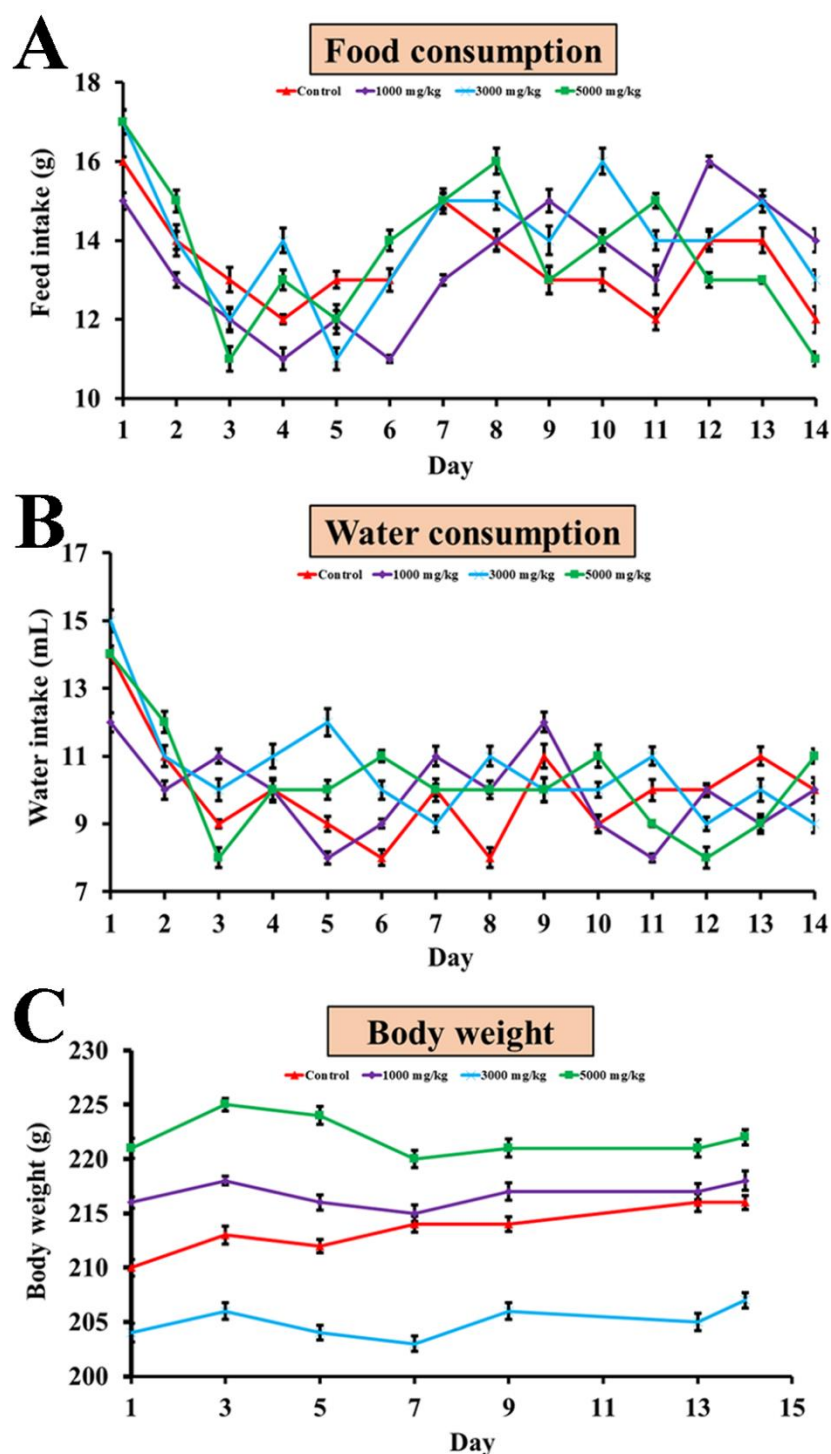


Figure 22. The impact of the methanolic extract derived from the seed pod of *Parkia timoriana* on the body weight, feed, and water intake of the Wistar rats that were exposed to it in a single-dose acute toxicity study. (A) The impact on daily food consumption. (B) The impact on the volume of water consumed daily. (C) The impact on the body weight was measured every alternate day for a period of 14 days.

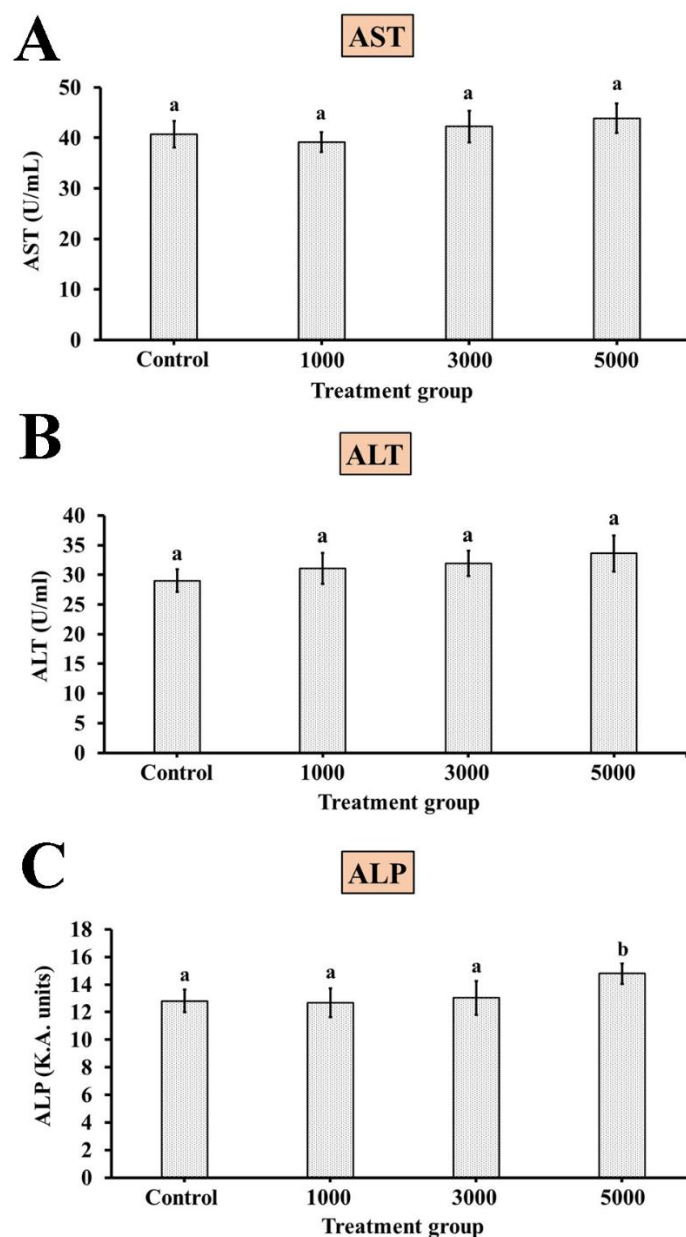


Figure 23. The effect of a single-dose of PTME on the liver (liver function test) of Wistar rats that were exposed to it in an acute toxicity study. (A) The level of AST (aspartate aminotransferase) showed no significant change between the treatment groups. (B) The level of ALT (alanine transaminase) showed no significant change between the treatment groups. (C) The level of ALP (alkaline phosphatase) was significantly high in 5000 mg/kg treatment group. All values are expressed as mean \pm SEM, $n = 5$. $p < 0.05$ shows a significant difference (one-way ANOVA/Tukey's multiple comparison). Statistically significant data are represented with different alphabetical letters.

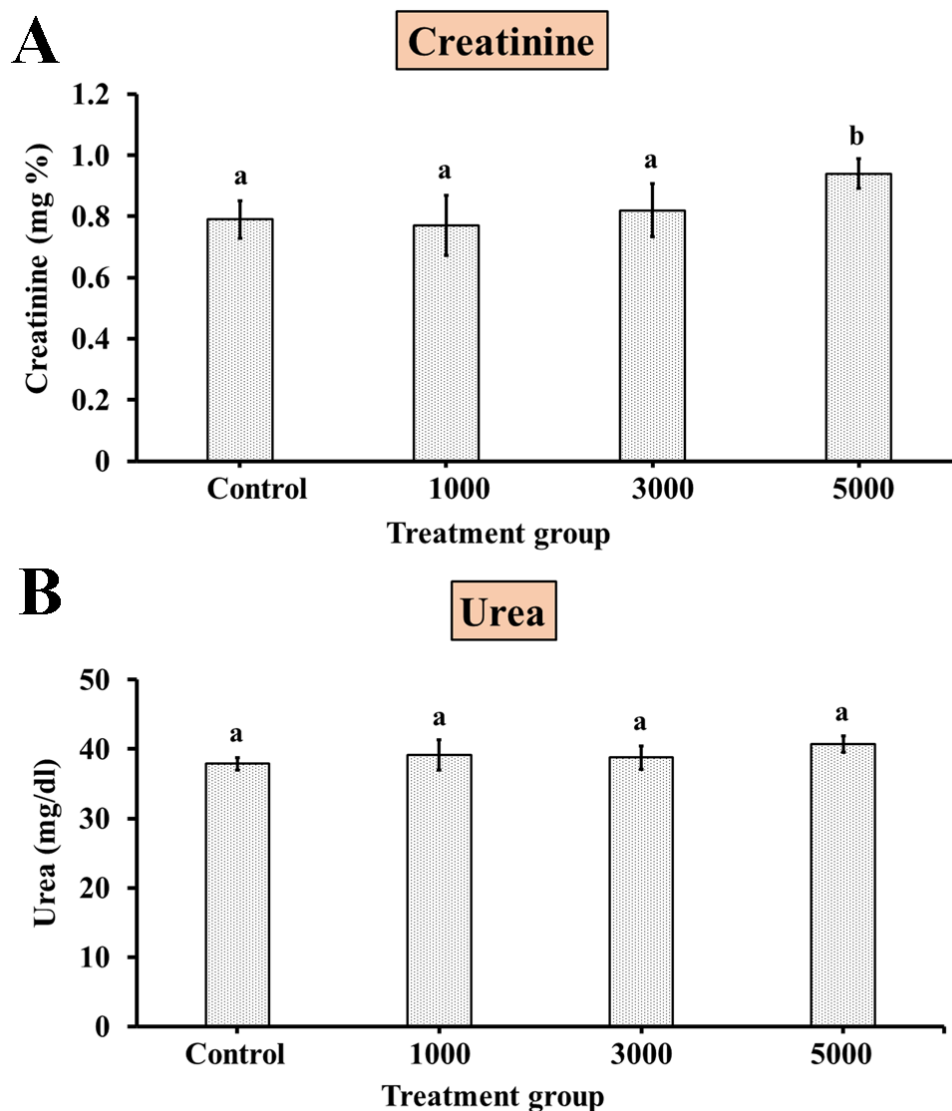


Figure 24. The effect of a single-dose of PTME on the kidney (kidney function test) of Wistar rats that were exposed to it in an acute toxicity study. (A) The level of creatinine was significantly high in the 5000 mg/kg treatment group. (B) The level of urea showed no significant change between the treatment groups. All values are expressed as mean \pm SEM, $n = 5$. $p < 0.05$ shows a significant difference (one-way ANOVA/Tukey's multiple comparison). Statistically significant data are represented with different alphabetical letters.

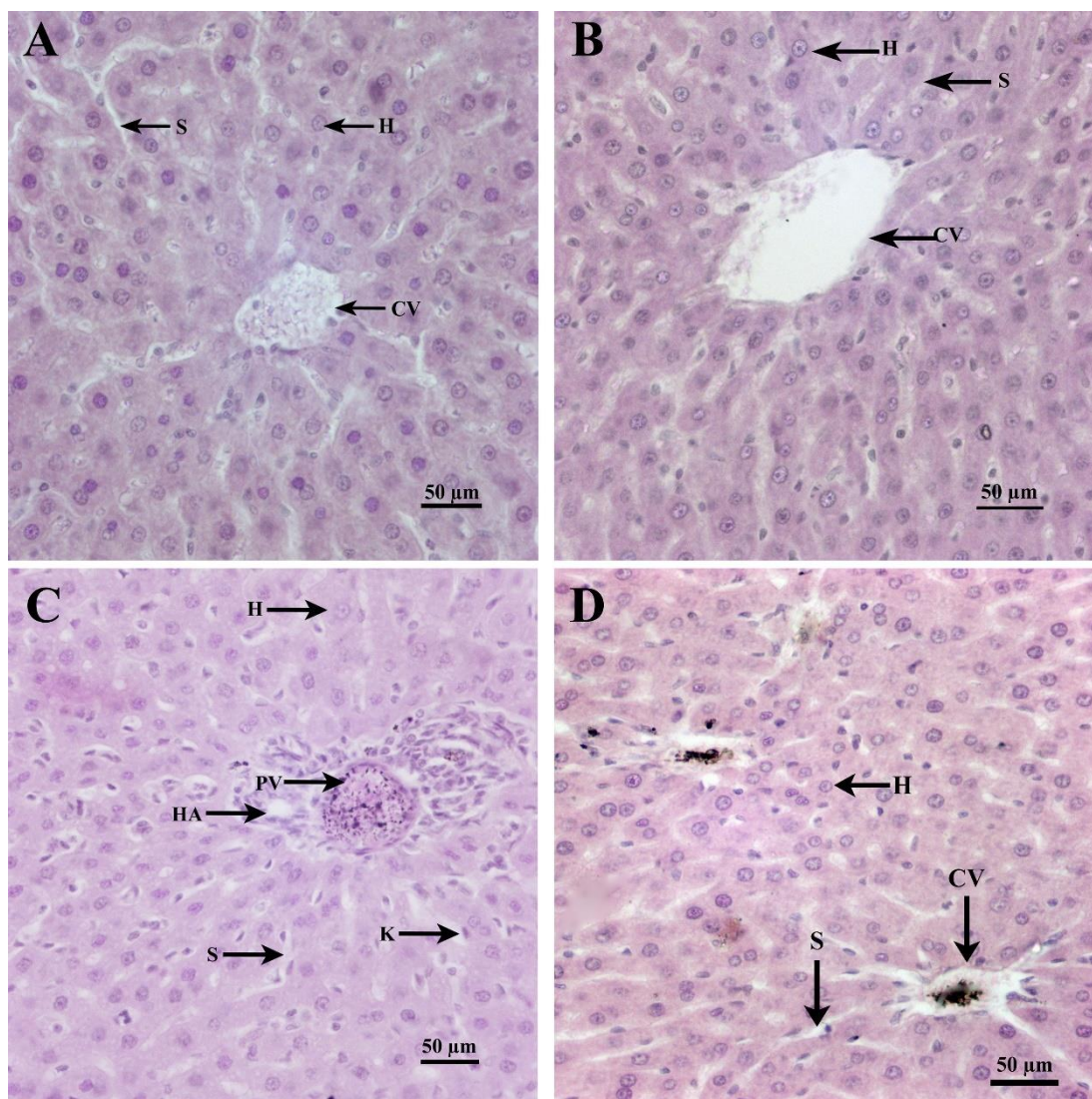


Figure 25. The effect of a single dose of PTME on the histopathological sections (40x magnification; H & E) of liver tissue of Wistar rats that were exposed to it in an acute toxicity study. (A) Control. (B) 1000 mg/kg treated group. (C) 3000 mg/kg treated group. (D) 5000 mg/kg treated group. The histopathological section of the 5000 mg/kg treated group showed alterations, with the central vein showing congestion, slight dilation in the sinusoids, and damaged hepatocytes. Whereas, the other groups showed normal liver architecture as the control. PV- portal vein, CV- central vein, H- hepatocyte, S- sinusoids, K- Kupffer's cell, and HA- hepatic artery.

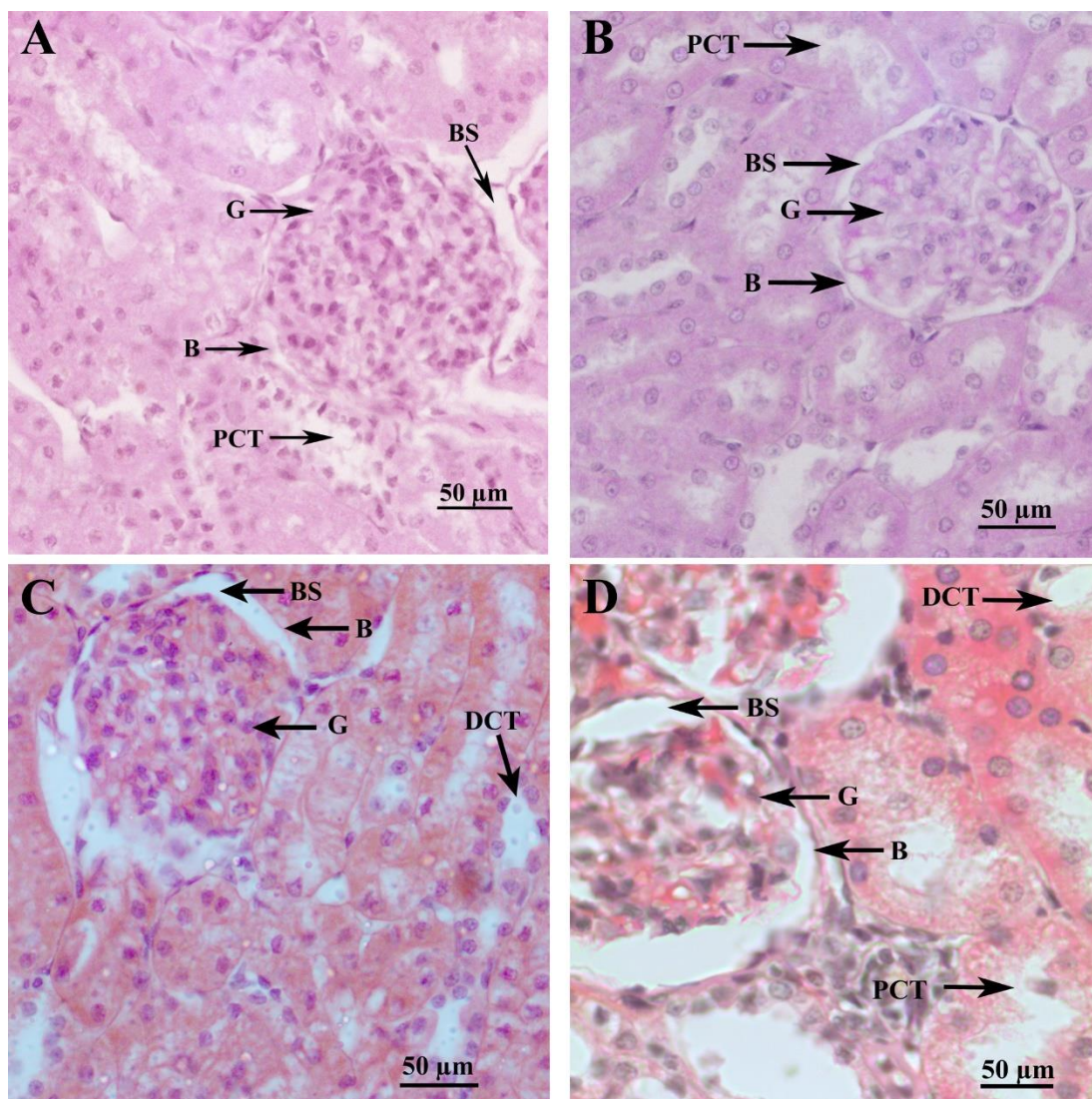


Figure 26. The effect of a single dose of PTME on the histopathological sections (40x magnification; H & E) of kidney tissue of Wistar rats that were exposed to it in an acute toxicity study. (A) Control. (B) 1000 mg/kg treated group. (C) 3000 mg/kg treated group. (D) 5000 mg/kg treated group. The histopathological section of the 5000 mg/kg treated group showed deteriorated alterations, with an enlarged Bowman's space around the glomerulus and an enlarged PCT. Whereas, the other groups showed normal structure of glomerulus, Bowman's capsule, DCT, and PCT. A slight enlargement in Bowman's capsule is seen in 3000 mg/kg treated group. G- glomerulus, B- Bowman's capsule, BS- Bowman's space, DCT- Distal convoluted tubule, and PCT- Proximal convoluted tubule.

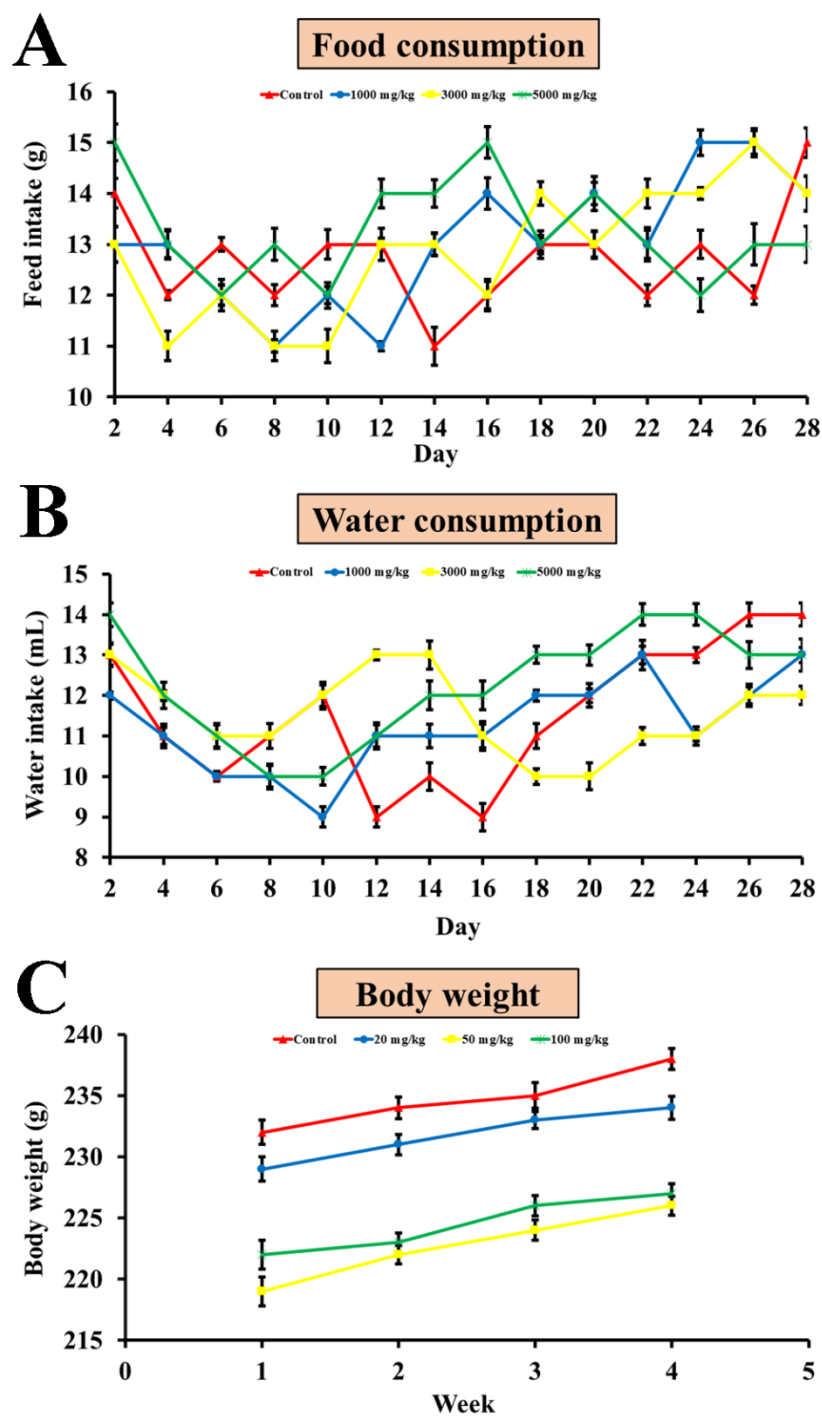


Figure 27. The impact of repeated-dose of the PTME on the body weight, feed and water intake by the Wistar rats that were exposed to it in a sub-acute toxicity study. (A) The impact on the food ingested was measured on an alternate day basis. (B) The impact on the volume of water consumed was recorded every other day. (C) The impact on the body weight was measured on a weekly basis for a period of 28 days.

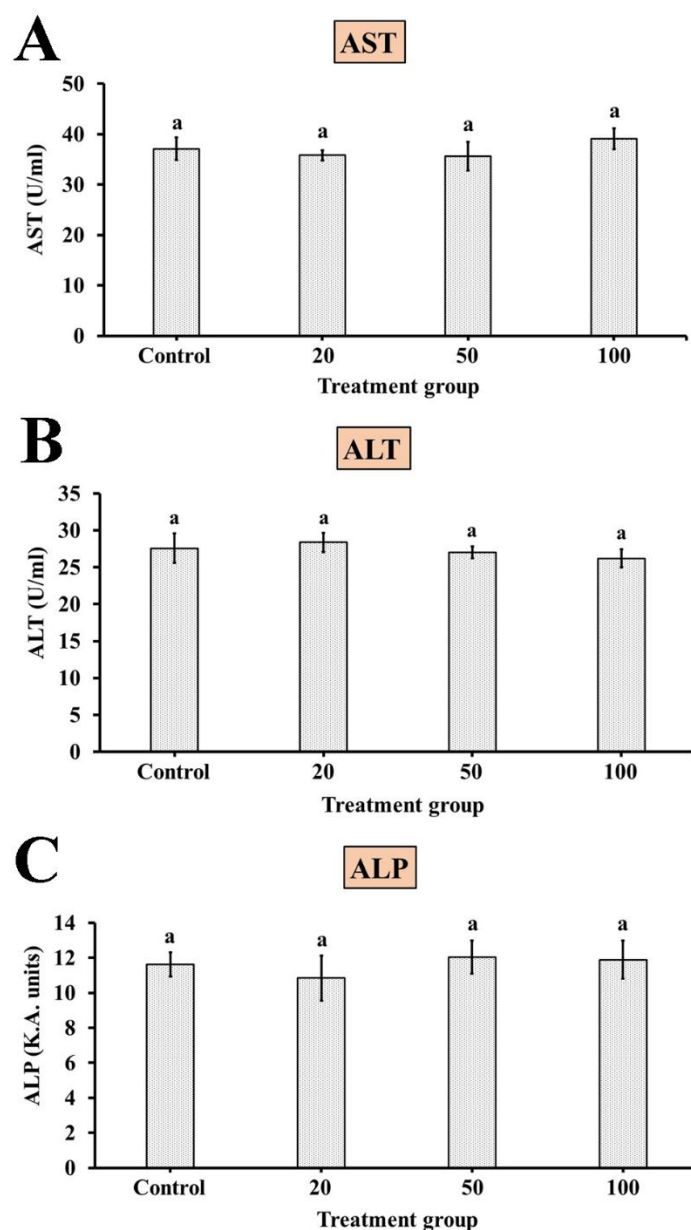


Figure 28. The effect of a repeated-dose of PTME on the liver (liver function test) of Wistar rats that were exposed to it in a sub-acute toxicity study. (A) The level of AST (aspartate aminotransferase) showed no significant change between the treatment groups. (B) The level of ALT (alanine transaminase) showed no significant change between the treatment groups. (C) The level of ALP (alkaline phosphatase) showed no significant change between the treatment groups. All values are expressed as mean \pm SEM, $n = 5$. $p < 0.05$ shows a significant difference (one-way ANOVA/Tukey's multiple comparison). Statistically significant data are represented with different alphabetical letters.

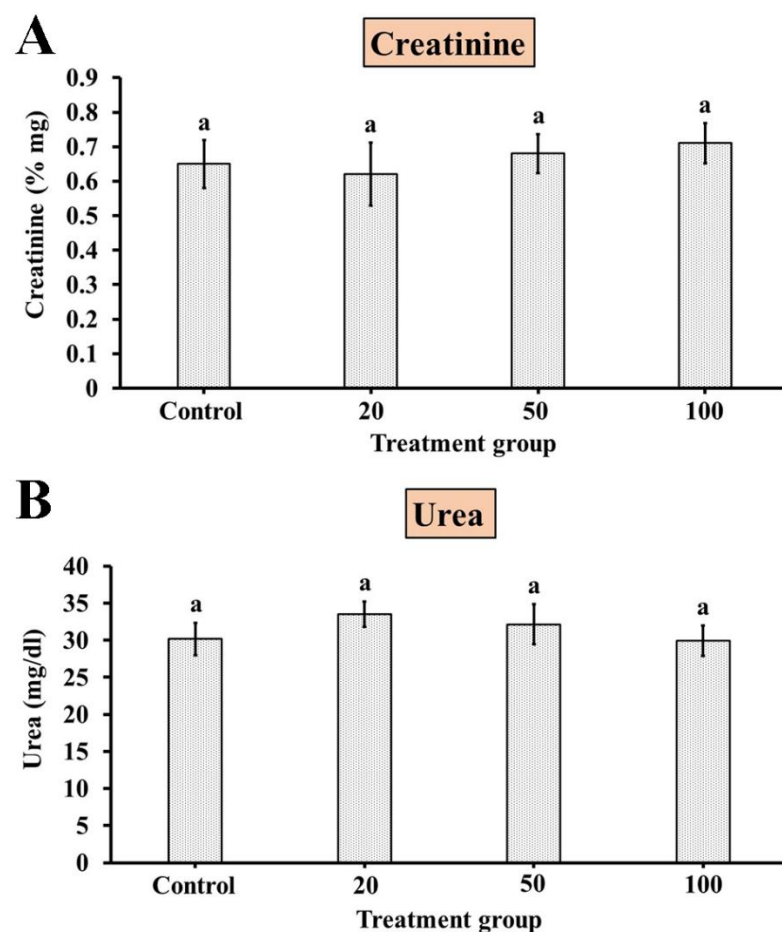


Figure 29. The effect of a repeated-dose of PTME on the kidney (kidney function test) of Wistar rats that were exposed to it in a sub-acute toxicity study. (A) The level of creatinine showed no significant change between the treatment groups. (B) The level of urea showed no significant change between the treatment groups. All values are expressed as mean \pm SEM, $n = 5$. $p < 0.05$ shows a significant difference (one-way ANOVA/Tukey's multiple comparison). Statistically significant data are represented with different alphabetical letters.

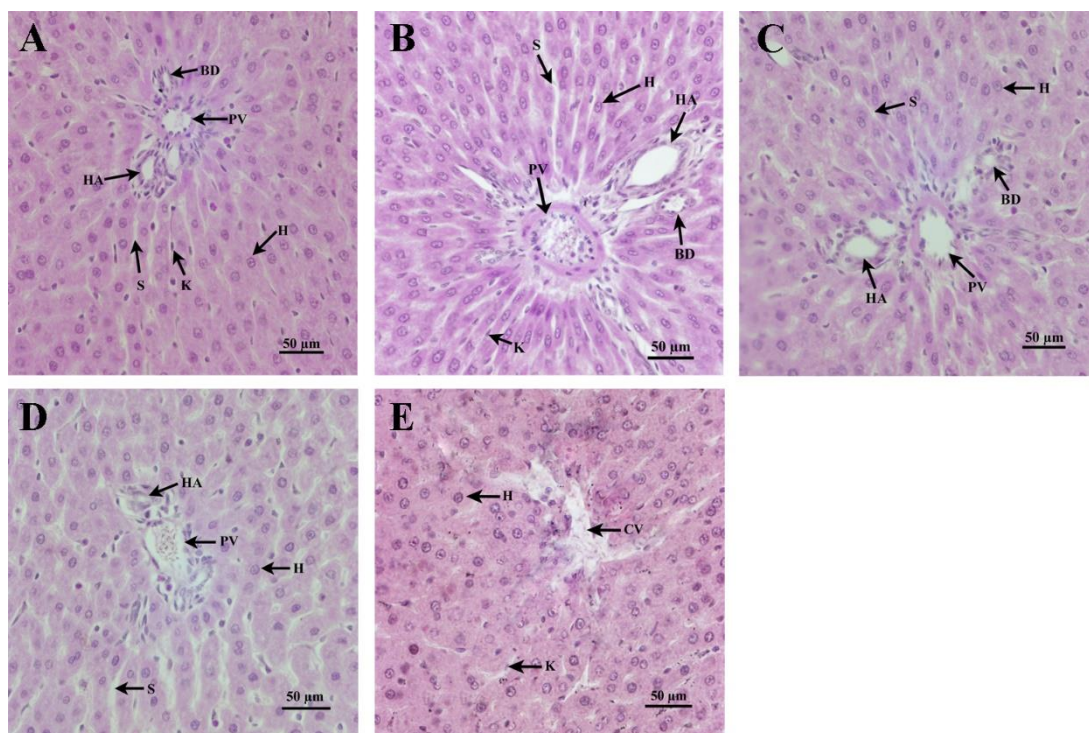


Figure 30. The effect of a repeated-dose of PTME on the histopathological sections (40x magnification; H & E) of liver tissue of Wistar rats that were exposed to it in a sub-acute toxicity study. (A) Control. (B) 20 mg/kg treated group. (C) 50 mg/kg treated group. (D) 100 mg/kg treated group. (E) 300 mg/kg treated group. The 300 mg/kg treated group's histopathological section showed a liver with a skewed structure, a congested central vein, and damaged hepatocytes. Whereas, the other treated groups showed normal hepatocytes, portal vein, sinusoids, and hepatic artery, similar to the control group. PV- portal vein, CV- central vein, H- hepatocyte, S- sinusoids, K- Kupffer's cell, HA- hepatic artery, and BD- bile duct.

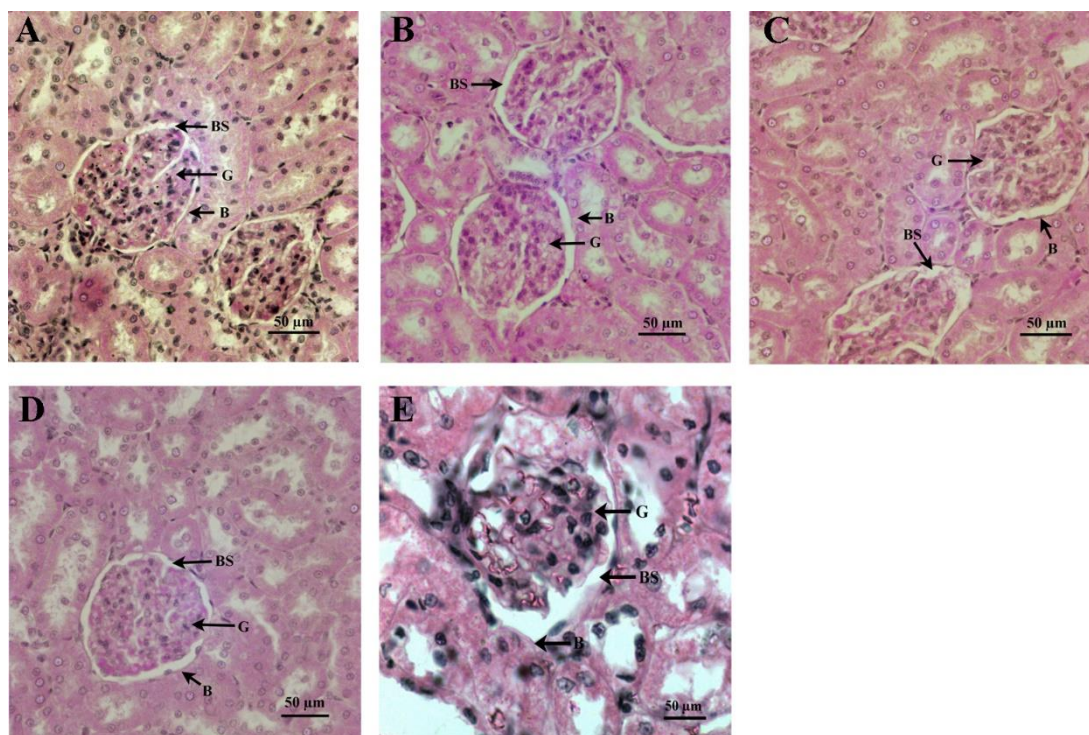


Figure 31. The effect of a repeated-dose of PTME on the histopathological sections (40x magnification; H & E) of kidney tissue of Wistar rats that were exposed to it in a sub-acute toxicity study. (A) Control. (B) 20 mg/kg treated group. (C) 50 mg/kg treated group. (D) 100 mg/kg treated group. (E) 300 mg/kg treated group. The histopathological section of the 300 mg/kg treated group showed significant damage. The kidney architecture of the other treated groups, comparable to the control group, was normal. G- glomerulus, B- Bowman's capsule, BS- Bowman's space.

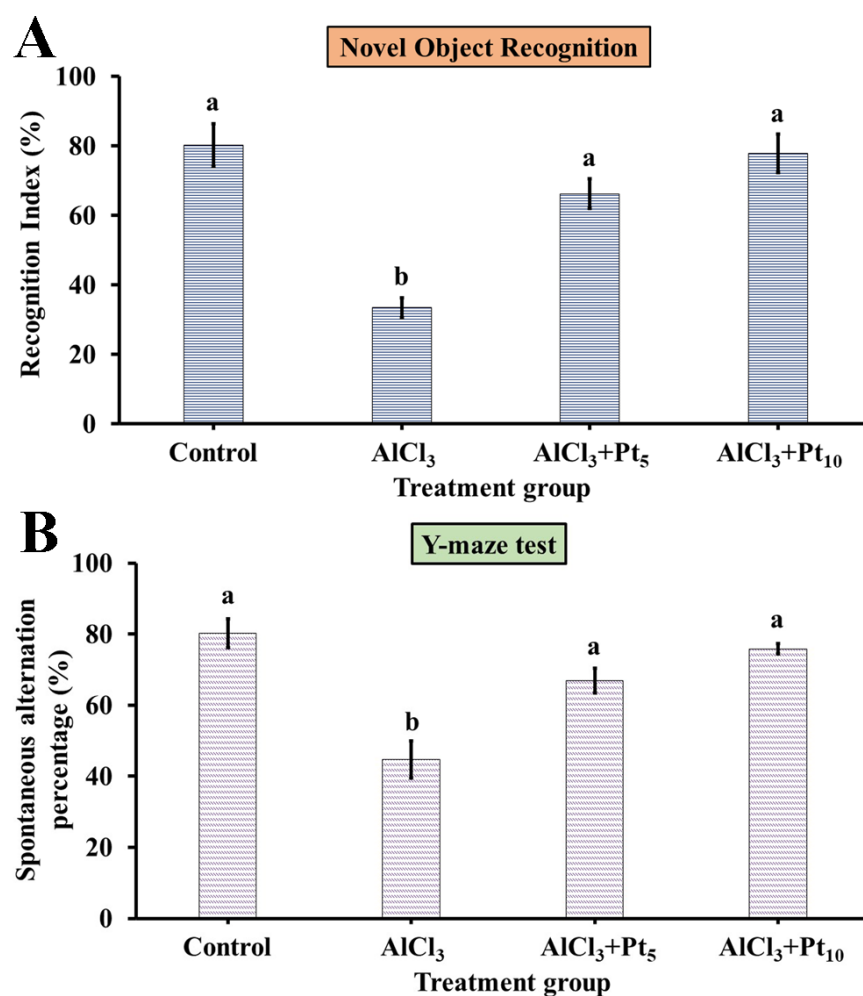


Figure 32. The methanolic extract of *Parkia timoriana* seed pod improved the cognitive impairment in an aluminum chloride-mediated Alzheimer's disease rat. (A) The effect of PTME on the recognition index percentage in a novel object recognition (NOR) test. (B) The effect of PTME on the spontaneous alternation percentage (SAP) in a Y-maze test. All values are expressed as mean \pm SEM, $n = 5$. $p < 0.05$ shows a significant difference (one-way ANOVA/Tukey's multiple comparison). Statistically significant data are represented with different alphabetical letters.

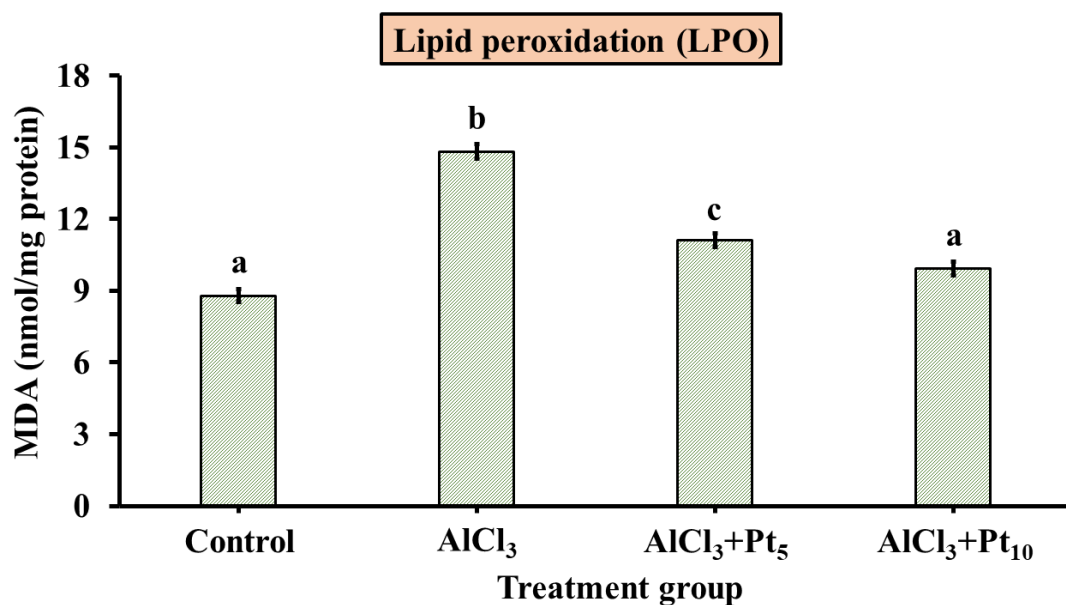


Figure 33. The methanolic extract of *Parkia timoriana* seed pod lowered lipid peroxidation (measured as MDA level), a sign of oxidative stress, in the hippocampus of an aluminum chloride-mediated Alzheimer's disease rat. All values are expressed as mean \pm SEM, $n = 5$. $p < 0.05$ shows a significant difference (one-way ANOVA/Tukey's multiple comparison). Statistically significant data are represented with different alphabetical letters.

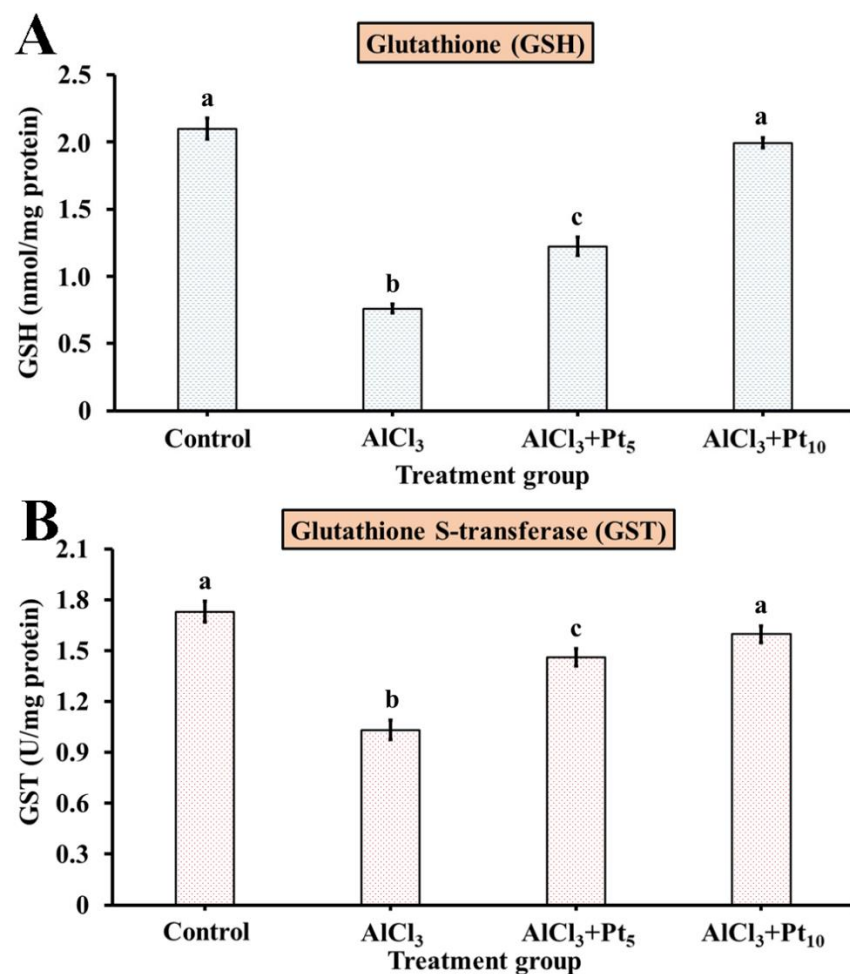


Figure 34. The methanolic extract of *Parkia timoriana* seed pod increased the anti-oxidant markers (glutathione, GSH; glutathione-S-transferase, GST) in the hippocampus of an aluminum chloride-mediated Alzheimer's disease rat. (A) The effect of PTME on the level of GSH in an AD rat. (B) The effect of PTME on GST levels in an AD rat. All values are expressed as mean \pm SEM, $n = 5$. $p < 0.05$ shows a significant difference (one-way ANOVA/Tukey's multiple comparison). Statistically significant data are represented with different alphabetical letters.

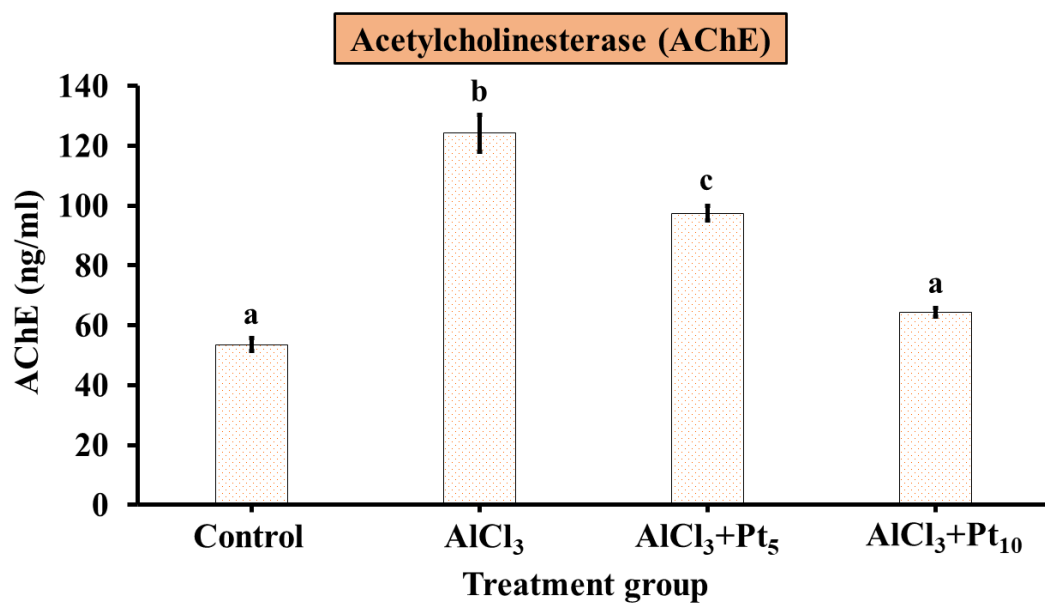


Figure 35. PTME decreased the level of acetylcholinesterase (AChE) in an aluminum chloride-mediated Alzheimer's disease rat. All values are expressed as mean \pm SEM, $n = 5$. $p < 0.05$ shows a significant difference (one-way ANOVA/Tukey's multiple comparison). Statistically significant data are represented with different alphabetical letters.

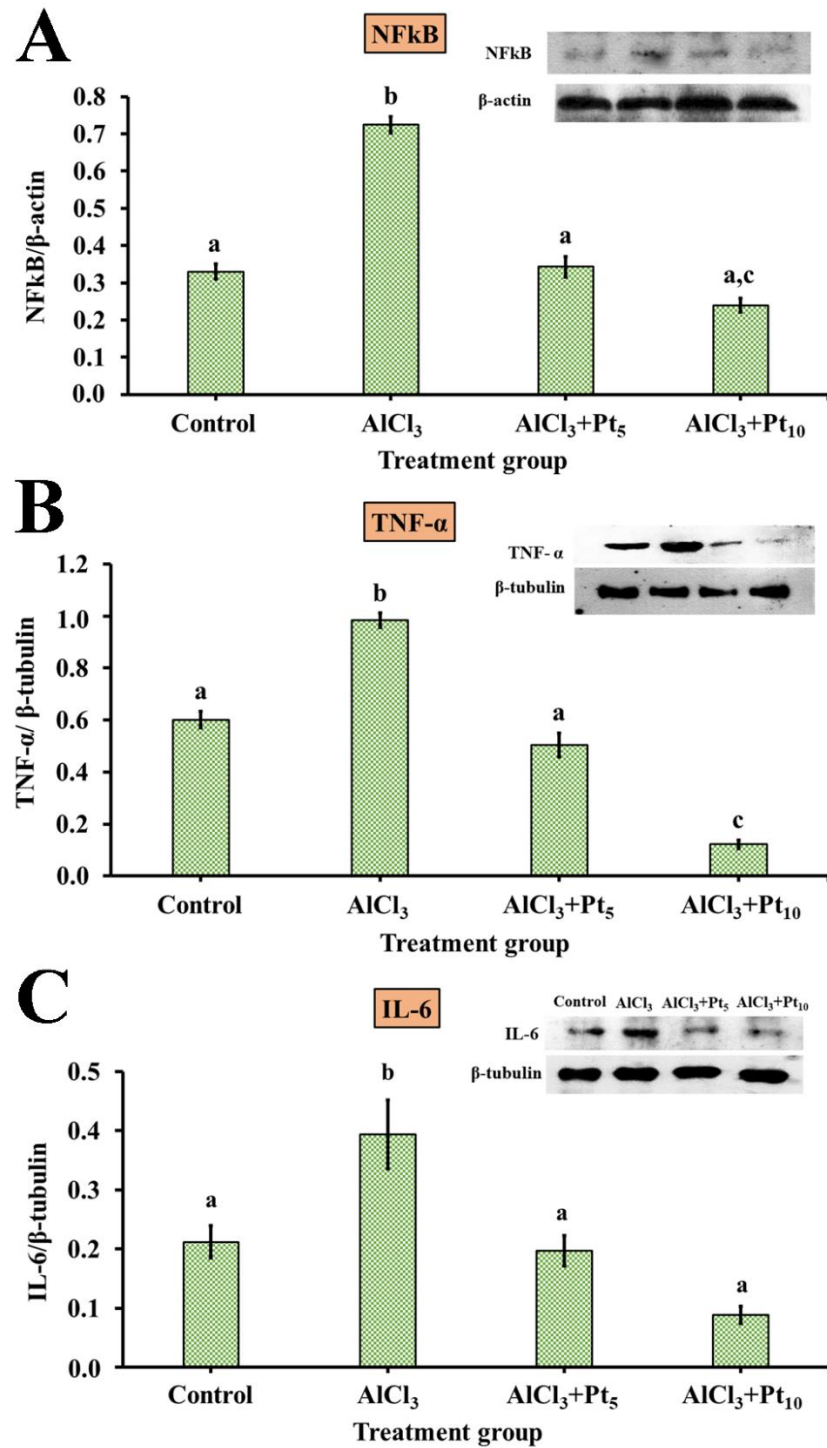


Figure 36. Neuroprotective effect of PTME on neuroinflammation in the hippocampus of an aluminum chloride-mediated Alzheimer's disease rat. (A) NF-κB. (B) TNF-α. (C) IL-6. All values are expressed as mean ± SEM, n = 5. p < 0.05 shows a significant difference (one-way ANOVA/Tukey's multiple comparison). Statistically significant data are represented with different alphabetical letters.

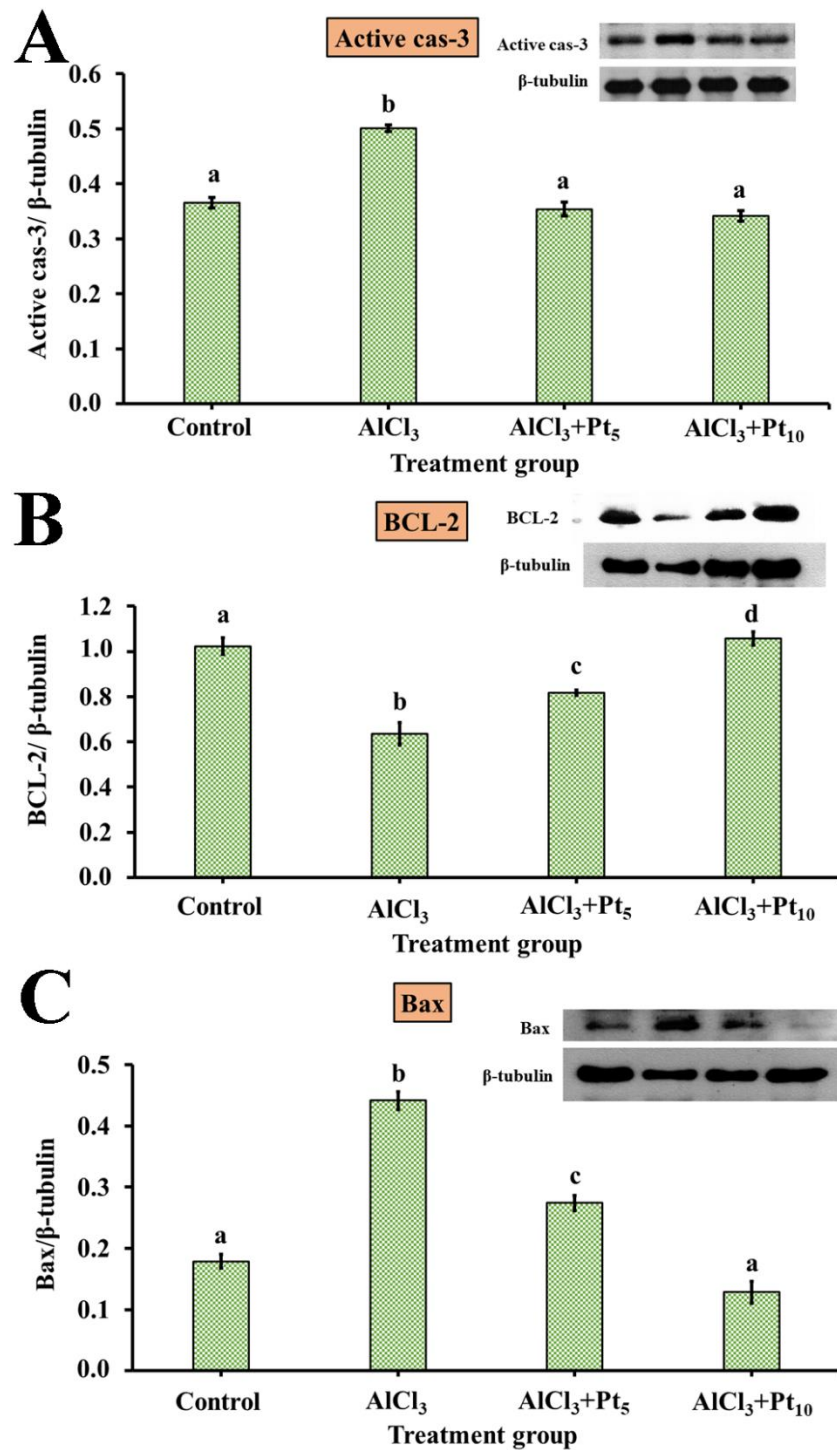


Figure 37. PTME treatment reduced apoptosis in the hippocampal region of an aluminum chloride-mediated Alzheimer's disease rat. (A) Active caspase-3. (B) BCL-2. (C) Bax. All values are expressed as mean \pm SEM, $n = 5$. $p < 0.05$ shows a significant difference (one-way ANOVA/Tukey's multiple comparison). Statistically significant data are represented with different alphabetical letters.

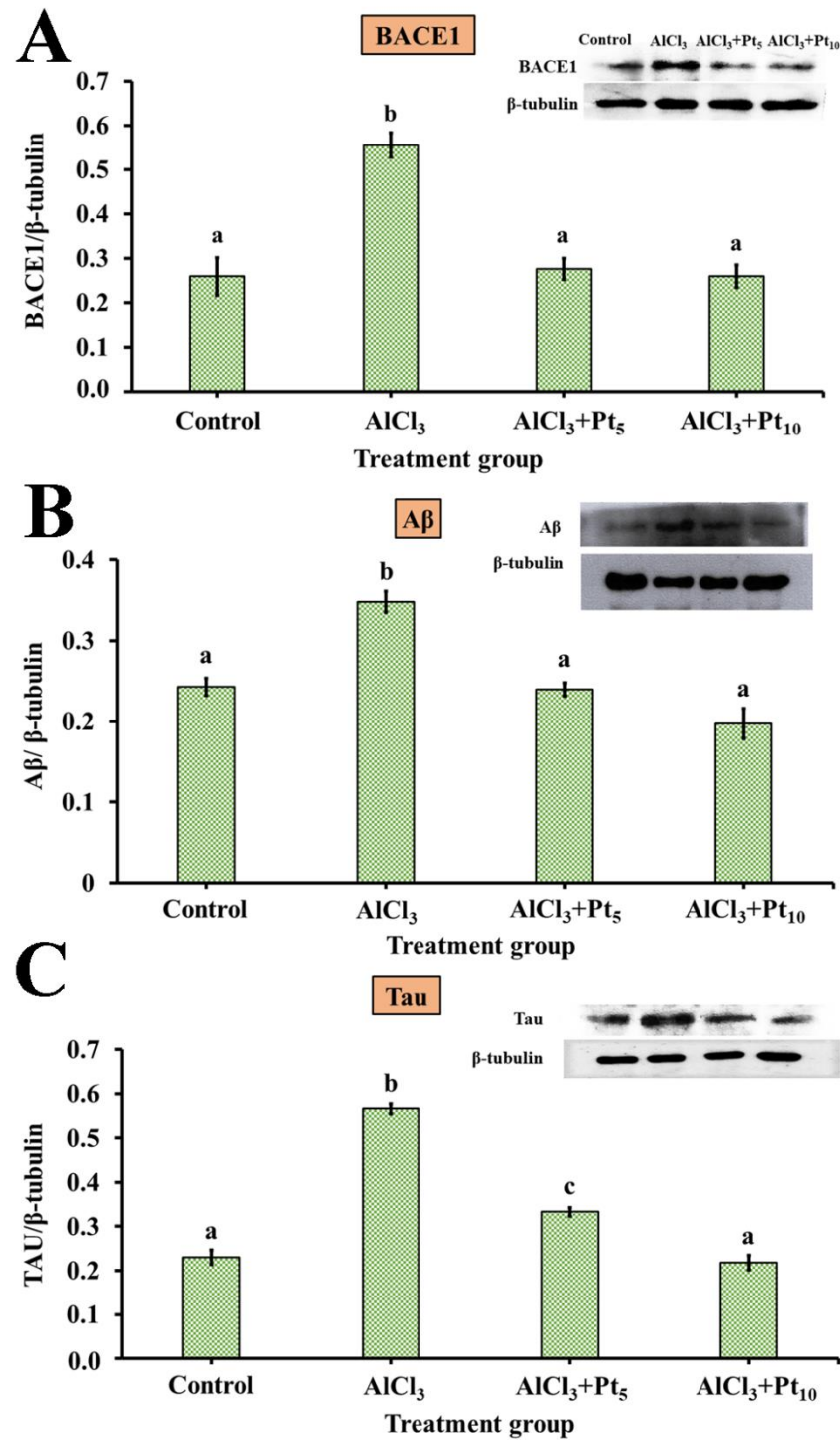


Figure 38. Ameliorative effect of PTME on the AD pathological markers in the hippocampal region of an aluminum chloride-mediated Alzheimer's disease rat. (A) BACE1. (B) Aβ. (C) Tau. All values are expressed as mean ± SEM, n = 5. p < 0.05 shows a significant difference (one-way ANOVA/Tukey's multiple comparison). Statistically significant data are represented with different alphabetical letters.

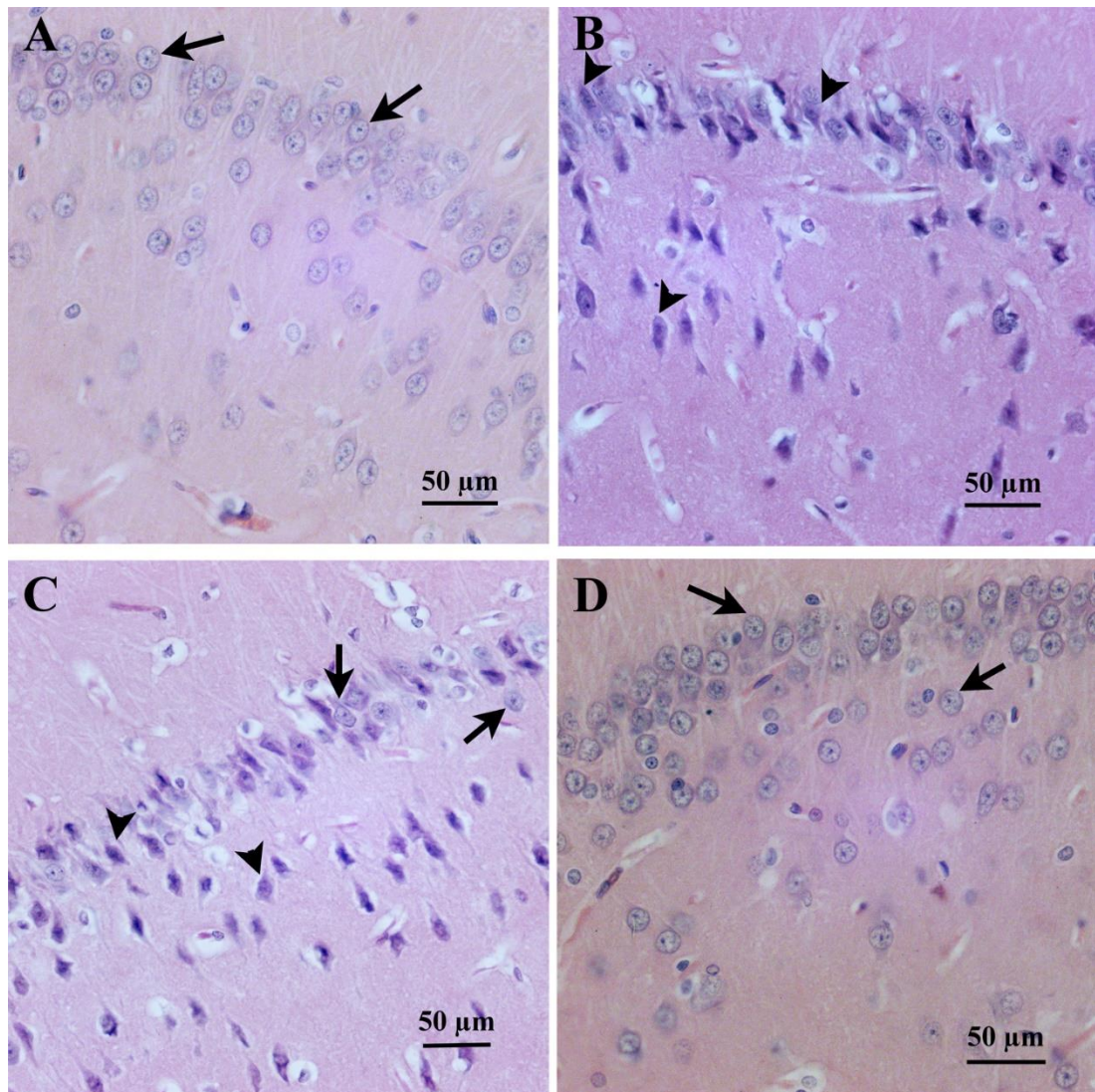


Figure 39. PTME administration improved the histopathological alterations in the hippocampus of an aluminum chloride-mediated Alzheimer's disease rat. (A) Group 1, or the control group, showed viable, well-defined neuronal cells with a distinct nucleus (arrow). (B) Group 2 or AlCl_3 group showed a large number of damaged, distorted, irregular neuronal cells (arrowhead) with shrunken cytoplasm and dark pyknotic nuclei. (C) Group 3 or $\text{AlCl}_3 + \text{Pt}_5$ group showed a bit of improvement from damaged neurons (arrowhead), as a greater number of normal neurons (arrow) were seen compared to group 2. (D) Group 4 or $\text{AlCl}_3 + \text{Pt}_{10}$ group showed a remarkable decrease in the number of injured or damaged cells and an increase in the number of viable neuronal cells. Arrow- viable and well-defined neuronal cells. Arrowhead- damaged, distorted, and irregular neuronal cells.

Table 17. The effect of a single-dose methanolic extract of *Parkia timoriana* seed pod on the physical observations of Wistar albino rats exposed to it in an acute toxicity study.

Observation	Control	1000 mg/kg	3000 mg/kg	5000 mg/kg
Change in temperature	X	X	X	X
Change in skin	X	X	X	X
Eye colour change	X	X	X	X
Food intake	Normal	Normal	Normal	Normal
General physique	Normal	Normal	Normal	Normal
Diarrhoea	X	X	X	X
Coma	X	X	X	X
Drowsiness	X	X	X	X
Breathing difficulties	X	X	X	X
Tremor	X	X	X	X
Fur	Normal	Normal	Normal	Normal
Salivation	X	X	X	X
Red tear	X	X	X	✓
Death	0	0	0	2

Note: X - Not observed; ✓ - Observed

Table 18. The impact of a single-dose methanolic extract of *Parkia timoriana* seed pod on the body weight and relative organ weight of Wistar albino rats exposed to it in an acute toxicity study.

Organ	Control	1000 mg/kg	3000 mg/kg	5000 mg/kg
Initial body weight	210 ± 0.98	216 ± 1.31	204 ± 0.81	221 ± 0.89
Final body weight	216 ± 0.81	218 ± 0.93	207 ± 0.98	222 ± 1.09
Kidney	0.63 ± 0.07	0.61 ± 0.06	0.62 ± 0.05	0.60 ± 0.05
Liver	2.93 ± 0.40	2.59 ± 0.38	2.56 ± 0.37	3.11 ± 0.36
Lungs	0.91 ± 0.09	0.81 ± 0.07	0.74 ± 0.11	0.84 ± 0.08
Spleen	0.22 ± 0.14	0.22 ± 0.13	0.21 ± 0.12	0.27 ± 0.10
Brain	0.99 ± 0.25	0.84 ± 0.19	0.80 ± 0.25	0.94 ± 0.27
Heart	0.42 ± 0.06	0.40 ± 0.04	0.40 ± 0.03	0.42 ± 0.07

Table 19. The impact of a single-dose methanolic extract of *Parkia timoriana* seed pod on the haematological parameters of Wistar albino rats exposed to it in an acute toxicity study. All values are expressed as mean \pm SEM, n = 5. p < 0.05 shows a significant difference (one-way ANOVA/Tukey's multiple comparison). Statistically significant data are represented with different alphabetical letters.

Parameter	Control	1000 mg/kg	3000 mg/kg	5000 mg/kg
RBC ($10^6/\mu\text{l}$)	6.69 \pm 0.36	6.99 \pm 0.51	6.37 \pm 0.83	6.62 \pm 0.24
WBC ($10^3/\mu\text{l}$)	9.05 \pm 0.43	8.99 \pm 0.27	9.35 \pm 0.46	9.98 \pm 0.32
Hb (g/dl)	13.2 \pm 0.46	12.56 \pm 0.23	13.61 \pm 0.41	12.98 \pm 0.66
Hematocrit (%)	45.12 \pm 1.6	44.86 \pm 1.42	45.98 \pm 1.03	45.26 \pm 1.20
MCV (fl)	69.65 \pm 3.81	68.76 \pm 3.37	70.56 \pm 3.41	68.12 \pm 2.81
MCH (pg)	19.64 \pm 1.52	18.98 \pm 1.03	20.97 \pm 1.18	20.05 \pm 1.38
MCHC (g/dl)	29.86 \pm 2.06	28.31 \pm 2.51	28.94 \pm 2.2	28.65 \pm 1.95

Table 20. The impact of a single-dose methanolic extract of *Parkia timoriana* seed pod on the biochemical analysis of Wistar albino rats exposed to it in an acute toxicity study. All values are expressed as mean \pm SEM, n = 5. *p < 0.05 shows a significant difference (one-way ANOVA/Tukey's multiple comparison). Statistically significant data are represented with different alphabetical letters.

Parameter	Control	1000 mg/kg	3000 mg/kg	5000 mg/kg
AST (U/ml)	40.67 \pm 2.62	39.17 \pm 1.97	42.26 \pm 3.12	43.86 \pm 2.89
ALT (U/ml)	29.01 \pm 1.91	31.07 \pm 2.62	31.91 \pm 2.14	33.61 \pm 3.02
ALP (K.A. Units)*	12.81 \pm 0.81 ^a	12.67 \pm 1.06 ^a	13.02 \pm 1.21 ^a	14.79 \pm 0.73 ^b
Creatinine (mg %)*	0.79 \pm 0.061 ^a	0.77 \pm 0.098 ^a	0.82 \pm 0.087 ^a	0.94 \pm 0.048 ^b
Urea (mg/dl)	37.89 \pm 0.92	39.12 \pm 2.18	38.78 \pm 1.72	40.71 \pm 1.21
Cholesterol (mg/dl)	58.56 \pm 3.01	54.81 \pm 2.09	57.82 \pm 2.81	59.03 \pm 1.63
Triglycerides (mg/dl)	30.21 \pm 1.90	31.78 \pm 2.11	28.56 \pm 1.02	30.88 \pm 1.91
HDL (mg/dl)	23.41 \pm 1.23	23.81 \pm 1.31	22.27 \pm 1.09	22.91 \pm 0.98
LDL (mg/dl)	9.12 \pm 1.03	10.28 \pm 0.92	8.89 \pm 1.26	9.87 \pm 0.79

Table 21. The effect of a repeated-dose methanolic extract of *Parkia timoriana* seed pod on the physical observations of Wistar albino rats exposed to it in a 28 days sub-acute toxicity study.

Observation	Control	20 mg/kg	50 mg/kg	100 mg/kg	300 mg/kg
Change in temperature	X	X	X	X	X
Change in skin	X	X	X	X	X
Eye colour change	X	X	X	X	X
Food intake	Normal	Normal	Normal	Normal	Normal
General physique	Normal	Normal	Normal	Normal	Normal
Diarrhoea	X	X	X	X	X
Coma	X	X	X	X	X
Drowsiness	X	X	X	X	X
Breathing difficulties	X	X	X	X	X
Tremor	X	X	X	X	X
Fur	Normal	Normal	Normal	Normal	Normal
Salivation	X	X	X	X	X
Red tear	X	X	X	X	X
Death	0	0	0	0	4

Note: X - Not observed; ✓ - Observed

Table 22. The effect of a repeated-dose methanolic extract of *Parkia timoriana* seed pod on the body weight and relative organ weight of Wistar albino rats exposed to it in a sub-acute toxicity study.

Organ	Control	20 mg/kg	50 mg/kg	100 mg/kg
Initial body weight	232 ± 0.98	229 ± 1.01	219 ± 0.76	222 ± 1.19
Final body weight	238 ± 0.87	234 ± 0.95	226 ± 0.88	227 ± 0.79
Kidney	0.72 ± 0.21	0.73 ± 0.18	0.68 ± 0.17	0.69 ± 0.16
Liver	3.25 ± 0.60	2.28 ± 0.43	3.20 ± 0.59	3.07 ± 0.57
Lungs	1.09 ± 0.33	1.11 ± 0.29	0.90 ± 0.21	0.98 ± 0.19
Spleen	0.24 ± 0.11	0.24 ± 0.10	0.34 ± 0.17	0.34 ± 0.17
Brain	0.94 ± 0.20	0.96 ± 0.18	0.91 ± 0.26	0.98 ± 0.24
Heart	0.47 ± 0.08	0.43 ± 0.17	0.36 ± 0.13	0.39 ± 0.12

Table 23. The effect of a repeated-dose methanolic extract of *Parkia timoriana* seed pod on the haematological parameters of Wistar albino rats exposed to it in a sub-acute toxicity study. All values are expressed as mean \pm SEM, n = 5. *p < 0.05 shows a significant difference (one-way ANOVA/Tukey's multiple comparison). Statistically significant data are represented with different alphabetical letters.

Parameter	Control	10 mg/kg	20 mg/kg	50 mg/kg
RBC ($10^6/\mu\text{l}$)	7.03 \pm 0.56	7.52 \pm 0.38	6.90 \pm 0.67	7.21 \pm 0.51
WBC ($10^3/\mu\text{l}$)	8.82 \pm 0.87	8.09 \pm 0.61	7.91 \pm 0.29	8.47 \pm 0.58
Hb (g/dl)	12.19 \pm 0.91	12.45 \pm 0.49	13.32 \pm 0.72	12.89 \pm 0.39
Hematocrit (%)	43.89 \pm 2.16	45.71 \pm 2.71	42.61 \pm 3.91	47.36 \pm 1.82
MCV (fl)	63.52 \pm 3.64	59.66 \pm 2.85	61.28 \pm 1.95	64.71 \pm 2.82
MCH (pg)	18.64 \pm 1.62	16.95 \pm 1.28	19.21 \pm 0.98	16.94 \pm 1.91
MCHC (g/dl)	26.99 \pm 1.09	27.81 \pm 2.01	30.62 \pm 2.71	27.81 \pm 1.92

Table 24. The impact of a repeated-dose methanolic extract of *Parkia timoriana* seed pod on the biochemical analysis of Wistar albino rats exposed to it in a sub-acute toxicity study. All values are expressed as mean \pm SEM, n = 5. *p < 0.05 shows a significant difference (one-way ANOVA/Tukey's multiple comparison). Statistically significant data are represented with different alphabetical letters.

Parameter	Control	20 mg/kg	50 mg/kg	100 mg/kg
AST (U/ml)	37.12 \pm 2.19	35.81 \pm 1.01	35.62 \pm 2.81	39.08 \pm 2.07
ALT (U/ml)	27.56 \pm 1.98	28.38 \pm 1.31	27.01 \pm 0.81	26.19 \pm 1.21
ALP (K.A. Units)	11.62 \pm 0.69	10.84 \pm 1.27	12.04 \pm 0.95	11.88 \pm 1.09
Creatinine (mg %)	0.65 \pm 0.069	0.62 \pm 0.091	0.68 \pm 0.057	0.71 \pm 0.058
Urea (mg/dl)	30.17 \pm 2.19	33.51 \pm 1.72	32.16 \pm 2.67	29.95 \pm 2.08
Cholesterol (mg/dl)	46.18 \pm 1.82	45.21 \pm 2.17	48.52 \pm 3.38	49.71 \pm 3.02
Triglycerides (mg/dl)	32.61 \pm 2.13	33.21 \pm 1.84	30.14 \pm 2.81	30.68 \pm 0.97
HDL (mg/dl)	27.21 \pm 0.89	24.67 \pm 2.73	25.43 \pm 1.79	26.89 \pm 1.28
LDL (mg/dl)	10.54 \pm 1.33	11.41 \pm 0.71	12.26 \pm 1.17	12.78 \pm 1.82

4.5. DISCUSSIONS

4.5.1. Acute and sub-acute toxicity study

Parkia timoriana, besides its significant nutritional content, has been shown to possess antioxidant, antibacterial, antidiabetic, anti-proliferative, and insecticidal activities (Angami et al., 2018). The pods of *P. timoriana* contain a significant quantity of tannins, flavonoids, saponins, anthocyanins, and leuco-anthocyanins (Salam et al., 2009). Similarly, this research demonstrated a significant concentration of flavonoids and phenols in the methanolic extract of the seed pods of *P. timoriana*. These phytochemical components in medicinal plants are responsible for their antioxidant properties and support bioactive activities (Aiyegoro and Okoh, 2010). Considering these properties of *P. timoriana*, the present study was designed to see the effect of PTME on Alzheimer's disease. However, the toxicity and food safety of *P. timoriana* have not been well explored. Before using traditional plants for their medicinal benefits, it is crucial to conduct a thorough scientific toxicological study to accurately estimate their toxicological characteristics. This evaluation is necessary even for the traditional plants with the most efficient therapeutic effect (Chanda et al., 2015; Jayesh et al., 2017).

The findings from the acute toxicity study demonstrate that the single-dose oral administration of the PTME to rats at doses of 1000, 3000, and 5000 mg/kg shows signs of mortality in two rats at a dose of 5000 mg/kg. However, the value of LD₅₀ was found to be more than 5000 mg/kg body weight. According to the Organisation for Economic Development (OECD) standards outlined in its Globally Harmonised Classification System (GHS) for chemical compounds and combinations, substances having an LD₅₀ greater than 2000 mg/kg are classified as either unclassified or in category 5 (Walum, 1998). In addition, the OECD 423 guidelines state that if all the animals in the study lived until the end of the experiment, it indicates that the extract has a low level of toxicity and should be classified in category 5 (Brondani et al. 2017). These findings indicate that the LD₅₀ of PTME may be considered safe. No sign of morphological change was observed at all doses, except for a rat treated with 5000

mg/kg who had a red tear. Red tears are often seen as an indication of stress or illness (**Mason et al., 2004**).

Acute toxicity findings often have minimal clinical relevance. Consequently, research on sub-acute toxicity was conducted. Substances used to treat chronic diseases may need a toxicological review to assess their potential for sub-acute toxicity. This is because regular use of these substances may lead to their buildup in the body, which can have progressive effects on tissues and organs (**Ugwah-Oguejiofor et al., 2019**). The repeated-dose administration of PTME at doses of 20 mg/kg, 50 mg/kg, and 100 mg/kg did not show any mortality. However, four rats (only one survived) died at a dose of 300 mg/kg. No morphological change was observed at all doses. The food and water intake, as well as body weight and relative organ weight, did not show any significant change in both the administration of single-dose and repeated-dose PTME. Body weight, feed, and water intake have been used as indications to assess the overall health state of experimental animals (**El-Hilaly et al., 2004**). Organ weight changes are highly responsive markers of toxicity in toxicity studies. They may reflect effects on enzymes, physiological disruptions, and injuries to target organs (**Michael et al., 2007**). A rise in organ weight indicates hypertrophy, whereas a reduction signals necrosis in the target organ (**Teo et al., 2002**). Although organ weights may offer valuable indications of the effects caused by the test article, it is important to interpret this data in conjunction with gross pathology, clinical pathology, and histopathological results in order to have a comprehensive understanding (**Sellers et al., 2007**).

Haematological parameter analysis is used to assess the level of toxicity of pharmacological compounds, including plant extracts (**Ibrahim et al., 2016**). Haematopoiesis refers to the biological process by which blood cells are produced. The predictive value of human toxicity is stronger when data from animal research is translated, particularly in relation to changes in the haematopoietic system (**Olson et al., 2000**). In this investigation, the administration of PTME in both acute and sub-acute studies did not result in any significant alterations in the blood parameters, except for a slight elevation of WBC in acute toxicity study. WBCs are highly adaptable cells that play a crucial role in initiating an immune response to foreign chemicals (**Pearce**

et al., 2013). The rise in lymphocytes indicates a potential immunostimulatory impact of the plant (**Ugwah-Oguejiofor et al., 2019**).

The liver and kidney functions play a crucial role in the survival of animals. Their functioning may be assessed using serum biochemical analysis, which is essential in the toxicological assessment of xenobiotics (**Bariweni et al., 2018**). Serum liver function tests provide insights into the condition of the liver. AST, ALP, and ALT are primarily synthesised by hepatocytes, and any damage to the liver might result in an elevation of these enzyme levels in the bloodstream (**Adedapo et al., 2004**). Elevated levels of liver enzymes are indicative of hepatocellular toxicity (**Brautbar and Williams, 2002**), whereas a reduction may suggest enzyme inhibition (**Akanji et al., 2013**). In the acute toxicity study, there was a significant increase in the level of ALP at a dose of 5000 mg/kg and a slight increase in the levels of AST and ALT. This shows acute hepatocellular toxicity at a higher single-dose administration of PTME. The histopathological study has confirmed the presence of deteriorated alterations in the liver tissue, providing further evidence of liver cell damage caused by PTME at a higher single dosage of 5000 mg/kg. No significant change was observed in the levels of AST, ALP, and ALT at 20 mg/kg, 50 mg/kg, and 100 mg/kg after repeated-dose administration of PTME for 28 days. As a result, the histological examination of the liver in these groups also showed normal architecture of the liver tissue. However, the administration of a repeated-dose of PTME at a dose of 300 mg/kg for 28 days caused the death of four rats, and the surviving rat showed deteriorated alterations in the liver tissue.

The kidney function test showed that the level of creatinine was significantly increased at a single-dose administration of 5000 mg/kg, and there was a slight increase in the level of urea. Renal toxicity is characterised by increased concentrations of creatinine, urea, and uric acid in the circulation as a result of impaired kidney function, which hinders the efficient removal of these waste products (**Feriani et al., 2017**). Therefore, a single-dose administration of PTME at a dose of 5000 mg/kg may cause nephrotoxicity, as creatinine levels are regarded as significant indicators of renal impairment (**Mukinda and Eagles, 2010; Chebaibi et al., 2019**). This was evident as the histological examination showed significant damage in the tissue of the kidney at

a dose of 5000 mg/kg. In the sub-acute toxicity study, no significant change was observed in the level of creatinine and urea at 20 mg/kg, 50 mg/kg, and 100 mg/kg repeated-dose administration of PTME for 28 days, and the histological examination at these doses showed normal hepatocytes displaying no apparent alterations in the morphological features. However, the repeated-dose administration of PTME at a dose of 300 mg/kg for 28 days caused the death of four rats, and the surviving rat showed highly damaged kidney tissue. The sub-acute toxicity study revealed that a repeated-dose administration of PTME at a dose of 300 mg/kg showed signs of mortality and toxicity in the surviving rat. Therefore, a lower dose ≤ 100 mg/kg may be preferred for chronic use to treat different types of diseases. The NOAEL of the methanolic extract of *Parkia timoriana* seed pods was found to be 100 mg/kg.

4.5.2. AlCl₃-mediated Alzheimer's disease treatment

The present work assesses the neurotoxic impacts of administering aluminum chloride to adult rats for a duration of 6 weeks, as well as the neuroprotective benefits of *Parkia timoriana*. The research emphasises the influence of aluminum on memory, presents more proof of the health risks linked to aluminum food additives, and explains the processes via which aluminum contributes to the development of Alzheimer's disease.

This research demonstrates that PTME has an ameliorative effect on the impairment of learning and memory caused by aluminum. This effect was shown in both the novel object recognition (NOR) and Y-maze tests, and it is associated with changes in biochemical indicators in the hippocampus. The Morris water maze is a well-established technique used to assess spatial learning and memory in rats. However, the experimental situation in NOR is conducive to the well-being of the animals and closely resembles the conditions of human behavioural examinations. Therefore, the Morris water maze might be supplanted by this test as the principal method for assessing the efficacy of new medications in treating Alzheimer's disease (**Zhang et al., 2012; Ennaceur and Delacour, 1988**). The Y-maze task is a precise and effective test for evaluating spatial recognition memory in rats. The test is based on the inherent inclination of rats to investigate a new environment (**Yusuf et al., 2009; Van der Borgh et al., 2007; Hidaka et al., 2011**). The Y-maze used in this investigation does

not employ any unpleasant stimuli and was deemed appropriate for assessing memory. Prior research has shown that elevated amounts of aluminum in the brain might hinder long-term potentiation, which is believed to be the primary physiological mechanism underlying learning and memory (**Llansola et al., 1999; Shuchang et al., 2008**).

Oxidative stress is a crucial factor that might impact the initiation and pathological advancement of Alzheimer's disease (**Wang et al., 2014; Zhao and Zhao, 2013**). The excessive accumulation of free radicals causes oxidative damage to macromolecules, which in turn leads to brain damage and cognitive deficits (**Bertram and Tanzi, 2008**). Reactive oxygen species (ROS) generated in brain tissues may regulate the transmission of signals between neurons, both at the synapses and outside of them. This can lead to inflammation in the brain and the death of cells, ultimately causing neurodegeneration and memory impairment (**Popa-Wagner et al., 2013**). GSH depletion is a key sign in patients throughout the course of neurodegenerative diseases (**Bharath et al., 2002**). In the present study, the administration of PTME reduced the negative effects caused by $AlCl_3$, such as decreased MDA levels and increased GST and GSH levels. This demonstrates that PTME improved the oxidative stress caused by $AlCl_3$ in the hippocampus. The hippocampus plays a crucial role in the development of recognition memory in both humans and animals (**Barker and Warburton, 2011**). It is often considered to be a significantly damaged region throughout the course of Alzheimer's disease (**Bingman and Jones, 1994**).

Acetylcholine (ACh) is the primary neurotransmitter responsible for learning and memory activities. Changes in cholinergic activity are the major cause of neurochemical abnormalities in Alzheimer's disease (**Rakonczay et al., 2005; Gold, 2003**). Acetylcholinesterase (AChE) is the enzyme used to identify and measure cholinergic activity. It breaks down and ends the natural effects of ACh in the body. Aluminum may increase the activity of AChE by interacting with its peripheral locations and altering the secondary structure (**Zatta et al., 1994; Liaquat et al., 2019; Thirunavukkarasu et al., 2012**). The current research attributes the increased activity of AChE in the group treated with $AlCl_3$ to the direct impact of Al. Our investigation revealed that the simultaneous administration of PTME resulted in a significant decrease in AChE activity in the hippocampus.

A significant discovery of this study is that PTME hindered the activation of NF- κ B in the hippocampus, which in turn reduced the occurrence of subsequent pathological events. A previous study has shown an increase in NF- κ B expression in rats treated with aluminum (Zhao et al., 2014). NF- κ B, once activated, moves into the nucleus and attaches to DNA, causing the activation of genes related to inflammation, such as IL-8 and IL-6 (Karin, 2009; Brasier, 2010). Furthermore, NF- κ B enhances the production of BACE1 and hinders the ability of microglial cells to engulf and remove A β 42 peptide monomers, leading to their accumulation and formation of larger amyloid structures (Tamagno et al., 2012; Zhao et al., 2014). In addition, the activation of NF- κ B leads to the production of suppressor of cytokine signaling-3 (SOCS3), which functions as a negative controller of the JAK/STAT3 pathway, therefore inhibiting STAT3 activation (McFarland et al., 2013). Therefore, NF- κ B is probably the primary upstream mediator responsible for the neuronal abnormalities seen in this research, such as A β accumulation, increased production of pro-inflammatory cytokines, and apoptosis.

In Alzheimer's disease (AD), neuroinflammation is a key process that is initiated by the introduction of aluminum and the deposition of the toxic A β protein. This leads to the activation of microglia and a rise in the number of astrocytes in the hippocampus (Glass et al., 2010). The production of pro-inflammatory cytokines, TNF- α and IL-6, in the hippocampal regions of aluminum-treated rats is likely associated with A β deposition, tau phosphorylation, and activation of NF- κ B (Rubio-Perez and Morillas-Ruiz, 2012; McFarland, 2013). IL-1b, IL-6, and TNF- α have been widely studied as pro-inflammatory mediators in the brain. They have a role in the development of memory and learning impairments in Alzheimer's disease (Akiyama et al., 2000; Li et al., 2015). In the present study, the administration of PTME lowered the expression of these pro-inflammatory cytokines, including IL-6 and TNF- α , probably by inhibiting the expression of NF- κ B.

Apoptosis has been a subject of significant concern due to its crucial role in the pathological progression of Alzheimer's disease (Paquet et al., 2018). Apoptosis is tightly controlled by two primary categories of Bcl-2 family proteins: the anti-apoptotic members, including Bcl-2 and Bcl-xL, and the pro-apoptotic members,

including Bax, Bak, and BH3-domain-only proteins (**Fiandalo and Kyprianou, 2012**). Upon receiving apoptotic signals, BH3-domain-only proteins interact with and disable the anti-apoptotic Bcl-2 protein, which typically deactivates the pro-apoptotic Bax/Bak proteins (**Cheng et al., 2001**). The Bax/Bak proteins become activated and form oligomers in the outer mitochondrial membrane. These oligomers create pores that cause the mitochondrial wall to become permeable, allowing cytochrome c to be released into the cytosol. This release of cytochrome c triggers the activation of caspase-9, which then acts on downstream targets, including caspase-3, ultimately leading to apoptotic cell death (**Zou et al., 1999; Wei et al., 2001; Ohtsuka et al., 2003**). In the current study, there is an increased expression of active caspase-3 and Bax by the aluminum exposure, which might be linked to the reduction of Bcl-2 expression levels. Interestingly, the administration of PTME caused a decrease in the levels of active caspase-3 and Bax, most likely by restoring the Bcl-2 expression level.

Rats treated with aluminum showed increased expression of BACE1, which was correlated with elevated hippocampus A β levels. In fact, BACE1 and γ -secretase cause two consecutive endoproteolytic cleavages of the amyloid precursor protein to produce A β (**Vardy et al., 2005**). The cleavage of APP by BACE1 is the first and necessary step for the formation of A β 42. Additionally, the levels of BACE1 are increased in both experimental models of Alzheimer's disease and in the brains of Alzheimer's disease patients (**Li et al., 2004; Harada et al., 2006; Zhao et al., 2007**). Downstream consequences of A β toxicity are the phosphorylation of tau and the disruption of microtubule networks, which are crucial underlying processes leading to neuronal death and the development of Alzheimer's disease (**Patrick et al., 1999**). A β stimulates the phosphorylation of tau, most likely via activating proteases generated by A β (**Park and Ferreira, 2005**) and increasing the activity of several kinases that target tau, such as glycogen synthase kinase-3 (GSK-3) (**Reifert et al., 2011**). The administration of PTME reduces the expression level of A β , probably by inhibiting the activity of BACE1. Furthermore, the reduction in the expression level of tau protein may be attributed to the suppression of A β toxicity by the administration of PTME.

The administration of the methanolic extract of *P. timoriana* seed pods successfully restored the histopathological alterations of the hippocampus caused by AlCl₃ toxicity.

It reduced the aberrant overexpression of BACE1, A β , and phosphorylated tau in the hippocampus. Furthermore, it successfully counteracted the increase in AChE level caused by aluminum, inhibited inflammation in neurons, reduced oxidative stress in neurons, and increased the activities of antioxidants GSH and GST in the hippocampus. Additionally, it decreased the activity of pro-apoptotic biomarkers, including caspase-3 and Bax, and increased the levels of Bcl-2, an anti-apoptotic biomarker.

4.6. KEY FINDINGS

- The acute toxicity study found that PTME, administered at doses of 1000, 3000, and 5000 mg/kg, caused mortality in two rats at 5000 mg/kg dosage, with a LD₅₀ value exceeding 5000 mg/kg body weight. According to the OECD, the LD₅₀ of PTME may be considered safe. There were no observable changes in the morphology of the subjects at any of the administered dosages, except for one rat treated with 5000 mg/kg which had a red tear.
- The repeated-dose administration of PTME at doses of 20 mg/kg, 50 mg/kg, and 100 mg/kg did not show any mortality. However, four rats (only one survived) died at a dose of 300 mg/kg. No morphological change was observed at all doses.
- The food and water intake, as well as body weight and relative organ weight, did not show any significant change in both the administration of single-dose and repeated-dose PTME.
- The administration of PTME in both acute and sub-acute studies did not result in any significant alterations in the blood parameters, except for a slight elevation of WBC in acute toxicity study.
- In the acute toxicity study, there was a significant increase in the level of ALP at a dose of 5000 mg/kg and a slight increase in the levels of AST and ALT. This shows acute hepatocellular toxicity at a higher single-dose administration of PTME. The histopathological study has confirmed the presence of deteriorated alterations in the liver tissue, providing further evidence of liver cell damage caused by PTME at a higher single dosage of 5000 mg/kg.

- In the sub-acute toxicity study, no significant change was observed in the levels of AST, ALP, and ALT at 20 mg/kg, 50 mg/kg, and 100 mg/kg after repeated-dose administration of PTME for 28 days. As a result, the histological examination of the liver in these groups also showed normal architecture of the liver tissue. However, the administration of a repeated-dose of PTME at a dose of 300 mg/kg for 28 days caused the death of four rats, and the surviving rat showed deteriorated alterations in the liver tissue.
- In the acute toxicity study, the kidney function test showed that the level of creatinine was significantly increased at a single-dose administration of 5000 mg/kg, and there was a slight increase in the level of urea. This was evident as the histological examination showed significant damage in the tissue of the kidney at a dose of 5000 mg/kg.
- In the sub-acute toxicity study, no significant change was observed in the level of creatinine and urea at 20 mg/kg, 50 mg/kg, and 100 mg/kg repeated-dose administration of PTME for 28 days, and the histological examination at these doses showed normal hepatocytes displaying no apparent alterations in the morphological features. However, the repeated-dose administration of PTME at a dose of 300 mg/kg for 28 days caused the death of four rats, and the surviving rat showed highly damaged kidney tissue.
- The sub-acute toxicity study revealed that a repeated-dose administration of PTME at a dose of 300 mg/kg showed signs of mortality and toxicity in the surviving rat. Therefore, a lower dose ≤ 100 mg/kg may be preferred for chronic use to treat different types of diseases. The NOAEL of the methanolic extract of *Parkia timoriana* seed pods was found to be 100 mg/kg.
- The novel object recognition (NOR) and Y-maze tests have demonstrated that PTME has an ameliorative effect on the learning and memory impairment caused by aluminum.
- The administration of PTME improved the oxidative stress (MDA) caused by AlCl_3 in the hippocampus and increased GST and GSH anti-oxidant levels.
- The current research attributes the increased activity of AChE in the group treated with AlCl_3 to the direct impact of Al. Our investigation revealed that

the simultaneous administration of PTME resulted in a significant decrease in AChE activity in the hippocampus.

- PTME hindered the activation of NF- κ B in the hippocampus, which in turn reduced the occurrence of subsequent pathological events, such as A β accumulation, increased production of pro-inflammatory cytokines, and apoptosis.
- The administration of PTME lowered the expression of pro-inflammatory cytokines, including IL-6 and TNF- α , in the hippocampus of AlCl₃-mediated AD rats, probably by inhibiting the expression of NF- κ B.
- The administration of PTME caused a decrease in the levels of active caspase-3 and Bax in the hippocampus of AlCl₃-mediated AD rats, most likely by restoring the Bcl-2 expression level.
- The administration of PTME reduces the expression level of A β in the hippocampus of AlCl₃-mediated AD rats, probably by inhibiting the activity of BACE1. Furthermore, the reduction in the expression level of tau protein may be attributed to the suppression of A β toxicity by the administration of PTME.
- The administration of the methanolic extract of *P. timoriana* seed pods successfully restored the histopathological alterations of the hippocampus caused by AlCl₃ toxicity.

CHAPTER-5

SUMMARY

Parkia timoriana is a nutritious, underutilized leguminous tree found in the north-eastern regions of India and other Southeast Asian nations. In addition to its significant nutritional content, *P. timoriana* has been shown to possess many biological activities, including antioxidant, antibacterial, antidiabetic, anti-proliferative, and insecticidal activities. The pods of *P. timoriana* also contain a significant quantity of tannins, flavonoids, saponins, anthocyanins, and leuco-anthocyanins. These phytochemical components in medicinal plants are responsible for their antioxidant properties and support bioactive activities. With these properties in consideration, the primary objective of this research is to evaluate the beneficial impact of *P. timoriana* seed pods on cognitive impairment in rats with Alzheimer's disease produced by AlCl_3 . However, the toxicity and food safety of *P. timoriana* have not been well explored. Therefore, prior to conducting the experiment, an analysis was performed on the phytochemical contents of *P. timoriana* seed pods, and their toxicity was evaluated using computational techniques. Furthermore, these phytocompounds were subjected to molecular docking, MD modelling, and free energy calculation to assess their interactions with BACE1 and AChE protein receptors. Acute and sub-acute toxicity studies were conducted to estimate the LD_{50} and NOAEL values of the plant.

In the present study, nine bioactive compounds were identified through GC-MS analysis and fifty-two bioactive compounds were identified through LC-MS analysis. The phytocompounds present in the methanolic extract of *P. timoriana* seed pod were mostly composed of flavonoids, alkaloids, and terpenoids. The PTME has a total phenol concentration of 421.64 ± 3.38 mg GAE/g of extract and total flavonoid concentration was measured to be 280.893 ± 4.31 mg QE/g of extract.

The predicted acute toxicity of phytocompounds from PTME showed four distinct hierarchies. a) fathead minnow > *T. pyriformis* > *D. magna* > rat; b) fathead minnow > *D. magna* > *T. pyriformis* > rat; c) *D. magna* > fathead minnow > *T. pyriformis* > rat; and d) *T. pyriformis* > fathead minnow > *D. magna* > rat. This shows that phytocompounds from PTME had less toxicity for mammalian species (rat/ LD_{50})

compared to aquatic organisms (LC₅₀/fathead minnow and *D. magna*, IGC₅₀/*T. pyriformis*). All of the phytocompounds found in PTME, except two, had a bioconcentration factor under 2000 and were therefore considered non-bioaccumulative. Forty-six out of sixty-one phytocompounds from PTME were considered toxic for the developmental stage, whereas apigenin glucoside arabinoside, isoschaftoside, maritimetin-6-O-glucoside, apiin, 3-oxo-C8-homoserine lactone, and ouabain were safe alternatives. The majority of the phytocompounds (fifty-one out of sixty-one) from PTME showed negative carcinogenic and mutagenic properties. The oral toxicity test revealed that 75% of the phytocompounds are highly toxic (Cramer/category III), while 64% do not affect fertility or possess reproductive toxicity. The study found that 37.70% of phytocompounds had a high NOAEL value, which indicated their safety and did not cause negative effects, while the remaining phytocompounds (62.29%) were toxic and had positive side effects. The repeated dose toxicity analysis of the phytocompounds showed forty-eight out of sixty-one are safe and do not cause any damage to organs, with a significant number of phytocompounds showing bioavailability, metabolized by cytochrome-P450 enzyme complex, and excreted from the body. The phytocompounds studied have properties for dementia treatment (thirty-one phytocompounds), cytochrome P450 stimulant (seventeen phytocompounds), anti-oxidant (forty-one phytocompounds), anti-inflammatory (forty-five phytocompounds), neurotrophic factor enhancer (twenty-three phytocompounds), amyloid- β aggregation inhibitor (five phytocompounds), acetylcholine stimulant (fifteen phytocompounds), and Alzheimer disease treatment (two phytocompounds).

The ADMET study using SwissADME demonstrated that forty compounds had drug-likeness properties as indicated by Lipinski's rule of five, thirty-two compounds were considered to have a good affinity for a lipophilic environment, thirty-one compounds that have the capacity to be absorbed by the body when taken orally and have the ability to reach certain target areas inside the body as per their TPSA value, forty-eight compounds have non-hydrogen atoms that falls under the acceptable range, sixteen compounds possess an acceptable molar volume, and thirty-six compounds were in the acceptable range of molar refractivity. No compound was found highly soluble as per

LogS value. However, six compounds showed solubility, twenty compounds slightly soluble, and thirty-five compounds lack solubility. Additionally, twenty-seven phytocompounds revealed high absorption in the gastrointestinal tract, and twenty compounds showed blood-brain barrier permeation. With respect to GPCR, ion channel modulator, kinase inhibitor, nuclear receptor ligand, protease inhibitor, and enzyme inhibitor, all the sixty-one phytocompounds of *Parkia timoriana* fall under the category of active and moderately active drugs. Thirty-eight phytocompounds successfully met the P-gp substrate criteria, fifty-three showed no alert for PAINS filters, and nineteen phytocompounds did not show alert for BRENK. The majority of the phytocompounds had lesser skin permeability. Similarly, the majority of the compounds indicated good oral bioavailability and can be moderately synthesized. Thirty-nine compounds inhibited one or the other enzyme of the cytochrome p450 enzyme complex.

The molecular docking analysis revealed that the phytocompounds from the methanolic extract of *Parkia timoriana* seed pods strongly bind to BACE1 and AChE receptors, with binding affinities ranging from -5.3 kcal/mol to -10.3 kcal/mol against the BACE1 receptor and from -6.0 kcal/mol to -10.3 kcal/mol against the AChE receptor. Sixteen and fifteen phytocompounds had binding affinity \leq -9.0 kcal/mol against BACE1 and AChE, respectively. The selected top hit ligands for the BACE1 receptor include ergocristine as the best-ranked ligand with a binding affinity of -10.3 kcal/mol, followed by nicotiflorin, voacamine, and isorhamnetin-3-O-rutinoside with binding affinity of -10.2 kcal/mol, -10.1 kcal/mol, and -10.1 kcal/mol, respectively. Whereas, the top hit ligands for the AChE receptor include apiin and maritimetin-6-O-glucoside as the best binding ligands with binding affinity of -10.3 kcal/mol each, followed by paeoniflorin and silychrystin with binding affinity of -10.2 kcal/mol and -9.8 kcal/mol, respectively. TRP76, PHE108, TYR71, LYS107, and ILE126 were the most common residues of BACE1, among the other interacting residues, that were interacting with the top hit ligands through hydrogen and hydrophobic bonds and therefore may be important in ligand binding. On the other hand, SER125, TYR341, TYR124, and TRP86 were the most common residues of AChE, among the other

interacting residues, that were interacting with the top hit ligands through hydrogen and hydrophobic bonds and therefore may be important in ligand binding.

The MD simulation studies confirmed that the top hit ligands formed a stable complex with BACE1 having RMSD, RMSF, and Rg values of ~ 0.2 nm, ~ 0.1 nm, and ~ 2.0 nm, respectively. However, the BACE1-nicotiflorin and BACE1-isorhamnetin-3-O-rutinoside complexes formed a significantly higher number of H-bonds of 4.94 and 3.88, respectively, compared to the other complexes. Similarly, the MD simulation studies confirmed that the top hit ligands formed a stable complex with AChE having RMSD, RMSF, and Rg values as ~ 0.24 nm, ~ 0.11 , and ~ 2.3 nm, respectively. On the other hand, the AChE-maritimetin-6-O glucoside and AChE-paeoniflorin complexes formed a higher number of H-bond of 3.27 and 2.76, respectively, compared to the other complexes.

The binding free energy calculation for BACE1 by MM/PBSA method showed that all the simulated complexes formed a strong bonding complex, with BACE1-voacamine complex showing exceptionally high binding free energy of -417.951 ± 31.736 kJ/mol. Similarly, the binding free energy calculation for AChE by MM/PBSA method showed that all the simulated complexes also formed a strong bonding complex, with AChE-silychristin complex showing exceptionally high binding free energy of -385.386 ± 18.965 kJ/mol. The main energy contribution of the BACE1 receptor's amino acids in the binding of lead ligands at the active site indicated that residues TYR 71, ASP 106, ASP 228, PHE 108, SER 35, ASP 32, and ASP 223 of the BACE1 receptor played a significant role in the intermolecular interaction and the binding of the ligands. However, in complexes involving AChE and ligands, distinct amino acid residues played a role in contributing to the binding energy for each of the lead ligands. The principal component analysis showed that the C α of both BACE1 and AChE when complexed with the top hit ligands occupied very less phase space further confirming the stability of the complex formed.

The acute toxicity study found that PTME, administered at doses of 1000, 3000, and 5000 mg/kg, caused mortality in two rats at 5000 mg/kg dosage, with a LD₅₀ value exceeding 5000 mg/kg body weight. According to the OECD, the LD₅₀ of PTME may

be considered safe. There were no observable changes in the morphology of the subjects at any of the administered dosages, except for one rat treated with 5000 mg/kg which had a red tear. The repeated-dose administration of PTME at doses of 20 mg/kg, 50 mg/kg, and 100 mg/kg did not show any mortality. However, four rats (only one survived) died at a dose of 300 mg/kg. No morphological change was observed at all doses. The food and water intake, as well as body weight and relative organ weight, did not show any significant change in both the administration of single-dose and repeated-dose PTME. The administration of PTME in both acute and sub-acute studies did not result in any significant alterations in the blood parameters, except for a slight elevation of WBC in acute toxicity study. In the acute toxicity study, there was a significant increase in the level of ALP at a dose of 5000 mg/kg and a slight increase in the levels of AST and ALT. This shows acute hepatocellular toxicity at a higher single-dose administration of PTME. The histopathological study has confirmed the presence of deteriorated alterations in the liver tissue, providing further evidence of liver cell damage caused by PTME at a higher single dosage of 5000 mg/kg. In the sub-acute toxicity study, no significant change was observed in the levels of AST, ALP, and ALT at 20 mg/kg, 50 mg/kg, and 100 mg/kg after repeated-dose administration of PTME for 28 days. As a result, the histological examination of the liver in these groups also showed normal architecture of the liver tissue. However, the administration of a repeated-dose of PTME at a dose of 300 mg/kg for 28 days caused the death of four rats, and the surviving rat showed deteriorated alterations in the liver tissue. In the acute toxicity study, the kidney function test showed that the level of creatinine was significantly increased at a single-dose administration of 5000 mg/kg, and there was a slight increase in the level of urea. This was evident as the histological examination showed significant damage in the tissue of the kidney at a dose of 5000 mg/kg. In the sub-acute toxicity study, no significant change was observed in the level of creatinine and urea at 20 mg/kg, 50 mg/kg, and 100 mg/kg repeated-dose administration of PTME for 28 days, and the histological examination at these doses showed normal hepatocytes displaying no apparent alterations in the morphological features. However, the repeated-dose administration of PTME at a dose of 300 mg/kg for 28 days caused the death of four rats, and the surviving rat showed highly damaged kidney tissue. The sub-acute toxicity study revealed that a repeated-dose administration of

PTME at a dose of 300 mg/kg showed signs of mortality and toxicity in the surviving rat. Therefore, a lower dose ≤ 100 mg/kg may be preferred for chronic use to treat different types of diseases. The NOAEL of the methanolic extract of *Parkia timoriana* seed pods was found to be 100 mg/kg.

The novel object recognition (NOR) and Y-maze tests have demonstrated that PTME has an ameliorative effect on the learning and memory impairment caused by aluminum. The administration of PTME improved the oxidative stress (MDA) caused by AlCl_3 in the hippocampus and increased GST and GSH anti-oxidant levels. The current research attributes the increased activity of AChE in the group treated with AlCl_3 to the direct impact of Al. Our investigation revealed that the simultaneous administration of PTME resulted in a significant decrease in AChE activity in the hippocampus. PTME hindered the activation of NF- κ B in the hippocampus, which in turn reduced the occurrence of subsequent pathological events, such as $\text{A}\beta$ accumulation, increased production of pro-inflammatory cytokines, and apoptosis. The administration of PTME has also lowered the expression of pro-inflammatory cytokines, including IL-6 and TNF- α , in the hippocampus of AlCl_3 -mediated AD rats, probably by inhibiting the expression of NF- κ B. It caused a decrease in the levels of active caspase-3 and Bax in the hippocampus of AlCl_3 -mediated AD rats, most likely by restoring the Bcl-2 expression level. The administration of PTME reduces the expression level of $\text{A}\beta$ in the hippocampus of AlCl_3 -mediated AD rats, probably by inhibiting the activity of BACE1. Furthermore, the reduction in the expression level of tau protein may be attributed to the suppression of $\text{A}\beta$ toxicity by the administration of PTME. The administration of the methanolic extract of *P. timoriana* seed pods successfully restored the histopathological alterations of the hippocampus caused by AlCl_3 toxicity.

CHAPTER 6

CONCLUSION

The majority of the compounds detected, using GC-MS and LC-MS analyses, in PTME are alkaloids, flavonoids, and terpenoids. A high content of total flavonoid and total phenol was found in the extract. The phytochemicals from PTME have higher toxicity (LC_{50} and IGC_{50}) for aquatic animals than for terrestrial mammals (LD_{50}). The phytochemicals from PTME are mostly not bioaccumulative, mutagenic, or carcinogenic and are bioavailable, metabolized by Cyt-P450 enzymes, and eliminated from the body. The phytochemicals have a wide range of biological effects, including dementia treatment, cytochrome P450 stimulant, anti-oxidant, anti-inflammatory, neurotrophic factor enhancer, amyloid- β aggregation inhibitor, acetylcholine stimulant, and Alzheimer's disease treatment activities. Potent developmental toxicants and low NOAEL values were predicted in *P. timoriana* phytochemicals. The phytochemicals had favourable pharmacokinetic and pharmacodynamic features, as well as a robust binding affinity, forming stable complexes with the BACE1 and AChE receptors. Ergocristine, nicotiflorin, voacamine, and isorhamnetin-3-O-rutinoside exhibited the strongest binding affinity (≤ -10.1 kcal/mol) against BACE1 and apiin, maritimetin-6-O-glucoside, paeoniflorin, and silychrystin (≤ -9.8 kcal/mol) against AChE. Additionally, these molecules displayed high energy non-bonded interactions, appropriate folding, stability, compactness, flexibility, and limited movements in the analysis of molecular dynamics simulation and free energy calculation. The drug-likeness, molecular docking, MD simulation, and free energy calculation investigations of the phytochemicals from PTME provide thorough validation of their neuroprotective potential. The acute toxicity analysis of the PTME demonstrated a high LD_{50} value > 5000 mg/kg, which corresponds to the anticipated high LD_{50} value in the computational research. However, the sub-acute toxicity exhibited a low NOAEL of ≤ 100 mg/kg, as predicted by the computational analysis. This research reveals the positive impacts of PTME in mitigating the pathological disruptions resembling Alzheimer's disease generated by aluminum. PTME successfully restored the histopathological alterations and reduced the aberrant overexpression of BACE1, A β , and p-tau. Additionally, it restored the cognitive

impairment caused by aluminum, repressed inflammation in neurons, reduced oxidative stress in neurons, decreased caspase-3 activation, and increased levels of GSH and GST. PTME likely provided protection by regulating NF- κ B activation, which in turn controls Bcl-2 signalling.

CHAPTER-7

REFERENCES

- Abera, B. (2014). Medicinal plants used in traditional medicine by Oromo people, Ghimbi District, Southwest Ethiopia. *Journal of ethnobiology and ethnomedicine*, 10, 40. <https://doi.org/10.1186/1746-4269-10-40>
- Abotsi, W. K., Ainooson, G. K., Gyasi, E. B., Abotsi, W. K. M. (2011). Acute and sub-acute toxicity studies of the ethanolic extract of the aerial parts of *Hillieria latifolia* (Lam.) H. Walt. (Phytolaccaceae) in rodents. *West African Journal of Pharmacy*. 22, 27e35.
- Abraham, M. J., Murtola, T., Schulz, R., Páll, S., Smith, J. C., Hess, B., and Lindahl, E. (2015). GROMACS: High performance molecular simulations through multi-level parallelism from laptops to supercomputers. *SoftwareX*, 1–2, 19–25. <https://doi.org/10.1016/j.softx.2015.06.001>
- Abramson, A., Caffarel-Salvador, E., Khang, M., Dellal, D., Silverstein, D., Gao, Y., Frederiksen, M. R., Vegge, A., Hubálek, F., Water, J. J., Friderichsen, A. V., Fels, J., Kirk, R. K., Cleveland, C., Collins, J., Tamang, S., Hayward, A., Landh, T., Buckley, S. T., Roxhed, N., ... Traverso, G. (2019). An ingestible self-orienting system for oral delivery of macromolecules. *Science* (New York, N.Y.), 363(6427), 611–615. <https://doi.org/10.1126/science.aau2277>
- Adedapo, A. A., Abatan, M. O., and Olorunsogo, O. O., 2004. Toxic effects of some plants in the genus Euphorbiaceae on haematological and biochemical parameters of rats. *Veterinarski arhiv*, 74 (1), 53e62.
- Agrawal, S. S., and Paridhavi, M. (2007). Herbal drug technology. Universities press, India. 2007:607-614.
- Ahmad, V., Khan, M. I., Jamal, Q. M. S., Alzahrani, F. A., and Albiheyri, R. (2023). Computational Molecular Docking and Simulation-Based Assessment of Anti-Inflammatory Properties of *Nyctanthes arbor-tristis* Linn Phytochemicals. *Pharmaceuticals* (Basel, Switzerland), 17(1), 18. <https://doi.org/10.3390/ph17010018>

- Aithal, G. P., Watkins, P. B., Andrade, R. J., Larrey, D., Molokhia, M., Takikawa, H., Hunt, C. M., Wilke, R. A., Avigan, M., Kaplowitz, N., Bjornsson, E., and Daly, A. K. (2011). Case definition and phenotype standardization in drug-induced liver injury. *Clinical pharmacology and therapeutics*, 89(6), 806–815. <https://doi.org/10.1038/clpt.2011.58>
- Aiyegoro, O. A., and Okoh, A. I. (2010). Preliminary phytochemical screening and in vitro antioxidant activities of the aqueous extract of *Helichrysum longifolium* DC. *BMC complementary and alternative medicine*, 10, 21. <https://doi.org/10.1186/1472-6882-10-21>
- Akanji, M. A., Yakubu, M. T., Kazeem, M. I. (2013). Hypolipidemic and toxicological potential of aqueous extract of *Rauwolfia vomitoria* Afzel root in Wistar rats. *The Journal of Medical Sciences*, 13, 253e260.
- Akiyama, H., Barger, S., Barnum, S., Bradt, B., Bauer, J., Cole, G. M., Cooper, N. R., Eikelenboom, P., Emmerling, M., Fiebich, B. L., Finch, C. E., Frautschy, S., Griffin, W. S., Hampel, H., Hull, M., Landreth, G., Lue, L., Mrak, R., Mackenzie, I. R., McGeer, P. L., ... Wyss-Coray, T. (2000). Inflammation and Alzheimer's disease. *Neurobiology of aging*, 21(3), 383–421. [https://doi.org/10.1016/s0197-4580\(00\)00124-x](https://doi.org/10.1016/s0197-4580(00)00124-x)
- Alam, N., Banu, N., Aziz, M. A., Barua, N., Ruman, U., Jahan, I., Chy, F. J., Denath, S., Paul, A., Chy, M. N. U., Sayeed, M. A., Emran, T. B., and Simal-Gandara, J. (2021). Chemical Profiling, Pharmacological Insights and In Silico Studies of Methanol Seed Extract of *Sterculia foetida*. *Plants* (Basel, Switzerland), 10(6), 1135. <https://doi.org/10.3390/plants10061135>
- Alawdi, S. H., El-Denshary, E. S., Safar, M. M., Eidi, H., David, M. O., and Abdel-Wahhab, M. A. (2017). Neuroprotective Effect of Nanodiamond in Alzheimer's Disease Rat Model: a Pivotal Role for Modulating NF-κB and STAT3 Signaling. *Molecular neurobiology*, 54(3), 1906–1918. <https://doi.org/10.1007/s12035-016-9762-0>

- Alempijevic, T., Zec, S., and Milosavljevic, T. (2017). Drug-induced liver injury: Do we know everything?. *World journal of hepatology*, 9(10), 491–502. <https://doi.org/10.4254/wjh.v9.i10.491>
- Alencar Filho, J. M. T., Teixeira, H. A. P., Sampaio, P. A., Pereira, E. C. V., Amariz, I. A. E., Rolim Neto, P. J., Rolim, L. A., and Araújo, E. C. D. C. (2020). Phytochemical analysis in *Alternanthera brasiliana* by LC-MS/MS and GC-MS. *Natural product research*, 34(3), 429–433. <https://doi.org/10.1080/14786419.2018.1533827>
- Alistair, B., Steve, I. (2009). Clinical review: Alzheimer's disease. *British medical journal*, 21(338), 467–71. <https://doi.org/doi:10.1136/bmj.b158>
- Alonso, H., Bliznyuk, A. A., and Gready, J. E. (2006). Combining docking and molecular dynamic simulations in drug design. *Medicinal research reviews*, 26(5), 531–568. <https://doi.org/10.1002/med.20067>
- Alzheimer, A., Stelzmann, R. A., Schnitzlein, H. N., and Murtagh, F. R. (1995). An English translation of Alzheimer's 1907 paper, "Über eine eigenartige Erkrankung der Hirnrinde". *Clinical anatomy* (New York, N.Y.), 8(6), 429–431. <https://doi.org/10.1002/ca.980080612>
- Alzheimer's Association (2024). 2024 Alzheimer's disease facts and figures. *Alzheimer's & dementia : the journal of the Alzheimer's Association*, 20(5), 3708–3821. <https://doi.org/10.1002/alz.13809>
- Amadei, A., Linssen, A. B., and Berendsen, H. J. (1993). Essential dynamics of proteins. *Proteins*, 17(4), 412–425. <https://doi.org/10.1002/prot.340170408>
- Amber, W., J., K., P. (1981). Assisted model building with energy refinement. A general program for modeling molecules and their interaction. *Journal of Computational Chemistry*, 2, 287-296. <https://doi:10.1002/jcc.540020311>
- Amenta, F., Parnetti, L., Gallai, V., and Wallin, A. (2001). Treatment of cognitive dysfunction associated with Alzheimer's disease with cholinergic precursors. Ineffective treatments or inappropriate approaches?. *Mechanisms of ageing and*

development, 122(16), 2025–2040. [https://doi.org/10.1016/s0047-6374\(01\)00310-4](https://doi.org/10.1016/s0047-6374(01)00310-4)

Ames, B. N., Durston, W. E., Yamasaki, E., and Lee, F. D. (1973). Carcinogens are mutagens: a simple test system combining liver homogenates for activation and bacteria for detection. *Proceedings of the National Academy of Sciences of the United States of America*, 70(8), 2281–2285. <https://doi.org/10.1073/pnas.70.8.2281>

Ames, B. N., Gurney, E. G., Miller, J. A., and Bartsch, H. (1972). Carcinogens as frameshift mutagens: metabolites and derivatives of 2-acetylaminofluorene and other aromatic amine carcinogens. *Proceedings of the National Academy of Sciences of the United States of America*, 69(11), 3128–3132. <https://doi.org/10.1073/pnas.69.11.3128>

Angami, T., Bhagawati, R., Touthang, L., Makdoh, B., Khatri, N., Singson, L., Bharati, K., Silambarasan, R., and Ayyanar, M. (2018). Traditional uses, phytochemistry and biological activities of *Parkia timoriana* (DC.) Merr., an underutilized multipurpose tree bean: a review. *Genetic Resources and Crop Evolution*, 65. <https://doi.org/10.1007/s10722-017-0595-0>

Annie, L., Gurusubramanian, G., and Roy, V. K. (2020). Changes in the localization of ovarian visfatin protein and its possible role during estrous cycle of mice. *Acta histochemica*, 122(8), 151630. <https://doi.org/10.1016/j.acthis.2020.151630>

Arboleda-Velasquez, J. F., Lopera, F., O'Hare, M., Delgado-Tirado, S., Marino, C., Chmielewska, N., Saez-Torres, K. L., Amarnani, D., Schultz, A. P., Sperling, R. A., Leyton-Cifuentes, D., Chen, K., Baena, A., Aguillon, D., Rios-Romenets, S., Giraldo, M., Guzmán-Vélez, E., Norton, D. J., Pardilla-Delgado, E., Artola, A., and Quiroz, Y. T. (2019). Resistance to autosomal dominant Alzheimer's disease in an APOE3 Christchurch homozygote: a case report. *Nature medicine*, 25(11), 1680–1683. <https://doi.org/10.1038/s41591-019-0611-3>

Arendt, T., Brückner, M. K., Morawski, M., Jäger, C., and Gertz, H. J. (2015). Early neurone loss in Alzheimer's disease: cortical or subcortical?. *Acta*

neuropathologica communications, 3, 10. <https://doi.org/10.1186/s40478-015-0187-1>

Arnot, J. A., and Gobas, F. A. (2006). A review of bioconcentration factor (BCF) and bioaccumulation factor (BAF) assessments for organic chemicals in aquatic organisms. *Environmental Reviews*, 14 (4), 257–297. <https://doi.org/10.1139/a06-005>

Ashafa, A. O., Orekoya, L. O., and Yakubu, M. T. (2012). Toxicity profile of ethanolic extract of *Azadirachta indica* stem bark in male Wistar rats. *Asian Pacific journal of tropical biomedicine*, 2(10), 811–817. [https://doi.org/10.1016/S2221-1691\(12\)60234-2](https://doi.org/10.1016/S2221-1691(12)60234-2)

Attia, H. N., and Ahmed, K. A. (2020). Protective role of functional food in cognitive deficit in young and senile rats. *Behavioural pharmacology*, 31(1), 81–96. <https://doi.org/10.1097/FBP.0000000000000522>

Bacci, A., Runfola, M., Sestito, S., and Rapposelli, S. (2021). Beyond Antioxidant Effects: Nature-Based Templates Unveil New Strategies for Neurodegenerative Diseases. *Antioxidants* (Basel, Switzerland), 10(3), 367. <https://doi.org/10.3390/antiox10030367>

Bagheri, M., Joghataei, M. T., Mohseni, S., and Roghani, M. (2011). Genistein ameliorates learning and memory deficits in amyloid β (1-40) rat model of Alzheimer's disease. *Neurobiology of learning and memory*, 95(3), 270–276. <https://doi.org/10.1016/j.nlm.2010.12.001>

Baker, D. J. (2016). The classification and properties of toxic hazards BT. In: Baker D.J., editor. *Toxic Trauma: A Basic Clinical Guide*. Springer International Publishing; Cham, Switzerland, 25–47.

Baker, N. A., Sept, D., Joseph, S., Holst, M. J., and McCammon, J. A. (2001). Electrostatics of nanosystems: application to microtubules and the ribosome. *Proceedings of the National Academy of Sciences of the United States of America*, 98(18), 10037–10041. <https://doi.org/10.1073/pnas.181342398>

- Bancroft, J.D. and Gamble, M. (2002). Theory and practice of histological techniques. 5th ed. Edinburgh: Churchill Livingstone Pub, 172, 593–620.
- Bariweni, M. W., Yibala, O. I., and Ozolua, R. I. (2018). Toxicological studies on the aqueous leaf extract of *Pavetta crassipes* (K. Schum) in rodents. *Journal of Pharmacy & Pharmacognosy Research*, 6 (1), 1–16.
- Barker, G. R., and Warburton, E. C. (2011). When is the hippocampus involved in recognition memory?. *The Journal of neuroscience: the official journal of the Society for Neuroscience*, 31(29), 10721–10731. <https://doi.org/10.1523/JNEUROSCI.6413-10.2011>
- Bekris, L. M., Yu, C. E., Bird, T. D., and Tsuang, D. W. (2010). Genetics of Alzheimer disease. *Journal of geriatric psychiatry and neurology*, 23(4), 213–227. <https://doi.org/10.1177/0891988710383571>
- Bellenguez, C., Küçükali, F., Jansen, I. E., Kleindam, L., Moreno-Grau, S., Amin, N., Naj, A. C., Campos-Martin, R., Grenier-Boley, B., Andrade, V., Holmans, P. A., Boland, A., Damotte, V., van der Lee, S. J., Costa, M. R., Kuulasmaa, T., Yang, Q., de Rojas, I., Bis, J. C., Yaqub, A., and Lambert, J. C. (2022). New insights into the genetic etiology of Alzheimer's disease and related dementias. *Nature genetics*, 54(4), 412–436. <https://doi.org/10.1038/s41588-022-01024-z>
- Benfenati, E., Benigni, R., Demarini, D. M., Helma, C., Kirkland, D., Martin, T. M., Mazzatorta, P., Ouédraogo-Arras, G., Richard, A. M., Schilter, B., Schoonen, W. G., Snyder, R. D., and Yang, C. (2009). Predictive models for carcinogenicity and mutagenicity: frameworks, state-of-the-art, and perspectives. *Journal of environmental science and health. Part C, Environmental carcinogenesis & ecotoxicology reviews*, 27(2), 57–90. <https://doi.org/10.1080/10590500902885593>
- Berendsen, H. J. C., Spoel, D. V. D., Drunen, R. V. (1995). GROMACS: a message-passing parallel molecular dynamics implementation. *Computer Physics Communications*, 91(1–3), 43–56. [https://doi.org/10.1016/0010-4655\(95\)00042-E](https://doi.org/10.1016/0010-4655(95)00042-E)

- Berendsen, H., Postma, J. P. M., van Gunsteren, W., DiNola, A. D., and Haak, J. R. (1984). Molecular-dynamics with coupling to an external bath. *The Journal of Chemical Physics*, 81, 3684. <https://doi.org/10.1063/1.448118>
- Bertram, L., and Tanzi, R. E. (2008). Thirty years of Alzheimer's disease genetics: the implications of systematic meta-analyses. *Nature reviews. Neuroscience*, 9(10), 768–778. <https://doi.org/10.1038/nrn2494>
- Bharath, S., Hsu, M., Kaur, D., Rajagopalan, S., and Andersen, J. K. (2002). Glutathione, iron and Parkinson's disease. *Biochemical pharmacology*, 64(5-6), 1037–1048. [https://doi.org/10.1016/s0006-2952\(02\)01174-7](https://doi.org/10.1016/s0006-2952(02)01174-7)
- Bingman, V. P. (1992). The importance of comparative studies and ecological validity for understanding hippocampal structure and cognitive function. *Hippocampus*, 2(3), 213–219. <https://doi.org/10.1002/hipo.450020302>
- Bingman, V. P., and Jones, T. J. (1994). Sun compass-based spatial learning impaired in homing pigeons with hippocampal lesions. *The Journal of neuroscience: the official journal of the Society for Neuroscience*, 14(11 Pt 1), 6687–6694. <https://doi.org/10.1523/JNEUROSCI.14-11-06687.1994>
- Bioten (2024). Biogen to realign resources for Alzheimer's disease franchise. Available at: <https://investors.biogen.com/newsreleases/news-release-details/biogen-realign-resources-alzheimers-disease-franchise>. Accessed January 31, 2024.
- Bodey, G. P., Bolivar, R., and Fainstein, V. (1982). Infectious complications in leukemic patients. *Seminars in hematology*, 19(3), 193–226.
- Bolós, M., Perea, J. R., and Avila, J. (2017). Alzheimer's disease as an inflammatory disease. *Biomolecular concepts*, 8(1), 37–43. <https://doi.org/10.1515/bmc-2016-0029>
- Bondi, M. W., Edmonds, E. C., and Salmon, D. P. (2017). Alzheimer's Disease: Past, Present, and Future. *Journal of the International Neuropsychological Society: JINS*, 23(9-10), 818–831. <https://doi.org/10.1017/S135561771700100X>

- Bonsnes, R.W., and Taussky, H.H. (1945). On the colorimetric determination of creatinine by the Jaffe reaction. *Journal of Biological Chemistry*. 158, 581–591.
- Boverhof, D. R., and Zacharewski, T. R. (2006). Toxicogenomics in risk assessment: applications and needs. *Toxicological sciences: an official journal of the Society of Toxicology*, 89(2), 352–360. <https://doi.org/10.1093/toxsci/kfj018>
- Braak, H., Braak, E., and Bohl, J. (1993). Staging of Alzheimer-related cortical destruction. *European neurology*, 33(6), 403–408. <https://doi.org/10.1159/000116984>
- Bradbury, C., and Murray, J. (2013). Investigating an incidental finding of thrombocytopenia. *BMJ* (Clinical research ed.), 346, f11. <https://doi.org/10.1136/bmj.f11>
- Bradford, M. M. (1976). A rapid and sensitive method for the quantitation of microgram quantities of protein utilizing the principle of protein-dye binding. *Analytical biochemistry*, 72, 248–254. <https://doi.org/10.1006/abio.1976.9999>
- Brasier, A. R. (2010). The nuclear factor-kappaB-interleukin-6 signalling pathway mediating vascular inflammation. *Cardiovascular research*, 86(2), 211–218. <https://doi.org/10.1093/cvr/cvq076>
- Brautbar, N., and Williams, J., 2nd (2002). Industrial solvents and liver toxicity: risk assessment, risk factors and mechanisms. *International journal of hygiene and environmental health*, 205(6), 479–491. <https://doi.org/10.1078/1438-4639-00175>
- Burden, N., Creton, S., Weltje, L., Maynard, S. K., and Wheeler, J. R. (2014). Reducing the number of fish in bioconcentration studies with general chemicals by reducing the number of test concentrations. *Regulatory toxicology and pharmacology: RTP*, 70(2), 442–445. <https://doi.org/10.1016/j.yrtph.2014.08.008>
- Butiuk, A. P., Martos, M. A., Adachi, O., and Hours, R. A. (2016) Study of the chlorogenic acid content of in yerba mate (*Ilex paraguariensis* St. Hil.): Effect of plant fraction, processing step and harvesting season. *Journal of Applied*

- Research on Medicinal and Aromatic Plants*, 2016, 3(1), 27–33.
<https://doi.org/10.1016/j.jarmap.2015.12.003>
- Forman, H. J., Davies, K. J., and Ursini, F. (2014). How do nutritional antioxidants really work: nucleophilic tone and para-hormesis versus free radical scavenging in vivo. *Free radical biology & medicine*, 66, 24–35.
<https://doi.org/10.1016/j.freeradbiomed.2013.05.045>
- Butterfield, D. A., Griffin, S., Munch, G., and Pasinetti, G. M. (2002). Amyloid beta-peptide and amyloid pathology are central to the oxidative stress and inflammatory cascades under which Alzheimer's disease brain exists. *Journal of Alzheimer's disease: JAD*, 4(3), 193–201. <https://doi.org/10.3233/jad-2002-4309>
- Butterweck, V., Winterhoff, H., and Herkenham, M. (2003). Hyperforin-containing extracts of St John's wort fail to alter gene transcription in brain areas involved in HPA axis control in a long-term treatment regimen in rats. *Neuropsychopharmacology: official publication of the American College of Neuropsychopharmacology*, 28(12), 2160–2168.
<https://doi.org/10.1038/sj.npp.1300253>
- Calil Brondani, J., Reginato, F. Z., da Silva Brum, E., de Souza Vencato, M., Lima Lhamas, C., Viana, C., da Rocha, M. I., de Freitas Bauermann, L., and Manfron, M. P. (2017). Evaluation of acute and subacute toxicity of hydroethanolic extract of *Dolichandra unguis-cati* L. leaves in rats. *Journal of ethnopharmacology*, 202, 147–153. <https://doi.org/10.1016/j.jep.2017.03.011>
- Cao, Z., Wang, F., Xiu, C., Zhang, J., and Li, Y. (2017). Hypericum perforatum extract attenuates behavioral, biochemical, and neurochemical abnormalities in Aluminum chloride-induced Alzheimer's disease rats. *Biomedicine & pharmacotherapy = Biomedecine & pharmacotherapie*, 91, 931–937.
<https://doi.org/10.1016/j.biopha.2017.05.022>
- Cassano, A., Manganaro, A., Martin, T., Young, D., Piclin, N., Pintore, M., Bigoni, D., and Benfenati, E. (2010). CAESAR models for developmental toxicity. *Chemistry Central journal*, 4 Suppl 1(Suppl 1), S4.
<https://doi.org/10.1186/1752-153X-4-S1-S4>

- Cendoya, X., Quevedo, C., Ipiñazar, M., and Planes, F. J. (2020). Computational approach for collection and prediction of molecular initiating events in developmental toxicity. *Reproductive toxicology* (Elmsford, N.Y.), 94, 55–64. <https://doi.org/10.1016/j.reprotox.2020.03.010>
- Cervellati, C., Valacchi, G., and Zuliani, G. (2021). BACE1: from biomarker to Alzheimer's disease therapeutical target. *Aging*, 13(9), 12299–12300. <https://doi.org/10.18632/aging.203064>
- Chanda, S., Parekh, J., Vaghasiya, Y., Dave, R., Baravalia, Y., and Nair, R. (2015). Medicinal plants - from traditional use to toxicity assessment: a review. *International journal of pharmaceutical sciences and research*, 6 (7), 2652–2670. [https://doi.org/10.13040/IJPSR.0975-8232.6\(7\).2652-70](https://doi.org/10.13040/IJPSR.0975-8232.6(7).2652-70)
- Chebaibi, M., Bousta, D., Chbani, L., Ezzoubi, Y., Touiti, N., and Achour, S. (2019). Acute toxicity of plants mixture used in traditional treatment of edema and colic renal in Morocco. *Scientific African*, 6, e00152. <https://doi.org/10.1016/j.sciaf.2019.e00152>
- Chekole, G., Asfaw, Z., and Kelbessa, E. (2015). Ethnobotanical study of medicinal plants in the environs of Tara-gedam and Amba remnant forests of Libo Kemkem District, northwest Ethiopia. *Journal of ethnobiology and ethnomedicine*, 11, 4. <https://doi.org/10.1186/1746-4269-11-4>
- Chen, F., Eckman, E. A., and Eckman, C. B. (2006). Reductions in levels of the Alzheimer's amyloid beta peptide after oral administration of ginsenosides. *FASEB journal: official publication of the Federation of American Societies for Experimental Biology*, 20(8), 1269–1271. <https://doi.org/10.1096/fj.05-5530fje>
- Chen, J., Wang, X., Zhu, T., Zhang, Q., and Zhang, J. Z. (2015). A Comparative Insight into Amprenavir Resistance of Mutations V32I, G48V, I50V, I54V, and I84V in HIV-1 Protease Based on Thermodynamic Integration and MM-PBSA Methods. *Journal of chemical information and modeling*, 55(9), 1903–1913. <https://doi.org/10.1021/acs.jcim.5b00173>

- Chen, R., Lai, U. H., Zhu, L., Singh, A., Ahmed, M., and Forsyth, N. R. (2018). Reactive Oxygen Species Formation in the Brain at Different Oxygen Levels: The Role of Hypoxia Inducible Factors. *Frontiers in cell and developmental biology*, 6, 132. <https://doi.org/10.3389/fcell.2018.00132>
- Cheng, E. H., Wei, M. C., Weiler, S., Flavell, R. A., Mak, T. W., Lindsten, T., and Korsmeyer, S. J. (2001). BCL-2, BCL-X(L) sequester BH3 domain-only molecules preventing BAX- and BAK-mediated mitochondrial apoptosis. *Molecular cell*, 8(3), 705–711. [https://doi.org/10.1016/s1097-2765\(01\)00320-3](https://doi.org/10.1016/s1097-2765(01)00320-3)
- Chiarini, A., Armato, U., Hu, P., and Dal Prà, I. (2020). Danger-Sensing/Patten Recognition Receptors and Neuroinflammation in Alzheimer's Disease. *International journal of molecular sciences*, 21(23), 9036. <https://doi.org/10.3390/ijms21239036>
- Chiroma, S. M., Mohd Moklas, M. A., Mat Taib, C. N., Baharuldin, M. T. H., and Amon, Z. (2018). d-galactose and aluminum chloride induced rat model with cognitive impairments. *Biomedicine & pharmacotherapy = Biomedecine & pharmacotherapie*, 103, 1602–1608. <https://doi.org/10.1016/j.biopha.2018.04.152>
- Cho, J. H., and Johnson, G. V. (2004). Primed phosphorylation of tau at Thr231 by glycogen synthase kinase 3beta (GSK3beta) plays a critical role in regulating tau's ability to bind and stabilize microtubules. *Journal of neurochemistry*, 88(2), 349–358. <https://doi.org/10.1111/j.1471-4159.2004.02155.x>
- Choi, J. S., Islam, M. N., Ali, M. Y., Kim, Y. M., Park, H. J., Sohn, H. S., and Jung, H. A. (2014). The effects of C-glycosylation of luteolin on its antioxidant, anti-Alzheimer's disease, anti-diabetic, and anti-inflammatory activities. *Archives of pharmacal research*, 37(10), 1354–1363. <https://doi.org/10.1007/s12272-014-0351-3>
- Choi, R. J., Roy, A., Jung, H. J., Ali, M. Y., Min, B. S., Park, C. H., Yokozawa, T., Fan, T. P., Choi, J. S., and Jung, H. A. (2016). BACE1 molecular docking and anti-

- Alzheimer's disease activities of ginsenosides. *Journal of ethnopharmacology*, 190, 219–230. <https://doi.org/10.1016/j.jep.2016.06.013>
- Chy, M. N. U., Chakrabarty, N., Roy, A., Paul, A., Emu, K. A., Dutta, T., Dutta, E., Ferdous, I., Das, R., Hasan, M. J., and Tasnim, S. M. (2019). Antibacterial, anthelmintic, and analgesic activities of *Piper sylvaticum* (Roxb.) leaves and in silico molecular docking and PASS prediction studies of its isolated compounds. *Journal of complementary & integrative medicine*, 16(4). <https://doi.org/10.1515/jcim-2018-0176>
- Clemmedson, C., Barile, F. A., Chesne, C., Cottin, M., Curren, R., Eckwall, B., Ferro, M., Gomez-Lechon, M. J., Imai, K., Janus, J., Kemp, R. B., Kerszman, G., Kjellstrand, P., Lavrijsen, K., Logemann, P., McFarlane-Abdulla, E., Roguet, R., Segner, H., Thuvander, A., Walum, E., and Ekwall, B. (2000). MEIC evaluation of acute systemic toxicity. Part VII. Prediction of human toxicity by results from testing of the first 30 reference chemicals with 27 further in vitro assays. *ATLA*, 28, 159–200.
- Colerangle, J. B. (2017). Preclinical Development of Nononcogenic Drugs (Small and Large Molecules). *A Comprehensive Guide to Toxicology in Nonclinical Drug Development* (Second Edition), Academic Press, 659-683. <https://doi.org/10.1016/B978-0-12-803620-4.00025-6>
- Comery, T. A., Martone, R. L., Aschmies, S., Atchison, K. P., Diamantidis, G., Gong, X., Zhou, H., Kreft, A. F., Pangalos, M. N., Sonnenberg-Reines, J., Jacobsen, J. S., and Marquis, K. L. (2005). Acute gamma-secretase inhibition improves contextual fear conditioning in the Tg2576 mouse model of Alzheimer's disease. *The Journal of neuroscience: the official journal of the Society for Neuroscience*, 25(39), 8898–8902. <https://doi.org/10.1523/JNEUROSCI.2693-05.2005>
- Corcoran, M. P., McKay, D. L., and Blumberg, J. B. (2012). Flavonoid basics: chemistry, sources, mechanisms of action, and safety. *Journal of nutrition in gerontology and geriatrics*, 31(3), 176–189. <https://doi.org/10.1080/21551197.2012.698219>

- Currais, A., Chiruta, C., Goujon-Svrzic, M., Costa, G., Santos, T., Batista, M. T., Paiva, J., do Céu Madureira, M., and Maher, P. (2014). Screening and identification of neuroprotective compounds relevant to Alzheimer's disease from medicinal plants of S. Tomé e Príncipe. *Journal of ethnopharmacology*, 155(1), 830–840. <https://doi.org/10.1016/j.jep.2014.06.046>
- Custer, L. L., and Sweder, K. S. (2008). The role of genetic toxicology in drug discovery and optimization. *Current drug metabolism*, 9(9), 978–985. <https://doi.org/10.2174/138920008786485191>
- Daina, A., and Zoete, V. (2016). A BOILED-Egg To Predict Gastrointestinal Absorption and Brain Penetration of Small Molecules. *ChemMedChem*, 11(11), 1117–1121. <https://doi.org/10.1002/cmdc.201600182>
- Daina, A., Michielin, O., and Zoete, V. (2014). iLOGP: a simple, robust, and efficient description of n-octanol/water partition coefficient for drug design using the GB/SA approach. *Journal of chemical information and modeling*, 54(12), 3284–3301. <https://doi.org/10.1021/ci500467k>
- Daina, A., Michielin, O., and Zoete, V. (2017). SwissADME: a free web tool to evaluate pharmacokinetics, drug-likeness and medicinal chemistry friendliness of small molecules. *Scientific reports*, 7, 42717. <https://doi.org/10.1038/srep42717>
- Dallakyan, S., Olson, A. J. (2015). Small-molecule library screening by docking with PyRx. *Methods in Molecular Biology*, 1263, 243–250. https://doi.org/10.1007/978-1-4939-2269-7_19
- Damayanti, S., Permana, J., and Tjahjono, D. H. (2015). The use of computational chemistry to predict toxicity of antioxidants food additives and its metabolites as a reference for food safety regulation. *Der Pharma Chemica*, 7(9), 174-181.
- Damiati, S. (2019). A Pilot Study to Assess Kidney Functions and Toxic Dimethyl-arginines as Risk Biomarkers in Women with Low Vitamin D Levels. *Journal of medical biochemistry*, 38(2), 145–152. <https://doi.org/10.2478/jomb-2018-0025>

- Daulatzai, M. A. (2016). Fundamental role of pan-inflammation and oxidative-nitrosative pathways in neuropathogenesis of Alzheimer's disease. *American journal of neurodegenerative disease*, 5(1), 1–28.
- de Jonge, W. J., van der Zanden, E. P., The, F. O., Bijlsma, M. F., van Westerloo, D. J., Bennink, R. J., Berthoud, H. R., Uematsu, S., Akira, S., van den Wijngaard, R. M., and Boeckxstaens, G. E. (2005). Stimulation of the vagus nerve attenuates macrophage activation by activating the Jak2-STAT3 signaling pathway. *Nature immunology*, 6(8), 844–851. <https://doi.org/10.1038/ni1229>
- Del Rio, D., Rodriguez-Mateos, A., Spencer, J. P., Tognolini, M., Borges, G., and Crozier, A. (2013). Dietary (poly)phenolics in human health: structures, bioavailability, and evidence of protective effects against chronic diseases. *Antioxidants & redox signaling*, 18(14), 1818–1892. <https://doi.org/10.1089/ars.2012.4581>
- DeTure, M. A., and Dickson, D. W. (2019). The neuropathological diagnosis of Alzheimer's disease. *Molecular neurodegeneration*, 14(1), 32. <https://doi.org/10.1186/s13024-019-0333-5>
- Devi, L., and Ohno, M. (2012). Mitochondrial dysfunction and accumulation of the β -secretase-cleaved C-terminal fragment of APP in Alzheimer's disease transgenic mice. *Neurobiology of disease*, 45(1), 417–424. <https://doi.org/10.1016/j.nbd.2011.09.001>
- D'Hooge, R., and De Deyn, P. P. (2001). Applications of the Morris water maze in the study of learning and memory. *Brain research. Brain research reviews*, 36(1), 60–90. [https://doi.org/10.1016/s0165-0173\(01\)00067-4](https://doi.org/10.1016/s0165-0173(01)00067-4)
- Di Carlo, P., Punzi, G., and Ursini, G. (2019). Brain-derived neurotrophic factor and schizophrenia. *Psychiatric genetics*, 29(5), 200–210. <https://doi.org/10.1097/YPG.0000000000000237>
- Dineley, K. T., Xia, X., Bui, D., Sweatt, J. D., and Zheng, H. (2002). Accelerated plaque accumulation, associative learning deficits, and up-regulation of alpha 7 nicotinic receptor protein in transgenic mice co-expressing mutant human

- presenilin 1 and amyloid precursor proteins. *The Journal of biological chemistry*, 277(25), 22768–22780. <https://doi.org/10.1074/jbc.M200164200>
- DiSabato, D. J., Quan, N., and Godbout, J. P. (2016). Neuroinflammation: the devil is in the details. *Journal of neurochemistry*, 139 Suppl 2(Suppl 2), 136–153. <https://doi.org/10.1111/jnc.13607>
- Duan, A. R., Jonasson, E. M., Alberico, E. O., Li, C., Scripture, J. P., Miller, R. A., Alber, M. S., and Goodson, H. V. (2017). Interactions between Tau and Different Conformations of Tubulin: Implications for Tau Function and Mechanism. *Journal of molecular biology*, 429(9), 1424–1438. <https://doi.org/10.1016/j.jmb.2017.03.018>
- Duke, J. A. (2000). Handbook of phytochemical constituent GRAS herbs and other economic plants. Herbal reference library, CRC Press, Boca Raton, FL, USA.
- Egbuna, C., Patrick-Iwuanyanwu, K. C., Onyeike, E. N., Khan, J., and Alshehri, B. (2022). FMS-like tyrosine kinase-3 (FLT3) inhibitors with better binding affinity and ADMET properties than sorafenib and gilteritinib against acute myeloid leukemia: in silico studies. *Journal of biomolecular structure & dynamics*, 40(22), 12248–12259. <https://doi.org/10.1080/07391102.2021.1969286>
- El Hilaly, J., Israili, Z. H., and Lyoussi, B. (2004). Acute and chronic toxicological studies of *Ajuga iva* in experimental animals. *Journal of ethnopharmacology*, 91(1), 43–50. <https://doi.org/10.1016/j.jep.2003.11.009>
- El-Guendy, N., and Rangnekar, V. M. (2003). Apoptosis by Par-4 in cancer and neurodegenerative diseases. *Experimental cell research*, 283(1), 51–66. [https://doi.org/10.1016/s0014-4827\(02\)00016-2](https://doi.org/10.1016/s0014-4827(02)00016-2)
- Elhabak, M., Salama, A. A. A., and Salama, A. H. (2023). Nose-to-brain delivery of galantamine loaded nanospray dried polyacrylic acid/taurodeoxycholate mixed matrix as a protective therapy in lipopolysaccharide-induced Alzheimer's in mice model. *International journal of pharmaceutics*, 632, 122588. <https://doi.org/10.1016/j.ijpharm.2023.122588>

- Ennaceur, A., and Delacour, J. (1988). A new one-trial test for neurobiological studies of memory in rats. 1: Behavioral data. *Behavioural brain research*, 31(1), 47–59. [https://doi.org/10.1016/0166-4328\(88\)90157-x](https://doi.org/10.1016/0166-4328(88)90157-x)
- Erhirhie, E. O., Ihekwereme, C. P., and Ilodigwe, E. E. (2018). Advances in acute toxicity testing: strengths, weaknesses and regulatory acceptance. *Interdisciplinary toxicology*, 11(1), 5–12. <https://doi.org/10.2478/intox-2018-0001>
- Ertl, P., and Schuffenhauer, A. (2009). Estimation of synthetic accessibility score of drug-like molecules based on molecular complexity and fragment contributions. *Journal of cheminformatics*, 1(1), 8. <https://doi.org/10.1186/1758-2946-1-8>
- Ertl, P., Roggo, S., and Schuffenhauer, A. (2008). Natural product-likeness score and its application for prioritization of compound libraries. *Journal of chemical information and modeling*, 48(1), 68–74. <https://doi.org/10.1021/ci700286x>
- Exley, C. (2013). Human exposure to aluminum. *Environmental science. Processes & impacts*, 15(10), 1807–1816. <https://doi.org/10.1039/c3em00374d>
- Farihi, A., Bouhrim, M., Chigr, F., Elbouzidi, A., Bencheikh, N., Zrouri, H., Nasr, F. A., Parvez, M. K., Alahdab, A., and Ahami, A. O. T. (2023). Exploring Medicinal Herbs' Therapeutic Potential and Molecular Docking Analysis for Compounds as Potential Inhibitors of Human Acetylcholinesterase in Alzheimer's Disease Treatment. *Medicina* (Kaunas, Lithuania), 59(10), 1812. <https://doi.org/10.3390/medicina59101812>
- Fathalla, N., Bishr, M., Nasser Singab, A., and Salama, O. (2019). GC-MS and LC-MS Identification of the Phenolic Compounds Present in the ethyl Acetate Fraction Obtained from Senna tora, L. Roxb. seeds. *Natural product research*, 33(19), 2878–2881. <https://doi.org/10.1080/14786419.2018.1508138>
- Fathalla, N., Bishr, M., Singab, A. N., Salama, O. (2015). Phytochemical and Biological Evaluation of Cassia tora, L. Seeds. *IOSR Journal of Pharmacy and Biological Sciences*, 10(1), 1–8.

- Fawcett, J. K., and Scott, J. E. (1960). A rapid and precise method for the determination of urea. *Journal of clinical pathology*, 13(2), 156–159. <https://doi.org/10.1136/jcp.13.2.156>
- Feldman, B.F., Zinkl, J.G., and Jain, V.C. (2000). Schalm's Veterinary Hematology, fifth ed. Lippincott Williams and Wilkins, Toronto, Canada, 1145–1146.
- Feriani, A., Contreras, M.M., Talhaoui, N., Gómez-Caravaca, A.M., Taamalli, A., Segura-Carretero, A., and Ghazouani, L. (2017). Protective effect of *Globularia alypum* leaves against deltamethrin-induced nephrotoxicity in rats and determination of its bioactive compounds using high-performance liquid chromatography coupled with electrospray ionization tandem quadrupole–time of-flight mass spectrometry. *Journal of Functional Foods*, 32, 139–148. <https://doi.org/10.1016/j.jff.2017.02.015>
- Fernie A. R. (2007). The future of metabolic phytochemistry: larger numbers of metabolites, higher resolution, greater understanding. *Phytochemistry*, 68(22–24), 2861–2880. <https://doi.org/10.1016/j.phytochem.2007.07.010>
- Ferreira, L. L. G., and Andricopulo, A. D. (2019). ADMET modeling approaches in drug discovery. *Drug discovery today*, 24(5), 1157–1165. <https://doi.org/10.1016/j.drudis.2019.03.015>
- Fiandalo, M. V., and Kyprianou, N. (2012). Caspase control: protagonists of cancer cell apoptosis. *Experimental oncology*, 34(3), 165–175.
- Fiehn, O., Kopka, J., Dörmann, P., Altmann, T., Trethewey, R. N., and Willmitzer, L. (2000). Metabolite profiling for plant functional genomics. *Nature biotechnology*, 18(11), 1157–1161. <https://doi.org/10.1038/81137>
- Fraga, C. G., and Oteiza, P. I. (2011). Dietary flavonoids: Role of (-)-epicatechin and related procyanidins in cell signaling. *Free radical biology & medicine*, 51(4), 813–823. <https://doi.org/10.1016/j.freeradbiomed.2011.06.002>
- Fraga, C. G., Croft, K. D., Kennedy, D. O., and Tomás-Barberán, F. A. (2019). The effects of polyphenols and other bioactives on human health. *Food & function*, 10(2), 514–528. <https://doi.org/10.1039/c8fo01997e>

- Fraga, C. G., Oteiza, P. I., and Galleano, M. (2018). Plant bioactives and redox signaling: (-)-Epicatechin as a paradigm. *Molecular aspects of medicine*, 61, 31–40. <https://doi.org/10.1016/j.mam.2018.01.007>
- Francis, P. T., Palmer, A. M., Snape, M., and Wilcock, G. K. (1999). The cholinergic hypothesis of Alzheimer's disease: a review of progress. *Journal of neurology, neurosurgery, and psychiatry*, 66(2), 137–147. <https://doi.org/10.1136/jnnp.66.2.137>
- Friedlander, R. M. (2003). Apoptosis and caspases in neurodegenerative diseases. *The New England journal of medicine*, 348(14), 1365–1375. <https://doi.org/10.1056/NEJMra022366>
- García Rodríguez, L. A., Ruigómez, A., and Jick, H. (1997). A review of epidemiologic research on drug-induced acute liver injury using the general practice research data base in the United Kingdom. *Pharmacotherapy*, 17(4), 721–728.
- García-Ayllón, M. S., Small, D. H., Avila, J., and Sáez-Valero, J. (2011). Revisiting the Role of Acetylcholinesterase in Alzheimer's Disease: Cross-Talk with P-tau and β -Amyloid. *Frontiers in molecular neuroscience*, 4, 22. <https://doi.org/10.3389/fnmol.2011.00022>
- Gheena, S., and Ezhilarasan, D. (2019). Syringic acid triggers reactive oxygen species-mediated cytotoxicity in HepG2 cells. *Human & experimental toxicology*, 38(6), 694–702. <https://doi.org/10.1177/0960327119839173>
- Ghosh, R., Chakraborty, A., Biswas, A., and Chowdhuri, S. (2021). Evaluation of green tea polyphenols as novel corona virus (SARS CoV-2) main protease (Mpro) inhibitors - an in silico docking and molecular dynamics simulation study. *Journal of biomolecular structure & dynamics*, 39(12), 4362–4374. <https://doi.org/10.1080/07391102.2020.1779818>
- Giacobini, E. (1998). Invited review: Cholinesterase inhibitors for Alzheimer's disease therapy: from tacrine to future applications. *Neurochemistry international*, 32(5-6), 413–419. [https://doi.org/10.1016/s0197-0186\(97\)00124-1](https://doi.org/10.1016/s0197-0186(97)00124-1)

- Gibson, G. L., Allsop, D., and Austen, B. M. (2004). Induction of cellular oxidative stress by the beta-amyloid peptide involved in Alzheimer's disease. *Protein and peptide letters*, 11(3), 257–270. <https://doi.org/10.2174/0929866043407101>
- Glass, C. K., Saijo, K., Winner, B., Marchetto, M. C., and Gage, F. H. (2010). Mechanisms underlying inflammation in neurodegeneration. *Cell*, 140(6), 918–934. <https://doi.org/10.1016/j.cell.2010.02.016>
- Goel, R. K., Singh, D., Lagunin, A., and Poroikov, V. (2011). PASS-assisted exploration of new therapeutic potential of natural products. *Medicinal Chemistry Research*, 20(2011), 1509.
- Gold, P. E. (2003). Acetylcholine modulation of neural systems involved in learning and memory. *Neurobiology of learning and memory*, 80(3), 194–210. <https://doi.org/10.1016/j.nlm.2003.07.003>
- Golde, T. E., Eckman, C. B., and Younkin, S. G. (2000). Biochemical detection of Abeta isoforms: implications for pathogenesis, diagnosis, and treatment of Alzheimer's disease. *Biochimica et biophysica acta*, 1502(1), 172–187. [https://doi.org/10.1016/s0925-4439\(00\)00043-0](https://doi.org/10.1016/s0925-4439(00)00043-0)
- Goldman, J. S., Hahn, S. E., Catania, J. W., LaRusse-Eckert, S., Butson, M. B., Rumbaugh, M., Strecker, M. N., Roberts, J. S., Burke, W., Mayeux, R., Bird, T., and American College of Medical Genetics and the National Society of Genetic Counselors (2011). Genetic counseling and testing for Alzheimer disease: joint practice guidelines of the American College of Medical Genetics and the National Society of Genetic Counselors. *Genetics in medicine: official journal of the American College of Medical Genetics*, 13(6), 597–605. <https://doi.org/10.1097/GIM.0b013e31821d69b8>
- Gounden, V., Bhatt, H., and Jialal, I. (2023). Renal Function Tests. In StatPearls. StatPearls Publishing.
- Green, R. C., Cupples, L. A., Go, R., Benke, K. S., Edeki, T., Griffith, P. A., Williams, M., Hipps, Y., Graff-Radford, N., Bachman, D., Farrer, L. A., and MIRAGE Study Group (2002). Risk of dementia among white and African American

- relatives of patients with Alzheimer disease. *JAMA*, 287(3), 329–336.
<https://doi.org/10.1001/jama.287.3.329>
- Gribaldo, L., Gennari, A., Blackburn, K., Clemenson, C., Deguerce, A., Meneguz, A., Pfaller, W., and Ruhdel, I. (2005). Acute toxicity. *Alternatives to laboratory animals: ATLA*, 33 (1), 27–34. <https://doi.org/10.1177/026119290503301s07>
- Griffiths, A., Wessler, S., Lewontin, R., and Carroll S. (2000). Relation between mutagens and carcinogens. In *An introduction to genetic analysis*. 7th ed. WH Freeman.
- Grossberg, G. T., and Desai, A. K. (2003). Management of Alzheimer's disease. The journals of gerontology. Series A, *Biological sciences and medical sciences*, 58(4), 331–353. <https://doi.org/10.1093/gerona/58.4.m331>
- Guan, L., Yang, H., Cai, Y., Sun, L., Di, P., Li, W., Liu, G., and Tang, Y. (2018). ADMET-score - a comprehensive scoring function for evaluation of chemical drug-likeness. *MedChemComm*, 10(1), 148–157.
<https://doi.org/10.1039/c8md00472b>
- Guerreiro, R., Wojtas, A., Bras, J., Carrasquillo, M., Rogaeva, E., Majounie, E., Cruchaga, C., Sassi, C., Kauwe, J. S., Younkin, S., Hazrati, L., Collinge, J., Pocock, J., Lashley, T., Williams, J., Lambert, J. C., Amouyel, P., Goate, A., Rademakers, R., Morgan, K., ... Alzheimer Genetic Analysis Group (2013). TREM2 variants in Alzheimer's disease. *The New England journal of medicine*, 368(2), 117–127. <https://doi.org/10.1056/NEJMoa1211851>
- Habig, W. H., Pabst, M. J., and Jakoby, W. B. (1974). Glutathione S-transferases. The first enzymatic step in mercapturic acid formation. *The Journal of biological chemistry*, 249(22), 7130–7139.
- Hajieva P. (2017). The Effect of Polyphenols on Protein Degradation Pathways: Implications for Neuroprotection. *Molecules* (Basel, Switzerland), 22(1), 159.
<https://doi.org/10.3390/molecules22010159>
- Hampel, H., Hardy, J., Blennow, K., Chen, C., Perry, G., Kim, S. H., Villemagne, V. L., Aisen, P., Vendruscolo, M., Iwatsubo, T., Masters, C. L., Cho, M., Lannfelt,

- L., Cummings, J. L., and Vergallo, A. (2021). The Amyloid- β Pathway in Alzheimer's Disease. *Molecular psychiatry*, 26(10), 5481–5503. <https://doi.org/10.1038/s41380-021-01249-0>
- Harada, H., Tamaoka, A., Ishii, K., Shoji, S., Kametaka, S., Kametani, F., Saito, Y., and Murayama, S. (2006). Beta-site APP cleaving enzyme 1 (BACE1) is increased in remaining neurons in Alzheimer's disease brains. *Neuroscience research*, 54(1), 24–29. <https://doi.org/10.1016/j.neures.2005.10.001>
- Hardy, J. (2009). The amyloid hypothesis for Alzheimer's disease: a critical reappraisal. *Journal of neurochemistry*, 110(4), 1129–1134. <https://doi.org/10.1111/j.1471-4159.2009.06181.x>
- Hardy, J., and Selkoe, D. J. (2002). The amyloid hypothesis of Alzheimer's disease: progress and problems on the road to therapeutics. *Science* (New York, N.Y.), 297(5580), 353–356. <https://doi.org/10.1126/science.1072994>
- Hasler, C. M. (2002). Functional foods: benefits, concerns and challenges-a position paper from the american council on science and health. *The Journal of nutrition*, 132(12), 3772–3781. <https://doi.org/10.1093/jn/132.12.3772>
- Havsteen, B. (1983). Flavonoids, a class of natural products of high pharmacological potency. *Biochemical pharmacology*, 32(7), 1141–1148. [https://doi.org/10.1016/0006-2952\(83\)90262-9](https://doi.org/10.1016/0006-2952(83)90262-9)
- Adnan, M., Patel, M., Deshpande, S., Alreshidi, M., Siddiqui, A. J., Reddy, M. N., Emira, N., and De Feo, V. (2020). Effect of Adiantum philippense Extract on Biofilm Formation, Adhesion with Its Antibacterial Activities Against Foodborne Pathogens, and Characterization of Bioactive Metabolites: An in vitro-in silico Approach. *Frontiers in microbiology*, 11, 823. <https://doi.org/10.3389/fmicb.2020.00823>
- Hebert, L. E., Weuve, J., Scherr, P. A., and Evans, D. A. (2013). Alzheimer disease in the United States (2010-2050) estimated using the 2010 census. *Neurology*, 80(19), 1778–1783. <https://doi.org/10.1212/WNL.0b013e31828726f5>

- Heneka, M. T., Kummer, M. P., and Latz, E. (2014). Innate immune activation in neurodegenerative disease. *Nature reviews. Immunology*, 14(7), 463–477. <https://doi.org/10.1038/nri3705>
- Hess, B., Bekker, H., Berendsen, H., and Fraaije, J. (1998) LINCS: a linear constraint solver for molecular simulations. *Journal of Computational Chemistry*, 18,1463–1472. [https://doi.org/10.1002/\(SICI\)1096-987X\(199709\)18:12<1463::AIDJCC4>3.0.CO;2-H](https://doi.org/10.1002/(SICI)1096-987X(199709)18:12<1463::AIDJCC4>3.0.CO;2-H)
- Hidaka, N., Suemaru, K., Takechi, K., Li, B., and Araki, H. (2011). Inhibitory effects of valproate on impairment of Y-maze alternation behavior induced by repeated electroconvulsive seizures and c-Fos protein levels in rat brains. *Acta medica Okayama*, 65(4), 269–277. <https://doi.org/10.18926/AMO/46853>
- Higgins, T., Beutler, E., and Dumas, B.T. (2008). Measurement of haemoglobin in blood. In: Burtis, C.A., Ashwood, E.R., Bruns, D.E. (Eds.), *Tietz Fundamentals of Clinical Chemistry*, sixth ed. Sanders Elsevier, Saint Louis, MO, USA, 524–525.
- Hodgson, J. (2001). ADMET--turning chemicals into drugs. *Nature biotechnology*, 19(8), 722–726. <https://doi.org/10.1038/90761>
- Hollingsworth, S. A., and Dror, R. O. (2018). Molecular Dynamics Simulation for All. *Neuron*, 99(6), 1129–1143. <https://doi.org/10.1016/j.neuron.2018.08.011>
- Holt, M., and Ju, C. (2010). Drug-induced liver injury. *Handbook of experimental pharmacology*, (196), 3–27. https://doi.org/10.1007/978-3-642-00663-0_1
- Homeyer, N., Stoll, F., Hillisch, A., and Gohlke, H. (2014). Binding Free Energy Calculations for Lead Optimization: Assessment of Their Accuracy in an Industrial Drug Design Context. *Journal of chemical theory and computation*, 10(8), 3331–3344. <https://doi.org/10.1021/ct5000296>
- Hong, S., Dissing-Olesen, L., and Stevens, B. (2016). New insights on the role of microglia in synaptic pruning in health and disease. *Current opinion in neurobiology*, 36, 128–134. <https://doi.org/10.1016/j.conb.2015.12.004>

- Hornak, V., Abel, R., Okur, A., Strockbine, B., Roitberg, A., and Simmerling, C. (2006). Comparison of multiple Amber force fields and development of improved protein backbone parameters. *Proteins*, 65(3), 712–725. <https://doi.org/10.1002/prot.21123>
- Hou, T., Wang, J., Li, Y., and Wang, W. (2011). Assessing the performance of the MM/PBSA and MM/GBSA methods. The accuracy of binding free energy calculations based on molecular dynamics simulations. *Journal of chemical information and modeling*, 51(1), 69–82. <https://doi.org/10.1021/ci100275a>
- Huang, S. Y., and Zou, X. (2010). Advances and challenges in protein-ligand docking. *International journal of molecular sciences*, 11(8), 3016–3034. <https://doi.org/10.3390/ijms11083016>
- Ibrahim, M. B., Sowemimo, A. A., Sofidiya, M. O., Badmos, K. B., Fageyinbo, M. S., Abdulkareem, F. B., and Odukoya, O. A. (2016). Sub-acute and chronic toxicity profiles of Markhamia tomentosa ethanolic leaf extract in rats. *Journal of ethnopharmacology*, 193, 68–75. <https://doi.org/10.1016/j.jep.2016.07.036>
- Izak, M., and Bussel, J. B. (2014). Management of thrombocytopenia. *F1000prime reports*, 6, 45. <https://doi.org/10.12703/P6-45>
- Jamal, Q. M. S., Khan, M. I., Alharbi, A. H., Ahmad, V., and Yadav, B. S. (2023). Identification of Natural Compounds of the Apple as Inhibitors against Cholinesterase for the Treatment of Alzheimer's Disease: An in silico Molecular Docking Simulation and ADMET Study. *Nutrients*, 15(7), 1579. <https://doi.org/10.3390/nu15071579>
- Jayesh, K., Helen, L. R., Vysakh, A., Binil, E., and Latha, M. S. (2017). In vivo toxicity evaluation of aqueous acetone extract of Terminalia bellirica (Gaertn.) Roxb. fruit. *Regulatory toxicology and pharmacology: RTP*, 86, 349–355. <https://doi.org/10.1016/j.yrtph.2017.04.002>
- Jegnie, M., Abula, T., Woldekidan, S., Chalchisa, D., Asmare, Z., and Afework, M. (2023). Acute and Sub-Acute Toxicity Evaluation of the Crude Methanolic

- Extract of *Justicia schimperiana* Leaf in Wistar Albino Rats. *Journal of experimental pharmacology*, 15, 467–483. <https://doi.org/10.2147/JEP.S441273>
- Jorge, T. F., Rodrigues, J. A., Caldana, C., Schmidt, R., van Dongen, J. T., Thomas-Oates, J., and António, C. (2016). Mass spectrometry-based plant metabolomics: Metabolite responses to abiotic stress. *Mass spectrometry reviews*, 35(5), 620–649. <https://doi.org/10.1002/mas.21449>
- Justin Thenmozhi, A., William Raja, T. R., Manivasagam, T., Janakiraman, U., and Essa, M. M. (2017). Hesperidin ameliorates cognitive dysfunction, oxidative stress and apoptosis against aluminum chloride induced rat model of Alzheimer's disease. *Nutritional neuroscience*, 20(6), 360–368. <https://doi.org/10.1080/1028415X.2016.1144846>
- Kamianowska, M., Szczepański, M., and Wasilewska, A. (2019). Tubular and Glomerular Biomarkers of Acute Kidney Injury in Newborns. *Current drug metabolism*, 20(5), 332–349. <https://doi.org/10.2174/1389200220666190321142417>
- Kamisah, Y., Zuhair, J. S. F., Juliana, A. H., and Jaarin, K. (2017). *Parkia speciosa* empty pod prevents hypertension and cardiac damage in rats given N(G)-nitro-l-arginine methyl ester. *Biomedicine & pharmacotherapy = Biomedecine & pharmacotherapie*, 96, 291–298. <https://doi.org/10.1016/j.biopha.2017.09.095>
- Kapetanovic, I., M. (2008). Computer-aided drug discovery and development (CADD): in silico-chemico-biological approach. *Chemico-biological interactions*, 171(2), 165–176. <https://doi.org/10.1016/j.cbi.2006.12.006>
- Kar, S., and Leszczynski, J. (2019). Exploration of Computational Approaches to Predict the Toxicity of Chemical Mixtures. *Toxics*, 7(1), 15. <https://doi.org/10.3390/toxics7010015>
- Karin, M. (2009). NF-kappaB as a critical link between inflammation and cancer. *Cold Spring Harbor perspectives in biology*, 1(5), a000141. <https://doi.org/10.1101/cshperspect.a000141>

- Katarey, D., and Verma, S. (2016). Drug-induced liver injury. *Clinical medicine* (London, England), 16(Suppl 6), s104–s109. <https://doi.org/10.7861/clinmedicine.16-6-s104>
- Kayed, R., Head, E., Thompson, J. L., McIntire, T. M., Milton, S. C., Cotman, C. W., and Glabe, C. G. (2003). Common structure of soluble amyloid oligomers implies common mechanism of pathogenesis. *Science* (New York, N.Y.), 300(5618), 486–489. <https://doi.org/10.1126/science.1079469>
- Kazius, J., McGuire, R., and Bursi, R. (2005). Derivation and validation of toxicophores for mutagenicity prediction. *Journal of medicinal chemistry*, 48(1), 312–320. <https://doi.org/10.1021/jm040835a>
- Keretsu, S., Bhujbal, S. P., and Cho, S. J. (2021). Molecular modeling studies of pyrrolo[2,3-d]pyrimidin-4-amine derivatives as JAK1 inhibitors based on 3D-QSAR, molecular docking, molecular dynamics (MD) and MM-PBSA calculations. *Journal of biomolecular structure & dynamics*, 39(3), 753–765. <https://doi.org/10.1080/07391102.2020.1714483>
- Khalifaoui, A., Noumi, E., Belaabed, S., Aouadi, K., Lamjed, B., Adnan, M., Defant, A., Kadri, A., Snoussi, M., Khan, M. A., and Mancini, I. (2021). LC-ESI/MS-Phytochemical Profiling with Antioxidant, Antibacterial, Antifungal, Antiviral and In Silico Pharmacological Properties of Algerian *Asphodelus tenuifolius* (Cav.) Organic Extracts. *Antioxidants* (Basel, Switzerland), 10(4), 628. <https://doi.org/10.3390/antiox10040628>
- Khalifa, M., Safar, M. M., Abdelsalam, R. M., and Zaki, H. F. (2020). Telmisartan Protects Against Aluminum-Induced Alzheimer-like Pathological Changes in Rats. *Neurotoxicity research*, 37(2), 275–285. <https://doi.org/10.1007/s12640-019-00085-z>
- Khan, T., Dixit, S., Ahmad, R., Raza, S., Azad, I., Joshi, S., and Khan, A. R. (2017). Molecular docking, PASS analysis, bioactivity score prediction, synthesis, characterization and biological activity evaluation of a functionalized 2-

- butanone thiosemicarbazone ligand and its complexes. *Journal of chemical biology*, 10(3), 91–104. <https://doi.org/10.1007/s12154-017-0167-y>
- Kim, H. K., Choi, Y. H., and Verpoorte, R. (2011). NMR-based plant metabolomics: where do we stand, where do we go?. *Trends in biotechnology*, 29(6), 267–275. <https://doi.org/10.1016/j.tibtech.2011.02.001>
- Kim, H. S., Quon, M. J., and Kim, J. A. (2014). New insights into the mechanisms of polyphenols beyond antioxidant properties; lessons from the green tea polyphenol, epigallocatechin 3-gallate. *Redox biology*, 2, 187–195. <https://doi.org/10.1016/j.redox.2013.12.022>
- Kim, R. (2005). Unknotting the roles of Bcl-2 and Bcl-xL in cell death. *Biochemical and biophysical research communications*, 333(2), 336–343. <https://doi.org/10.1016/j.bbrc.2005.04.161>
- Kind, P. R., and King, E. J. (1954). Estimation of plasma phosphatase by determination of hydrolysed phenol with amino-antipyrine. *Journal of clinical pathology*, 7(4), 322–326. <https://doi.org/10.1136/jcp.7.4.322>
- Kirkland, D., Aardema, M., Henderson, L., and Müller, L. (2005). Evaluation of the ability of a battery of three in vitro genotoxicity tests to discriminate rodent carcinogens and non-carcinogens I. Sensitivity, specificity and relative predictivity. *Mutation research*, 584(1-2), 1–256. <https://doi.org/10.1016/j.mrgentox.2005.02.004>
- Koelsch G. (2017). BACE1 Function and Inhibition: Implications of Intervention in the Amyloid Pathway of Alzheimer's Disease Pathology. *Molecules* (Basel, Switzerland), 22(10), 1723. <https://doi.org/10.3390/molecules22101723>
- Kola, I., and Landis, J. (2004). Can the pharmaceutical industry reduce attrition rates?. *Nature reviews. Drug discovery*, 3(8), 711–715. <https://doi.org/10.1038/nrd1470>
- Kolodziejczyk-Czepas, J., Pasiński, B., Ponczek, M. B., Moniuszko-Szajwaj, B., Kowalczyk, M., Pecio, Ł., Nowak, P., and Stochmal, A. (2018). Bufadienolides from *Kalanchoe daigremontiana* modulate the enzymatic activity of plasmin - In

- vitro and in silico analyses. *International journal of biological macromolecules*, 120(Pt B), 1591–1600. <https://doi.org/10.1016/j.ijbiomac.2018.09.143>
- Kong, D. X., Li, X. J., and Zhang, H. Y. (2009). Where is the hope for drug discovery? Let history tell the future. *Drug discovery today*, 14(3-4), 115–119. <https://doi.org/10.1016/j.drudis.2008.07.002>
- Koutsoukis, C., Roukos, C., Demertzis, P., G., Kandrelis, S., and Akrida-Demertzi, K. (2019). The variation of the chemical composition of the main plant species in a subalpine grassland in northwestern Greece. *Legume Science*, 1 (1), e23.
- Kramer, J. A., Sagartz, J. E., and Morris, D. L. (2007). The application of discovery toxicology and pathology towards the design of safer pharmaceutical lead candidates. *Nature reviews. Drug discovery*, 6(8), 636–649. <https://doi.org/10.1038/nrd2378>
- Kuete, V., Tangmouo, J. G., Penlap Beng, V., Ngounou, F. N., and Lontsi, D. (2006). Antimicrobial activity of the methanolic extract from the stem bark of *Tridestemon omphalocarpoides* (Sapotaceae). *Journal of ethnopharmacology*, 104(1-2), 5–11. <https://doi.org/10.1016/j.jep.2005.08.002>
- Kumar, A., Srivastava, G., Negi, A. S., and Sharma, A. (2019). Docking, molecular dynamics, binding energy-MM-PBSA studies of naphthofuran derivatives to identify potential dual inhibitors against BACE-1 and GSK-3 β . *Journal of biomolecular structure & dynamics*, 37(2), 275–290. <https://doi.org/10.1080/07391102.2018.1426043>
- Kumari, R., Kumar, R., Open Source Drug Discovery Consortium, and Lynn, A. (2014). g_mmpbsa--a GROMACS tool for high-throughput MM-PBSA calculations. *Journal of chemical information and modeling*, 54(7), 1951–1962. <https://doi.org/10.1021/ci500020m>
- Lam, K., Pan, K., Linnekamp, J. F., Medema, J. P., and Kandimalla, R. (2016). DNA methylation based biomarkers in colorectal cancer: A systematic review. *Biochimica et biophysica acta*, 1866(1), 106–120. <https://doi.org/10.1016/j.bbcan.2016.07.001>

- Lasagna-Reeves, C. A., Castillo-Carranza, D. L., Guerrero-Muoz, M. J., Jackson, G. R., and Kaye, R. (2010). Preparation and characterization of neurotoxic tau oligomers. *Biochemistry*, 49(47), 10039–10041. <https://doi.org/10.1021/bi1016233>
- Lautenschlager, N. T., Cupples, L. A., Rao, V. S., Auerbach, S. A., Becker, R., Burke, J., Chui, H., Duara, R., Foley, E. J., Glatt, S. L., Green, R. C., Jones, R., Karlinsky, H., Kukull, W. A., Kurz, A., Larson, E. B., Martelli, K., Sadovnick, A. D., Volker, L., Waring, S. C., and Farrer, L. A. (1996). Risk of dementia among relatives of Alzheimer's disease patients in the MIRAGE study: What is in store for the oldest old?. *Neurology*, 46(3), 641–650. <https://doi.org/10.1212/wnl.46.3.641>
- Lauterbach, E. C., Victoroff, J., Coburn, K. L., Shillcutt, S. D., Doonan, S. M., and Mendez, M. F. (2010). Psychopharmacological neuroprotection in neurodegenerative disease: assessing the preclinical data. *The Journal of neuropsychiatry and clinical neurosciences*, 22(1), 8–18. <https://doi.org/10.1176/jnp.2010.22.1.8>
- Le Guilloux, V., Schmidtke, P., and Tuffery, P. (2009). Fpocket: an open-source platform for ligand pocket detection. *BMC bioinformatics*, 10, 168. <https://doi.org/10.1186/1471-2105-10-168>
- Lee, S. J., Nam, E., Lee, H. J., Savelieff, M. G., and Lim, M. H. (2017). Towards an understanding of amyloid- β oligomers: characterization, toxicity mechanisms, and inhibitors. *Chemical Society reviews*, 46(2), 310–323. <https://doi.org/10.1039/c6cs00731g>
- Leenaars, C. H. C., Kouwenaar, C., Stafleu, F. R., Bleich, A., Ritskes-Hoitinga, M., De Vries, R. B. M., and Meijboom, F. L. B. (2019). Animal to human translation: a systematic scoping review of reported concordance rates. *Journal of translational medicine*, 17(1), 223. <https://doi.org/10.1186/s12967-019-1976-2>
- Li, R., Lindholm, K., Yang, L. B., Yue, X., Citron, M., Yan, R., Beach, T., Sue, L., Sabbagh, M., Cai, H., Wong, P., Price, D., and Shen, Y. (2004). Amyloid beta

- peptide load is correlated with increased beta-secretase activity in sporadic Alzheimer's disease patients. *Proceedings of the National Academy of Sciences of the United States of America*, 101(10), 3632–3637. <https://doi.org/10.1073/pnas.0205689101>
- Li, Z., Tong, Q., Xu, H., Hu, L., Zhao, R., Zhou, F., Pan, W., and Zhou, L. (2015). Therapeutic Effects of TianDiJingWan on the A β 25-35-Induced Alzheimer's Disease Model Rats. *Evidence-based complementary and alternative medicine: eCAM*, 2015, 307350. <https://doi.org/10.1155/2015/307350>
- Liaquat, L., Sadir, S., Batool, Z., Tabassum, S., Shahzad, S., Afzal, A., and Haider, S. (2019). Acute aluminum chloride toxicity revisited: Study on DNA damage and histopathological, biochemical and neurochemical alterations in rat brain. *Life sciences*, 217, 202–211. <https://doi.org/10.1016/j.lfs.2018.12.009>
- Lipinski C. A. (2004). Lead- and drug-like compounds: the rule-of-five revolution. *Drug discovery today. Technologies*, 1(4), 337–341. <https://doi.org/10.1016/j.ddtec.2004.11.007>
- Lista, S., Vergallo, A., Teipel, S. J., Lemercier, P., Giorgi, F. S., Gabelle, A., Garaci, F., Mercuri, N. B., Babiloni, C., Gaire, B. P., Koronyo, Y., Koronyo-Hamaoui, M., Hampel, H., Nisticò, R., and Neurodegeneration Precision Medicine Initiative (NPMI) (2023). Determinants of approved acetylcholinesterase inhibitor response outcomes in Alzheimer's disease: relevance for precision medicine in neurodegenerative diseases. *Ageing research reviews*, 84, 101819. <https://doi.org/10.1016/j.arr.2022.101819>
- Livingston, G., Huntley, J., Sommerlad, A., Ames, D., Ballard, C., Banerjee, S., Brayne, C., Burns, A., Cohen-Mansfield, J., Cooper, C., Costafreda, S. G., Dias, A., Fox, N., Gitlin, L. N., Howard, R., Kales, H. C., Kivimäki, M., Larson, E. B., Ogunniyi, A., Orgeta, V., and Mukadam, N. (2020). Dementia prevention, intervention, and care: 2020 report of the Lancet Commission. *Lancet* (London, England), 396(10248), 413–446. [https://doi.org/10.1016/S0140-6736\(20\)30367-6](https://doi.org/10.1016/S0140-6736(20)30367-6)

- Llansola, M., Miñana, M. D., Montoliu, C., Saez, R., Corbalán, R., Manzo, L., and Felipo, V. (1999). Prenatal exposure to aluminum reduces expression of neuronal nitric oxide synthase and of soluble guanylate cyclase and impairs glutamatergic neurotransmission in rat cerebellum. *Journal of neurochemistry*, 73(2), 712–718. <https://doi.org/10.1046/j.1471-4159.1999.0730712.x>
- Long, S., Benoist, C., and Weidner, W. (2023). World Alzheimer Report 2023: Reducing dementia risk: never too early, never too late. London, England: Alzheimer's Disease International.
- Longvah, T., and Deosthale, Y. G. (1998). Nutrient composition and food potential of *Parkia roxburghii*, a less known tree legume from northeast India. *Food chemistry*, 62(4), 477–481. [https://doi.org/10.1016/S0308-8146\(97\)00179-9](https://doi.org/10.1016/S0308-8146(97)00179-9)
- Loomis, T. A., Hayes, A.W. (1996). Loomis's essentials of toxicology. 4th ed., California, Academic press: 208–245.
- Lopera, F., Marino, C., Chandrahas, A. S., O'Hare, M., Villalba-Moreno, N. D., Aguillon, D., Baena, A., Sanchez, J. S., Vila-Castelar, C., Ramirez Gomez, L., Chmielewska, N., Oliveira, G. M., Littau, J. L., Hartmann, K., Park, K., Krasemann, S., Glatzel, M., Schoemaker, D., Gonzalez-Buendia, L., Delgado-Tirado, S., and Quiroz, Y. T. (2023). Resilience to autosomal dominant Alzheimer's disease in a Reelin-COLBOS heterozygous man. *Nature medicine*, 29(5), 1243–1252. <https://doi.org/10.1038/s41591-023-02318-3>
- López-Vallejo, F., Caulfield, T., Martínez-Mayorga, K., Giulianotti, M. A., Nefzi, A., Houghten, R. A., and Medina-Franco, J. L. (2011). Integrating virtual screening and combinatorial chemistry for accelerated drug discovery. *Combinatorial chemistry & high throughput screening*, 14(6), 475–487. <https://doi.org/10.2174/138620711795767866>
- Loukrakpam, B., Rajendran, A., Chyne, D., A., L., and Longvah, T. (2019). 12th IFDC 2017 Special Issue—Nutrient and phytonutrient profiles of some indigenous vegetables of Manipur, Northeast India. *Journal of Food Composition and Analysis*, 79, 12–22.

- Loy, C. T., Schofield, P. R., Turner, A. M., and Kwok, J. B. (2014). Genetics of dementia. *Lancet* (London, England), 383(9919), 828–840. [https://doi.org/10.1016/S0140-6736\(13\)60630-3](https://doi.org/10.1016/S0140-6736(13)60630-3)
- Lühe, A., Suter, L., Ruepp, S., Singer, T., Weiser, T., and Albertini, S. (2005). Toxicogenomics in the pharmaceutical industry: hollow promises or real benefit?. *Mutation research*, 575(1-2), 102–115. <https://doi.org/10.1016/j.mrfmmm.2005.02.009>
- Lunardi, P. S. (2010). Effect of Huperzine-A on secretion of S100B in primary culture
- Ma, W., Ding, B., Yu, H., Yuan, L., Xi, Y., and Xiao, R. (2015). Genistein alleviates β -amyloid-induced inflammatory damage through regulating Toll-like receptor 4/nuclear factor κ B. *Journal of medicinal food*, 18(3), 273–279. <https://doi.org/10.1089/jmf.2014.3150>
- Macalalad, M. A. B., and Gonzales, A. A., 3rd (2022). In-silico screening and identification of phytochemicals from *Centella asiatica* as potential inhibitors of sodium-glucose co-transporter 2 for treating diabetes. *Journal of biomolecular structure & dynamics*, 40(22), 12221–12238. <https://doi.org/10.1080/07391102.2021.1969282>
- Machauer, R., Lueoend, R., Hurth, K., Veenstra, S. J., Rueeger, H., Voegtli, M., Tintelnot-Blomley, M., Rondeau, J. M., Jacobson, L. H., Laue, G., Beltz, K., and Neumann, U. (2021). Discovery of Umibecestat (CNP520): A Potent, Selective, and Efficacious β -Secretase (BACE1) Inhibitor for the Prevention of Alzheimer's Disease. *Journal of medicinal chemistry*, 64(20), 15262–15279. <https://doi.org/10.1021/acs.jmedchem.1c01300>
- Madi, Y. F., Choucry, M. A., El-Marasy, S. A., Meselhy, M. R., and El-Kashoury, E. A. (2020). UPLC-Orbitrap HRMS metabolic profiling of *Cymbopogon citratus* cultivated in Egypt; neuroprotective effect against $AlCl_3$ -induced neurotoxicity in rats. *Journal of ethnopharmacology*, 259, 112930. <https://doi.org/10.1016/j.jep.2020.112930>

- Mahdi, O., Baharuldin, M. T. H., Mohd Nor, N. H., Chiroma, S. M., Jagadeesan, S., and Moklas, M. A. M (2019). Chemicals used for the induction of Alzheimer's disease-like cognitive dysfunctions in rodents. *Biomedical research journal*, 6(11), 3460-3484. <https://doi.org/10.15419/bmrat.v6i11.575>
- Mahnashi, M. H., Ashraf, M., Alhasaniah, A. H., Ullah, H., Zeb, A., Ghufran, M., Fahad, S., Ayaz, M., and Daglia, M. (2023). Polyphenol-enriched *Desmodium elegans* DC. ameliorate scopolamine-induced amnesia in animal model of Alzheimer's disease: In Vitro, In Vivo and In Silico approaches. *Biomedicine & pharmacotherapy = Biomedecine & pharmacotherapie*, 165, 115144. <https://doi.org/10.1016/j.biopha.2023.115144>
- Majumder, R., and Mandal, M. (2022). Screening of plant-based natural compounds as a potential COVID-19 main protease inhibitor: an in silico docking and molecular dynamics simulation approach. *Journal of biomolecular structure & dynamics*, 40(2), 696–711. <https://doi.org/10.1080/07391102.2020.1817787>
- Manach, C., Williamson, G., Morand, C., Scalbert, A., and Rémésy, C. (2005). Bioavailability and bioefficacy of polyphenols in humans. I. Review of 97 bioavailability studies. *The American journal of clinical nutrition*, 81(1 Suppl), 230S–242S. <https://doi.org/10.1093/ajcn/81.1.230S>
- Manikandan, P., and Nagini, S. (2018). Cytochrome P450 Structure, Function and Clinical Significance: A Review. *Current drug targets*, 19(1), 38–54. <https://doi.org/10.2174/1389450118666170125144557>
- Manoharan, S., Guillemin, G. J., Abiramasundari, R. S., Essa, M. M., Akbar, M., and Akbar, M. D. (2016). The Role of Reactive Oxygen Species in the Pathogenesis of Alzheimer's Disease, Parkinson's Disease, and Huntington's Disease: A Mini Review. *Oxidative medicine and cellular longevity*, 2016, 8590578. <https://doi.org/10.1155/2016/8590578>
- Marak, C. C., Marak, B. N., Singh, V. P., Gurusubramanian, G., and Roy, V. K. (2023). Phytochemical analysis, in silico study and toxicity profile of *Cycas pectinata*

- Buch.-Ham seed in mice. *Drug and chemical toxicology*, 46(2), 330–342.
<https://doi.org/10.1080/01480545.2022.2033258>
- Martin, T. M. (2020). User's Guide for T.E.S.T. (Toxicity Estimation Software Tool) Version 5.1: A Java Application to Estimate Toxicities and Physical Properties from Molecular Structure. U.S. Environmental Protection Agency.
- Martin, T. M., and Young, D. M. (2001). Prediction of the acute toxicity (96-h LC50) of organic compounds to the fathead minnow (*Pimephales promelas*) using a group contribution method. *Chemical research in toxicology*, 14(10), 1378–1385. <https://doi.org/10.1021/tx0155045>
- Martin, T. M., Harten, P., Venkatapathy, R., Das, S., and Young, D. M. (2008). A hierarchical clustering methodology for the estimation of toxicity. *Toxicology mechanisms and methods*, 18(2-3), 251–266.
<https://doi.org/10.1080/15376510701857353>
- Marucci, G., Buccioni, M., Ben, D. D., Lambertucci, C., Volpini, R., and Amenta, F. (2021). Efficacy of acetylcholinesterase inhibitors in Alzheimer's disease. *Neuropharmacology*, 190, 108352.
<https://doi.org/10.1016/j.neuropharm.2020.108352>
- Mason, G., Wilson, D., Hampton, C., and Würbel, H. (2004). Non-invasively assessing disturbance and stress in laboratory rats by scoring chromodacryorrhoea. *Alternatives to laboratory animals: ATLA*, 32 Suppl 1A, 153–159.
<https://doi.org/10.1177/026119290403201s25>
- Maurer, K., Maurer, U (2003). Alzheimer: The life of a physician and career of a disease. New York: Columbia University Press.
- Maust, D. T., Kim, H. M., Seyfried, L. S., Chiang, C., Kavanagh, J., Schneider, L. S., and Kales, H. C. (2015). Antipsychotics, other psychotropics, and the risk of death in patients with dementia: number needed to harm. *JAMA psychiatry*, 72(5), 438–445. <https://doi.org/10.1001/jamapsychiatry.2014.3018>
- McFarland, B. C., Gray, G. K., Nozell, S. E., Hong, S. W., and Benveniste, E. N. (2013). Activation of the NF- κ B pathway by the STAT3 inhibitor JSI-124 in

- human glioblastoma cells. *Molecular cancer research: MCR*, 11(5), 494–505.
<https://doi.org/10.1158/1541-7786.MCR-12-0528>
- Meng, X. Y., Zhang, H. X., Mezei, M., and Cui, M. (2011). Molecular docking: a powerful approach for structure-based drug discovery. *Current computer-aided drug design*, 7(2), 146–157. <https://doi.org/10.2174/157340911795677602>
- Meng, Z., Chen, H., Deng, C., and Meng, S. (2022). Multiple Roles of Paeoniflorin in Alzheimer's Disease. *Evidence-based complementary and alternative medicine: eCAM*, 2022, 2464163. <https://doi.org/10.1155/2022/2464163>
- Mi, K., and Johnson, G. V. (2006). The role of tau phosphorylation in the pathogenesis of Alzheimer's disease. *Current Alzheimer research*, 3(5), 449–463. <https://doi.org/10.2174/156720506779025279>
- Michael, B., Yano, B., Sellers, R. S., Perry, R., Morton, D., Roome, N., Johnson, J. K., Schafer, K., and Pitsch, S. (2007). Evaluation of organ weights for rodent and non-rodent toxicity studies: a review of regulatory guidelines and a survey of current practices. *Toxicologic pathology*, 35(5), 742–750. <https://doi.org/10.1080/01926230701595292>
- Michael, J., Derelanko, Carol, S., and Auletta (2014). Handbook of Toxicology, 3rd edition. CRC Press.
- Miller, D. B., and O'Callaghan, J. P. (2005). Aging, stress and the hippocampus. *Ageing research reviews*, 4(2), 123–140. <https://doi.org/10.1016/j.arr.2005.03.002>
- Mohandas, E., Rajmohan, V., and Raghunath, B. (2009). Neurobiology of Alzheimer's disease. *Indian journal of psychiatry*, 51(1), 55–61. <https://doi.org/10.4103/0019-5545.44908>
- Mohmmad Abdul, H., Sultana, R., Keller, J. N., St Clair, D. K., Markesbery, W. R., and Butterfield, D. A. (2006). Mutations in amyloid precursor protein and presenilin-1 genes increase the basal oxidative stress in murine neuronal cells and lead to increased sensitivity to oxidative stress mediated by amyloid beta-peptide (1-42), HO and kainic acid: implications for Alzheimer's disease.

Journal of neurochemistry, 96(5), 1322–1335. <https://doi.org/10.1111/j.1471-4159.2005.03647.x>

Molinspiration cheminformatics server (free web services). Slovensky Grob, Slovakia.
Retrieved on 5 September, 2022. Available at <http://www.molinspiration.com>

Moron, M. S., Depierre, J. W., and Mannervik, B. (1979). Levels of glutathione, glutathione reductase and glutathione S-transferase activities in rat lung and liver. *Biochimica et biophysica acta*, 582(1), 67–78.
[https://doi.org/10.1016/0304-4165\(79\)90289-7](https://doi.org/10.1016/0304-4165(79)90289-7)

Morphy, R., and Rankovic, Z. (2009). Designing multiple ligands - medicinal chemistry strategies and challenges. *Current pharmaceutical design*, 15(6), 587–600. <https://doi.org/10.2174/138161209787315594>

Morris, G. M., and Lim-Wilby, M. (2008). Molecular docking. *Methods in molecular biology* (Clifton, N.J.), 443, 365–382. https://doi.org/10.1007/978-1-59745-177-2_19

Morris, R. (1984). Developments of a water-maze procedure for studying spatial learning in the rat. *Journal of neuroscience methods*, 11(1), 47–60.
[https://doi.org/10.1016/0165-0270\(84\)90007-4](https://doi.org/10.1016/0165-0270(84)90007-4)

Mortelmans, K., and Zeiger, E. (2000). The Ames Salmonella/microsome mutagenicity assay. *Mutation research*, 455(1-2), 29–60.
[https://doi.org/10.1016/s0027-5107\(00\)00064-6](https://doi.org/10.1016/s0027-5107(00)00064-6)

Mostrag-Szlichtyng, A., Zaldívar Comenges, J. M., and Worth, A. P. (2010). Computational toxicology at the European Commission's Joint Research Centre. *Expert opinion on drug metabolism & toxicology*, 6(7), 785–792.
<https://doi.org/10.1517/17425255.2010.489551>

Moussa-Pacha, N. M., Abdin, S. M., Omar, H. A., Alniss, H., and Al-Tel, T. H. (2020). BACE1 inhibitors: Current status and future directions in treating Alzheimer's disease. *Medicinal research reviews*, 40(1), 339–384.
<https://doi.org/10.1002/med.21622>

- Mu, Y., and Gage, F. H. (2011). Adult hippocampal neurogenesis and its role in Alzheimer's disease. *Molecular neurodegeneration*, 6, 85. <https://doi.org/10.1186/1750-1326-6-85>
- Mujika, J. I., Rezabal, E., Mercero, J. M., Ruipérez, F., Costa, D., Ugalde, J. M., and Lopez, X. (2014). Aluminum in biological environments: a computational approach. *Computational and structural biotechnology journal*, 9, e201403002. <https://doi.org/10.5936/csbj.201403002>
- Mukinda, J. T., and Eagles, P. F. (2010). Acute and sub-chronic oral toxicity profiles of the aqueous extract of *Polygala fruticosa* in female mice and rats. *Journal of ethnopharmacology*, 128(1), 236–240. <https://doi.org/10.1016/j.jep.2010.01.022>
- Nallagouni, C. S., and Reddy, K. P. (2017). Aluminum and fluoride impacts cortex, hippocampus and dentate gyrus structure in rats: protective effect of resveratrol. *International Journal of Applied Biology and Pharmaceutical Technology*, 8, 89–97.
- Naven, R. T., Louise-May, S., and Greene, N. (2010). The computational prediction of genotoxicity. *Expert opinion on drug metabolism & toxicology*, 6(7), 797–807. <https://doi.org/10.1517/17425255.2010.495118>
- Naz, T., Mosaddik, A., Rahman, M., Muhammad, I., Haque, E., and Cho, S. K. (2012). Antimicrobial, antileishmanial and cytotoxic compounds from *Piper chaba*. *Natural product research*, 26(11), 979–986. <https://doi.org/10.1080/14786419.2010.535166>
- Neidle, S. (2012). Design principles for quadruplex-binding small molecules. In: *Therapeutic applications of quadruplex nucleic acids*. US: Academic Press, pp 151–174. <https://doi.org/10.1016/b9780-12-375138-6.00009-1>
- Nelson, P. T., Head, E., Schmitt, F. A., Davis, P. R., Neltner, J. H., Jicha, G. A., Abner, E. L., Smith, C. D., Van Eldik, L. J., Kryscio, R. J., and Scheff, S. W. (2011). Alzheimer's disease is not "brain aging": neuropathological, genetic, and

- epidemiological human studies. *Acta neuropathologica*, 121(5), 571–587.
<https://doi.org/10.1007/s00401-011-0826-y>
- Newman, D. J., and Cragg, G. M. (2007). Natural products as sources of new drugs over the last 25 years. *Journal of natural products*, 70(3), 461–477.
<https://doi.org/10.1021/np068054v>
- Nianogo, R. A., Rosenwohl-Mack, A., Yaffe, K., Carrasco, A., Hoffmann, C. M., and Barnes, D. E. (2022). Risk Factors Associated with Alzheimer Disease and Related Dementias by Sex and Race and Ethnicity in the US. *JAMA neurology*, 79(6), 584–591. <https://doi.org/10.1001/jamaneurol.2022.0976>
- Nie, L., He, K., Xie, F., Xiao, S., Li, S., Xu, J., Zhang, K., Yang, C., Zhou, L., Liu, J., Zou, L., and Yang, X. (2021). Loganin substantially ameliorates molecular deficits, pathologies and cognitive impairment in a mouse model of Alzheimer's disease. *Aging*, 13(20), 23739–23756. <https://doi.org/10.18632/aging.203646>
- Nordberg, A., Ballard, C., Bullock, R., Darreh-Shori, T., and Somogyi, M. (2013). A review of butyrylcholinesterase as a therapeutic target in the treatment of Alzheimer's disease. *The primary care companion for CNS disorders*, 15(2), PCC.12r01412. <https://doi.org/10.4088/PCC.12r01412>
- Noumi, E., Snoussi, M., Anouar, E. H., Alreshidi, M., Veettil, V. N., Elkahoui, S., Adnan, M., Patel, M., Kadri, A., Aouadi, K., De Feo, V., and Badraoui, R. (2020). HR-LCMS-Based Metabolite Profiling, Antioxidant, and Anticancer Properties of Teucrium polium L. Methanolic Extract: Computational and In Vitro Study. *Antioxidants* (Basel, Switzerland), 9(11), 1089. <https://doi.org/10.3390/antiox9111089>
- OECD, (2008). Test No. 407: Repeated Dose 28-day Oral Toxicity Study in Rodents, OECD Guidelines for the Testing of Chemicals, Section 4, OECD Publishing, Paris, <https://doi.org/10.1787/9789264070684-en>
- Ogu, C. C., and Maxa, J. L. (2000). Drug interactions due to cytochrome P450. *Proceedings* (Baylor University. Medical Center), 13(4), 421–423. <https://doi.org/10.1080/08998280.2000.11927719>

- Ohkawa, H., Ohishi, N., and Yagi, K. (1979). Assay for lipid peroxides in animal tissues by thiobarbituric acid reaction. *Analytical biochemistry*, 95(2), 351–358. [https://doi.org/10.1016/0003-2697\(79\)90738-3](https://doi.org/10.1016/0003-2697(79)90738-3)
- Ohtsuka, T., Buchsbaum, D., Oliver, P., Makhija, S., Kimberly, R., and Zhou, T. (2003). Synergistic induction of tumor cell apoptosis by death receptor antibody and chemotherapy agent through JNK/p38 and mitochondrial death pathway. *Oncogene*, 22(13), 2034–2044. <https://doi.org/10.1038/sj.onc.1206290>
- Okoro, R. N., and Farate, V. T. (2019). The use of nephrotoxic drugs in patients with chronic kidney disease. *International journal of clinical pharmacy*, 41(3), 767–775. <https://doi.org/10.1007/s11096-019-00811-9>
- Olson, H., Betton, G., Robinson, D., Thomas, K., Monro, A., Kolaja, G., Lilly, P., Sanders, J., Sipes, G., Bracken, W., Dorato, M., Van Deun, K., Smith, P., Berger, B., and Heller, A. (2000). Concordance of the toxicity of pharmaceuticals in humans and in animals. *Regulatory toxicology and pharmacology: RTP*, 32(1), 56–67. <https://doi.org/10.1006/rtp.2000.1399>
- Opo, F. A. D. M., Rahman, M. M., Ahammad, F., Ahmed, I., Bhuiyan, M. A., and Asiri, A. M. (2021). Structure based pharmacophore modeling, virtual screening, molecular docking and ADMET approaches for identification of natural anti-cancer agents targeting XIAP protein. *Scientific reports*, 11(1), 4049. <https://doi.org/10.1038/s41598-021-83626-x>
- Organization for Economic Development, 2001. Guideline for Testing of Chemicals. Guidance, no. 425.
- Padrón, J. A., Carrasco, R., and Pellón, R. F. (2002). Molecular descriptor based on a molar refractivity partition using Randic-type graph-theoretical invariant. *Journal of pharmacy & pharmaceutical sciences: a publication of the Canadian Society for Pharmaceutical Sciences, Societe canadienne des sciences pharmaceutiques*, 5(3), 258–266.
- Palladini, J., Bagnati, R., Passoni, A., Davoli, E., Lanno, A., Terzaghi, E., Falakdin, P., and Di Guardo, A. (2022). Bioaccumulation of PCBs and their hydroxy and

- sulfonated metabolites in earthworms: Comparing lab and field results. *Environmental pollution* (Barking, Essex : 1987), 293, 118507. <https://doi.org/10.1016/j.envpol.2021.118507>
- Pandey, K. B., and Rizvi, S. I. (2009). Plant polyphenols as dietary antioxidants in human health and disease. *Oxidative medicine and cellular longevity*, 2(5), 270–278. <https://doi.org/10.4161/oxim.2.5.9498>
- Pankaj, P. P., and Varma, M. C. (2013). Potential role of *Spirulina platensis* in maintaining blood parameters in alloxan induced diabetic mice. *International Journal of Pharmacy and Pharmaceutical Sciences*, 5, 450-456.
- Paolicelli, R. C., Bolasco, G., Pagani, F., Maggi, L., Scianni, M., Panzanelli, P., Giustetto, M., Ferreira, T. A., Guiducci, E., Dumas, L., Ragozzino, D., and Gross, C. T. (2011). Synaptic pruning by microglia is necessary for normal brain development. *Science* (New York, N.Y.), 333(6048), 1456–1458. <https://doi.org/10.1126/science.1202529>
- Paquet, C., Nicoll, J. A., Love, S., Mouton-Liger, F., Holmes, C., Hugon, J., and Boche, D. (2018). Downregulated apoptosis and autophagy after anti-A β immunotherapy in Alzheimer's disease. *Brain pathology* (Zurich, Switzerland), 28(5), 603–610. <https://doi.org/10.1111/bpa.12567>
- Pardridge, W. M. (2009). Alzheimer's disease drug development and the problem of the blood-brain barrier. *Alzheimer's & dementia: the journal of the Alzheimer's Association*, 5(5), 427–432. <https://doi.org/10.1016/j.jalz.2009.06.003>
- Park S. Y. (2010). Potential therapeutic agents against Alzheimer's disease from natural sources. *Archives of pharmacal research*, 33(10), 1589–1609. <https://doi.org/10.1007/s12272-010-1010-y>
- Park, S. Y., and Ferreira, A. (2005). The generation of a 17 kDa neurotoxic fragment: an alternative mechanism by which tau mediates beta-amyloid-induced neurodegeneration. *The Journal of neuroscience: the official journal of the Society for Neuroscience*, 25(22), 5365–5375. <https://doi.org/10.1523/JNEUROSCI.1125-05.2005>

- Parrinello, M., and Rahman, A. (1981). Polymorphic transitions in single crystals: a new molecular dynamics method. *Journal of Applied Physics*, 52, 7182-7190. <https://doi.org/10.1063/1.328693>
- Patel, C., Shukla, P., Pande, S., Punamiya, R., Ranch, K., and Boddu, S. H. S. (2022). Acute and sub-acute toxicity study of anti-obesity herbal granules in Sprague Dawley rats. *Brazilian journal of biology= Revista brasleira de biologia*, 84, e264320. <https://doi.org/10.1590/1519-6984.264320>
- Patrick, G. N., Zukerberg, L., Nikolic, M., de la Monte, S., Dikkes, P., and Tsai, L. H. (1999). Conversion of p35 to p25 deregulates Cdk5 activity and promotes neurodegeneration. *Nature*, 402(6762), 615–622. <https://doi.org/10.1038/45159>
- Patterson, K. R., Remmers, C., Fu, Y., Brooker, S., Kanaan, N. M., Vana, L., Ward, S., Reyes, J. F., Philibert, K., Glucksman, M. J., and Binder, L. I. (2011). Characterization of prefibrillar Tau oligomers in vitro and in Alzheimer disease. *The Journal of biological chemistry*, 286(26), 23063–23076. <https://doi.org/10.1074/jbc.M111.237974>
- Pavan, M., Netzeva, T. I., and Worth, A. P. (2008). Review of literature-based quantitative structure-activity relationship models for bioconcentration. *QSAR & Combinatorial Science*, 27 (1), 21–31. <https://doi.org/10.1002/qsar.200710102>
- Pearce, E. L., Poffenberger, M. C., Chang, C. H., and Jones, R. G. (2013). Fueling immunity: insights into metabolism and lymphocyte function. *Science* (New York, N.Y.), 342(6155), 1242454. <https://doi.org/10.1126/science.1242454>
- Persson, T., Popescu, B. O., and Cedazo-Minguez, A. (2014). Oxidative stress in Alzheimer's disease: why did antioxidant therapy fail?. *Oxidative medicine and cellular longevity*, 2014, 427318. <https://doi.org/10.1155/2014/427318>
- Pettersen, E. F., Goddard, T. D., Huang, C. C., Couch, G. S., Greenblatt, D. M., Meng, E. C., and Ferrin, T. E. (2004). UCSF Chimera--a visualization system for exploratory research and analysis. *Journal of computational chemistry*, 25(13), 1605–1612. <https://doi.org/10.1002/jcc.20084>

- Piršelová, K., Baláž, Š. and Schultz, T. W. (1996). Model-based QSAR for ionizable compounds: Toxicity of phenols against *Tetrahymena pyriformis*. *Archives of Environmental Contamination and Toxicology*, 30, 170–177. <https://doi.org/10.1007/BF00215795>
- Pizzo, F., Gadaleta, D., and Benfenati, E. (2022). In Silico Models for Repeated-Dose Toxicity (RDT): Prediction of the No Observed Adverse Effect Level (NOAEL) and Lowest Observed Adverse Effect Level (LOAEL) for Drugs. *Methods in molecular biology* (Clifton, N.J.), 2425, 241–258. https://doi.org/10.1007/978-1-0716-1960-5_11
- Pognan, F., Beilmann, M., Boonen, H. C. M., Czich, A., Dear, G., Hewitt, P., Mow, T., Oinonen, T., Roth, A., Steger-Hartmann, T., Valentin, J. P., Van Goethem, F., Weaver, R. J., and Newham, P. (2023). The evolving role of investigative toxicology in the pharmaceutical industry. *Nature reviews. Drug discovery*, 22(4), 317–335. <https://doi.org/10.1038/s41573-022-00633-x>
- Popa-Wagner, A., Mitran, S., Sivanesan, S., Chang, E., and Buga, A. M. (2013). ROS and brain diseases: the good, the bad, and the ugly. *Oxidative medicine and cellular longevity*, 2013, 963520. <https://doi.org/10.1155/2013/963520>
- Potts, R. O., and Guy, R. H. (1992). Predicting skin permeability. *Pharmaceutical research*, 9(5), 663–669. <https://doi.org/10.1023/a:1015810312465>
- Prachayasittikul, V., and Prachayasittikul, V. (2016). P-glycoprotein transporter in drug development. *EXCLI journal*, 15, 113–118. <https://doi.org/10.17179/excli2015-768>
- Prakash, A., Kumar, V., Lynn, A. M., and Haque, R. (2019). Insights into the DNA binding induced thermal stabilization of transcription factor FOXP3. *Journal of biomolecular structure & dynamics*, 37(9), 2219–2229. <https://doi.org/10.1080/07391102.2018.1486228>
- Price, E. A., and Schrier, S. L. (2008). Anemia in the elderly: introduction. *Seminars in hematology*, 45(4), 207–209. <https://doi.org/10.1053/j.seminhematol.2008.07.001>

- Qian, D., Wang, Q., Lin, S., Li, Y., Gu, X., Xia, C., Xu, Y., Zhang, T., Yang, L., Wu, Q., Sun, J., Liu, Y., and Zhou, M. (2022). Identification of potential targets of cinnamon for treatment against Alzheimer's disease-related GABAergic synaptic dysfunction using network pharmacology. *Scientific reports*, 12(1), 19959. <https://doi.org/10.1038/s41598-022-24378-0>
- Rafi, M. O., Bhattacharje, G., Al-Khafaji, K., Taskin-Tok, T., Alfasane, M. A., Das, A. K., Parvez, M. A. K., and Rahman, M. S. (2022). Combination of QSAR, molecular docking, molecular dynamic simulation and MM-PBSA: analogues of lopinavir and favipiravir as potential drug candidates against COVID-19. *Journal of biomolecular structure & dynamics*, 40(8), 3711–3730. <https://doi.org/10.1080/07391102.2020.1850355>
- Raies, A. B., and Bajic, V. B. (2016). In silico toxicology: computational methods for the prediction of chemical toxicity. Wiley interdisciplinary reviews. *Computational molecular science*, 6(2), 147–172. <https://doi.org/10.1002/wcms.1240>
- Rakonczay, Z., Horváth, Z., Juhász, A., and Kálmán, J. (2005). Peripheral cholinergic disturbances in Alzheimer's disease. *Chemico-biological interactions*, 157-158, 233–238. <https://doi.org/10.1016/j.cbi.2005.10.034>
- Ralph, S. J., and Espinet, A. J. (2018). Increased All-Cause Mortality by Antipsychotic Drugs: Updated Review and Meta-Analysis in Dementia and General Mental Health Care. *Journal of Alzheimer's disease reports*, 2(1), 1–26. <https://doi.org/10.3233/ADR-170042>
- Ralte, L., Khiangte, L., Thangjam, N. M., Kumar, A., and Singh, Y. T. (2022). GC-MS and molecular docking analyses of phytochemicals from the underutilized plant, *Parkia timoriana* revealed candidate anti-cancerous and anti-inflammatory agents. *Scientific reports*, 12(1), 3395. <https://doi.org/10.1038/s41598-022-07320-2>
- Ramaiah, S. K. (2011). Preclinical safety assessment: current gaps, challenges, and approaches in identifying translatable biomarkers of drug-induced liver injury.

Clinics in laboratory medicine, 31(1), 161–172.
<https://doi.org/10.1016/j.cll.2010.10.004>

Ravi, S. K., Ramesh, B. N., Mundugaru, R., and Vincent, B. (2018). Multiple pharmacological activities of *Caesalpinia crista* against aluminum-induced neurodegeneration in rats: Relevance for Alzheimer's disease. *Environmental toxicology and pharmacology*, 58, 202–211.
<https://doi.org/10.1016/j.etap.2018.01.008>

Reddy, M. N., Adnan, M., Alreshidi, M. M., Saeed, M., and Patel, M. (2020). Evaluation of Anticancer, Antibacterial and Antioxidant Properties of a Medicinally Treasured Fern *Tectaria coadunata* with its Phytoconstituents Analysis by HR-LCMS. *Anti-cancer agents in medicinal chemistry*, 20(15), 1845–1856. <https://doi.org/10.2174/1871520620666200318101938>

Reifert, J., Hartung-Cranston, D., and Feinstein, S. C. (2011). Amyloid beta-mediated cell death of cultured hippocampal neurons reveals extensive Tau fragmentation without increased full-length tau phosphorylation. *The Journal of biological chemistry*, 286(23), 20797–20811. <https://doi.org/10.1074/jbc.M111.234674>

Reitman, S., and Frankel, S. (1957). A colorimetric method for the determination of serum glutamic oxalacetic and glutamic pyruvic transaminases. *American journal of clinical pathology*, 28(1), 56–63. <https://doi.org/10.1093/ajcp/28.1.56>

Rekha, K. R., Selvakumar, G. P., and Sivakamasundari, R. I. (2014). Effects of syringic acid on chronic MPTP/probenecid induced motor dysfunction, dopaminergic markers expression and neuroinflammation in C57BL/6 mice. *Biomedicine & Aging Pathology*, 4, 95–104.

Rhodes, C., Thomas, M., Athis, J. (1993). Principles of testing for acute toxic effects. In: General and Applied Toxicology. Vol 1 (Ballantyne B, Marrs T, Turner P, eds). New York: Stockton Press, 49-87.

Rollinger, J. M., Langer, T., and Stuppner, H. (2006). Strategies for efficient lead structure discovery from natural products. *Current medicinal chemistry*, 13(13), 1491–1507. <https://doi.org/10.2174/092986706777442075>

- Rubio-Perez, J. M., and Morillas-Ruiz, J. M. (2012). A review: inflammatory process in Alzheimer's disease, role of cytokines. *The Scientific World Journal*, 2012, 756357. <https://doi.org/10.1100/2012/756357>
- Saha, R., and Tomar, J. M. S., and Ghosh, P. K. (2007). Evaluation and selection of multipurpose tree for improving soil hydro-physical behavior under hilly ecosystem of Northeast India. *Agroforestry Systems*, 69, 239-247. <https://doi.org/10.1007/s10457-007-9044-y>
- Salam, J., S., Singh, P., K., Dutta, B., K., and Sahoo, U., K. (2009). Chemical composition and nutritive indices in *Parkia roxburghii*, a leguminous plant of India. *Indian Journal of Agricultural Biochemistry*, 22(2), 87–93.
- Salomone, S., Caraci, F., Leggio, G. M., Fedotova, J., and Drago, F. (2012). New pharmacological strategies for treatment of Alzheimer's disease: focus on disease modifying drugs. *British journal of clinical pharmacology*, 73(4), 504–517. <https://doi.org/10.1111/j.1365-2125.2011.04134.x>
- Salter, M. W., and Stevens, B. (2017). Microglia emerge as central players in brain disease. *Nature medicine*, 23(9), 1018–1027. <https://doi.org/10.1038/nm.4397>
- Sanchez-Varo, R., Trujillo-Estrada, L., Sanchez-Mejias, E., Torres, M., Baglietto-Vargas, D., Moreno-Gonzalez, I., De Castro, V., Jimenez, S., Ruano, D., Vizuite, M., Davila, J. C., Garcia-Verdugo, J. M., Jimenez, A. J., Vitorica, J., and Gutierrez, A. (2012). Abnormal accumulation of autophagic vesicles correlates with axonal and synaptic pathology in young Alzheimer's mice hippocampus. *Acta neuropathologica*, 123(1), 53–70. <https://doi.org/10.1007/s00401-011-0896-x>
- Sass, N. (2000). Humane endpoints and acute toxicity testing. *ILAR journal*, 41(2), 114–123. <https://doi.org/10.1093/ilar.41.2.114>
- Schmidtke, P., Le Guilloux, V., Maupetit, J., and Tufféry, P. (2010). fpocket: online tools for protein ensemble pocket detection and tracking. *Nucleic acids research*, 38(Web Server issue), W582–W589. <https://doi.org/10.1093/nar/gkq383>

- Schneider, G. (2013). Prediction of drug-like properties. In: Madame Curie Bioscience Database [Internet]. Landes Bioscience, 2000, 2013. <https://www.ncbi.nlm.nih.gov/books/NBK6404/>
- Schrage, A., Hempel, K., Schulz, M., Kolle, S. N., van Ravenzwaay, B., and Landsiedel, R. (2011). Refinement and reduction of acute oral toxicity testing: a critical review of the use of cytotoxicity data. *Alternatives to laboratory animals: ATLA*, 39(3), 273–295. <https://doi.org/10.1177/026119291103900311>
- Seal, T. (2011). Nutritional composition of wild edible fruits in Meghalaya state of India and their ethno-botanical importance. *Research Journal of Botany*, 6 (2), 58–67. <https://doi.org/10.3923/rjb.2011.58.67>
- Selick, H. E., Beresford, A. P., and Tarbit, M. H. (2002). The emerging importance of predictive ADME simulation in drug discovery. *Drug discovery today*, 7(2), 109–116. [https://doi.org/10.1016/s1359-6446\(01\)02100-6](https://doi.org/10.1016/s1359-6446(01)02100-6)
- Selkoe, D. J. (2001). Alzheimer's disease: genes, proteins, and therapy. *Physiological reviews*, 81(2), 741–766. <https://doi.org/10.1152/physrev.2001.81.2.741>
- Sellers, R. S., Morton, D., Michael, B., Roome, N., Johnson, J. K., Yano, B. L., Perry, R., and Schafer, K. (2007). Society of Toxicologic Pathology position paper: organ weight recommendations for toxicology studies. *Toxicologic pathology*, 35(5), 751–755. <https://doi.org/10.1080/01926230701595300>
- Selvaraj, C., Dinesh, D. C., Panwar, U., Abhirami, R., Boura, E., and Singh, S. K. (2021). Structure-based virtual screening and molecular dynamics simulation of SARS-CoV-2 Guanine-N7 methyltransferase (nsp14) for identifying antiviral inhibitors against COVID-19. *Journal of biomolecular structure & dynamics*, 39(13), 4582–4593. <https://doi.org/10.1080/07391102.2020.1778535>
- Sen, S., De, B., Devanna, N., and Chakraborty, R. (2013). Total phenolic, total flavonoid content, and antioxidant capacity of the leaves of *Meyna spinosa* Roxb., an Indian medicinal plant. *Chinese journal of natural medicines*, 11(2), 149–157. [https://doi.org/10.1016/S1875-5364\(13\)60042-4](https://doi.org/10.1016/S1875-5364(13)60042-4)

- Serrano-Pozo, A., Frosch, M. P., Masliah, E., and Hyman, B. T. (2011). Neuropathological alterations in Alzheimer disease. *Cold Spring Harbor perspectives in medicine*, 1(1), a006189. <https://doi.org/10.1101/cshperspect.a006189>
- Sharififar, F., Nudeh-dehghn, G., and Mirtajaldini, M. (2008). Major flavonoids with antioxidant activity from *Teucrium polium* L. *Food Chemistry*, 112, 885-888.
- Sharma, A., Vora, J., Patel, D., Sinha, S., Jha, P. C., and Shrivastava, N. (2022). Identification of natural inhibitors against prime targets of SARS-CoV-2 using molecular docking, molecular dynamics simulation and MM-PBSA approaches. *Journal of biomolecular structure & dynamics*, 40(7), 3296–3311. <https://doi.org/10.1080/07391102.2020.1846624>
- Sheikh, Y., Maibam, B. C., Talukdar, N. C., Deka, D. C., and Borah, J. C. (2016). In vitro and in vivo anti-diabetic and hepatoprotective effects of edible pods of *Parkia roxburghii* and quantification of the active constituent by HPLC-PDA. *Journal of ethnopharmacology*, 191, 21–28. <https://doi.org/10.1016/j.jep.2016.06.015>
- Shirts, M. R., Mobley, D. L., and Chodera, J. D. (2007). Alchemical free energy calculations: ready for prime time? *Annual Reports in Computational Chemistry*, 3, 41-59.
- Shuchang, H., Qiao, N., Piye, N., Mingwei, H., Xiaoshu, S., Feng, S., Sheng, W., and Opler, M. (2008). Protective effects of *gastrodia elata* on aluminum-chloride-induced learning impairments and alterations of amino acid neurotransmitter release in adult rats. *Restorative neurology and neuroscience*, 26(6), 467–473.
- Siddiqui, A. J., Danciu, C., Ashraf, S. A., Moin, A., Singh, R., Alreshidi, M., Patel, M., Jahan, S., Kumar, S., Alkhinjar, M. I. M., Badraoui, R., Snoussi, M., and Adnan, M. (2020). Plants-Derived Biomolecules as Potent Antiviral Phytomedicines: New Insights on Ethnobotanical Evidences against Coronaviruses. *Plants* (Basel, Switzerland), 9(9), 1244. <https://doi.org/10.3390/plants9091244>

- Singha, W. R., Kurmi, B., Sahoo, U. K., Sileshi, G. W., Nath, A. J., and Das, A. K. (2021). *Parkia roxburghii*, an underutilized tree bean for food, nutritional and regional climate security. *Trees, Forests and People*, 4, 100065. <https://doi.org/10.1016/j.tfp.2021.100065>
- Skovronsky, D. M., Lee, V. M., and Trojanowski, J. Q. (2006). Neurodegenerative diseases: new concepts of pathogenesis and their therapeutic implications. *Annual review of pathology*, 1, 151–170. <https://doi.org/10.1146/annurev.pathol.1.110304.100113>
- Snow, C. D., Sorin, E. J., Rhee, Y. M., and Pande, V. S. (2005). How well can simulation predict protein folding kinetics and thermodynamics?. *Annual review of biophysics and biomolecular structure*, 34, 43–69. <https://doi.org/10.1146/annurev.biophys.34.040204.144447>
- Soldatow, V. Y., Lecluyse, E. L., Griffith, L. G., and Rusyn, I. (2013). In vitro models for liver toxicity testing. *Toxicology research*, 2(1), 23–39. <https://doi.org/10.1039/C2TX20051A>
- Song, H. L., Demirev, A. V., Kim, N. Y., Kim, D. H., and Yoon, S. Y. (2019). Ouabain activates transcription factor EB and exerts neuroprotection in models of Alzheimer's disease. *Molecular and cellular neurosciences*, 95, 13–24. <https://doi.org/10.1016/j.mcn.2018.12.007>
- Sripriya, S., Ranjith, K. M., Karthick, A. N., Bhuvaneswari, S., and Prakash, U. N. K., (2021). In silico evaluation of multispecies toxicity of natural compounds. *Drug and chemical toxicology*, 44(5), 480–486. <https://doi.org/10.1080/01480545.2019.1614023>
- Suarez-Torres, J. D., Ciangherotti, C. E., and Jimenez-Orozco, F. A. (2020). The predictivity of the -alert performance- functionality of the OECD QSAR-Toolbox (c/w further issues on the predictivity of nonclinical testing). *Toxicology in vitro: an international journal published in association with BIBRA*, 66, 104858. <https://doi.org/10.1016/j.tiv.2020.104858>

- Sugimoto, H., Ogura, H., Arai, Y., Limura, Y., and Yamanishi, Y. (2002). Research and development of donepezil hydrochloride, a new type of acetylcholinesterase inhibitor. *Japanese journal of pharmacology*, 89(1), 7–20. <https://doi.org/10.1254/jjp.89.7>
- Suh, Y. H., and Checler, F. (2002). Amyloid precursor protein, presenilins, and alpha-synuclein: molecular pathogenesis and pharmacological applications in Alzheimer's disease. *Pharmacological reviews*, 54(3), 469–525. <https://doi.org/10.1124/pr.54.3.469>
- Swerdlow, R. H., and Khan, S. M. (2004). A "mitochondrial cascade hypothesis" for sporadic Alzheimer's disease. *Medical hypotheses*, 63(1), 8–20. <https://doi.org/10.1016/j.mehy.2003.12.045>
- Tabernilla, A., Dos Santos Rodrigues, B., Pieters, A., Caufriez, A., Leroy, K., Van Campenhout, R., Cooreman, A., Gomes, A. R., Arnesdotter, E., Gijbels, E., and Vinken, M. (2021). In Vitro Liver Toxicity Testing of Chemicals: A Pragmatic Approach. *International journal of molecular sciences*, 22(9), 5038. <https://doi.org/10.3390/ijms22095038>
- Taidi, L., Maurady, A., and Britel, M. R. (2022). Molecular docking study and molecular dynamic simulation of human cyclooxygenase-2 (COX-2) with selected eutypoids. *Journal of biomolecular structure & dynamics*, 40(3), 1189–1204. <https://doi.org/10.1080/07391102.2020.1823884>
- Tamagno, E., Guglielmotto, M., Monteleone, D., Vercelli, A., and Tabaton, M. (2012). Transcriptional and post-transcriptional regulation of β -secretase. *IUBMB life*, 64(12), 943–950. <https://doi.org/10.1002/iub.1099>
- Tapan, S. (2011). Evaluation of antioxidant activity of some wild edible fruits of Meghalaya state in India. *International Journal of Pharmacy and Pharmaceutical Sciences*, 3(4), 233–236. <https://doi.org/10.5897/IJNAM11.060>
- Tarragon, E., Lopez, D., Estrada, C., Ana, G. C., Schenker, E., Pifferi, F., Bordet, R., Richardson, J. C., and Herrero, M. T. (2013). Octodon degus: a model for the

- cognitive impairment associated with Alzheimer's disease. *CNS neuroscience & therapeutics*, 19(9), 643–648. <https://doi.org/10.1111/cns.12125>
- Teixeira, J., Silva, T., Andrade, P. B., and Borges, F. (2013). Alzheimer's disease and antioxidant therapy: how long how far?. *Current medicinal chemistry*, 20(24), 2939–2952. <https://doi.org/10.2174/1871523011320240001>
- Teo, S., Stirling, D., Thomas, S., Hoberman, A., Kiorpes, A., and Khetani, V. (2002). A 90-day oral gavage toxicity study of D-methylphenidate and D,L-methylphenidate in Sprague-Dawley rats. *Toxicology*, 179(3), 183–196. [https://doi.org/10.1016/s0300-483x\(02\)00338-4](https://doi.org/10.1016/s0300-483x(02)00338-4)
- Terry, A. V., Jr, and Buccafusco, J. J. (2003). The cholinergic hypothesis of age and Alzheimer's disease-related cognitive deficits: recent challenges and their implications for novel drug development. *The Journal of pharmacology and experimental therapeutics*, 306(3), 821–827. <https://doi.org/10.1124/jpet.102.041616>
- Thangjam R. (2014). Inter-simple sequence repeat (ISSR) marker analysis in *Parkia timoriana* (DC.) Merr. populations from Northeast India. *Applied biochemistry and biotechnology*, 172(4), 1727–1734. <https://doi.org/10.1007/s12010-013-0639-7>
- Thawkar, B. S., and Kaur, G. (2019). Inhibitors of NF- κ B and P2X7/NLRP3/Caspase 1 pathway in microglia: Novel therapeutic opportunities in neuroinflammation induced early-stage Alzheimer's disease. *Journal of neuroimmunology*, 326, 62–74. <https://doi.org/10.1016/j.jneuroim.2018.11.010>
- Theodoridis, G., Gika, H. G., and Wilson, I. D. (2011). Mass spectrometry-based holistic analytical approaches for metabolite profiling in systems biology studies. *Mass spectrometry reviews*, 30(5), 884–906. <https://doi.org/10.1002/mas.20306>
- Thirunavukkarasu, S. V., Venkataraman, S., Raja, S., and Upadhyay, L. (2012). Neuroprotective effect of Manasamitra vatakam against aluminum induced cognitive impairment and oxidative damage in the cortex and hippocampus of

- rat brain. *Drug and chemical toxicology*, 35(1), 104–115.
<https://doi.org/10.3109/01480545.2011.589442>
- Thrall, M.A., and Weiser, M.G. (2002). Hematology in laboratory procedures for veterinary technicians. In: Hendrix, C.M. (Ed.), Saint Louis, MO, fourth ed. Mosby, USA, 29–74.
- Tosun, M., Ercisli, S., Sengul, M., Ozer, H., Polat, T., and Ozturk, E. (2009). Antioxidant properties and total phenolic content of eight *Salvia* species from Turkey. *Biological research*, 42(2), 175–181.
- Trinder, P. (1969). Enzymatic calorimetric determination of triglycerides by GOP-PAP method. *Annals of Clinical Biochemistry*. 6, 24–27.
- Trott, O., and Olson, A. J. (2010). AutoDock Vina: improving the speed and accuracy of docking with a new scoring function, efficient optimization, and multithreading. *Journal of computational chemistry*, 31(2), 455–461.
<https://doi.org/10.1002/jcc.21334>
- Truong, H., Nguyen, D., Ta, N., Bui Anh, V., Do, T., and Nguyen, H. C. (2019). Evaluation of the Use of Different Solvents for Phytochemical Constituents, Antioxidants, and In Vitro Anti-Inflammatory Activities of *Severinia buxifolia*. *Journal of Food Quality*. 2019. 1-9. <https://doi.org/10.1155/2019/8178294>
- Tuccinardi T. (2009). Docking-based virtual screening: recent developments. *Combinatorial chemistry & high throughput screening*, 12(3), 303–314.
<https://doi.org/10.2174/138620709787581666>
- U.S.E.P.A, ECOTOX Database, (2016) Available from: <http://cfpub.epa.gov/ecotox/>
- Ugwah-Oguejiofor, C. J., Okoli, C. O., Ugwah, M. O., Umaru, M. L., Ogbulie, C. S., Mshelia, H. E., Umar, M., and Njan, A. A. (2019). Acute and sub-acute toxicity of aqueous extract of aerial parts of *Caralluma dalzielii* N. E. Brown in mice and rats. *Heliyon*, 5(1), e01179. <https://doi.org/10.1016/j.heliyon.2019.e01179>
- Ul Haq, F., Abro, A., Raza, S., Liedl, K. R., and Azam, S. S. (2017). Molecular dynamics simulation studies of novel β -lactamase inhibitor. *Journal of*

molecular graphics & modelling, 74, 143–152.
<https://doi.org/10.1016/j.jmgm.2017.03.002>

Upadhyay, P., Shukla, R., and Mishra, S. K. (2019). Acute and sub-acute toxicity study of hydro-alcoholic leaves extract of *Reinwardtia indica* in rats. *Biomedicine & pharmacotherapy= Biomedecine & pharmacotherapie*, 111, 36–41.
<https://doi.org/10.1016/j.biopha.2018.12.056>

Vaidya, A. D., and Devasagayam, T. P. (2007). Current status of herbal drugs in India: an overview. *Journal of clinical biochemistry and nutrition*, 41(1), 1–11.
<https://doi.org/10.3164/jcbtn.2007001>

Valerio, L. G., Jr, Arvidson, K. B., Chanderbhan, R. F., and Contrera, J. F. (2007). Prediction of rodent carcinogenic potential of naturally occurring chemicals in the human diet using high-throughput QSAR predictive modeling. *Toxicology and applied pharmacology*, 222(1), 1–16.
<https://doi.org/10.1016/j.taap.2007.03.012>

Vallés, S. L., Borrás, C., Gambini, J., Furriol, J., Ortega, A., Sastre, J., Pallardó, F. V., and Viña, J. (2008). Oestradiol or genistein rescues neurons from amyloid beta-induced cell death by inhibiting activation of p38. *Aging cell*, 7(1), 112–118.
<https://doi.org/10.1111/j.1474-9726.2007.00356.x>

Van der Borght, K., Havekes, R., Bos, T., Eggen, B. J., and Van der Zee, E. A. (2007). Exercise improves memory acquisition and retrieval in the Y-maze task: relationship with hippocampal neurogenesis. *Behavioral neuroscience*, 121(2), 324–334. <https://doi.org/10.1037/0735-7044.121.2.324>

Van der Mussele, S., Le Bastard, N., Saelens, J., Somers, N., Mariën, P., Goeman, J., De Deyn, P. P., and Engelborghs, S. (2015). Agitation-associated behavioral symptoms in mild cognitive impairment and Alzheimer's dementia. *Aging & mental health*, 19(3), 247–257. <https://doi.org/10.1080/13607863.2014.924900>

van Dyck, C. H., Swanson, C. J., Aisen, P., Bateman, R. J., Chen, C., Gee, M., Kanekiyo, M., Li, D., Reyderman, L., Cohen, S., Froelich, L., Katayama, S., Sabbagh, M., Vellas, B., Watson, D., Dhadda, S., Irizarry, M., Kramer, L. D., and

- Iwatsubo, T. (2023). Lecanemab in Early Alzheimer's Disease. *The New England journal of medicine*, 388(1), 9–21. <https://doi.org/10.1056/NEJMoa2212948>
- Van Norman, G. A. (2020). Limitations of Animal Studies for Predicting Toxicity in Clinical Trials: Part 2: Potential Alternatives to the Use of Animals in Preclinical Trials. *JACC. Basic to translational science*, 5(4), 387–397. <https://doi.org/10.1016/j.jacbts.2020.03.010>
- van Wyk, A. S., and Prinsloo, G. (2020). Health, safety and quality concerns of plant-based traditional medicines and herbal remedies. *South African Journal of Botany*, 133, 54. <https://doi.org/10.1016/j.sajb.2020.06.031>
- Vardy, E. R., Catto, A. J., and Hooper, N. M. (2005). Proteolytic mechanisms in amyloid-beta metabolism: therapeutic implications for Alzheimer's disease. *Trends in molecular medicine*, 11(10), 464–472. <https://doi.org/10.1016/j.molmed.2005.08.004>
- Veber, D. F., Johnson, S. R., Cheng, H. Y., Smith, B. R., Ward, K. W., and Kopple, K. D. (2002). Molecular properties that influence the oral bioavailability of drug candidates. *Journal of medicinal chemistry*, 45(12), 2615–2623. <https://doi.org/10.1021/jm020017n>
- Venigalla, M., Gyengesi, E., and Münch, G. (2015). Curcumin and Apigenin - novel and promising therapeutics against chronic neuroinflammation in Alzheimer's disease. *Neural regeneration research*, 10(8), 1181–1185. <https://doi.org/10.4103/1673-5374.162686>
- Venugopal, P. P., Das, B. K., Soorya, E., and Chakraborty, D. (2020). Effect of hydrophobic and hydrogen bonding interactions on the potency of β -alanine analogs of G-protein coupled glucagon receptor inhibitors. *Proteins*, 88(2), 327–344. <https://doi.org/10.1002/prot.25807>
- Villaflors, O. B., Chen, Y. J., Chen, C. P., Yeh, J. M., and Wu, T. Y. (2012). Effects of curcumin and demethoxycurcumin on amyloid- β precursor and tau proteins through the internal ribosome entry sites: a potential therapeutic for Alzheimer's

- disease. *Taiwanese journal of obstetrics & gynecology*, 51(4), 554–564.
<https://doi.org/10.1016/j.tjog.2012.09.010>
- Villemagne, V. L., Burnham, S., Bourgeat, P., Brown, B., Ellis, K. A., Salvado, O., Szoek, C., Macaulay, S. L., Martins, R., Maruff, P., Ames, D., Rowe, C. C., Masters, C. L., and Australian Imaging Biomarkers and Lifestyle (AIBL) Research Group (2013). Amyloid β deposition, neurodegeneration, and cognitive decline in sporadic Alzheimer's disease: a prospective cohort study. *The Lancet. Neurology*, 12(4), 357–367. [https://doi.org/10.1016/S1474-4422\(13\)70044-9](https://doi.org/10.1016/S1474-4422(13)70044-9)
- Walton, J. R. (2007). An aluminum-based rat model for Alzheimer's disease exhibits oxidative damage, inhibition of PP2A activity, hyperphosphorylated tau, and granulovacuolar degeneration. *Journal of inorganic biochemistry*, 101(9), 1275–1284. <https://doi.org/10.1016/j.jinorgbio.2007.06.001>
- Walum, E. (1998). Acute oral toxicity. *Environmental health perspectives*, 106 Suppl 2(Suppl 2), 497–503. <https://doi.org/10.1289/ehp.98106497>
- Wang, X., Wang, W., Li, L., Perry, G., Lee, H. G., and Zhu, X. (2014). Oxidative stress and mitochondrial dysfunction in Alzheimer's disease. *Biochimica et biophysica acta*, 1842(8), 1240–1247. <https://doi.org/10.1016/j.bbadis.2013.10.015>
- Waring, M. J., Arrowsmith, J., Leach, A. R., Leeson, P. D., Mandrell, S., Owen, R. M., Pairaudeau, G., Pennie, W. D., Pickett, S. D., Wang, J., Wallace, O., and Weir, A. (2015). An analysis of the attrition of drug candidates from four major pharmaceutical companies. *Nature reviews. Drug discovery*, 14(7), 475–486. <https://doi.org/10.1038/nrd4609>
- Wassenaar, P. N. H., Verbruggen, E. M. J., Cieraad, E., Peijnenburg, W. J. G. M., and Vijver, M. G. (2020). Variability in fish bioconcentration factors: Influences of study design and consequences for regulation. *Chemosphere*, 239, 124731. <https://doi.org/10.1016/j.chemosphere.2019.124731>

- Watkins, P. B., Zimmerman, H. J., Knapp, M. J., Gracon, S. I., and Lewis, K. W. (1994). Hepatotoxic effects of tacrine administration in patients with Alzheimer's disease. *JAMA*, 271(13), 992–998.
- Wei, M. C., Zong, W. X., Cheng, E. H., Lindsten, T., Panoutsakopoulou, V., Ross, A. J., Roth, K. A., MacGregor, G. R., Thompson, C. B., and Korsmeyer, S. J. (2001). Proapoptotic BAX and BAK: a requisite gateway to mitochondrial dysfunction and death. *Science* (New York, N.Y.), 292(5517), 727–730. <https://doi.org/10.1126/science.1059108>
- Willhite, C. C., Karyakina, N. A., Yokel, R. A., Yenugadhati, N., Wisniewski, T. M., Arnold, I. M., Momoli, F., and Krewski, D. (2014). Systematic review of potential health risks posed by pharmaceutical, occupational and consumer exposures to metallic and nanoscale aluminum, aluminum oxides, aluminum hydroxide and its soluble salts. *Critical reviews in toxicology*, 44 Suppl 4(Suppl 4), 1–80. <https://doi.org/10.3109/10408444.2014.934439>
- Williams, M. D., Reeves, R., Resar, L. S., and Hill, H. H., Jr (2013). Metabolomics of colorectal cancer: past and current analytical platforms. *Analytical and bioanalytical chemistry*, 405(15), 5013–5030. <https://doi.org/10.1007/s00216-013-6777-5>
- Wincewicz, D., and Braszko, J. J. (2014). Telmisartan attenuates cognitive impairment caused by chronic stress in rats. *Pharmacological reports: PR*, 66(3), 436–441. <https://doi.org/10.1016/j.pharep.2013.11.002>
- Woo, Y., and Lai, D. (2003). Mechanisms of action of chemical carcinogens, and their role in Structure-Activity Relationships (SAR) analysis and risk assessment. In: Benigni R (ed) Quantitative Structure-Activity Relationship (QSAR) models of mutagens and carcinogens. CRC, Boca Raton, FL, 41–80.
- World Health Organization (2023). Dementia, accessed July 31, 2023, <https://www.who.int/news-room/facts-in-pictures/detail/dementia>.

- Wu, X., Xu, L. Y., Li, E. M., and Dong, G. (2022). Application of molecular dynamics simulation in biomedicine. *Chemical biology & drug design*, 99(5), 789–800. <https://doi.org/10.1111/cbdd.14038>
- Wu, Y., and Wang, G. (2018). Machine Learning Based Toxicity Prediction: From Chemical Structural Description to Transcriptome Analysis. *International journal of molecular sciences*, 19(8), 2358. <https://doi.org/10.3390/ijms19082358>
- Xie, X., Wang, H. T., Li, C. L., Gao, X. H., Ding, J. L., Zhao, H. H., and Lu, Y. L. (2010). Ginsenoside Rb1 protects PC12 cells against β -amyloid-induced cell injury. *Molecular medicine reports*, 3(4), 635–639. https://doi.org/10.3892/mmr_00000308
- Xiong, G., Wu, Z., Yi, J., Fu, L., Yang, Z., Hsieh, C., Yin, M., Zeng, X., Wu, C., Lu, A., Chen, X., Hou, T., and Cao, D. (2021). ADMETlab 2.0: an integrated online platform for accurate and comprehensive predictions of ADMET properties. *Nucleic acids research*, 49(W1), W5–W14. <https://doi.org/10.1093/nar/gkab255>
- Xu, C., Cheng, F., Chen, L., Du, Z., Li, W., Liu, G., Lee, P. W., and Tang, Y. (2012). In silico prediction of chemical Ames mutagenicity. *Journal of chemical information and modeling*, 52(11), 2840–2847. <https://doi.org/10.1021/ci300400a>
- Xu, Q. Q., Su, Z. R., Yang, W., Zhong, M., Xian, Y. F., and Lin, Z. X. (2023). Patchouli alcohol attenuates the cognitive deficits in a transgenic mouse model of Alzheimer's disease via modulating neuropathology and gut microbiota through suppressing C/EBP β /AEP pathway. *Journal of neuroinflammation*, 20(1), 19. <https://doi.org/10.1186/s12974-023-02704-1>
- Yakubu, M. T., Akanji, M. A., and Oladiji, A. T. (2007). Hematological evaluation in male albino rats following chronic administration of aqueous extract of *Fadogia agrestis* stem. *Pharmacognosy Magazine*, 3: 34.

- Yargicoglu, P., Sahin, E., Gümüşlü, S., and Açar, A. (2007). The effect of sulfur dioxide inhalation on active avoidance learning, antioxidant status and lipid peroxidation during aging. *Neurotoxicology and teratology*, 29(2), 211–218. <https://doi.org/10.1016/j.ntt.2006.11.002>
- Ye, H., Nelson, L. J., Gómez Del Moral, M., Martínez-Naves, E., and Cubero, F. J. (2018). Dissecting the molecular pathophysiology of drug-induced liver injury. *World journal of gastroenterology*, 24(13), 1373–1385. <https://doi.org/10.3748/wjg.v24.i13.1373>
- Yin, S., Ran, Q., Yang, J., Zhao, Y., and Li, C. (2020). Nootropic effect of neferine on aluminum chloride-induced Alzheimer's disease in experimental models. *Journal of biochemical and molecular toxicology*, 34(2), e22429. <https://doi.org/10.1002/jbt.22429>
- Youn, K., Park, J. H., Lee, S., Lee, S., Lee, J., Yun, E. Y., Jeong, W. S., and Jun, M. (2018). BACE1 Inhibition by Genistein: Biological Evaluation, Kinetic Analysis, and Molecular Docking Simulation. *Journal of medicinal food*, 21(4), 416–420. <https://doi.org/10.1089/jmf.2017.4068>
- Yu, Y. C., Mao, Y. M., Chen, C. W., Chen, J. J., Chen, J., Cong, W. M., Ding, Y., Duan, Z. P., Fu, Q. C., Guo, X. Y., Hu, P., Hu, X. Q., Jia, J. D., Lai, R. T., Li, D. L., Liu, Y. X., Lu, L. G., Ma, S. W., Ma, X., Nan, Y. M., ... Chinese Medical Association (CMA) (2017). CSH guidelines for the diagnosis and treatment of drug-induced liver injury. *Hepatology international*, 11(3), 221–241. <https://doi.org/10.1007/s12072-017-9793-2>
- Yuriev, E., Agostino, M., and Ramsland, P. A. (2011). Challenges and advances in computational docking: 2009 in review. *Journal of molecular recognition: JMR*, 24(2), 149–164. <https://doi.org/10.1002/jmr.1077>
- Yusuf, S., Adelaiye, B. A., and Agunu, A. (2009). Effect of Ziziphus mauritania (L.) seed extracts on spatial recognition memory of rats as measured by the Y-maze test. *Journal of Natural Products*, 2, 31–39.

- Zatta, P., Zambenedetti, P., Bruna, V., and Filippi, B. (1994). Activation of acetylcholinesterase by aluminum(III): the relevance of the metal species. *Neuroreport*, 5(14), 1777–1780. <https://doi.org/10.1097/00001756-199409080-00023>
- Zhang, A., Sun, H., Wang, P., Han, Y., and Wang, X. (2012). Modern analytical techniques in metabolomics analysis. *The Analyst*, 137(2), 293–300. <https://doi.org/10.1039/c1an15605e>
- Zhang, B., Gaiteri, C., Bodea, L. G., Wang, Z., McElwee, J., Podtelezhnikov, A. A., Zhang, C., Xie, T., Tran, L., Dobrin, R., Fluder, E., Clurman, B., Melquist, S., Narayanan, M., Suver, C., Shah, H., Mahajan, M., Gillis, T., Mysore, J., MacDonald, M. E., ... Emilsson, V. (2013). Integrated systems approach identifies genetic nodes and networks in late-onset Alzheimer's disease. *Cell*, 153(3), 707–720. <https://doi.org/10.1016/j.cell.2013.03.030>
- Zhang, J. H., Zhang, Y., and Herman, B. (2003). Caspases, apoptosis and aging. *Ageing research reviews*, 2(4), 357–366. [https://doi.org/10.1016/s1568-1637\(03\)00026-6](https://doi.org/10.1016/s1568-1637(03)00026-6)
- Zhang, M., Cao, J., Dai, X., Chen, X., and Wang, Q. (2012). Flavonoid Contents and Free Radical Scavenging Activity of Extracts from Leaves, Stems, Rachis and Roots of *Dryopteris erythrosora*. *Iranian journal of pharmaceutical research: IJPR*, 11(3), 991–997.
- Zhang, R., Xue, G., Wang, S., Zhang, L., Shi, C., and Xie, X. (2012). Novel object recognition as a facile behavior test for evaluating drug effects in A β PP/PS1 Alzheimer's disease mouse model. *Journal of Alzheimer's disease : JAD*, 31(4), 801–812. <https://doi.org/10.3233/JAD-2012-120151>
- Zhao, C., Boriani, E., Chana, A., Roncaglioni, A., and Benfenati, E. (2008). A new hybrid system of QSAR models for predicting bioconcentration factors (BCF). *Chemosphere*, 73(11), 1701–1707. <https://doi.org/10.1016/j.chemosphere.2008.09.033>

- Zhao, J., Fu, Y., Yasvoina, M., Shao, P., Hitt, B., O'Connor, T., Logan, S., Maus, E., Citron, M., Berry, R., Binder, L., and Vassar, R. (2007). Beta-site amyloid precursor protein cleaving enzyme 1 levels become elevated in neurons around amyloid plaques: implications for Alzheimer's disease pathogenesis. *The Journal of neuroscience: the official journal of the Society for Neuroscience*, 27(14), 3639–3649. <https://doi.org/10.1523/JNEUROSCI.4396-06.2007>
- Zhao, Y., and Zhao, B. (2013). Oxidative stress and the pathogenesis of Alzheimer's disease. *Oxidative medicine and cellular longevity*, 2013, 316523. <https://doi.org/10.1155/2013/316523>
- Zhao, Y., Dang, M., Zhang, W., Lei, Y., Ramesh, T., Veeraraghavan, V. P., and Hou, X. (2020). Neuroprotective effects of Syringic acid against aluminum chloride induced oxidative stress mediated neuroinflammation in rat model of Alzheimer's disease. *Journal of Functional Foods*, 71, 104009. <https://doi.org/10.1016/j.jff.2020.104009>
- Zhao, Y., Hill, J. M., Bhattacharjee, S., Percy, M. E., Pogue, A. I., and Lukiw, W. J. (2014). Aluminum-induced amyloidogenesis and impairment in the clearance of amyloid peptides from the central nervous system in Alzheimer's disease. *Frontiers in neurology*, 5, 167. <https://doi.org/10.3389/fneur.2014.00167>
- Zhong, B. R., Zhou, G. F., Song, L., Wen, Q. X., Deng, X. J., Ma, Y. L., Hu, L. T., and Chen, G. J. (2021). TUFM is involved in Alzheimer's disease-like pathologies that are associated with ROS. *FASEB journal: official publication of the Federation of American Societies for Experimental Biology*, 35(5), e21445. <https://doi.org/10.1096/fj.202002461R>
- Zhou, X., Li, Y., Shi, X., and Ma, C. (2016). An overview on therapeutics attenuating amyloid β level in Alzheimer's disease: targeting neurotransmission, inflammation, oxidative stress and enhanced cholesterol levels. *American journal of translational research*, 8(2), 246–269.
- Zhu, H., Martin, T. M., Ye, L., Sedykh, A., Young, D. M., and Tropsha, A. (2009). Quantitative structure-activity relationship modeling of rat acute toxicity by oral

exposure. *Chemical research in toxicology*, 22(12), 1913–1921.
<https://doi.org/10.1021/tx900189p>

Zou, H., Li, Y., Liu, X., and Wang, X. (1999). An APAF-1.cytochrome c multimeric complex is a functional apoptosome that activates procaspase-9. *The Journal of biological chemistry*, 274(17), 11549–11556.
<https://doi.org/10.1074/jbc.274.17.11549>

BRIEF BIO-DATA OF THE CANDIDATE

Name : Nisekphoto Nisa

Father's Name : Kekoyato Nisa

Mobile : +91 7085121322; +91 9089580431

Email id : edwinnisa1996@gmail.com

Gender : Male

Date of Birth : 07-08-1996

Marital Status : Single

Religion : Christian

Nationality : Indian

Permanent address : Jotsoma Village, Kohima-797002, Nagaland

Address for correspondence: Department of Zoology, Mizoram University,
Aizawl-796004, Mizoram

Educational Qualification:

Course	Institute Name	Year of Passing	Marks Percentage
HSLC	St. Andrew's School Jotsoma	2012	78.67
HSSLC	Kohima Science College Jotsoma	2014	77.4
B.Sc. (Hons)	Kohima Science College Jotsoma	2017	94.2
M.Sc. (Zoology)	Kohima Science College Jotsoma	2019	82.2
Additional qualification			
Exam	Year of passing		Ranking
CSIR NET JRF	2020		121 (AIR)
CSIR SRF	2022		

LIST OF CONFERENCE/WORKSHOP/SEMINAR ATTENDED

1. Presented a paper entitled ‘Screening of polyphenols from *Parkia* spp. as a potential inhibitor of β -site amyloid precursor protein cleaving enzyme 1 (BACE1): an in-silico molecular docking, molecular dynamics simulation and MM/PBSA binding energy study’ at the International Conference on “Bioresources & Bioeconomy” organized by the Department of Botany, Nagaland University, Lumami, Nagaland. September, 2022.
2. Presented a paper entitled ‘Bioactive compounds from honey-bee products as potential inhibitors of β -site APP cleaving enzyme 1 (BACE-1): an in silico molecular docking, molecular dynamics simulation and MM-PBSA binding energy studies’ at the 3rd International Conference on “Traditional and Alternative Medicine” organized by the Conference Mind, Goa, India in November, 2022.
3. Participated in the National Workshop on “Molecular phylogeny and molecular docking” organized by the Department of Zoology, Mizoram University in January, 2021.
4. Participated in the National Workshop on “Bee keeping and management” organized by the Department of Zoology, Mizoram University in January, 2021.
5. Participated in the National Workshop on “Sequence to Database & Database to Sequence” organized by the Department of Zoology, Mizoram University in January, 2021.
6. Participated in the National Workshop on “Statistical data analysis and interpretation” organized by the Department of Zoology, Mizoram University in January, 2021.
7. Participated in the National Workshop on “Basic and advanced molecular techniques” organized by the Department of Zoology, Mizoram University in January, 2021.
8. Participated in the National Workshop on “Basic and advanced molecular techniques” organized by the Department of Zoology, Mizoram University in January, 2021.

9. Participated in the National Workshop on “Computer-aided Molecular Modeling & Drug Discovery” organized by the Center for Bioinformatics, Computational and Systems Biology, PRTF, Noida in 2021.
10. Participated in the Online Skill Development Program “DATA INTERPRETATION OF GCMS & LCMS” organized by CytoGene Research & Development, Lucknow in March, 2022.
11. Participated in the International Workshop on “The Value and Interconnections of Human, Animal, Plant, and Microorganisms: Metataxonomics and Metagenomics Approach” organized by the Department of Zoology, Mizoram University in March, 2023.
12. Participated in the International Workshop on “Computational Genomics With R: A Hands-On Course on NGS Data Analysis” organized by the Department of Zoology, Mizoram University in March, 2023.
13. Participated in the International Workshop on “Nanopore Sequencing and Data Analysis: Opportunities for Rapid Biodiversity and Biosurveillance Programs and Local Capacity Building” organized by the Department of Zoology, Mizoram University in March, 2023.
14. Participated in the webinar on “Introduction to data visualization using R-Studio for Biologists” organized by the NyBerMan Bioinformatique d’Europe in April, 2023.



CERTIFICATE OF RECOGNITION

This certificate goes to


Mr. Nisekphoto Nisa

Department of Zoology, Mizoram University Aizawl-796004, Mizoram, India


For his phenomenal and worthy oral presentation with the paper entitled

"Bioactive compounds from honey-bee products as potential inhibitors of β -site APP cleaving enzyme 1 (BACE-1): an in silico molecular docking, molecular dynamics simulation and MM-PBSA binding energy studies" & contribution as a speaker at the **3rd International Hybrid**

Conference on Traditional & Alternative Medicine, was held on **November 17-18, 2022**
at **Goa, India.**


Dr. K. Radhakrishnan
Principal Scientist (Retd.), JNTBGL, Palode,
Thiruvananthapuram, Kerala State, India,
or Former Chief Executive Officer in Charge,
State Medicinal Plants Board, Kerala State, India.
(ORGANIZING COMMITTEE MEMBER)


Dr. Murat Topoglu
President
Turkish Acupuncture Society, Turkey
(Session Chair)


Dr. Mohammad Bagher Rezaee
Chairman, Iranian Society of Medicinal
Plants, Iran (Session Co-Chair)


CMTRMS1088 Activate Window
Go to Settings to activate
<https://www.conferencemind.com/>



International Conference on 'Bioresources & Bioeconomy' (ICBB-2022)

Organized By
Department of Botany, Nagaland University, Lumami 798627, Nagaland, India

In Collaboration With

Nagaland Forest Management Project, Department of Environment,
Forest and Climate Change, Govt. of Nagaland, India.
September 19-21, 2022

CERTIFICATE OF PRESENTATION

This is to certify that

Mr./Miss/Dr. Nisekphoto Nisa of Mizoram University, India

has presented a paper (Oral/poster) titled

'Screening of Polyphenols from Parkia spp. as a Potential Inhibitor of β -site Amyloid Precursor Protein Cleaving Enzyme 1 (BACE1): an in silico Molecular Docking, Molecular Dynamics Simulation and MM/PBSA Binding Energy Study' in the ICBB-2022 organized by the Department of Botany, Nagaland University, Lumami 798627, Nagaland, India, held on September 19-21, 2022.


(Prof. M. S. Rawat)
Dean, School of Sciences


(Prof. Chitta Ranjan Deb)
Convener cum Organizing Secretary
ICBB-22

LIST OF RESEARCH PUBLICATIONS

1. **Nisa, N.**, Rasmita, B., Arati, C., Uditraj, C., Siddhartha, R., Dinata, R., Bhanushree, B., Bidanchi, R. M., Manikandan, B., Laskar, S. A., Abinash, G., Pori, B., Roy, V. K., and Gurusubramanian, G. (2023). Repurposing of phyto-ligand molecules from the honey bee products for Alzheimer's disease as novel inhibitors of BACE-1: small molecule bioinformatics strategies as amyloid-based therapy. *Environmental science and pollution research international*, 30(17), 51143–51169. <https://doi.org/10.1007/s11356-023-25943-4>
2. **Nisa, N.**, Dinata, R., Arati, C., Abdelgani-Baraka, G. A., Bhanushree, B., Bidanchi, R. M., Manikandan, B., Saeed, A. L., Abinash, G., Pori, B., Lalrinzuali, S., Khushboo, M., Indira, S., Roy, V. K., Rao, K. R. S. S., and Gurusubramanian, G. (2023). Computational toxicology and food safety assessment of *Parkia timoriana* phytoconstituents using quantitative structure-activity relationship (QSAR) modeling approaches. *Indian Journal of Biochemistry & Biophysics*, 60, 896-918. <https://doi.org/10.56042/ijbb.v60i12.6933>
3. Dinata, R., **Nisa, N.**, Arati, C., Rasmita, B., Uditraj, C., Siddhartha, R., Bhanushree, B., Saeed-Ahmed, L., Manikandan, B., Bidanchi, R. M., Abinash, G., Pori, B., Khushboo, M., Roy, V. K., and Gurusubramanian, G. (2024). Repurposing immune boosting and anti-viral efficacy of *Parkia* bioactive entities as multi-target directed therapeutic approach for SARS-CoV-2: exploration of lead drugs by drug likeness, molecular docking and molecular dynamics simulation methods. *Journal of biomolecular structure & dynamics*, 42(1), 43–81. <https://doi.org/10.1080/07391102.2023.2192797>
4. Dinata, R., Arati, C., Manikandan, B., Abinash, G., **Nisa, N.**, Bhanushree, B., Saeed, A. L., Bidanchi, R. M., Pori, B., Khushboo, Indira, S., Roy, V. K., Rao, K. R. S. S., and Gurusubramanian, G. (2023). Pharmacological and therapeutic potential of honey bee antimicrobial peptides. *Indian Journal of Biochemistry & Biophysics*, 60, 365-384. <https://doi.org/10.56042/ijbb.v60i5.552>
5. Khushboo, M., Sanjeev, S., Murthy, M. K., Sunitadevi, M., Dinata, R., Bhanushree, B., Bidanchi, R. M., **Nisa, N.**, Lalrinzuali, S., Manikandan, B.,

- Saeed, A. L., Abinash, G., Pori, B., Arati, C., Roy, V. K., and Gurusubramanian, G. (2023). Dietary phytoestrogen diosgenin interrupts metabolism, physiology, and reproduction of Swiss albino mice: Possible mode of action as an emerging environmental contaminant, endocrine disruptor and reproductive toxicant. *Food and chemical toxicology*, 176, 113798. <https://doi.org/10.1016/j.fct.2023.113798>
6. Lalrinzuali, S., Khushboo, M., Dinata, R., Bhanushree, B., **Nisa, N.**, Bidanchi, R. M., Laskar, S. A., Manikandan, B., Abinash, G., Pori, B., Roy, V. K., and Gurusubramanian, G. (2023). Long-term consumption of fermented pork fat-based diets differing in calorie, fat content, and fatty acid levels mediates oxidative stress, inflammation, redox imbalance, germ cell apoptosis, disruption of steroidogenesis, and testicular dysfunction in Wistar rats. *Environmental science and pollution research international*, 30(18), 52446–52471. <https://doi.org/10.1007/s11356-023-26018-0>
 7. Bidanchi, R. M., Lalrindika, L., Khushboo, M., Bhanushree, B., Dinata, R., Das, M., **Nisa, N.**, Lalrinzuali, S., Manikandan, B., Saeed-Ahmed, L., Sanjeev, S., Murthy, M. K., Roy, V. K., and Gurusubramanian, G. (2022). Antioxidative, anti-inflammatory and anti-apoptotic action of ellagic acid against lead acetate induced testicular and hepato-renal oxidative damages and pathophysiological changes in male Long Evans rats. *Environmental pollution* (Barking, Essex: 1987), 302, 119048. <https://doi.org/10.1016/j.envpol.2022.119048>



Repurposing of phyto-ligand molecules from the honey bee products for Alzheimer's disease as novel inhibitors of BACE-1: small molecule bioinformatics strategies as amyloid-based therapy

Nisekhot Nisa¹ · Borgohain Rasmita¹ · Chettri Arati¹ · Chetia Uditraj¹ · Rajkonwar Siddhartha¹ · Roy Dinata¹ · Baishya Bhanushree¹ · Rema Momin Bidanchi¹ · Bose Manikandan¹ · Saeed Ahmed Laskar¹ · Giri Abinash¹ · Buragohain Pori¹ · Vikas Kumar Roy¹ · Guruswami Gurusubramanian¹

Received: 25 August 2022 / Accepted: 10 February 2023
© The Author(s), under exclusive licence to Springer-Verlag GmbH Germany, part of Springer Nature 2023

Abstract

Alzheimer's disease (AD) is one of the neurodegenerative diseases, manifesting dementia, spatial disorientation, language, cognitive, and functional impairment, mainly affects the elderly population with a growing concern about the financial burden on society. Repurposing can improve the traditional progress of drug design applications and could speed up the identification of innovative remedies for AD. The pursuit of potent anti-BACE-1 drugs for AD treatment has become a hot boiler topic in the recent past and to instigate the design of novel improved inhibitors from the bee products. Drug-likeness characteristics (ADMET: absorption, distribution, metabolism, excretion, and toxicity), docking (AutoDock Vina), simulation (GROMACS), and free energy interaction (MM-PBSA, molecular mechanics Poisson–Boltzmann surface area) analyses were performed to identify the lead candidates from the bee products (500 bioactives from the honey, royal jelly, propolis, bee bread, bee wax, and bee venom) for Alzheimer's disease as novel inhibitors of BACE-1 (beta-site amyloid precursor protein cleaving enzyme (1) receptor using appropriate bioinformatics tools. Forty-four bioactive lead compounds were screened from the bee products through high throughput virtual screening on the basis of their pharmacokinetic and pharmacodynamics characteristics, showing favorable intestinal and oral absorption, bioavailability, blood brain barrier penetration, less skin permeability, and no inhibition of cytochrome P450 inhibitors. The docking score of the forty-four ligand molecules was found to be between -4 and -10.3 kcal/mol, respectively, exhibiting strong binding affinity to BACE1 receptor. The highest binding affinity was observed in the rutin (-10.3 kcal/mol), 3,4-dicaffeoylquinic acid (-9.5 kcal/mol), nemorosone (-9.5 kcal/mol), and luteolin (-8.9 kcal/mol). Furthermore, these compounds demonstrated high total binding energy -73.20 to -105.85 kJ/mol, and low root mean square deviation (0.194 – 0.202 nm), root mean square fluctuation (0.0985 – 0.1136 nm), radius of gyration (2.12 nm), number of H-bonds (0.778 – 5.436), and eigenvector values (2.39 – 3.54 nm²) in the molecular dynamic simulation, signifying restricted motion of C α atoms, proper folding and flexibility, and highly stable with compact of the BACE1 receptor with the ligands. Docking and simulation studies concluded that rutin, 3,4-dicaffeoylquinic acid, nemorosone, and luteolin are plausibly used as novel inhibitors of BACE1 to combat AD, but further in-depth experimental investigations are warranted to prove these in silico findings.

Keywords ADMET · Alzheimer's disease · BACE1 · Honeybee products · Repurposing · Molecular dynamics

Nisekhot Nisa and Vikas Kumar Roy contributed equally to this work.

Responsible Editor: Lotfi Aleya

✉ Guruswami Gurusubramanian
gurus64@yahoo.com; mzut036@mzu.edu.in

¹ Department of Zoology, Mizoram University, Aizawl, Mizoram 796004, India

Introduction

Alzheimer's disease (AD) is an irreversible progressive neurodegenerative disorder leading to deterioration in cognitive functions and changes in behavior and personality (Martins et al. 2018). AD causes cognitive and functional impairment, including dementia and disability in the older people and it is documented as a public health precedence by the WHO (Scott et al. 2016; WHO 2021). Aging is the main

Published online: 20 February 2023

Springer



Computational toxicology and food safety assessment of *Parkia timoriana* phytoconstituents using quantitative structure-activity relationship (QSAR) modeling approaches

Nisekhoto Nisa¹, Roy Dinata¹, Chettri Arati¹, Gumaa Abdelmualaa Abdelgani-Baraka¹, Baishya Bhanushree¹, Rema Momin Bidanchi¹, Bose Manikandan¹, Ahmed-Laskar Saeed¹, Giri Abinash¹, Buragohain Pori¹, Sailo Lalrinzuali¹, Maurya Khushboo¹, Sonar Indira¹, Vikas Kumar Roy¹, KRS Sambasiva Rao^{2*} & Guruswami Gurusubramanian^{2*}

¹Department of Zoology, Mizoram University (A Central University), Aizawl-796 004, Mizoram, India

²Department of Pharmacy, Mangalayatan University-Jabalpur, Jabalpur-483 001, Madhya Pradesh, India

Received 24 November 2023; revised 27 December 2023

As a lead compound, natural compounds have undergone extensive research in different enterprises. Since they might also have other adverse effects, determining their toxicity is crucial. Computational methods can circumvent the main challenges associated with assessing the toxicity of substances using *in vivo* and *in vitro* techniques, including time, money, labor, and the use of animal models. Although *Parkia timoriana* (PT) has a significant economic potential, its exploitation has yet to be thoroughly explored in terms of its toxicity and food safety. In PT seed pod extracts, 61 phytochemicals with a predominance of alkaloids, flavonoids, and terpenoids were identified using GC-MS and LC-MS/MS analysis. Utilizing the TEST, OECD QSAR toolkit, VEGA-HUB, Toxtree, and PASS tools, phytochemicals from PT were assessed for toxicity, food safety risk assessment, and biological activity. The phytochemicals were tested on multiple species, including *Daphnia magna*, *Pimephales promelas*, *Tetrahymena pyriformis*, and rats, to determine their toxicity using the QSAR-TEST tool. For aquatic and mammalian organisms, the phytochemicals from PT were shown to be hazardous in the following four hierarchical orders: i) *P. promelas*>*T. pyriformis*>*D. magna*>*R. norvegicus*, ii) *P. promelas*>*D. magna*>*T. pyriformis*>*R. norvegicus*, iii) *D. magna*>*P. promelas*>*T. pyriformis*>*R. norvegicus*, and *T. pyriformis*>*P. promelas*>*D. magna*>*R. norvegicus*. Despite being non-bioaccumulative, non-mutagenic, and non-carcinogenic in nature, the majority of phytochemicals were developmental toxins. More than half of the phytochemicals derived from PT were highly toxic (Cramer oral toxicity) and manifested negative side effects (with a lower NOAEL value). Most of the substances did not exhibit organ toxicity in the repeated dose toxicity test, were bioavailable, metabolized by cytochrome-P450 pathway, and were excreted from the body. PASS predicted that the examined phytoconstituents from PT were to demonstrate a wide range of anti-oxidant, free radical scavenger, anti-inflammatory, antiviral, anti-fungal, anti-neoplastic, antibacterial, and anti-protozoal activities. For the purpose of exploring drug discovery, additional research of the phytochemicals on *in vivo* models is advised.

Keywords: Computational toxicology, Food safety, GC-MS, LC-MS/MS, *Parkia timoriana*, Quantitative structure-activity relationship modeling, Risk assessment

Parkia timoriana (PT, Fabaceae), also known as the tree bean, is a nutritionally rich, underutilized leguminous tree that grows in northeastern India and various Southeast Asian countries. From an ethnobotanical standpoint, tree beans are significant to ethnic groups in a number of provinces of Northeast India, Burma, Bangladesh, Pakistan, China, Thailand, Malaysia, and the Gambia. Numerous ailments are treated with concoctions of bark, fruit, and leaf portions. All edible parts of this plant, from the flowers and young pods through the mature seeds, are in

seasonally high demand and offer a good supply of nutrients¹. If utilized properly, tree beans could serve as an additional source of vegetable proteins. The protein level of pods ranged from 12.1% in tender to 18.8% in mature pods, but kernels had substantially greater protein content (28.8%) than pods¹ it has been found that the pods of PT contain significant amounts of tannins, flavonoids, saponins, anthocyanins, and leuco-anthocyanins². Tree bean has been found to have antioxidant, α -glucosidase and α -amylase inhibitory, antibacterial, antidiabetic, antiproliferative, antiviral, immune boosting, and insecticidal effects. It has also been used to treat liver and skin diseases, ulcer, colon cancer, leprosy, hypertension, and painful eyes³. In the case of PT pods, leaves, and other plant parts are eaten

*Correspondence:

Phone: +91-7630079075 (Mob); +91-9862399411 (Mob)

E-mail: krssrao@yahoo.com; gurus64@yahoo.com

Repurposing immune boosting and anti-viral efficacy of *Parkia* bioactive entities as multi-target directed therapeutic approach for SARS-CoV-2: exploration of lead drugs by drug likeness, molecular docking and molecular dynamics simulation methods

Roy Dinata^a, Nisekhoto Nisa^a, Chettri Arati, Borgohain Rasmita, Chetia Uditraj, Rajkonwar Siddhartha, Baishya Bhanushree, Laskar Saeed-Ahmed, Bose Manikandan, Rema Momin Bidanchi, Giri Abinash, Buragohain Pori, Maurya Khushboo, Vikas Kumar Roy^a and Guruswami Gurusubramanian^a

Department of Zoology, Mizoram University, Aizawl, Mizoram, India

ABSTRACT

The COVID-19 pandemic has caused adverse health (severe respiratory, enteric and systemic infections) and environmental impacts that have threatened public health and the economy worldwide. Drug repurposing and small molecule multi-target directed herbal medicine therapeutic approaches are the most appropriate exploration strategies for SARS-CoV-2 drug discovery. This study identified potential multi-target-directed *Parkia* bioactive entities against SARS-CoV-2 receptors (S-protein, ACE2, TMPRSS2, RBD/ACE2, RdRp, MPro, and PLPro) using ADMET, drug-likeness, molecular docking (AutoDock, FireDock and HDOCK), molecular dynamics simulation and MM-PBSA tools. One thousand *Parkia* bioactive entities were screened out by virtual screening and forty-five bioactive phytochemicals were selected based on favorable binding affinity and acceptable pharmacokinetic and pharmacodynamics properties. The binding affinity values of *Parkia* phyto-ligands (AutoDock: -6.00—10.40 kcal/mol; FireDock: -31.00—62.02 kcal/mol; and HDOCK: -150.0—294.93 kcal/mol) were observed to be higher than the reference antiviral drugs (AutoDock: -5.90—9.10 kcal/mol; FireDock: -35.64—59.35 kcal/mol; and HDOCK: -132.82—211.87 kcal/mol), suggesting a potent modulatory action of *Parkia* bioactive entities against the SARS-CoV-2. Didymine, rutin, epigallocatechin gallate, epicatechin-3-O-gallate, hyperin, ursolic acid, lupeol, stigmasta-5,24(28)-diene-3-ol, ellagic acid, apigenin, stigmasterol, and campesterol strongly bound with the multiple targets of the SARS-CoV-2 receptors, inhibiting viral entry, attachment, binding, replication, transcription, maturation, packaging and spread. Furthermore, ACE2, TMPRSS2, and MPro receptors possess significant molecular dynamic properties, including stability, compactness, flexibility and total binding energy. Residues GLU-589, and LEU-95 of ACE2, GLN-350, HIS-186, and ASP-257 of TMPRSS2, and GLU-14, MET-49, and GLN-189 of MPro receptors contributed to the formation of hydrogen bonds and binding interactions, playing vital roles in inhibiting the activity of the receptors. Promising results were achieved by developing multi-targeted antiviral *Parkia* bioactive entities as lead and prospective candidates under a small molecule strategy against SARS-CoV-2 pathogenesis. The antiviral activity of *Parkia* bioactive entities needs to be further validated by pre-clinical and clinical trials.

ARTICLE HISTORY

Received 9 December 2022
Accepted 10 March 2023

KEYWORDS

Parkia bioactive entities;
SARS-CoV-2 receptors;
multi-target-directed-
approach; ADMET;
molecular-docking;
molecular-simulation



CONTACT G. Gurusubramanian gurus64@yahoo.com Department of Zoology, Mizoram University, Aizawl, Mizoram 796004, India

Supplemental data for this article can be accessed online at <https://doi.org/10.1080/07391102.2023.2192797>.

*These authors contributed equally to this work.

© 2023 Informa UK Limited, trading as Taylor & Francis Group

Pharmacological and therapeutic potential of honey bee antimicrobial peptides

Dinata Roy¹, Chettri Arati¹, Bose Manikandan¹, Giri Abinash¹, Nisekhoto Nisa¹, Baishya Bhanushree¹,
Laskar Saeed-Ahmed¹, Rema Momin Bidanchi¹, Buragohain Pori¹, Maurya Khushboo¹, Sonar Indira¹,
Vikas Kumar Roy¹, KRS Sambasiva Rao^{2*} & Guruswami Gurusubramanian^{1*}

¹Department of Zoology; & ²Department of Biotechnology, Mizoram University (A Central University), Aizawl-796 004, Mizoram, India

Received 13 April 2023; revised 09 June 2023

Honey bees (Apidae: Apini) and stingless bees (Apidae: Meliponini) act as the main pollinators for many wild and cultivated tropical plants, playing a vital role in the ecology, economy, and culture. Honey bees and stingless bees are one of the major sources of antimicrobial peptides/proteins (AMPs) synthesized in fat bodies and blood cells of bees. Bee AMPs are a class of small peptides having amino acid residues between 9 and 340, classified based on source, activity, structural characteristics, and amino acid-rich species. AMPs have a wide range of inhibitory effects against bacteria, fungi, parasites, and viruses. Four antimicrobial peptide families, *i.e.*, apidaecins (proline-rich), abaecin (proline-rich), hymenoptaecin (glycine-rich), and defensin (cystine-rich) are synthesized in the haemolymph, signifying a broad spectrum of antimicrobial activity. Jelleines (I-IV), royalisin, apisimin (serine-valine-rich peptide), 10 HDA, apalbumin, and apisin, which are present in royal jelly, have antimicrobial, mast cell degranulating, and hemolysis activity. Bee venom also contains several bioactive peptides, such as apamin (leucine-cystine-rich), melittin (leucine-alanine-rich), melectin (lysine-rich), adolapin, secapin (proline-rich), and tertiapin (cystine-lysine-rich). Currently, AMPs databases are displaying an essential role in exploration, identification, characterization, and annotation. Several AMPs databases (CAMP, DRAMP, APD, InverPep, LAMP, ADAPTABLE, ADAM, AntiBP, AMPper, AVPPred, EFC-FCBF, and class AMP) are open-access resources that have been developed to enhance research on antimicrobial peptides. Bee immune responses are composed of a multifaceted group of individual immune mechanisms and special types of behavioral adaptations. Given the importance of drug discovery from honey bee AMPs, this review is aimed at providing an exhaustive screening of the AMPs detected in honey and honeybee products and their classification, databases, computational tools, physicochemical properties, signaling pathways, pharmaceutical and clinical uses, application status, prospects, and problems to be solved.

Keywords: AMPs, Databases, Honey bees, Signaling pathways, Therapeutic applications

Introduction

Honey bees and stingless bees, act as one of the major pollinators in wild forest and agriculture systems, are indispensable for conserving ecological biodiversity, global ecological stability, productivity and economy¹. Besides, both honey bees and stingless bees are capable to produce different types of honey, royal jelly, bee wax, propolis, bee bread and bee venom based on diverse floral resources visit and can yield significant contributions to human society (Fig. 1). Nevertheless, several factors seemingly lead to bee depopulation and colony/brood loss events, including pathogens (parasites, fungi, bacteria and viruses), ecosystem alteration or loss, and the use of pesticides and antibiotics intimidate wild plant diversity, terrestrial ecosystem stability, crop

production, global food supply, and human welfare². The immune system of bees is capable of changing its defence mechanisms, so it is essential to understand how it works in order to examine how it reacts to various pathogenic and stressful situations that affect the health and behaviour of bee colonies (Fig. 1).

Bee immunity serves as an example of the superorganism theory since it relies on both individual and colony-level defence mechanisms to protect bees from infections and stressful situations³. Additionally, bees' social immunity—a network of behavioural, physiological, and organizational responses that prevents the admission, establishment, expansion, and transmission of parasites and microbial diseases in the colony—supplements their physiological immune systems. Bee immune responses are comprised of distinctive categories of behavioral adaptations, evolutionary conserved defense strategies (cellular and humoral responses) and assemblage of multifaceted discrete immune mechanisms that afford

*Correspondence:

Phone: +91-7630079075; +91-9862399411 (Mob)

E-mail: krssrno@yahoo.com (KRSSR); gurus64@yahoo.com (GG)



Contents lists available at ScienceDirect

Food and Chemical Toxicology

journal homepage: www.elsevier.com/locate/foodchemtox

Dietary phytoestrogen diosgenin interrupts metabolism, physiology, and reproduction of Swiss albino mice: Possible mode of action as an emerging environmental contaminant, endocrine disruptor and reproductive toxicant

Maurya Khushboo, Sanasam Sanjeev, Meesala Krishna Murthy, Maibam Sunitadevi, Roy Dinata, Baishya Bhanushree, Rema Momin Bidanchi, Nisekhot Nisa, Sailo Lalrinzuali, Bose Manikandan, Ahmed-Laskar Saeed, Giri Abinash, Buragohain Pori, Chettri Arati, Vikas Kumar Roy, Guruswami Gurusubramanian*

Department of Zoology, Mizoram University, Aizawl, 796004, Mizoram, India

ARTICLE INFO

Handling Editor: Dr. Bryan Delaney

Keywords:

Dietary diosgenin
Environmental contaminant
Phytoestrogen
Reproductive
Toxicity
Endocrine disruptor
Steroidogenesis
Apoptosis

ABSTRACT

Dietary phytoestrogens are the main source of environmental contamination due to their estrogen-mimicking and endocrine-disrupting effects, posing a threat to microbial, soil, plant, and animal health. Diosgenin, a phytosteroid saponin, is used in many traditional medicines, nutraceuticals, dietary supplements, contraceptives, and hormone replacement therapies against numerous diseases and disorders. It is important to be aware of the potential risks associated with diosgenin, as well as its potential to cause reproductive and endocrine toxicity. Due to the lack of research on the safety and probable adverse side effects of diosgenin, this work evaluated the endocrine-disrupting and reproductive toxicity of diosgenin in albino mice by following acute toxicity (OECD-423), repeated dose 90-day oral toxicity (OECD-408), and F₁ extended one-generation reproductive toxicity (OECD-443) studies. Diosgenin was found to be slightly toxic, with LD₅₀ for male and female mice being 546.26 and 538.72 mg/kg, respectively. Chronic exposure of diosgenin (10, 50, 100, and 200 mg/kg) generated oxidative stress, depleted antioxidant enzymes, disturbed homeostasis of the reproductive hormones, and interrupted steroidogenesis, germ cell apoptosis, gametogenesis, sperm quality, estrous cycle, and reproductive performance in the F₀ and F₁ offspring. Long-term oral exposure of diosgenin to the mice disturbed the endocrine and reproductive functions and generated transgenerational reproductive toxic effects in F₂ and F₃ offspring. These results suggest that diosgenin should be used carefully in food products and medical applications due to its potential endocrine-disrupting and reproductive toxic effects. The findings of this study provide a better understanding of the potential adverse effects of diosgenin and the need for appropriate risk assessment and management of its use.

1. Introduction

Phytoestrogens are plant-derived polyphenolic compounds found in various foods that demonstrate a structural resemblance to endogenous human hormones and have numerous health benefits. With their promising recognition as a drug for hormonal replacement therapy, contraceptives, nutraceuticals, functional foods, and dietary

supplements, their consumption has been augmented worldwide to the tune of 15–200 mg, especially in the Asian region (Rietjens et al., 2017).

Preclinical studies have evidenced that the intake of phytoestrogens may affect the physiology (hormones and health), and reproduction in humans depending on the exposure (phytoestrogen category, milliequivalent/capsule, dose, and bioavailability), race, hormone proportion (associated with age, sex, and physiological status), and health status of

* Corresponding author.

E-mail addresses: khushbooverma206@gmail.com (M. Khushboo), sanasamsanjeev@gmail.com (S. Sanjeev), krishnameesala6@gmail.com (M.K. Murthy), sunitamailam@gmail.com (M. Sunitadevi), dnataroy9@gmail.com (R. Dinata), bhanushreebaishya55@gmail.com (B. Bhanushree), bidanrema@gmail.com (R.M. Bidanchi), edwinisa1996@gmail.com (N. Nisa), lalrinzualisailo24@gmail.com (S. Lalrinzuali), selvamanikandan784@gmail.com (B. Manikandan), ahmed06super@gmail.com (A.-L. Saeed), abinashgiri888@gmail.com (G. Abinash), poriburagohain16@gmail.com (B. Pori), aratichettri8198@gmail.com (C. Arati), vikasroy4araria@gmail.com (V.K. Roy), guruswami@yahoo.com, mzuti036@mzu.edu.in (G. Gurusubramanian).

<https://doi.org/10.1016/j.fct.2023.113798>

Received 13 November 2022; Received in revised form 14 April 2023; Accepted 20 April 2023

Available online 3 May 2023

0278-6915/© 2023 Elsevier Ltd. All rights reserved.



Long-term consumption of fermented pork fat-based diets differing in calorie, fat content, and fatty acid levels mediates oxidative stress, inflammation, redox imbalance, germ cell apoptosis, disruption of steroidogenesis, and testicular dysfunction in Wistar rats

Sailo Lalrinzuali¹ · Maurya Khushboo¹ · Roy Dinata¹ · Balshya Bhanushree¹ · Nisekhot Nisa¹ · Rema Momin Bidanchi¹ · Saeed-Ahmed Laskar¹ · Bose Manikandan¹ · Giri Abinash¹ · Buragohain Pori¹ · Vikas Kumar Roy¹ · Guruswami Gurusubramanian¹

Received: 1 July 2022 / Accepted: 15 February 2023

© The Author(s), under exclusive licence to Springer-Verlag GmbH Germany, part of Springer Nature 2023

Abstract

There is a dearth of experimental evidence available as to whether the consumption of fermented pork fat (FPF) food has any harmful effects on metabolism and reproduction due to its excessive calories, high fat content, and fatty acid methyl ester (FAME) levels. We hypothesized that exposure to a FPF-diet with excessive calories, a high fat content, and high FAME levels alters testicular physiology and metabolism, leading to permanent damage to the testicular system and its function. Thirteen-week-old male rats ($n=20$) were assigned to a high-calorie, high-fat diet (FPF-H, fat-60%, 23 kJ/g), a moderate-calorie, moderate-fat diet (FPF-M, fat-30%, 17.5 kJ/g), a low-calorie and low-fat diet (FPF-L, fat-15%, 14.21 kJ/g) compared to the standard diet (Control, fat-11%, 12.56 kJ/g) orally for 90 days. GC-MS analysis of the three FPF-diets showed high quantities of saturated fatty acids (SFAs) and polyunsaturated fatty acids- $\omega 6$ (PUFA- $\omega 6$) and low levels of monounsaturated fatty acids (MUFAs) and polyunsaturated fatty acids- $\omega 3$ (PUFA- $\omega 3$) compared to the control diet. Consequently, the levels of serum FAMES of the FPF-diet fed rats were significantly increased. In addition, a high level of n-6:n-3 PUFA towards PUFA- $\omega 6$ was observed in the serum of FPF-diet fed rats due to the high content of linoleic, γ -linolenic, and arachidonic acid. Long-term consumption of FPF-diets disturbed the anthropometrical, nutritional, physiological, and metabolic profiles. Furthermore, administration of FPF-diets generated metabolic syndrome (dyslipidemia, leptinemia, insulin resistance, obesity, hepato-renal disorder and function), increased the cardiovascular risk factors, and triggered serum and testis inflammatory markers (interleukin-1 \uparrow , interleukin-6 \uparrow , interleukin-10 \downarrow , leukotriene B $4\uparrow$, prostaglandin \uparrow , nitric oxide \uparrow , myeloperoxidase \uparrow , lactate dehydrogenase \uparrow , and tumor necrosis factor- $\alpha\uparrow$). Activated testis oxidative stress (conjugated dienes \uparrow , lipid hydroperoxides \uparrow , malondialdehyde \uparrow , protein carbonyl \uparrow , and fragmented DNA \uparrow) and depleted antioxidant reserve (catalase \downarrow , superoxide dismutase \downarrow , glutathione S-transferase \downarrow , reduced glutathione \downarrow , glutathione disulfide \uparrow , and GSH:GSSG ratio \downarrow) were observed in FPF-diet fed rats. Disrupted testis histoarchitecture, progressive deterioration of spermatogenesis, poor sperm quality and functional indices, significant alterations in the reproductive hormones (serum and testis testosterone \downarrow , serum estradiol \uparrow , serum luteinizing hormone \downarrow , and follicle-stimulating hormone \uparrow), were noted in rats fed with FPF diets than in the control diet. Severe steroidogenic impairment (steroidogenic acute regulatory protein, StAR \downarrow ; 3 β -hydroxysteroid dehydrogenase, 3 β -HSD \downarrow ; and luteinizing hormone receptor, LHR \downarrow), deficiency in germ cells proliferation (proliferating cell nuclear antigen, PCNA \downarrow), and abnormally enhanced testicular germ cell apoptosis (terminal deoxynucleotidyl transferase dUTP nick end labeling, TUNEL assay \uparrow ; B-cell lymphoma-2, BCL-2 \downarrow ; Bcl-2-associated X protein, BAX \uparrow ; and BAX/BCL-2 ratio \uparrow) were remarked in the FPF-diet administered rats in comparison with the control diet. In conclusion, the long-term feeding of an FPF-diet with excessive calories, a high fat content, and high FAME levels induced oxidative stress, inflammation, and

Responsible Editor: Mohamed M. Abdel-Daim

Sailo Lalrinzuali, Maurya Khushboo and Vikas Kumar Roy contributed equally to this work.

Extended author information available on the last page of the article

Published online: 25 February 2023

Springer



Contents lists available at ScienceDirect

Environmental Pollution

journal homepage: www.elsevier.com/locate/envpol

Antioxidative, anti-inflammatory and anti-apoptotic action of ellagic acid against lead acetate induced testicular and hepato-renal oxidative damages and pathophysiological changes in male Long Evans rats[☆]

Rema Momin Bidanchi, Lalrinsanga Lalrindika, Maurya Khushboo, Baishya Bhanushree, Roy Dinata, Milirani Das, Nisekhoto Nisa, Sailo Lalrinzuali, Bose Manikandan, Laskar Saeed-Ahmed, Sanasam Sanjeev, Meesala Krishna Murthy, Vikas Kumar Roy, Guruswami Gurusubramanian^{*}

Department of Zoology, Mizoram University, Aizawl, 796004, Mizoram, India

ARTICLE INFO

Keywords:

Lead toxicity
Ellagic acid
Oxidative stress
Antioxidant defense
Inflammation
Apoptosis

ABSTRACT

Lead (Pb), is an environmental toxicant, causes multi-organ dysfunction including reproductive impairments. This study designed to investigate the prospective antioxidative, anti-inflammatory and anti-apoptotic effects of ellagic acid (EA) on Pb-mediated testicular and hepato-renal toxicity. Four experimental groups of five male Long-Evans rats each were used: control, Pb (60 mg/kg), EA (30 mg/kg), and Pb + EA groups. All groups were given their respective treatment orally for 30 days. Pb exposure altered body and organs weight, food and water consumption, rectal temperature, Pb residue levels in tissues, liver and kidney function, sperm quality parameters, serum metabolic and hematology profiles, and impaired the oxidative/antioxidative balance in the testicular and hepato-renal tissue, as shown by the decreased antioxidant proteins (superoxide dismutase, catalase, glutathione peroxidase, and reduced glutathione) and increased the oxidative (MDA, lipid hydroperoxides, conjugated dienes, protein carbonyl, fragmented DNA and GSH:GSSG ratio) stress and inflammatory (IL-1, IL-6, TNF- α , prostaglandin, LTB $_4$, NO, myeloperoxidase, LDH) markers. Moreover, a dysregulation in the stress response (HSP-70) and apoptotic-regulating proteins (BAX, BCL-2, and active Caspase-3) were recorded upon Pb exposure. Remarkably, EA oral administration reduced the Pb residue levels in tissues, improved the liver and kidney function, revived the spermatogenesis and sperm quality, restored redox homeostasis, suppressed the oxidative stress, inflammatory and apoptotic responses in the liver, kidney and testis tissue. Our findings point out that EA can be used as a phyto-chelator to overcome the adverse effects of Pb exposure due to its potent antioxidant, anti-inflammatory, and anti-apoptotic effects.

1. Introduction

Lead (Pb) has become a global health hazard (0.6%) because of exposure to animals and human beings with ingestion of feed and food, inhalation of industrial emissions, food chain, environment, and water resources (Ericson et al., 2016; Rehman et al., 2018). Globally, blood lead levels of 1 in 3 children (800 million) are estimated to be $\geq 5 \mu\text{g}/\text{dL}$ and over 275 million children in India suffer mild to severe effects of lead poisoning (Rees and Fuller, 2020). Pb is absorbed by the duodenum via DMT1 (divalent metal transporter 1), combined with erythrocyte

protein and later dispensed to tissues and organs (García-Niño and Pedraza-Chaverri, 2014). One third of the total absorbed Pb is stored in the liver due to hepatic conjugation, followed by the kidney and finally the residual quantity is accumulated in various tissues and organs causing biomolecules (DNA, lipid, protein, RNA) injury, cell damage and cell death (Flora et al., 2006; Chen et al., 2019). Pb is multi-organ cumulative toxicants that cause oxidative damage, hemato-biochemical alterations (Al-Omair et al., 2017) and interrupts organ functions causing various metabolic disorders (Caito et al., 2017; Gandhi et al., 2017; Park et al., 2019). Inflammation and oxidative stress that play a

[☆] This paper has been recommended for acceptance by Wen Chen.

^{*} Corresponding author.

E-mail address: gurus64@yahoo.com (G. Gurusubramanian).

<https://doi.org/10.1016/j.envpol.2022.119048>

Received 19 November 2021; Received in revised form 14 February 2022; Accepted 21 February 2022

Available online 24 February 2022

0269-7491/© 2022 Elsevier Ltd. All rights reserved.

PLAGIARISM CERTIFICATE



Similarity Report ID: oid:10015:62693125

PAPER NAME

Core (1).pdf

AUTHOR

Nisekphoto Nisa

WORD COUNT

49639 Words

CHARACTER COUNT

261167 Characters

PAGE COUNT

190 Pages

FILE SIZE

9.9MB

SUBMISSION DATE

Jul 11, 2024 5:02 PM GMT+5:30

REPORT DATE

Jul 11, 2024 5:04 PM GMT+5:30

● 0% Overall Similarity

This submission did not match any of the content we compared it against.

- 0% Internet database
- 0% Publications database
- Crossref database
- Crossref Posted Content database
- 0% Submitted Works database

● Excluded from Similarity Report

- Bibliographic material
- Quoted material
- Cited material
- Small Matches (Less than 14 words)
- Manually excluded sources
- Manually excluded text blocks

PAPER NAME

Non core.pdf

AUTHOR

Nisekphoto Nisa

WORD COUNT

10726 Words

CHARACTER COUNT

59198 Characters

PAGE COUNT

32 Pages

FILE SIZE

323.0KB

SUBMISSION DATE

Jul 11, 2024 3:22 PM GMT+5:30

REPORT DATE

Jul 11, 2024 3:24 PM GMT+5:30**7% Overall Similarity**

The combined total of all matches, including overlapping sources, for each database.

- 5% Internet database
- 5% Publications database
- Crossref database
- Crossref Posted Content database
- 2% Submitted Works database

Excluded from Similarity Report

- Bibliographic material
- Quoted material
- Cited material
- Small Matches (Less than 14 words)
- Manually excluded sources
- Manually excluded text blocks

PARTICULARS OF THE CANDIDATE

NAME OF THE CANDIDATE : NISEKHOTO NISA

DEGREE : DOCTOR OF PHILOSOPHY

DEPARTMENT : DEPARTMENT OF ZOOLOGY

TITLE OF THE THESIS : Neuroprotective activity of *Parkia timoriana* in
aluminum chloride mediated Alzheimer's
disease rats

DATE OF ADMISSION : 04-11-2020

APPROVAL OF RESEARCH PROPOSAL

DRC : 16-04-2021

BOS : 20-04-2021

SCHOOL BOARD : 29-04-2021

MZU REGISTRATION NO. : 2010594

REGISTRATION NO. & DATE : MZU/Ph.D./1539 of 04.11.2020

EXTENSION : Nil

(PROF. H. T. LALREMSANGA)

Head

Department of Zoology

Mizoram University

ABSTRACT

NEUROPROTECTIVE ACTIVITY OF *PARKIA TIMORIANA* IN ALUMINUM CHLORIDE MEDIATED ALZHEIMER'S DISEASE RATS

**AN ABSTRACT SUBMITTED IN PARTIAL FULFILLMENT OF
THE REQUIREMENTS FOR THE DEGREE OF DOCTOR OF
PHILOSOPHY**

NISEKHOTO NISA

MZU REGN NO.: 2010594

Ph.D. REGN NO.: MZU/Ph.D./1539 OF 04.11.2020



DEPARTMENT OF ZOOLOGY

SCHOOL OF LIFE SCIENCES

JULY, 2024

**NEUROPROTECTIVE ACTIVITY OF *PARKIA TIMORIANA* IN
ALUMINUM CHLORIDE MEDIATED ALZHEIMER'S DISEASE
RATS**

BY

Nisekphoto Nisa

Department of Zoology

Name of supervisor: Prof. G. Gurusubramanian

Submitted

**In partial fulfillment of the requirement of the Degree of Doctor of
Philosophy in Zoology of Mizoram University, Aizawl.**

1. INTRODUCTION

Alzheimer's disease (AD) is a neurodegenerative disease that is the most prevalent and complex type of dementia, exhibiting a variety of cognitive deficits, altered personality traits, and aberrant behaviour (**Alzheimer's association, 2024; Ravi et al., 2018**). The World Health Organisation (WHO) projects that there will be 139 million dementia patients worldwide by 2050, up from 55 million in 2019 (**WHO, 2023**). Additionally, it is predicted that the expenses related to dementia would double, reaching \$2.8 trillion by 2030 from US\$1.3 trillion annually in 2019 (**Long et al., 2023**).

The two main pathogenic markers seen in AD are neurofibrillary tangles (NFTs) and senile plaques, although the precise processes causing these changes are yet unknown. Senile plaque is produced when extracellular A β peptide aggregate, while aberrant hyperphosphorylated tau protein deposits result in NFTs. In addition, AD has been associated with mitochondrial malfunction, neuroinflammatory, impaired neurotransmissions, hormonal changes, and cell cycle abnormalities (**Tarragon et al., 2013; Lam et al., 2016**). The amyloid-beta (A β) peptide is formed from the APP (amyloid precursor protein) by a sequence of proteolytic cleavages and subsequent post-translational modifications, resulting in the generation of amyloid plaque (**Hardy and Selkoe, 2002**). BACE1 is responsible for the crucial, or first, cleavage of APP at the β site. The cleavage of APP by BACE1 leads to a diversion from the normal non-amyloidogenic route, which is controlled by α secretase. This diversion results in the production of two peptides: APPs β (soluble ectodomain) and C99 (membrane-bound C terminus). γ -secretase further processes the C99 to produce A β 40 and A β 42 (**Golde et al., 2000; Suh and Checler, 2002**). A β 42 is highly neurotoxic and is synthesised to generate the senile plaques, which are the pathological characteristics of Alzheimer's disease (**Sanchez-Varo et al., 2012**). According to the amyloid cascade hypothesis, the buildup of A β 42 is a subsequent occurrence in AD. It occurs before and probably plays a role in triggering the excessive phosphorylation of tau, leading to the formation of intracellular NFTs (neurofibrillary tangles). The presence of this secondary pathology, together with the buildup of A β , plays a role in a series of abnormal processes that result in the death of brain synapses and neurons (**Cervellati et al., 2021**). Because of this factor, BACE1 has been extensively researched in relation to

brain amyloidogenesis and has been shown to have a direct role in the generation of A β based on evidence from several mice knockout models. Pharmacological interventions have been used to target BACE1, resulting in the invention and testing of several inhibitory drugs. These compounds have effectively reduced the levels of A β in human subjects (**Park, 2010; Hampel et al., 2021**). The BACE1 level was discovered to be greatest in the postnatal brain of mice and in extracts from the brains of humans with AD. In both AD animal models and AD brains, there was a significant buildup of BACE1 in neuritic dystrophies around A β plaques. This accumulation is presumably due to a post-translational process. Inducing autophagy in mutated human neurons increases the accumulation of BACE1 in distant axons via autophagy, resulting in improved β -cleavage of APP (**Hampel et al., 2021**).

AChE plays a crucial role as an enzyme in the cholinergic nerve system. Throughout the course of Alzheimer's disease, several kinds of neurons deteriorate. There is a significant loss of cholinergic neurons in the brain of AD, which is followed by a gradual decrease in acetylcholine (**García-Ayllón et al., 2011**). In the brain tissue of people with AD, the enzyme acetylcholinesterase (AChE) is more prevalent than butyrylcholinesterase (BuChE). This abundance of AChE leads to the breakdown of acetylcholine (ACh) in the cerebral cortex and hippocampus (**Nordberg et al., 2013**). Currently, the improvement of cholinergic neurons remains a primary strategy in the symptomatic management of cognitive and behavioural symptoms in individuals with mild and moderate stages of AD. As part of this treatment approach, many substances were used which enhances the release of ACh in the hippocampus (**Lista et al., 2023; Nordberg et al., 2013**).

Currently, Alzheimer's disease has no known treatment and no known means of prevention. Research centres worldwide are focusing on finding ways to cure or prevent dementia, given that over 55 million people worldwide suffer from Alzheimer's and other dementias, which have a terrible impact on people's lives (**Alzheimer's association, 2024; WHO, 2023**). There are now eight medications, including, lecanemab, aducanumab, galantamine, rivastigmine, donepezil, memantine, brexpiprazole, and a combination of donepezil and memantine, on the market that can treat Alzheimer's disease (**Alzheimer's association, 2024**).

Parkia timoriana (DC.) Merr., also commonly known as tree bean, is a versatile tree belonging to the Leguminosae family and the Mimosoideae sub-family. This species is the most prevalent *Parkia* in the Indo-Pacific region, ranging from northeast India to Irian Jaya. It is a medium-height tree, reaching 10–12 meters, with numerous branches, and holds significant commercial and ecological value in the region (Singha et al., 2021). The indigenous people of northeast India use the pods and seeds of this tree as vegetables, chutneys, and salads at various stages of development or dry them in the sun for use during the off-season. It is a superior source of carbohydrates, proteins, minerals, and vitamins when compared to other legumes (Saha et al., 2007; Seal, 2011). The tree is well-suited to diverse agro-climatic regions, thriving in both cold hilly areas and hot plains. It typically grows wild in forests, Jhum fields, and backyards across northeast India without requiring special care. This tree is valued for its high medicinal and nutritional properties (Thangjam, 2014). Tree bean can serve as an excellent source of a variety of nutrients and supplements. The seeds of *P. timoriana* are abundant in protein- globulins and albumins; minerals- phosphorus, manganese, magnesium, zinc, potassium, and iron; essential amino acids – tyrosine, phenylalanine, leucine, and isoleucine; and fatty acids- linoleic and oleic acids. The essential amino acid composition found in the kernel of *P. timoriana* is similar to the essential amino acid requirement pattern outlined by FAO/WHO/UNU (1985) for preschool children (Longvah and Deosthale, 1998; Angami et al., 2018). Tree bean has demonstrated a wide range of medicinal properties, including antioxidant, antiviral, antidiabetic, insecticidal effects, antibacterial, immune-boosting, and antiproliferative. Additionally, it has been used in the treatment of colon cancer, skin and liver diseases, ulcers, eyes, hypertension, and leprosy. In addition to containing antioxidants that help prevent various diseases, tree bean can also enhance children's learning abilities (Sheikh et al., 2016; Tapan, 2011; Angami et al., 2018).

Since time immemorial, plants have been widely recognised as a source of medicine for various human diseases (Siddiqui et al., 2020). Despite the discovery of numerous plant-derived drugs, the exploration of new bioactive compounds remains necessary to expand the range and find less toxic, more effective medications (Noumi et al., 2020; Reddy et al., 2020). Herbal medications have recently garnered significant

interest due to their safety and cost-effectiveness. Bioactive compounds, which are secondary metabolites of plants, can produce pharmacological and toxicological effects in living organisms (López-Vallejo et al., 2011). Preclinical toxicity and adverse drug reactions account for approximately one-third of product failures (Van Norman, 2020). Screening each phytocompound for toxicity through *in vitro* and *in vivo* techniques is challenging. However, computational techniques are crucial for studying the toxicity and properties of both chemical and natural compounds, as they facilitate early drug development by enabling the early detection of substances lacking experimental data. These methodologies also provide a substitute for toxicity studies conducted on animal models (Pognan et al., 2023). In silico prediction approaches use the physiochemical features of a substance to estimate its activity in a given biological system. QSAR (quantitative structure activity relationship) and SAR (structure activity relationship) are mathematical models that predict the relative structures' activities in a compound (Kar and Leszczynski, 2019).

Utilising in silico research is the optimal approach for initiating pharmacological target development. Traditional methods are insufficient for the timely discovery of drug targets. Attaining majority aims using considerably rapid methods is challenging. Computational methods, such as molecular docking, MD simulations, and MM/PBSA computations, are significantly contributing to the field of drug discovery (Hou et al., 2011; Keretsu et al., 2021).

The primary objective of this research is to evaluate the beneficial impact of *P. timoriana* seed pods on cognitive impairment in rats with Alzheimer's disease induced by AlCl₃. However, the toxicity and food safety of *P. timoriana* have not been well explored. Therefore, prior to conducting the experiment, an analysis was performed on the phytochemical contents of methanolic extract of *P. timoriana* seed pods, and their toxicity was evaluated using computational techniques. Furthermore, these phytocompounds were subjected to molecular docking, MD simulation, and free energy calculation to assess their interactions with BACE1 and AChE protein receptors. Acute and sub-acute toxicity studies were conducted to estimate the LD₅₀ and NOAEL values of the plant extract.

2. OBJECTIVES

- GC-MS and LC-MS analysis of phytocompounds of *P. timoriana* and evaluation of phytocompounds toxicity using in silico tools.
- Molecular docking and molecular dynamics simulation of phytocompounds from *P. timoriana* to BACE1 and cholinesterase protein receptor: an in silico therapeutic intervention study on Alzheimer's disease.
- Biological evaluation of *P. timoriana* in ameliorating learning and memory processes in an aluminum chloride induced Alzheimer's disease rat model.

3. MATERIALS AND METHODS

3.1. Phytochemical analysis and computational toxicology

3.1.1. Collection, identification and extraction of *Parkia timoriana* seed pods

Parkia timoriana seed pods were collected from Tanhril village in Aizawl, Mizoram. The species bearing the accession number 1016 was identified by the BSI (Botanical Survey of India), Eastern Regional Centre, Shillong. They were air-dried and crushed into a powder and immersed in methanol for 72 hours. The extract was then filtered through Whatman filter paper No.1 and subjected to evaporation in an oven at 40 °C. The resulting dry extract was stored at 4°C until used (Kuethe et al., 2006; Sen et al., 2013).

3.1.2. Total flavonoid content

A solution was prepared by dissolving 0.2 g of extract in 10 mL of distilled water, using a ratio of 1:50 (w/v). This solution was then used to determine the total phenolic and flavonoid content. The total flavonoid content was quantified using the method reported by Zhang et al. (2012), with minor adjustments. The extract was mixed with a 5% NaNO₂ solution, 10% AlCl₃ solution, and 1M sodium hydroxide. The absorbance was measured using a spectrophotometer at a wavelength of 510 nm. Quercetin was used as a standard to generate a calibration curve. The total flavonoid content (TFC) was reported as quercetin equivalents in mg QE/g of the dried extract.

3.1.3. Total phenol content

The Folin-Ciocalteu reagent technique was used to quantify the total phenolic content. The extract was added to a test tube containing 2.5 mL of 10 % Folin-Ciocalteu reagent and 2.0 mL of 2 % Na₂CO₃ and incubated for 60 minutes. The absorbance at 765 nm was measured using a spectrophotometer, and gallic acid was used as a standard to generate a calibration curve. The total phenolic content was quantified as gallic acid equivalents in mg GAE/g of the dried extract (Sen et al., 2013).

3.1.4. Gas chromatography-mass spectrometry analysis

The PT seed pod extracts were analyzed using the GC-MS-2010 (Shimadzu, Japan) in EI mode at 70 eV electron ionisation energy. A Restek-5MS column was used, with pure helium gas flowing at a constant rate of 1 mL/min. The GC-MS spectrum was detected using an electron ionisation energy technique. The injector temperature was maintained at 260°C, and a flow control mode was used. The column oven temperature was set at 120°C for two minutes, then increased by 10°C each minute until reaching 280°C. Finally, it was raised to 300°C and maintained at that temperature for 20 minutes. The chromatogram and mass spectra were analyzed using the Xcalibur™ software integrated into the GC-MS/LC-MS equipment. The phytochemical contents of the test samples were determined by comparing their retention time, mass spectral patterns, peak height, and peak area with those stored in the NIST library and Dr. Duke's ethnobotanical phytochemical databases (Duke, 2000).

3.1.5. Liquid chromatography-mass spectrometry analysis

The Acquity UPLC H-Class equipment was used to separate phytochemicals using various chromatographic conditions, including mobile phase composition, injection volume, flow rate, and gradient programmes. The mobile phase consisted of a 0.1% (v/v) aqueous solution of formic acid (A) and acetonitrile (B) at a flow rate of 1.5 mL/min. The ideal conditions for separation were column pressure ranging from 0 to 300 bar and column temperature of 30 °C. The compounds were separated using an Acquity CSH C18 column at a temperature of 30 °C. Two solvents, 0.1% (v/v) formic acid in water (A) and methanol (B), were used to create a gradient elution at a flow rate of 1.5 ml/min. The gradient programme started with an initial concentration of 5%

(B) and increased to 30% (B) from 6 to 12 minutes, 60% (B) from 12 to 16 minutes, and 80% (B) from 16 to 20 minutes. The concentration of component D started at 95% and remained constant for 1 minute. The sample injection volume was 10 μ L. The MS analysis was conducted on the Water UPLC-TQD Mass Spectrometer using data-dependent automated switching between MS and MS/MS collection modes. The spectra were recorded using both positive and negative ionisation modes, with a mass acquisition range of 150–2000 m/z.

3.1.6. Toxicity prediction by QSAR-TEST

The toxicity of the phytocompounds found in *Parkia timoriana* seed pods was evaluated using QSAR-TEST (Version 5.1.2), a tool created by the US EPA (**Martin, 2020**). This programme uses many QSAR tactics, such as hierarchical, single-model, group contribution, nearest neighbour, and consensus mode of action approaches, to accurately assess the toxicity of a chemical for each specific endpoint (**Martin et al., 2008**). The TEST programme has models for predicting different toxicities: 96-hour fathead minnow and 48-hour *Daphnia magna* to test median lethal concentration (LC_{50}) (**Martin and Young, 2001; U.S.E.P.A., 2016**). *Tetrahymena pyriformis*, a single-celled organism, is to show a 50 percent growth inhibition concentration (IGC_{50}). Median lethal dose (LD_{50}) prediction using rats (**Zhu et al., 2009**). Also, bioconcentration factor (BCF) (**Zhao et al., 2008**), developmental toxicity (**Cassano et al., 2010**), and mutagenicity (Ames's test) (**Benfenati et al., 2009**).

3.1.7. Toxicity prediction by VEGA HUB, OECD QSAR and Toxtree

The toxicological properties, including repeated dose toxicity (HESS), oral toxicity, and Lipinski rule oasis, were predicted using the OECD QSAR toolbox (<https://qsartoolbox.org/download/>) (**Suarez-Torres et al., 2020**). The web programme VEGAHUB (www.vegahub.eu) was used to predict carcinogenicity, ADI, no observed adverse effect level (NOAEL), and developmental toxicity. The Toxtree platform, which is an open-source tool, was used to predict drug metabolism mediated by cytochrome P450.

3.1.8. Biological activity prediction

The PASS prediction online tool (<https://www.way2drug.com/passonline/>) was used to predict the different biological activities such as dementia treatment, cytochrome P450 stimulant, antioxidant, anti-inflammatory, neurotrophic factor enhancer, amyloid- β aggregation inhibitor, acetylcholine stimulant, and Alzheimer disease treatment. The PASS programme calculates the anticipated activity spectrum of a phytocompound, providing a prediction of likely activity (Pa) and probable inactivity (Pi). Only the biological activities with a Pa value greater than the Pi value are considered for a specific phytocompound (Goel et al., 2011).

3.2. Molecular docking, MD simulation and free energy calculation

3.2.1. Retrieval of ligand and its preparation

The sixty-one phytocompounds were analyzed for molecular docking against BACE1 and AChE protein receptors. The 2D and 3D structures of each ligand were obtained from PubChem, while the 3D structures were saved in sdf format. The phytocompounds were imported using the PyRx 0.8 programme and stabilized using the UFF energy minimization parameter and conjugate gradient descent optimization technique. The ligands were then transformed into pdbqt forms before molecular docking (Dallakyan and Olson, 2015).

3.2.2. ADMET

The SMILES format of sixty-one phytocompounds in PTME was obtained from PubChem and used for ADMET webserver. Physicochemical and molecular characteristics were determined using Molinspiration Cheminformatics Software (Kolodziejczyk-Czepas et al., 2018). ADMET properties, including water solubility, lipophilicity, and pharmacokinetic bioactivity score, were assessed using the SwissADME server. The study also examined medicinal chemistry, drug likeness, and bioavailability scores of the ligands (Daina et al., 2017).

3.2.3. Retrieval of protein and its preparation

The 3D structures of BACE1 (5I3V, 1.62 Å) and AChE (7E3D, 2.5 Å) were obtained from the Protein Data Bank under RCSB. The receptors' structures were constructed

using UCSF Chimera 1.15 before docking, eliminating co-crystallized ligand, solvent, and metal ions (**Pettersen et al., 2004**). Modifications included adding polar hydrogen atoms and partial charges, restoring shortened side chains, and adding gasteiger charges using the integrated dock prep programme (**Opo et al., 2021**).

3.2.4. Predicting the active site of the protein receptor

The fpocket web server was used to identify the active sites of BACE1 and AChE receptors in molecular docking investigations (**Le Guilloux et al., 2009**). The tool uses Voronoi tessellation and α -spheres to detect protein binding sites. The fpocket accurately detected 94% and 92% of known binding sites from the top three ranked pockets, with the highest rated pocket chosen for the receptor (**Schmidtke et al., 2010**). The findings were visualized using Schrödinger's Pymol 2.4.0 software.

3.2.5. Molecular docking

The study used the Autodock Vina plug-in tool in PyRx 0.8 to conduct molecular docking on receptors and ligands (**Trott and Olson, 2010**). The "Vina Wizard" feature was used to load receptors and ligands into the program. PyRx was used to identify, analyze, and classify the residue of the active pocket of the receptor. A grid box was positioned on the receptor and adjusted to include the whole active pocket. The AutoDock Vina programme was developed and executed to perform molecular docking. The optimal interaction conformation for each ligand was chosen. The most significant protein-ligand complexes were selected for further investigation. The chosen complexes were visualized using BIOVIA Discovery Studio Visualizer v21.1.0.20298 and Schrödinger's Pymol 2.4.0 software.

3.2.6. Molecular dynamics simulation

The molecular docking investigations were analyzed using MD simulations using GROMACS v5.1.5 (**Abraham et al., 2015; Berendsen et al., 1995**). The GAFF and AMBER99SB were used to create force field and parameter files for the ligand and protein, respectively (**Hornak et al., 2006**). A cubic box with periodic boundaries was placed around the complex, and a three-point water model known as TIP3P was used to nullify the system. In order to nullify the system, Na⁺ and Cl⁻ ions were introduced

as counter ions (**Sharma et al., 2022**). Energy minimization and equilibration were then performed, with the system subjected to energy reduction using the steepest descent minimization technique for 1000 steps (**Selvaraj et al., 2021**). An equilibration process was conducted for 500 ps at 300 K using the Berendsen Thermostat coupling in the NVT ensemble (**Berendsen et al., 1984**). The NPT ensemble equilibration was conducted for 1000 picoseconds (1 nanosecond). The Parrinello-Rahman barostat was used to couple the pressure at 1 bar (**Parrinello and Rahman, 1981**). The Particle Mesh Ewald (PME) method was used to compute long-range electrostatic interactions, and the LINear Constraint Solver (LINCS) method was used to limit bond lengths (**Hess et al., 1998; Sharma et al., 2022**). The system was exposed to unconstrained production molecular dynamics (MD) simulations lasting 100 nanoseconds while maintaining a goal temperature of 300 K and a pressure of 1 bar. The trajectories from a 100 ns MD simulation were used for dynamic studies, including RMSD, RMSF, Rg, and hydrogen bond determination. These analyses were performed using the built-in scripts of GROMACS.

3.2.7. Free energy binding

The binding free energy of a complex was determined using the MM-PBSA technique. The energy is calculated using MD trajectory data recorded at 500 picosecond intervals. The non-polar solvation energy was calculated using the SASA model. The energy obtained from MD simulation trajectories was computed using the default settings of the `g_mmpbsa` programme. The 'MmPbSaDecomp.py' script of the `g_mmpbsa` programme was used to calculate the energy contributed by individual residues to the overall binding energy (**Baker et al., 2001; Kumari et al., 2014**).

3.2.8. Principal component analysis

Principal component analysis (PCA) is a statistical method used to identify the combined and connected movements of atoms in biological macromolecules. It was conducted on snapshots taken every 2 picoseconds from 100 nanosecond simulations. The important collective movements of the protein receptor with ligands were captured by constructing covariance matrices of C α atoms (**Amadei et al., 1993; Prakash et al., 2019**). A positive value in the covariance matrix indicates associated motion, while

a negative value shows anti-correlated motion between two C α atoms. The covariance matrices were diagonalized, resulting in eigenvectors and their equivalent eigenvalues. Principal components (PCs) were derived by projecting the movement of C α atoms at each period onto the eigenvectors. The covariance matrices, eigenvectors, and two-dimensional graphs of PC1 vs PC2 were generated using Gromacs built-in tools (Taidi, 2022).

3.3. Toxicity study and AlCl₃-induced Alzheimer's disease treatment

3.3.1. Animal ethics

The animal experiments were carried out in compliance with the ethical guidelines for the maintenance and usage of laboratory animals and were authorised by the Mizoram University Institutional Animal Ethics Committee, situated in Aizawl, Mizoram, India (approval no. **MZU/IAEC/2021-22/09**).

3.3.2. Experimental animals

Adult Wistar albino rats weighing 130-160 g were used for the experiment. Animals were housed in polypropylene rat cages (421 × 290 × 190 mm) and kept under controlled environmental conditions: room temperature (25 ± 2 °C), constant humidity (60 ± 10 %), and constant photoperiodic conditions (12:12 h day light/darkness cycles) in the animal facility of the Department of Zoology, Mizoram University, Aizawl. The standard pellet diet and water were allowed ad libitum.

3.3.3. Toxicity study

3.3.3.1. Acute toxicity study

The study tested the acute toxicity of *P. timoriana* methanolic extract (PTME) on male adult Wistar albino rats, following OECD guideline no. 423. The rats were divided into four groups, each consisting of five animals. A single dosage of 1000 mg/kg, 3000 mg/kg, and 5000 mg/kg of PTME was given orally to the overnight fasted rats, while control animals received distilled water. The rats were observed for symptoms of acute toxicity for four hours, eight hours, and 14 days. Observations included morphological changes, such as rectal temperature, skin and eye color, food intake, and overall

physique. The initial body weight was measured before PTME administration, and the final weight was measured at the experiment's conclusion.

3.3.3.2. Sub-acute toxicity study

A study involving male Wistar albino rats was conducted to investigate the sub-acute toxicity of PTME. Four groups were given PTME orally at different concentrations (20 mg/kg, 50 mg/kg, 100 mg/kg, and 300 mg/kg) for 28 days, while the control group received distilled water. Throughout the investigation, we observed all the common indicators of toxicity in animals. The animals' initial body weight was recorded before and after PTME administration. The study aimed to understand the effects of PTME on animals.

3.3.3.3. Haematological parameters assessment

The toxicity experiment involved haematological assays on all surviving animals, collected on the 15th and 29th days. Blood samples were collected and analyzed for parameters such as red blood cells, white blood cells, hemoglobin, haematocrit, mean cell volume, mean corpuscular haemoglobin, and mean corpuscular haemoglobin concentration (**Thrall and Weiser, 2002; Higgins et al., 2008; Feldman et al., 2000**).

3.3.3.4. Serum biochemical parameters assessment

Biochemical parameters were assessed by collecting blood from surviving rats and centrifuging it at 3500 rpm for 30 minutes. The serum was collected and stored at -20 °C until analysis. The levels of serum alanine aminotransferase (ALT, EC.2.6.1.2, **Reitman and Frankel, 1957**), aspartate aminotransferase (AST, EC.2.6.1.1, **Reitman and Frankel, 1957**), alkaline phosphatase (ALP, EC.3.1.3.1, **Kind and King, 1954**), creatinine (**Bonsnes and Taussky, 1945**), urea (**Fawcett and Scott, 1960**), cholesterol, triglycerides, high-density lipoprotein (HDL), and low-density lipoprotein (LDL) (**Trinder, 1969**) were measured using a diagnostic kit from Coral Clinical Systems, Goa, India.

3.3.3.5. Relative organ weight measurement

Rats were sacrificed after acute and sub-acute toxicity treatment, and their organs, including liver, kidney, lungs, heart, and spleen were measured for weight. The relative organ's weight was determined as a ratio to the bodyweight using a specific equation.

$$\text{Relative organ weight} = (\text{Absolute organ weight/body weight}) \times 100$$

3.3.3.6. Histopathological assessment

The liver and kidney samples from acute and sub-acute cases were analyzed using histological testing. After retrieval, the organs were immersed in Bouin's fixative for 24 hours, then moved into 70% ethanol solution. They were then immersed in paraffin wax, sliced with a 7 μm thickness using a Leica rotary microtome, and stained with haematoxylin and eosin for general histology. The histopathology was then analyzed using an Olympus CX41 microscope, and images were captured for further examination (**Bancroft and Gamble, 2002**).

3.3.4. AlCl_3 -mediated Alzheimer's disease treatment

3.3.4.1. Experimental design

Wistar adult rats were randomly divided into four groups ($n = 5$) as follows:

- a) Group I: Rat administered saline water (0.5 ml, i.p) daily once for 42 days.
- b) Group II: Rat intraperitoneally treated with AlCl_3 (17 mg/kg b.w., i.p) (Sigma-Aldrich) for 42 days. The dose of AlCl_3 used is according to the previous study by Alawdi et al. (**2016**).
- c) Group III: Rat administered orally using intragastric tubes with PTME (5 mg/kg b.w., p.o.) dissolved in saline (1 h prior to AlCl_3 administration) and intraperitoneally treated with AlCl_3 as in group II for 42 days.
- d) Group IV: Rat administered orally using intragastric tubes with PTME (10 mg/kg b.w., p.o.) dissolved in saline (1 h prior to AlCl_3) and intraperitoneally treated with AlCl_3 as in group II for 42 days.

3.3.4.2. Behavioural experiment

3.3.4.2.1. Novel object recognition (NOR) test

The NOR test strategy involved rats in a rectangular open box with two stages: habituation and testing (**Ennaceur and Delacour, 1988**). Rats were given unrestricted access to the apparatus for three days, with a ten-minute daily time limit. The testing phase began on the fourth day, with two trials: a familiarisation trial lasting ten minutes and a test trial lasting five minutes. Rats were introduced to the apparatus containing two similar items, released oriented towards the wall, and then returned to their cages. After an hour, they were placed back in the apparatus, and one of the familiar items was replaced with a new one, marking the start of a five-minute testing session. The animal's exploration time was recorded when it approached an item with its snout within 2 cm or when it pawed or smelled the object. The recognition index (RI) of the testing trial was calculated using the formula (**Zhang et al., 2012**):

$$\text{RI (\%)} = \frac{\text{Time exploring novel object}}{(\text{time exploring novel object} + \text{time exploring familiar object})} \times 100$$

3.3.4.2.2. Y-maze test

The Y-maze test was used to assess spontaneous alteration behavior in short-term memory in rats. The test involved three arms, labeled A, B, and C, arranged perpendicularly. Rats were given five minutes of unrestricted movement in the labyrinth, with arm entrance only permitted once both hind paws were fully within the arm. Alterations involved entering three different arms in a row inside overlapping triplets (**Alawdi et al., 2017**). Every instance of arm entries and alternations was documented, and the spontaneous alternation percentage (SAP) was computed.

$$\text{SAP (\%)} = \frac{\text{Number of alternations}}{(\text{total arm entries} - 2)} \times 100$$

3.3.4.4. Oxidative and anti-oxidant parameters assessment

3.3.4.4.1. Protein estimation

The Bradford method was used for protein estimation in hippocampus tissue (**Bradford, 1976**). The sample was homogenized in phosphate buffered saline,

centrifuged, and the supernatant was recovered. 0.1 ml of protein sample was added to a test tube and mixed with 0.5 mL of Bradford reagent, and the absorbance at 595 nm was measured spectrophotometrically after 2 minutes against a reagent blank made from distilled water and 0.5 ml of Bradford reagent.

3.3.4.4.2. Lipid peroxidation (LPO)

Lipid peroxidation (LPO) levels in hippocampus tissue were measured using the thiobarbiturate test (**Ohkawa et al., 1979**). The tissue was homogenized, centrifuged, and the supernatant was collected. The supernatant was then mixed with 15% trichloroacetic acid (TCA) and 8% thiobarbituric acid (TBA). The sample was incubated at 95°C for 25 minutes, then analyzed using spectrophotometry at 540 nm. The LPO was expressed as the level of MDA in nmol/mg of protein.

3.3.4.4.3. Glutathione-S-transferase (GST)

GST was assayed spectrophotometrically at 340 nm by conjugating 1-chloro-2,4-dinitrobenzene (CDNB) with glutathione (GSH) at 37 °C (**Habig et al., 1974**). The test combination included 0.5 nM CDNB, 1 mM GSH, and 100 nM phosphate buffer at pH 6.5. CDNB was dissolved in ethanol and introduced into the phosphate buffer. The reaction was initiated with GSH and 10% tissue homogenate. The spectrophotometer quantified the rate of absorbance at 340 nm against a blank without homogenate, and the GST level was expressed as U/mg of protein.

3.3.4.4.4. Glutathione (GSH)

The concentration of reduced glutathione (GSH) was determined by reacting it with 5,5'-dithiobis(2-nitrobenzoic acid) (DTNB) to form a detectable product at 412 nm (**Moron et al., 1979**). The sample tubes were filled with 0.6 mM DTNB, 0.2 M sodium phosphate, 10% tissue homogenate, and 0.2 M phosphate buffer, with a reference tube filled with GSH solution. The reaction was initiated by adding the supernatant to the sample tube. GSH levels were expressed as nmol/mg of protein.

3.3.4.5. Enzyme-linked immunosorbent assay (ELISA)

The activity of acetylcholinesterase (AChE) in the hippocampus was measured using commercially available ELISA kit from Elabscience, USA (Rat AChE ELISA Kit;

Catalog No.: E-EL-R0355). The manufacturer's instructions were followed for the detection process. A spectrophotometer was used to detect the change in absorbance at 450 nm.

3.3.4.6. Western blotting

The western blotting was performed to study the expression of NF- κ B, TNF- α , IL-6, active caspase-3, BCL-2, Bax, A β , BACE1, and Tau protein in the hippocampus. The western blot technique was similar to the one previously described by Annie et al. (2020). A tissue homogenate (50 μ g) of the hippocampus was separated on a 10% sodium dodecyl sulphate (SDS)–polyacrylamide gel. The gel was then transferred to a polyvinylidene difluoride membrane (PVDF, Millipore, India) using a semi-dry apparatus for a duration of 30 minutes. In order to avoid non-specific binding, the membranes were treated with a blocking agent (5% skim milk, Sigma-Aldrich, USA) for 30 minutes. Subsequently, the membranes were incubated overnight at 4 °C with the primary antibodies. Subsequently, the membranes were exposed to the suitable HRP-conjugated secondary antibody and incubated for 3 hours at room temperature. The visualisation was performed using the ECL detection technique. The internal control used was β -tubulin and β -actin. The levels of the proteins were calculated using densitometric analysis using ImageJ.

3.3.4.7. Histopathological examination

The hippocampus was dissected and analyzed using histological testing. After retrieval, it was immersed in Bouin's fixative for 24 hours, then moved into 70% ethanol solution. They were then immersed in paraffin wax, sliced with a 7 μ m thickness using a Leica rotary microtome, and stained with haematoxylin and eosin for general histology. The histopathology was then analyzed using an Olympus CX41 microscope, and images were captured for further examination (**Bancroft and Gamble, 2002**).

3.3.5. Statistical analysis

The data were represented and given as mean \pm standard error of the mean (SEM). The threshold for statistical significance was established at a p-value < 0.05. The data were

analysed using a one-way ANOVA to compare means. Significant differences were then analysed using Tukey's multiple comparisons in GraphPad Prism (version 9, GraphPad Software, La Jolla, CA).

4. SUMMARY

4.1. Phytochemical analysis and computational toxicology

- In the present study, nine bioactive compounds were identified through GC-MS analysis and fifty-two bioactive compounds were identified through LC-MS analysis. The phytocompounds present in the methanolic extract of *P. timoriana* seed pods (PTME) were mostly composed of flavonoids, alkaloids, and terpenoids.
- The PTME has a total phenol concentration of 421.64 ± 3.38 mg GAE/g of extract and a total flavonoid concentration was measured to be 280.893 ± 4.31 mg QE/g of extract.
- The predicted acute toxicity of phytocompounds from PTME showed four distinct hierarchies. a) fathead minnow > *T. pyriformis* > *D. magna* > rat; b) fathead minnow > *D. magna* > *T. pyriformis* > rat; c) *D. magna* > fathead minnow > *T. pyriformis* > rat; and d) *T. pyriformis* > fathead minnow > *D. magna* > rat.
- The acute toxicity prediction revealed that phytocompounds from PTME had less toxicity for mammalian species (rat/LD₅₀) compared to aquatic organisms (LC₅₀/fathead minnow and *D. magna*, IGC₅₀/*T. pyriformis*).
- All of the phytocompounds found in PTME, except two, had a bioconcentration factor under 2000 and were therefore considered non-bioaccumulative.
- Forty-six out of sixty-one phytocompounds from PTME were considered toxic for the developmental stage, whereas apigenin glucoside arabinoside, isoschaftoside, maritimetin-6-O-glucoside, apiin, 3-oxo-C8-homoserine lactone, and ouabain were safe alternatives.
- The majority of the phytocompounds (fifty-one out of sixty-one) from PTME showed negative carcinogenic and mutagenic properties.

- The oral toxicity test revealed that 75% of the phytochemicals are highly toxic (Cramer/category III), while 64% do not affect fertility or possess reproductive toxicity.
- The study found that 37.70% of phytochemicals had a high NOAEL value, which indicated their safety and did not cause negative effects, while the remaining phytochemicals (62.29%) were toxic and had positive side effects.
- The repeated dose toxicity analysis of the phytochemicals showed forty-eight out of sixty-one are safe and do not cause any damage to organs, with a significant number of phytochemicals showing bioavailability, metabolized by cytochrome-P450 enzyme complex, and excreted from the body.
- The phytochemicals studied have properties for dementia treatment (thirty-one phytochemicals), cytochrome P450 stimulant (seventeen phytochemicals), anti-oxidant (forty-one phytochemicals), anti-inflammatory (forty-five phytochemicals), neurotrophic factor enhancer (twenty-three phytochemicals), amyloid- β aggregation inhibitor (five phytochemicals), acetylcholine stimulant (fifteen phytochemicals), and Alzheimer disease treatment (two phytochemicals).

4.2. Molecular docking, MD simulation and free energy calculation

- From the ADMET studies, forty compounds showed drug-likeness properties as indicated by Lipinski's rule of five, thirty-two compounds were considered to have a good affinity for a lipophilic environment, thirty-one compounds that have the capacity to be absorbed by the body when taken orally and have the ability to reach certain target areas inside the body as per their TPSA value, forty-eight compounds have non-hydrogen atoms that falls under the acceptable range, sixteen compounds possess an acceptable molar volume, and thirty-six compounds were in the acceptable range of molar refractivity. No compound was found highly soluble as per LogS value. However, six compounds showed solubility, twenty compounds slightly soluble, and thirty-five compounds lack solubility.
- Additionally, twenty-seven phytochemicals revealed high absorption in the gastrointestinal tract, and twenty compounds showed blood-brain barrier

permeation. With respect to GPCR, ion channel modulator, kinase inhibitor, nuclear receptor ligand, protease inhibitor, and enzyme inhibitor, all the sixty-one phytocompounds of *Parkia timoriana* fall under the category of active and moderately active drugs. Thirty-eight phytocompounds successfully met the P-gp substrate criteria, fifty-three showed no alert for PAINS filters, and nineteen phytocompounds did not show alert for BRENK. The majority of the phytocompounds had lesser skin permeability. Similarly, the majority of the compounds indicated good oral bioavailability and can be moderately synthesize. Thirty-nine compounds inhibited one or the other enzyme of the cytochrome p450 enzyme complex.

- The molecular docking analysis revealed that the phytocompounds from the methanolic extract of *Parkia timoriana* seed pods strongly bind to BACE1 and AChE receptors, with binding affinities ranging from -5.3 kcal/mol to -10.3 kcal/mol against the BACE1 receptor and from -6.0 kcal/mol to -10.3 kcal/mol against the AChE receptor. Sixteen and fifteen phytocompounds had binding affinity \leq -9.0 kcal/mol against BACE1 and AChE, respectively.
- The selected top hit ligands for the BACE1 receptor include ergocristine as the best-ranked ligand with a binding affinity of -10.3 kcal/mol, followed by nicotiflorin, voacamine, and isorhamnetin-3-O-rutinoside with binding affinity of -10.2 kcal/mol, -10.1 kcal/mol, and -10.1 kcal/mol, respectively.
- The top hit ligands for the AChE receptor include apiin and maritimetin-6-O-glucoside as the best binding ligands with binding affinity of -10.3 kcal/mol each, followed by paeoniflorin and silychrystin with binding affinity of -10.2 kcal/mol and 9.8 kcal/mol, respectively.
- TRP76, PHE108, TYR71, LYS107, and ILE126 were the most common residues of BACE1, among the other interacting residues, that were interacting with the top hit ligands through hydrogen and hydrophobic bonds and therefore may be important in ligand binding.
- SER125, TYR341, TYR124, and TRP86 were the most common residues of AChE, among the other interacting residues, that were interacting with the top

hit ligands through hydrogen and hydrophobic bonds and therefore may be important in ligand binding.

- The MD simulation studies confirmed that the top hit ligands formed a stable complex with BACE1 having RMSD, RMSF, and Rg values of ~0.2 nm, ~0.1 nm, and ~2.0 nm, respectively. However, the BACE1-nicotiflorin and BACE1-isorhamnetin-3-O-rutinoside complexes formed a significantly higher number of H-bonds of 4.94 and 3.88, respectively, compared to the other complexes.
- Similarly, the MD simulation studies confirmed that the top hit ligands formed a stable complex with AChE having RMSD, RMSF, and Rg values as ~0.24 nm, ~0.11, and ~2.3 nm, respectively. On the other hand, the AChE-maritimetin-6-O glucoside and AChE-paeoniflorin complexes formed a higher number of H-bond of 3.27 and 2.76, respectively, compared to the other complexes.
- The binding free energy calculation for BACE1 by MM/PBSA method showed that all the simulated complexes formed a strong bonding complex, with BACE1-voacamine complex showing exceptionally high binding free energy of -417.951 ± 31.736 kJ/mol.
- Similarly, the binding free energy calculation for AChE by MM/PBSA method showed that all the simulated complexes also formed a strong bonding complex, with AChE-silychristin complex showing exceptionally high binding free energy of -385.386 ± 18.965 kJ/mol.
- The main energy contribution of the BACE1 receptor's amino acids in the binding of lead ligands at the active site indicated that residues TYR 71, ASP 106, ASP 228, PHE 108, SER 35, ASP 32, and ASP 223 of the BACE1 receptor played a significant role in the intermolecular interaction and the binding of the ligands. However, in complexes involving AChE and ligands, distinct amino acid residues played a role in contributing to the binding energy for each of the lead ligands.
- The principal component analysis showed that the C α of both BACE1 and AChE when complexed with the top hit ligands occupied very less phase space further confirming the stability of the complex formed.

4.3. Toxicity study and AlCl₃-induced Alzheimer's disease treatment

- The acute toxicity study found that PTME, administered at doses of 1000, 3000, and 5000 mg/kg, caused mortality in two rats at 5000 mg/kg dosage, with a LD₅₀ value exceeding 5000 mg/kg body weight. According to the OECD, the LD₅₀ of PTME may be considered safe. There were no observable changes in the morphology of the subjects at any of the administered dosages, except for one rat treated with 5000 mg/kg which had a red tear.
- The repeated-dose administration of PTME at doses of 20 mg/kg, 50 mg/kg, and 100 mg/kg did not show any mortality. However, four rats (only one survived) died at a dose of 300 mg/kg. No morphological change was observed at all doses.
- The food and water intake, as well as body weight and relative organ weight, did not show any significant change in both the administration of single-dose and repeated-dose PTME.
- The administration of PTME in both acute and sub-acute studies did not result in any significant alterations in the blood parameters, except for a slight elevation of WBC in acute toxicity study.
- In the acute toxicity study, there was a significant increase in the level of ALP at a dose of 5000 mg/kg and a slight increase in the levels of AST and ALT. This shows acute hepatocellular toxicity at a higher single-dose administration of PTME. The histopathological study has confirmed the presence of deteriorated alterations in the liver tissue, providing further evidence of liver cell damage caused by PTME at a higher single dosage of 5000 mg/kg.
- In the sub-acute toxicity study, no significant change was observed in the levels of AST, ALP, and ALT at 20 mg/kg, 50 mg/kg, and 100 mg/kg after repeated-dose administration of PTME for 28 days. As a result, the histological examination of the liver in these groups also showed normal architecture of the liver tissue. However, the administration of a repeated-dose of PTME at a dose of 300 mg/kg for 28 days caused the death of four rats, and the surviving rat showed deteriorated alterations in the liver tissue.

- In the acute toxicity study, the kidney function test showed that the level of creatinine was significantly increased at a single-dose administration of 5000 mg/kg, and there was a slight increase in the level of urea. This was evident as the histological examination showed significant damage in the tissue of the kidney at a dose of 5000 mg/kg.
- In the sub-acute toxicity study, no significant change was observed in the level of creatinine and urea at 20 mg/kg, 50 mg/kg, and 100 mg/kg repeated-dose administration of PTME for 28 days, and the histological examination at these doses showed normal hepatocytes displaying no apparent alterations in the morphological features. However, the repeated-dose administration of PTME at a dose of 300 mg/kg for 28 days caused the death of four rats, and the surviving rat showed highly damaged kidney tissue.
- The sub-acute toxicity study revealed that a repeated-dose administration of PTME at a dose of 300 mg/kg showed signs of mortality and toxicity in the surviving rat. Therefore, a lower dose ≤ 100 mg/kg may be preferred for chronic use to treat different types of diseases. The NOAEL of the methanolic extract of *Parkia timoriana* seed pods was found to be 100 mg/kg.
- The novel object recognition (NOR) and Y-maze tests have demonstrated that PTME has an ameliorative effect on the learning and memory impairment caused by aluminum.
- The administration of PTME improved the oxidative stress (MDA) caused by AlCl_3 in the hippocampus and increased GST and GSH anti-oxidant levels.
- The current research attributes the increased activity of AChE in the group treated with AlCl_3 to the direct impact of Al. Our investigation revealed that the simultaneous administration of PTME resulted in a significant decrease in AChE activity in the hippocampus.
- PTME hindered the activation of NF- κ B in the hippocampus, which in turn reduced the occurrence of subsequent pathological events, such as $\text{A}\beta$ accumulation, increased production of pro-inflammatory cytokines, and apoptosis.

- The administration of PTME lowered the expression of pro-inflammatory cytokines, including IL-6 and TNF- α , in the hippocampus of AlCl₃-mediated AD rats, probably by inhibiting the expression of NF- κ B.
- The administration of PTME caused a decrease in the levels of active caspase-3 and Bax in the hippocampus of AlCl₃-mediated AD rats, most likely by restoring the Bcl-2 expression level.
- The administration of PTME reduces the expression level of A β in the hippocampus of AlCl₃-mediated AD rats, probably by inhibiting the activity of BACE1. Furthermore, the reduction in the expression level of tau protein may be attributed to the suppression of A β toxicity by the administration of PTME.
- The administration of the methanolic extract of *P. timoriana* seed pods successfully restored the histopathological alterations of the hippocampus caused by AlCl₃ toxicity.

5. REFERENCES

- Abraham, M. J., Murtola, T., Schulz, R., Páll, S., Smith, J. C., Hess, B., and Lindahl, E. (2015). GROMACS: High performance molecular simulations through multi-level parallelism from laptops to supercomputers. *SoftwareX*, 1–2, 19–25. <https://doi.org/10.1016/j.softx.2015.06.001>
- Alawdi, S. H., El-Denshary, E. S., Safar, M. M., Eidi, H., David, M. O., and Abdel-Wahhab, M. A. (2017). Neuroprotective Effect of Nanodiamond in Alzheimer's Disease Rat Model: a Pivotal Role for Modulating NF- κ B and STAT3 Signaling. *Molecular neurobiology*, 54(3), 1906–1918. <https://doi.org/10.1007/s12035-016-9762-0>
- Alzheimer's Association (2024). 2024 Alzheimer's disease facts and figures. *Alzheimer's & dementia: the journal of the Alzheimer's Association*, 20(5), 3708–3821. <https://doi.org/10.1002/alz.13809>
- Amadei, A., Linssen, A. B., and Berendsen, H. J. (1993). Essential dynamics of proteins. *Proteins*, 17(4), 412–425. <https://doi.org/10.1002/prot.340170408>

- Angami, T., Bhagawati, R., Touthang, L., Makdoh, B., Khatri, N., Singson, L., Bharati, K., Silambarasan, R., and Ayyanar, M. (2018). Traditional uses, phytochemistry and biological activities of *Parkia timoriana* (DC.) Merr., an underutilized multipurpose tree bean: a review. *Genetic Resources and Crop Evolution*, 65. <https://doi.org/10.1007/s10722-017-0595-0>
- Annie, L., Gurusubramanian, G., and Roy, V. K. (2020). Changes in the localization of ovarian visfatin protein and its possible role during estrous cycle of mice. *Acta histochemica*, 122(8), 151630. <https://doi.org/10.1016/j.acthis.2020.151630>
- Baker, N. A., Sept, D., Joseph, S., Holst, M. J., and McCammon, J. A. (2001). Electrostatics of nanosystems: application to microtubules and the ribosome. *Proceedings of the National Academy of Sciences of the United States of America*, 98(18), 10037–10041. <https://doi.org/10.1073/pnas.181342398>
- Bancroft, J. D. and Gamble, M. (2002). Theory and practice of histological techniques. 5th ed. Edinburgh: Churchill Livingstone Pub, 172, 593–620.
- Benfenati, E., Benigni, R., Demarini, D. M., Helma, C., Kirkland, D., Martin, T. M., Mazzatorta, P., Ouédraogo-Arras, G., Richard, A. M., Schilter, B., Schoonen, W. G., Snyder, R. D., and Yang, C. (2009). Predictive models for carcinogenicity and mutagenicity: frameworks, state-of-the-art, and perspectives. *Journal of environmental science and health. Part C, Environmental carcinogenesis & ecotoxicology reviews*, 27(2), 57–90. <https://doi.org/10.1080/10590500902885593>
- Berendsen, H. J. C., Spoel, D. V. D., Drunen, R. V. (1995). GROMACS: a message-passing parallel molecular dynamics implementation. *Computer Physics Communications*, 91(1–3), 43–56. [https://doi.org/10.1016/0010-4655\(95\)00042-E](https://doi.org/10.1016/0010-4655(95)00042-E)
- Berendsen, H., Postma, J. P. M., van Gunsteren, W., DiNola, A. D., and Haak, J. R. (1984). Molecular-dynamics with coupling to an external bath. *The Journal of Chemical Physics*, 81, 3684. <https://doi.org/10.1063/1.448118>

- Bonsnes, R. W., and Taussky, H. H. (1945). On the colorimetric determination of creatinine by the Jaffe reaction. *Journal of Biological Chemistry*. 158, 581–591.
- Bradford, M. M. (1976). A rapid and sensitive method for the quantitation of microgram quantities of protein utilizing the principle of protein-dye binding. *Analytical biochemistry*, 72, 248–254. <https://doi.org/10.1006/abio.1976.9999>
- Cassano, A., Manganaro, A., Martin, T., Young, D., Piclin, N., Pintore, M., Bigoni, D., and Benfenati, E. (2010). CAESAR models for developmental toxicity. *Chemistry Central journal*, 4 Suppl 1(Suppl 1), S4. <https://doi.org/10.1186/1752-153X-4-S1-S4>
- Cervellati, C., Valacchi, G., and Zuliani, G. (2021). BACE1: from biomarker to Alzheimer's disease therapeutical target. *Aging*, 13(9), 12299–12300. <https://doi.org/10.18632/aging.203064>
- Daina, A., Michielin, O., and Zoete, V. (2017). SwissADME: a free web tool to evaluate pharmacokinetics, drug-likeness and medicinal chemistry friendliness of small molecules. *Scientific reports*, 7, 42717. <https://doi.org/10.1038/srep42717>
- Dallakyan, S., Olson, A. J. (2015). Small-molecule library screening by docking with PyRx. *Methods in Molecular Biology*, 1263, 243–250. https://doi.org/10.1007/978-1-4939-2269-7_19
- Duke, J. A. (2000). Handbook of phytochemical constituent GRAS herbs and other economic plants. Herbal reference library, CRC Press, Boca Raton, FL, USA.
- Ennaceur, A., and Delacour, J. (1988). A new one-trial test for neurobiological studies of memory in rats. 1: Behavioral data. *Behavioural brain research*, 31(1), 47–59. [https://doi.org/10.1016/0166-4328\(88\)90157-x](https://doi.org/10.1016/0166-4328(88)90157-x)
- Fawcett, J. K., and Scott, J. E. (1960). A rapid and precise method for the determination of urea. *Journal of clinical pathology*, 13(2), 156–159. <https://doi.org/10.1136/jcp.13.2.156>

- Feldman, B.F., Zinkl, J.G., and Jain, V.C. (2000). Schalm's Veterinary Hematology, fifth ed. Lippincott Williams and Wilkins, Toronto, Canada, 1145–1146.
- García-Ayllón, M. S., Small, D. H., Avila, J., and Sáez-Valero, J. (2011). Revisiting the Role of Acetylcholinesterase in Alzheimer's Disease: Cross-Talk with P-tau and β -Amyloid. *Frontiers in molecular neuroscience*, 4, 22. <https://doi.org/10.3389/fnmol.2011.00022>
- Goel, R. K., Singh, D., Lagunin, A., and Poroikov, V. (2011). PASS-assisted exploration of new therapeutic potential of natural products. *Medicinal Chemistry Research*, 20(2011), 1509.
- Golde, T. E., Eckman, C. B., and Younkin, S. G. (2000). Biochemical detection of Abeta isoforms: implications for pathogenesis, diagnosis, and treatment of Alzheimer's disease. *Biochimica et biophysica acta*, 1502(1), 172–187. [https://doi.org/10.1016/s0925-4439\(00\)00043-0](https://doi.org/10.1016/s0925-4439(00)00043-0)
- Habig, W. H., Pabst, M. J., and Jakoby, W. B. (1974). Glutathione S-transferases. The first enzymatic step in mercapturic acid formation. *The Journal of biological chemistry*, 249(22), 7130–7139.
- Hampel, H., Hardy, J., Blennow, K., Chen, C., Perry, G., Kim, S. H., Villemagne, V. L., Aisen, P., Vendruscolo, M., Iwatsubo, T., Masters, C. L., Cho, M., Lannfelt, L., Cummings, J. L., and Vergallo, A. (2021). The Amyloid- β Pathway in Alzheimer's Disease. *Molecular psychiatry*, 26(10), 5481–5503. <https://doi.org/10.1038/s41380-021-01249-0>
- Hardy, J., and Selkoe, D. J. (2002). The amyloid hypothesis of Alzheimer's disease: progress and problems on the road to therapeutics. *Science* (New York, N.Y.), 297(5580), 353–356. <https://doi.org/10.1126/science.1072994>
- Hess, B., Bekker, H., Berendsen, H., and Fraaije, J. (1998) LINCS: a linear constraint solver for molecular simulations. *Journal of Computational Chemistry*, 18,1463–1472. [https://doi.org/10.1002/\(SICI\)1096-987X\(199709\)18:12<1463::AIDJCC4>3.0.CO;2-H](https://doi.org/10.1002/(SICI)1096-987X(199709)18:12<1463::AIDJCC4>3.0.CO;2-H)

- Higgins, T., Beutler, E., and Dumas, B.T. (2008). Measurement of haemoglobin in blood. In: Burtis, C.A., Ashwood, E.R., Bruns, D.E. (Eds.), *Tietz Fundamentals of Clinical Chemistry*, sixth ed. Sanders Elsevier, Saint Louis, MO, USA, 524–525.
- Hornak, V., Abel, R., Okur, A., Strockbine, B., Roitberg, A., and Simmerling, C. (2006). Comparison of multiple Amber force fields and development of improved protein backbone parameters. *Proteins*, 65(3), 712–725. <https://doi.org/10.1002/prot.21123>
- Hou, T., Wang, J., Li, Y., and Wang, W. (2011). Assessing the performance of the MM/PBSA and MM/GBSA methods. The accuracy of binding free energy calculations based on molecular dynamics simulations. *Journal of chemical information and modeling*, 51(1), 69–82. <https://doi.org/10.1021/ci100275a>
- Kar, S., and Leszczynski, J. (2019). Exploration of Computational Approaches to Predict the Toxicity of Chemical Mixtures. *Toxics*, 7(1), 15. <https://doi.org/10.3390/toxics7010015>
- Keretsu, S., Bhujbal, S. P., and Cho, S. J. (2021). Molecular modeling studies of pyrrolo[2,3-d]pyrimidin-4-amine derivatives as JAK1 inhibitors based on 3D-QSAR, molecular docking, molecular dynamics (MD) and MM-PBSA calculations. *Journal of biomolecular structure & dynamics*, 39(3), 753–765. <https://doi.org/10.1080/07391102.2020.1714483>
- Kind, P. R., and King, E. J. (1954). Estimation of plasma phosphatase by determination of hydrolysed phenol with amino-antipyrine. *Journal of clinical pathology*, 7(4), 322–326. <https://doi.org/10.1136/jcp.7.4.322>
- Kolodziejczyk-Czepas, J., Pasiński, B., Ponczek, M. B., Moniuszko-Szajwaj, B., Kowalczyk, M., Pecio, Ł., Nowak, P., and Stochmal, A. (2018). Bufadienolides from *Kalanchoe daigremontiana* modulate the enzymatic activity of plasmin - In vitro and in silico analyses. *International journal of biological macromolecules*, 120(Pt B), 1591–1600. <https://doi.org/10.1016/j.ijbiomac.2018.09.143>

- Kuete, V., Tangmouo, J. G., Penlap Beng, V., Ngounou, F. N., and Lontsi, D. (2006). Antimicrobial activity of the methanolic extract from the stem bark of *Tridestemon omphalocarpoides* (Sapotaceae). *Journal of ethnopharmacology*, 104(1-2), 5–11. <https://doi.org/10.1016/j.jep.2005.08.002>
- Kumari, R., Kumar, R., Open Source Drug Discovery Consortium, and Lynn, A. (2014). g_mmpbsa--a GROMACS tool for high-throughput MM-PBSA calculations. *Journal of chemical information and modeling*, 54(7), 1951–1962. <https://doi.org/10.1021/ci500020m>
- Lam, K., Pan, K., Linnekamp, J. F., Medema, J. P., and Kandimalla, R. (2016). DNA methylation based biomarkers in colorectal cancer: A systematic review. *Biochimica et biophysica acta*, 1866(1), 106–120. <https://doi.org/10.1016/j.bbcan.2016.07.001>
- Le Guilloux, V., Schmidtke, P., and Tuffery, P. (2009). Fpocket: an open-source platform for ligand pocket detection. *BMC bioinformatics*, 10, 168. <https://doi.org/10.1186/1471-2105-10-168>
- Lista, S., Vergallo, A., Teipel, S. J., Lemercier, P., Giorgi, F. S., Gabelle, A., Garaci, F., Mercuri, N. B., Babiloni, C., Gaire, B. P., Koronyo, Y., Koronyo-Hamaoui, M., Hampel, H., Nisticò, R., and Neurodegeneration Precision Medicine Initiative (NPMI) (2023). Determinants of approved acetylcholinesterase inhibitor response outcomes in Alzheimer's disease: relevance for precision medicine in neurodegenerative diseases. *Ageing research reviews*, 84, 101819. <https://doi.org/10.1016/j.arr.2022.101819>
- Long, S., Benoist, C., and Weidner, W. (2023). World Alzheimer Report 2023: Reducing dementia risk: never too early, never too late. London, England: Alzheimer's Disease International.
- Longvah, T., Deosthale, Y. G. (1998). Nutrient composition and food potential of *Parkia roxburghii*, a less known tree legume from northeast India. *Food chemistry*, 62(4), 477–481. [https://doi.org/10.1016/S0308-8146\(97\)00179-9](https://doi.org/10.1016/S0308-8146(97)00179-9)

- López-Vallejo, F., Caulfield, T., Martínez-Mayorga, K., Giulianotti, M. A., Nefzi, A., Houghten, R. A., and Medina-Franco, J. L. (2011). Integrating virtual screening and combinatorial chemistry for accelerated drug discovery. *Combinatorial chemistry & high throughput screening*, 14(6), 475–487. <https://doi.org/10.2174/138620711795767866>
- Martin, T. M. (2020). User's Guide for T.E.S.T. (Toxicity Estimation Software Tool) Version 5.1: A Java Application to Estimate Toxicities and Physical Properties from Molecular Structure. U.S. Environmental Protection Agency.
- Martin, T. M., and Young, D. M. (2001). Prediction of the acute toxicity (96-h LC50) of organic compounds to the fathead minnow (*Pimephales promelas*) using a group contribution method. *Chemical research in toxicology*, 14(10), 1378–1385. <https://doi.org/10.1021/tx0155045>
- Martin, T. M., Harten, P., Venkatapathy, R., Das, S., and Young, D. M. (2008). A hierarchical clustering methodology for the estimation of toxicity. *Toxicology mechanisms and methods*, 18(2-3), 251–266. <https://doi.org/10.1080/15376510701857353>
- Moron, M. S., Depierre, J. W., and Mannervik, B. (1979). Levels of glutathione, glutathione reductase and glutathione S-transferase activities in rat lung and liver. *Biochimica et biophysica acta*, 582(1), 67–78. [https://doi.org/10.1016/0304-4165\(79\)90289-7](https://doi.org/10.1016/0304-4165(79)90289-7)
- Nordberg, A., Ballard, C., Bullock, R., Darreh-Shori, T., and Somogyi, M. (2013). A review of butyrylcholinesterase as a therapeutic target in the treatment of Alzheimer's disease. *The primary care companion for CNS disorders*, 15(2), PCC.12r01412. <https://doi.org/10.4088/PCC.12r01412>
- Noumi, E., Snoussi, M., Anouar, E. H., Alreshidi, M., Veettil, V. N., Elkahoui, S., Adnan, M., Patel, M., Kadri, A., Aouadi, K., De Feo, V., and Badraoui, R. (2020). HR-LCMS-Based Metabolite Profiling, Antioxidant, and Anticancer Properties of *Teucrium polium* L. Methanolic Extract: Computational and In Vitro Study.

- Antioxidants* (Basel, Switzerland), 9(11), 1089.
<https://doi.org/10.3390/antiox9111089>
- Ohkawa, H., Ohishi, N., and Yagi, K. (1979). Assay for lipid peroxides in animal tissues by thiobarbituric acid reaction. *Analytical biochemistry*, 95(2), 351–358.
[https://doi.org/10.1016/0003-2697\(79\)90738-3](https://doi.org/10.1016/0003-2697(79)90738-3)
- Opo, F. A. D. M., Rahman, M. M., Ahammad, F., Ahmed, I., Bhuiyan, M. A., and Asiri, A. M. (2021). Structure based pharmacophore modeling, virtual screening, molecular docking and ADMET approaches for identification of natural anti-cancer agents targeting XIAP protein. *Scientific reports*, 11(1), 4049.
<https://doi.org/10.1038/s41598-021-83626-x>
- Park S. Y. (2010). Potential therapeutic agents against Alzheimer's disease from natural sources. *Archives of pharmacal research*, 33(10), 1589–1609.
<https://doi.org/10.1007/s12272-010-1010-y>
- Parrinello, M., and Rahman, A. (1981). Polymorphic transitions in single crystals: a new molecular dynamics method. *Journal of Applied Physics*, 52, 7182–7190.
<https://doi.org/10.1063/1.328693>
- Pettersen, E. F., Goddard, T. D., Huang, C. C., Couch, G. S., Greenblatt, D. M., Meng, E. C., and Ferrin, T. E. (2004). UCSF Chimera--a visualization system for exploratory research and analysis. *Journal of computational chemistry*, 25(13), 1605–1612. <https://doi.org/10.1002/jcc.20084>
- Pognan, F., Beilmann, M., Boonen, H. C. M., Czich, A., Dear, G., Hewitt, P., Mow, T., Oinonen, T., Roth, A., Steger-Hartmann, T., Valentin, J. P., Van Goethem, F., Weaver, R. J., and Newham, P. (2023). The evolving role of investigative toxicology in the pharmaceutical industry. *Nature reviews. Drug discovery*, 22(4), 317–335. <https://doi.org/10.1038/s41573-022-00633-x>
- Prakash, A., Kumar, V., Lynn, A. M., and Haque, R. (2019). Insights into the DNA binding induced thermal stabilization of transcription factor FOXP3. *Journal of biomolecular structure & dynamics*, 37(9), 2219–2229.
<https://doi.org/10.1080/07391102.2018.1486228>

- Ravi, S. K., Ramesh, B. N., Mundugaru, R., and Vincent, B. (2018). Multiple pharmacological activities of *Caesalpinia crista* against aluminum-induced neurodegeneration in rats: Relevance for Alzheimer's disease. *Environmental toxicology and pharmacology*, 58, 202–211. <https://doi.org/10.1016/j.etap.2018.01.008>
- Reddy, M. N., Adnan, M., Alreshidi, M. M., Saeed, M., and Patel, M. (2020). Evaluation of Anticancer, Antibacterial and Antioxidant Properties of a Medicinally Treasured Fern *Tectaria coadunata* with its Phytoconstituents Analysis by HR-LCMS. *Anti-cancer agents in medicinal chemistry*, 20(15), 1845–1856. <https://doi.org/10.2174/1871520620666200318101938>
- Reitman, S., and Frankel, S. (1957). A colorimetric method for the determination of serum glutamic oxalacetic and glutamic pyruvic transaminases. *American journal of clinical pathology*, 28(1), 56–63. <https://doi.org/10.1093/ajcp/28.1.56>
- Saha, R., and Tomar, J. M. S., and Ghosh, P. K. (2007). Evaluation and selection of multipurpose tree for improving soil hydro-physical behavior under hilly ecosystem of Northeast India. *Agroforestry Systems*, 69, 239–247. <https://doi.org/10.1007/s10457-007-9044-y>
- Sanchez-Varo, R., Trujillo-Estrada, L., Sanchez-Mejias, E., Torres, M., Baglietto-Vargas, D., Moreno-Gonzalez, I., De Castro, V., Jimenez, S., Ruano, D., Vizuite, M., Davila, J. C., Garcia-Verdugo, J. M., Jimenez, A. J., Vitorica, J., and Gutierrez, A. (2012). Abnormal accumulation of autophagic vesicles correlates with axonal and synaptic pathology in young Alzheimer's mice hippocampus. *Acta neuropathologica*, 123(1), 53–70. <https://doi.org/10.1007/s00401-011-0896-x>
- Schmidtke, P., Le Guilloux, V., Maupetit, J., and Tufféry, P. (2010). fpocket: online tools for protein ensemble pocket detection and tracking. *Nucleic acids research*, 38(Web Server issue), W582–W589. <https://doi.org/10.1093/nar/gkq383>

- Seal, T. (2011). Nutritional composition of wild edible fruits in Meghalaya state of India and their ethno-botanical importance. *Research Journal of Botany*, 6 (2), 58–67. <https://doi.org/10.3923/rjb.2011.58.67>
- Selvaraj, C., Dinesh, D. C., Panwar, U., Abhirami, R., Boura, E., and Singh, S. K. (2021). Structure-based virtual screening and molecular dynamics simulation of SARS-CoV-2 Guanine-N7 methyltransferase (nsp14) for identifying antiviral inhibitors against COVID-19. *Journal of biomolecular structure & dynamics*, 39(13), 4582–4593. <https://doi.org/10.1080/07391102.2020.1778535>
- Sen, S., De, B., Devanna, N., and Chakraborty, R. (2013). Total phenolic, total flavonoid content, and antioxidant capacity of the leaves of *Meyna spinosa* Roxb., an Indian medicinal plant. *Chinese journal of natural medicines*, 11(2), 149–157. [https://doi.org/10.1016/S1875-5364\(13\)60042-4](https://doi.org/10.1016/S1875-5364(13)60042-4)
- Sharma, A., Vora, J., Patel, D., Sinha, S., Jha, P. C., and Shrivastava, N. (2022). Identification of natural inhibitors against prime targets of SARS-CoV-2 using molecular docking, molecular dynamics simulation and MM-PBSA approaches. *Journal of biomolecular structure & dynamics*, 40(7), 3296–3311. <https://doi.org/10.1080/07391102.2020.1846624>
- Sheikh, Y., Maibam, B. C., Talukdar, N. C., Deka, D. C., and Borah, J. C. (2016). In vitro and in vivo anti-diabetic and hepatoprotective effects of edible pods of *Parkia roxburghii* and quantification of the active constituent by HPLC-PDA. *Journal of ethnopharmacology*, 191, 21–28. <https://doi.org/10.1016/j.jep.2016.06.015>
- Siddiqui, A. J., Danciu, C., Ashraf, S. A., Moin, A., Singh, R., Alreshidi, M., Patel, M., Jahan, S., Kumar, S., Alkhinjar, M. I. M., Badraoui, R., Snoussi, M., and Adnan, M. (2020). Plants-Derived Biomolecules as Potent Antiviral Phytomedicines: New Insights on Ethnobotanical Evidences against Coronaviruses. *Plants* (Basel, Switzerland), 9(9), 1244. <https://doi.org/10.3390/plants9091244>
- Singha, W. R., Kurmi, B., Sahoo, U. K., Sileshi, G. W., Nath, A. J., and Das, A. K. (2021). *Parkia roxburghii*, an underutilized tree bean for food, nutritional and

- regional climate security. *Trees, Forests and People*, 4, 100065. <https://doi.org/10.1016/j.tfp.2021.100065>
- Suarez-Torres, J. D., Ciangherotti, C. E., and Jimenez-Orozco, F. A. (2020). The predictivity of the -alert performance- functionality of the OECD QSAR-Toolbox (c/w further issues on the predictivity of nonclinical testing). *Toxicology in vitro: an international journal published in association with BIBRA*, 66, 104858. <https://doi.org/10.1016/j.tiv.2020.104858>
- Suh, Y. H., and Checler, F. (2002). Amyloid precursor protein, presenilins, and alpha-synuclein: molecular pathogenesis and pharmacological applications in Alzheimer's disease. *Pharmacological reviews*, 54(3), 469–525. <https://doi.org/10.1124/pr.54.3.469>
- Taidi, L., Maurady, A., and Britel, M. R. (2022). Molecular docking study and molecular dynamic simulation of human cyclooxygenase-2 (COX-2) with selected eutypoids. *Journal of biomolecular structure & dynamics*, 40(3), 1189–1204. <https://doi.org/10.1080/07391102.2020.1823884>
- Tapan, S. (2011). Evaluation of antioxidant activity of some wild edible fruits of Meghalaya state in India. *International Journal of Pharmacy and Pharmaceutical Sciences*, 3(4), 233–236. <https://doi.org/10.5897/IJNAM11.060>
- Tarragon, E., Lopez, D., Estrada, C., Ana, G. C., Schenker, E., Pifferi, F., Bordet, R., Richardson, J. C., and Herrero, M. T. (2013). Octodon degus: a model for the cognitive impairment associated with Alzheimer's disease. *CNS neuroscience & therapeutics*, 19(9), 643–648. <https://doi.org/10.1111/cns.12125>
- Thangjam R. (2014). Inter-simple sequence repeat (ISSR) marker analysis in *Parkia timoriana* (DC.) Merr. populations from Northeast India. *Applied biochemistry and biotechnology*, 172(4), 1727–1734. <https://doi.org/10.1007/s12010-013-0639-7>
- Thrall, M.A., and Weiser, M.G. (2002). Hematology in laboratory procedures for veterinary technicians. In: Hendrix, C.M. (Ed.), Saint Louis, MO, fourth ed. Mosby, USA, 29–74.

- Trinder, P. (1969). Enzymatic calorimetric determination of triglycerides by GOP-PAP method. *Annals of Clinical Biochemistry*. 6, 24–27.
- Trott, O., and Olson, A. J. (2010). AutoDock Vina: improving the speed and accuracy of docking with a new scoring function, efficient optimization, and multithreading. *Journal of computational chemistry*, 31(2), 455–461. <https://doi.org/10.1002/jcc.21334>
- U.S.E.P.A, ECOTOX Database, (2016) Available from: <http://cfpub.epa.gov/ecotox/>
- Van Norman, G. A. (2020). Limitations of Animal Studies for Predicting Toxicity in Clinical Trials: Part 2: Potential Alternatives to the Use of Animals in Preclinical Trials. *JACC. Basic to translational science*, 5(4), 387–397. <https://doi.org/10.1016/j.jacbts.2020.03.010>
- World Health Organization (2023). Dementia, accessed July 31, 2023, <https://www.who.int/news-room/facts-in-pictures/detail/dementia>
- Zhang, M., Cao, J., Dai, X., Chen, X., and Wang, Q. (2012). Flavonoid Contents and Free Radical Scavenging Activity of Extracts from Leaves, Stems, Rachis and Roots of *Dryopteris erythrosora*. *Iranian journal of pharmaceutical research: IJPR*, 11(3), 991–997.
- Zhang, R., Xue, G., Wang, S., Zhang, L., Shi, C., and Xie, X. (2012). Novel object recognition as a facile behavior test for evaluating drug effects in A β PP/PS1 Alzheimer's disease mouse model. *Journal of Alzheimer's disease : JAD*, 31(4), 801–812. <https://doi.org/10.3233/JAD-2012-120151>
- Zhao, C., Boriani, E., Chana, A., Roncaglioni, A., and Benfenati, E. (2008). A new hybrid system of QSAR models for predicting bioconcentration factors (BCF). *Chemosphere*, 73(11), 1701–1707. <https://doi.org/10.1016/j.chemosphere.2008.09.033>
- Zhu, H., Martin, T. M., Ye, L., Sedykh, A., Young, D. M., and Tropsha, A. (2009). Quantitative structure-activity relationship modeling of rat acute toxicity by oral exposure. *Chemical research in toxicology*, 22(12), 1913–1921. <https://doi.org/10.1021/tx900189p>